FACULTY OF SCIENCE
UNIVERSITY OF COPENHAGEN

PhD thesis

Selma Maric

Development of a Stealth Carrier System for Structural Studies of Membrane Proteins in Solution

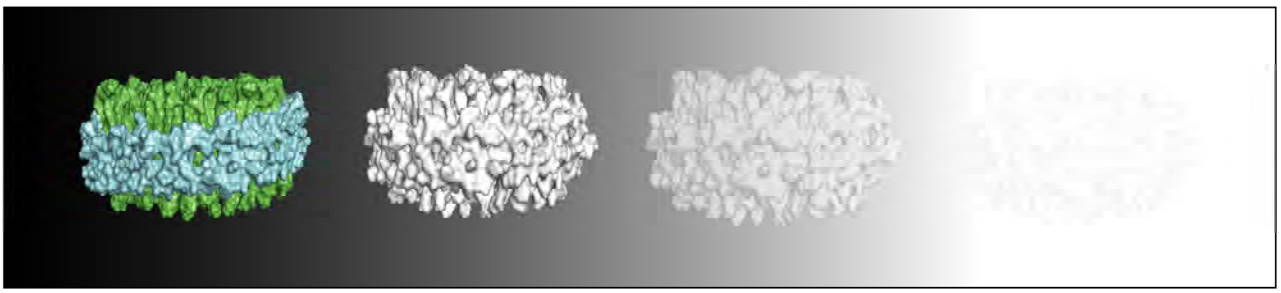

Academic advisors: Lise Arleth and Thomas Günther Pomorski
Submitted: 6th of February 2014

Structural Biophysics
Neutron and X-ray Scattering Group
The Niels Bohr Institute
Faculty of Science
University of Copenhagen

Development of a Stealth Carrier System for Structural Studies of Membrane Proteins in Solution

PhD thesis by
Selma Maric
Submitted: 6th of February 2014

Academic supervisors:
Professor Lise Arleth (principal)
Associate Professor Thomas Günther Pomorski

Structural Biophysics
Neutron and X-ray Scattering Group
The Niels Bohr Institute
Faculty of Science
University of Copenhagen

Front cover: Schematic representation of the stealth nanodisc system in a buffer solution with a gradually increasing level of D_2O (decreasing grayscale). From left to right: hydrogenated nanodisc consisting of a phospholipid bilayer (green) and membrane scaffold protein MSP (light blue), stealth nanodisc comprised of deuterated lipid and deuterated MSP at 60% D2O, stealth nanodisc at 80% D_2O, stealth nanodisc at 100% D_2O. Illustration by Selma Maric.

Preface

This thesis represents research from a three-year long PhD carried out under the Centre for Synthetic Biology at the University of Copenhagen with co-funding by the European Spallation Source, ESS in Lund, Sweden. The project was done as a collaboration between groups within the Center where the expression and purification steps in the production of physiologically relevant lipids were done in the Biomembrane group at the Department of Plant and Environmental Sciences led by Assoc. Prof. Thomas Günther Pomorski while the nanodisc carrier assembly and small angle scattering measurements and data analysis were done in the Structural Biophysics group at the Niels Bohr Institute led by Prof. Lise Arleth. The cross-disciplinary nature of the Center for Synthetic Biology further provided easy and fast access to other techniques and facilities relevant to the project such as NMR available in the Chemistry group led by Prof. Knud Jensen. All sets of deuteration were performed at the Life Sciences Group at the Institut Laue Langevin in Grenoble, France during several short term research stays hosted by Prof. Trevor Forsyth.

The thesis is comprised of seven chapters where the first chapter, the introduction, gives the main background and objectives of the thesis. The following five chapters represent five studies forming the main part of the PhD and a seventh chapter which is composed of the conclusions and future perspectives. The work from this thesis has resulted in three manuscripts, two of which are published, and one that is in preparation.

Selma Maric

5th of February 2014
Copenhagen, Denmark

Acknowledgements

It is difficult to acknowledge everyone who has contributed to the research presented in this thesis but I would like to start by thanking both Lise Arleth and Thomas Günther Pomorski for not only giving me the opportunity to join this exciting project but for your excellent supervision and guidance throughout the project. This thesis would never have been possible without your expertise, your mentorship and continuous support that you have provided me during these three fantastic, and sometimes challenging, years.

I would like to thank the many collaborators and colleagues that have always been so kind and helpful making it a pleasure to work here. First of all thank you to my colleagues Nicholas Skar-Gislinge, Martin Cramer Pedersen, Søren Kynde and the rest of the Structural Biophysics Group for the invaluable help with the acquisition, interpretation and analysis of small-angle scattering data and to Pie Huda and Søren Roi Midtgaard for all the help in the lab and especially for providing the sensory rhodopsin and extra deuterated belt protein used for the first trial reconstitution into invisible nanodiscs. I would also like to thank my collaborators Mikkel Boas Thygesen and Jürgen Schiller for your fruitful discussions, the help with data analysis and interpretation as well as important input on the manuscripts. Thank you to my colleagues Gerdi Kemmer, Magdalena Marek, Merethe Mørch Frøsig, Maria Stumph Jensen, Iwona Ziomkiewicz, Anne-Mette Bjerg Petersen, Bo Højen Justesen, Lisa Theorin, Rosa Lopez and the rest of the Transport Biology Group for all the help in the lab, the constant support, many interesting discussions and for simply being great colleagues. Thank you also to all the great scientists whom I have had the pleasure to work with within the Synthetic Biology community in Copenhagen for providing such a stimulating and interdisciplinary environment. Furthermore, I would like to thank the Life Science Group at the Institut Laue Langevin and especially Trevor Forsyth, Michael Haertlein and Martine Moulin for your invaluable contributions to this research and for making me feel so welcome and a part of your group during my many stays in Grenoble.

Finally, I wish to thank my fantastic family and friends for your continuous support throughout my time as a PhD student. Special thank you goes to my father for always taking the time to listen, to come up with great solutions to any problem that I might have and for always being there for me during this long and often challenging time. To you I dedicate this thesis.

Summary

Structural studies of membrane proteins remain a great experimental challenge. Functional reconstitution into artificial nano-scale bilayer disc carriers that mimic the native bilayer environment allows for the handling of membrane proteins in solution. This potentially enables the use of small-angle scattering techniques for fast and reliable structural analysis. The difficulty with this approach is that the carrier discs contribute to the measured scattering intensity in a highly non-trivial fashion, making subsequent data analysis challenging.

This thesis presents the development of a specifically deuterated, stealth nanodisc system which can be used for SANS structural analysis of membrane proteins in solution. In combination with the D_2O/H_2O-based contrast variation method it is demonstrated that it is possible to prepare specifically deuterated analogues of the nanodisc, which give minimal contribution to the neutron scattering data when used in 100% D_2O. An important challenge in the project was obtaining selective partial deuteration of the nanodisc system necessary for the total matching at 100% D_2O. This was achieved through an *E. coli* based biosynthesis for both deuterated phosphatidylcholines as well as membrane scaffolding protein. To obtain physiologically relevant deuterated phosphatidylcholine (PC) species with the required scattering length density a novel method for deuteration of PC was developed to separately control the deuteration levels of three different parts of the phospholipid molecule: the lipid head-group, glycerol-backbone and fatty-acyl tails. This could be achieved via a biosynthetic pathway in a genetically modified *E. coli* strain adapted to growth in D_2O in combination with a systematic supplementation with deuterated nutrients.

The stealth discs produced in this way should be generally usable in low-resolution structural studes of many membrane proteins and their complexes in solution as the analysis of SANS data for this platform is greatly simplified and allows for the application of existing data analysis tools already available for soluble proteins.

Resumé (Dansk)

Strukturelle studier af membranproteiner er til stadighed en stor eksperimentel udfordring. Funktionel rekonstituering i syntetiske modelmembraner, som efterligner de naturlige omgivelser i lipid-dobbeltlaget, muliggør studier af membranproteiner i opløsning. Herved kan metoder som små-vinkel spredning benyttes til at opnå hurtig og pålidelig strukturel information om membranproteiners struktur. Problemet ved denne fremgangsmåde er, at modelmembranerne selv bidrager væsentligt til den målte spredningsintensitet, så den efterfølgende dataanalyse bliver vanskelig.

Denne PhD-afhandling omhandler udviklingen af et specifikt deuteriseret usynligt nanodisc-system, der kan bruges til strukturel analyse med SANS af membranproteiner i opløsning. I kombination med metoder for D_2O/H_2O-baseret kontrastvariation demonstreres her, at det er muligt at fremstille specifikt deuteriserede analoger af nanodiscs, der bidrager minimalt til neutronspredningen i 100% D_2O. En særlig udfordring har været at kontrollere selektive deutereringsniveauer i nanodisc-systemet, der muliggør et total match i 100% D_2O. Dette er opnået via *E. coli*-baseret biosyntese af både deuterisede fosfatidylkoliner samt de membran-stabiliserende proteiner. For at producere fysiologisk relevante deuteriserede fosfatidylkoliner (PC) med den ønskede spredningslængdedensitet blev en ny metode til PC-deuterisering udviklet, hvor deuteriseringsniveauet af henholdsvis hoved-grupperne, glycerol-backbonet og fedtsyrekæderne kan kontrolleres separat. Dette kan opnås via en biosyntetisk pathway i en genmodificeret *E. coli*-stamme, som er tilpasset vækst i D_2O kombineret med tilsætning af deuteriserede næringsstoffer.

De usynlige nanodiscs produceret på denne måde vil være generelt anvendelige i strukturelle lavopløsningsstudier af forskellige membranproteiner og komplekser i opløsning. Analyser af SANS-data for denne metode vil blive væsentligt simplificeret da den tillader brug af de eksisterende dataanalyseværktøjer, der allerede er tilgængelige for vandopløselige proteiner.

List of Abbreviations

7TM	Seven transmembrane
9-AA	9-aminoacridine
Apo-A1	Apolipoprotein A1
ATP	Adenosine triphosphate
CDP	Cytidine diphosphate
CL	Cardiolipin
COSY	Correlation spectroscopy
DHB	acidic 2,5-dihydroxybenzoic acid
DMPC	1,2-dimyristoyl-*sn*-glycero-3-phosphocholine
DMPG	1,2-dimyristoyl-*sn*-glycero-3-phospho-(1'-*rac*-glycerol)
DNA	Deoxyribonucleic acid
EDTA	Ethylenediaminetetraacetic acid
EGFR	Epidermal growth factor receptor
EM	Electron microscopy
GLC	Gas-liquid chromatography
GPCR	G-protein coupled receptor
HDL	High-density lipo-protein
IPTG	Isopropyl b-D-1-thiogalactopyranoside
MALDI	Matrix-assisted laser desorption/ionization
MSP	Membrane scaffold protein
NMR	Nuclear magnetic resonance
NTA	Nitrilotriacetic acid
OD	Optical density
PA	Phosphatidic acid
PAGE	Polyacrylamide gel electrophoresis

PC	Phosphatidylcholine
PDB	Protein Data Bank
PE	Phosphatidylethanolamine
PG	Phosphatidylglycerol
PI	Phosphatidylinositol
PLA_2	Phospholipase A_2
PMSF	Phenylmethanesulfonyl fluoride
POPC	1-palmitoyl-2-oleoyl-*sn*-glycero-3-phosphocholine
PS	Phosphatidylserine
PSD	Post source decay
SANS	Small-angle neutron scattering
SAS	Small-angle scattering
SAXS	Small-angle x-ray scattering
SDS	Sodium dodecyl sulfate
SLD	Scattering length density
TLC	Thin-layer chromatography
TMS	Tetramethylsilane
TOF	Time of flight

Contents

Chapter 1

General introduction

The biological membrane surrounds every living cell and defines the boundary between the cell and the outside environment. Eukaryotic cells contain in addition numerous subcellular membranes that divide the cytoplasm into multiple organelles, thereby allowing different functions to occur efficiently and simultaneously in different parts of the cell.[1] Many cellular processes depend on this semi-permeable barrier which plays a role in intracellular metabolism, allows and regulates the traffic of nutrients and small molecules in and out of the cell and cellular compartments, and is responsible for sensing the environment.[1] The composition and architecture of biological membranes can vary greatly between cells as well as between different organelles of the same cell.[1-4] The understanding of the architecture of biological membranes has long been the target of biochemical and biophysical studies[5,6] but it is the fluid mosaic membrane model suggested by Singer and Nicolson in 1972[7] that is still the basis for our current view on membrane structure. This model proposed a matrix made up of a mostly fluid phospholipid bilayer containing integral membrane proteins able to diffuse freely while the membrane lipids were considered to have little function of their own and serve mainly as solutes (Fig. 1.1).[7] It has become increasingly evident however that the lipid bilayer has a profound effect on membrane proteins[8-11] resulting in numerous studies of the relationship between membrane proteins and their lipid environment.[12-16] Both structural and functional data of several well-characterized membrane proteins show specific interactions of the proteins with the bilayer indicating that lipids are not just bystanders but actively participate in many of the cellular processes.[8,16-24]

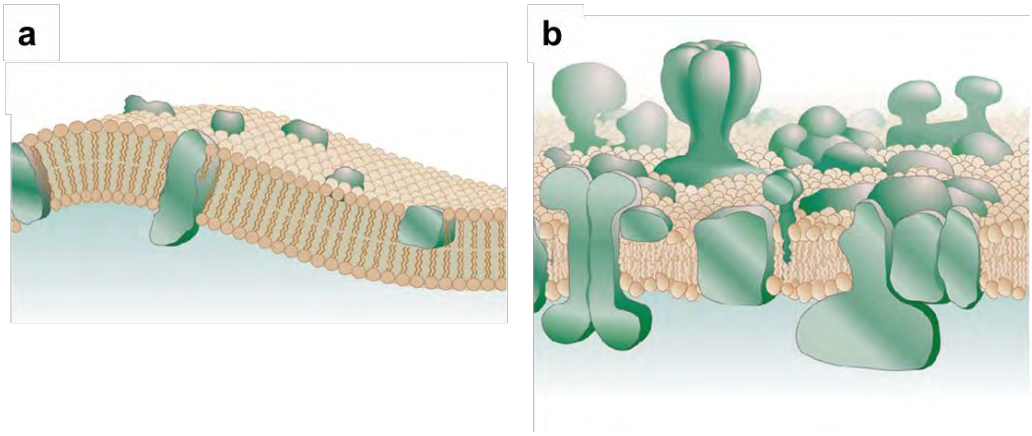

Figure 1.1. Fluid mosaic model of a membrane. (**a**) Classical representation. (**b**) Amended and updated version of the fluid mosaic model. Lipid bilayer is shown in yellow and membrane proteins in green. For details see text. Reprinted by permission from Macmillan Publishers Ltd: Nature, Engelman, copyright 2005.

Membrane lipids

Lipids are in fact involved in several important cell functions. Besides providing the necessary amphiphilic matrix for membrane proteins and giving the cell its barrier, lipids are also involved in energy storage, cell division, biological reproduction and intracellular trafficking.[1] They act as messengers in signal transduction and molecular recognition and define specific membrane domains for recruitment of proteins from the cytosol for secondary signalling.[2] A great variety of membrane lipids have been characterized through both biochemical and biophysical studies aiming to explain differences in phase behaviour, arrangements within the bilayer and the significance this has on membrane organization.[1,2,4] Lateral segregation of lipids to e.g. form physically distinct domains in model membrane systems was reported already in the 1970s,[25,26] and a number of models on the specific packing of lipids and the influence of this on membrane proteins have been proposed.[27-30]

The three major lipid classes in a eukaryotic cell are phospholipids, glycolipids and sterols with phospholipids representing most largest lipid class.[1,3] Most phospholipids consist of two fatty acyl chains (saturated or *cis*-unsaturated) which correspond to the hydrophobic part of the molecule and a glycerol backbone carrying a hydrophilic head-group.[1] Figure 1.2 shows the major phospholipids in eukaryotes where the glycerol backbone carries a phosphate (phosphatidic acid) esterified to either a choline (phosphatidylcholine), ethanolamine (phosphatidylethanolamine), serine (phosphatidylserine), glycerol (phosphatidylglycerol), diphosphatidylcglycerol which contains two phosphatidic acids (cardiolipin) and inositol (phosphatidylinositol).[1] It is the amphipathic nature of phospholipids and their ability to form bilayers that sets the physical basis for the spontaneous formation of membranes.[1] Phosphatidylcholine (PC) which accounts for more than 50% of phospholipids in most eukaryotic membranes[2] has a cylindrical molecular geometry which gives it the ability to spontaneously self-assemble into planar bilayers with the acyl residues facing each other and the polar head-groups interacting with the aqueous phase while the *cis*-unsaturated fatty acyl chain makes PC fluid at room temperature.[2] Phosphatidylethanolamine (PE) on the other hand comes with a conical molecular geometry due to the smaller size of its head-group.[2] The inclusion of PE in PC bilayers and the asymmetric distribution of various lipids between the two bilayer leaflets enforces a curvature stress in biomembranes which can lead to budding, fission and fusion.[2] In addition, the non-bilayer lipids like PE and cardiolipin are also

important for membrane protein embedment and regulation of membrane protein function.[2]

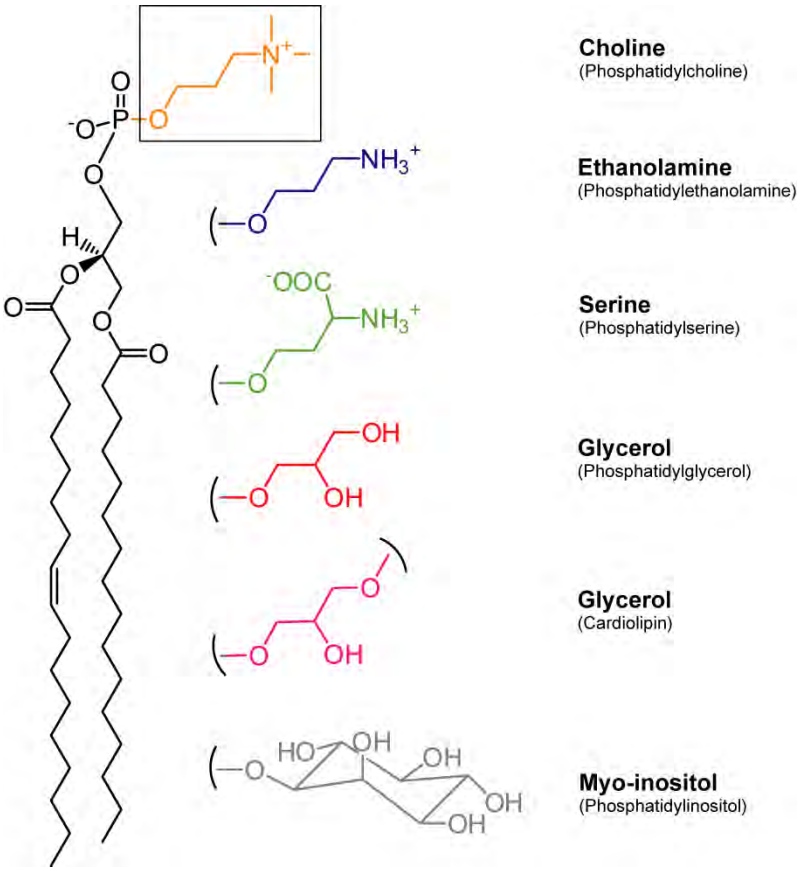

Figure 1.2. Structure of phospholipids. The complete structure presented is of 1-palmitoyl-2-oleoyl-*sn*-glycero-3-phosphocholine (POPC). Other possible head-groups at the *sn*-3 position of the glycerol backbone are shown on the right. Adapted from Biochemistry of Lipids, Lipoproteins and Membranes, 4th edition (2002).[1]

Sterols and sphingolipids are two other major components of membranes in plants, fungi and animal cells.[1,2] Sphingolipids consist of a ceramide backbone which is amide-linked to a fatty acyl residue and the major sphingolipids in mammalian cells are sphingomyelin and the glycosphingolipids.[1,2] Sphingolipids play an important role in membrane rafts as their saturated or *trans*-unsaturated acyl residues lead to the forming of taller, narrower cylinders than PC lipids of the same chain length which results in tighter packing.[1,2] Intermixed with sphingolipids are also sterols, the major non-polar lipids of cell membranes such as cholesterol in mammalian membranes and ergosterol in yeast.[1,2]

More than 1000 different lipid species exist across different cells as a result of the possible variation in their head-groups and fatty acyl chains.[2] Together with membrane

proteins and carbohydrates they build up the very complex membrane mosaic that can be extremely challenging to study *in vivo*. Most of our understanding of biological membranes gained over the last 90 years has thus been derived through the use of simplified model membrane systems often consisting of only one or two kinds of phospholipids (see below).[31]

Membrane proteins

Membrane proteins account for more than 50% of the total cell membrane[12] where they interact with both the lipid bilayer as well as the aqueous environment.[32-34] They are involved in many basic cellular activities such as solute and ion transport, energy conversion and signal transduction and information processing. It is therefore not surprising that they represent the majority of drug targets today.[35] Although ~30% of all genes encode membrane proteins[36] there is an extremely low number of unique membrane protein structures available in the Protein Data Bank (http://www.rcsb.org). Out of the ~90,000 available protein structures to date about 400 represent membrane proteins with only a dozen of those being human membrane protein structures.[37] This important lack of structural insight into membrane proteins and their complexes is due to the notorious difficulties associated with solubilisation of membrane proteins.[38,39]

Membrane proteins are represented by two different types; (i) peripheral proteins anchored to the hydrophilic regions of the membrane through electrostatic and other non-hydrophobic interactions and (ii) integral membrane proteins embedded in the membrane.[7,40-44] Integral proteins typically span the entire phospholipid bilayer and can contain one or more membrane-spanning domains, such as e.g. the seven transmembrane (7TM) domain receptors, while often containing domains outside the membrane. Some integral proteins are anchored to one of the membrane leaflets by covalently bound fatty acids. Figure 1.3 shows examples of membrane proteins and their functions. These include transport of molecules across the membrane carried out by transporters, channels and pores, signal transduction carried out by various receptors and the catalysis of various reactions such as immunoreactions, endo- and exocytosis and cell-cell interactions carried out by various enzymes.[43] Membrane proteins also help in shaping and stabilizing membranes by e.g. interaction with the membrane skeleton.[43]

The specific nature of membrane proteins whereby they interact with both water and the membrane lipid bilayer greatly affects their function.[17,45,46] This has been obser-

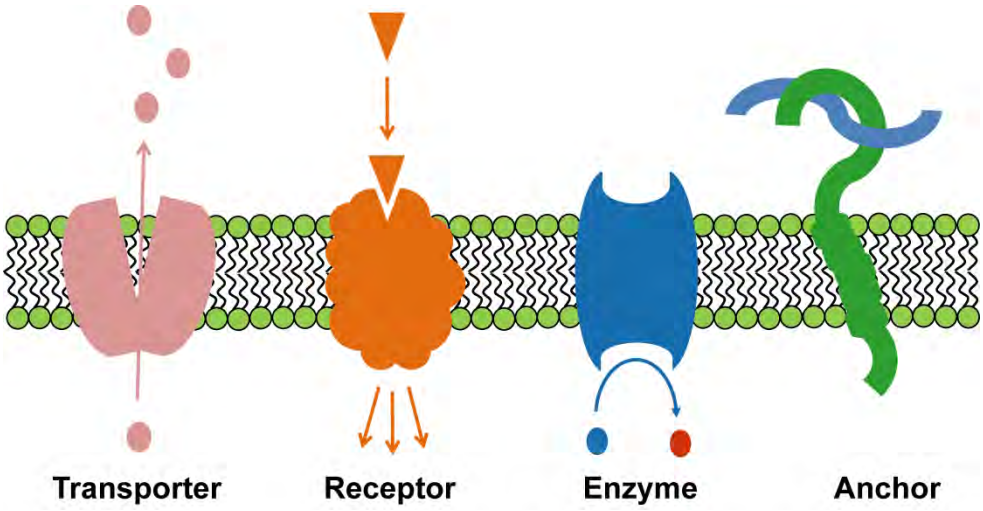

Figure 1.3: Examples of trans-membrane protein functions. Transporters control the transport of molecules from one side of the membrane to the other, receptors bind extracellular molecules (triangle) and activate intracellular processes, enzyme complexes catalyse cellular reactions, and anchor proteins can link intracellular structures with extracellular structures. To fulfil these different tasks, many membrane proteins form multimeric complexes that can vary and adapt to the functional state of the cell. Adapted from Nature Education copyright 2010.

ved for G-protein coupled receptors (GPCRs),[18,47,48] ion-channels,[16,19] and transporters.[49] X-ray crystallography of membrane proteins has led to several breakthroughs in our understanding of this important class of drug targts,[50-64] giving insightful details into their inner workings. However, current studies rely mainly on detergent-solubilized proteins and therefore cannot provide the precise picture of the membrane protein in its native configuration inside a lipid environment. Also cellular membranes are dynamic assemblies of both lipids and proteins existing in a liquid-crystalline phase,[10,15,65-70] and a static depiction is simply not sufficient. Furthermore, many membrane proteins form multimeric complexes that can vary and adapt to the functional state of the cell. Taken together, obtaining information beyond the crystalline state is therefore necessary to fully comprehend the roles of membrane-membrane protein systems at the molecular and cellular levels.[32] Both the specific polypeptide compositions as well as the assembly into quaternary structures inside the lipid bilayer are thus fundamental for the understanding of membrane protein functionality and methods that allow them to be studied inside their native or native-like environment have led to the development of many model membrane systems.

Model membrane systems

Carrier systems that mimic the native membrane environment are a prerequisite for the reconstitution of membrane proteins to enable their structural and functional studies and the available model membrane systems have been reviewed.[31,71,72] Some of the most commonly used systems composed of e.g. phospholipids such as lipid micelles, supported bilayers, lipid bicelles, lipid vesicles and most recent development of phospholipid bilayer nanodiscs can be seen in Figure 1.4. The use of these systems has enabled investigations of lipid dynamics, molecular relationships between lipids and proteins and other small molecules and some have even been used in drug delivery applications.[31,71,72] A schematic representation of membrane protein reconstitution into two of these systems (phospholipid vesicles and phospholipid bilayer nanodiscs) is shown in Figure 1.5.

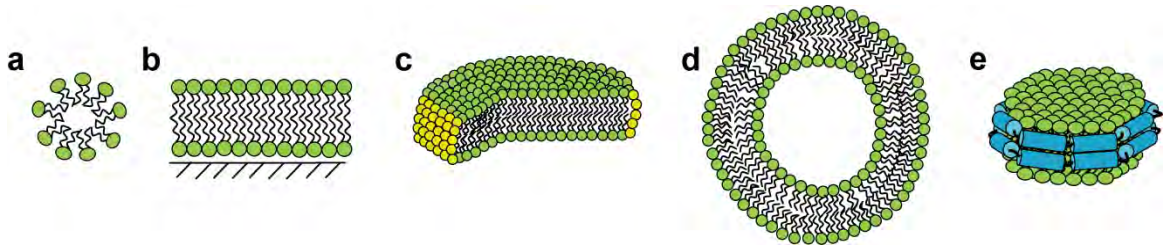

Figure 1.4. Examples of lipid assemblies which can be used for solubilisation of proteins. (**a**) Lipid micelle, (**b**) supported phospholipid bilayer, (**c**) lipid bicelle, (**d**) phospholipid vesicle and (**e**) phospholipid bilayer encircled by two membrane scaffold proteins constituting the nanodisc. Not on scale.

Phospholipid vesicles are closed, spherical phospholipid structures consisting of a curved bilayer which enclose a part of the surrounding solvent inside their interior.[72] They offer both a native-like membrane environment as well as compartmentalization and are useful when membrane transport through ion pumps and channels is studied.[71,72] Membrane protein reconstitution into phospholipid vesicles has been widely used in membrane protein research as shown by the large amount of studies done using this system.[71] Procedures for the reconstitution of unilamellar vesicles of different sizes are well-established and reconstitution of membrane proteins into these systems can be done through various methods. Usually detergent intermediated reconstitution is preferred as it offers the most gentle and quick approach and many different detergent systems and detergent removal procedures tailored to particular proteins are available.[71] A

homogenous size which is often required can be achieved through filtration under high pressure through a membrane of a selected size (extrusion). However the number of proteins that can be reconstituted per carrier can be unpredictable and the reconstitution is often associated with protein aggregate formation within the lipid vesicle environment.[71,72] Phospholipid vesicles are optimal systems in cases of very large membrane protein complexes, where reconstitution into smaller carriers is not appropriate or where a more cell-like environment is desired, e.g. in electrolyte or pH gradient studies.

Phospholipid bilayer nanodiscs, developed in the last decade, have proven a promising new platform for studies of membrane anchored and integral membrane proteins under defined experimental conditions.[73] They are derived from high density lipoprotein particles and consist of a phospholipid bilayer, encircled by two amphipathic membrane scaffold protein (MSP) belts,[74] where the size of the belts constraints the size of the discs (see Chapter 2 for more details). This allows for the reconstitution of different sized discs specifically tailored for different membrane proteins.[74-76] This defined carrier size also makes it a promising new platform for structural studies of membrane proteins using solution scattering techniques.[77-79]

The structural approach to membrane protein function

The only two techniques that can provide atomic resolution information on proteins are crystallography and nuclear magnetic resonance (NMR). X-ray crystallography is one of the most succesful methods for determining the three-dimensional structure of membrane proteins[80-85] and has led to numerous structural breakthroughs for important membrane protein complexes such as GPCRs[51,64] and several membrane pumps[86-88] giving insightful details into the inner workings of these important drug targets. However the requirement for obtaining crystals that diffract sufficiently well is not always possible for membrane protein systems which require a membrane mimicking carrier for stability and function.[38,89] This has in turn led to studies of truncated versions of membrane proteins such as e.g. in the case of the epidermal growth factor receptor and the 60 or so other proteins in this family of tyrosine kinases.[38] Many crystallographers doubt the structure of a full length receptor tyrosine kinase will ever be possible through crystallography as these proteins consist of both extra-cellular and intracellular domains

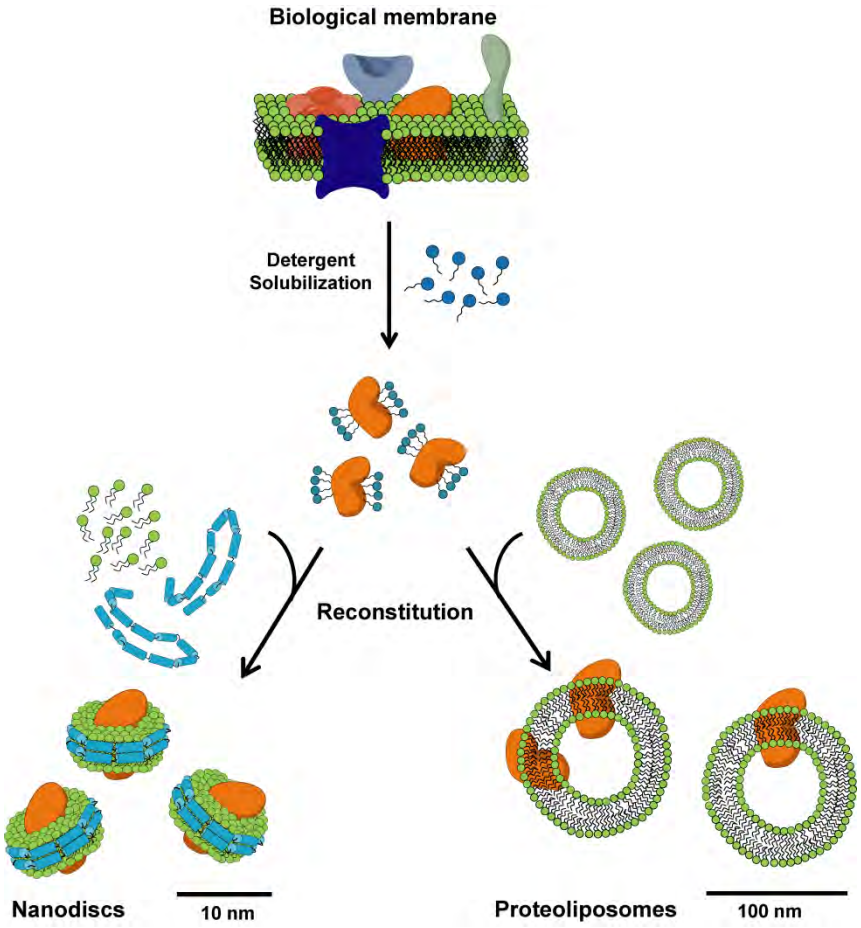

Figure 1.5. Membrane protein reconstitution into bilayer mimics. Membrane proteins are solubilized from the biological membrane using detergents. Reconstitution of membrane proteins into phospholipid vesicles can be achieved by combining a suspension of vesicles obtained by sonication or extrusion in aqueous medium with the isolated and detergent solubilized membrane protein. Removal of the detergent leads to spontaneous incorporation of the protein into the phospholipid bilayer. The self-assembly of the phospholipid bilayer nanodiscs is initiated upon detergent removal from a mixture of detergent solubilized nanodisc components (membrane scaffold protein and phospholipids) and detergent solubilized membrane protein.[92] Additional purification steps to separate membrane protein containing from empty discs are possible. Not to scale.

held together by a single transmembrane spanning domain and where the flexibility of the soluble domains makes it difficult for the protein to form ordered crystals.[38,90,91] Granted that the sample can be crystallized however, there are no practical limitations on the size of system that can be studied using this approach.

A competing structural biology technique which can also provide atomic-resolution information on proteins in solution is NMR. While NMR provides possibilities of studying a membrane proteins in a lipid bilayer under near-native conditions the limitations of this technique are related to the maximum size of the system that can be

studied.[93-95] This is much smaller than the multisubunit complexes which make up the molecular machines of living cells.

Electron microscopy (EM) is another structural technique which can be applied to membrane protein systems and other biological macromolecules. EM can provide structures at around 15-30 Å resolution which makes it a very powerful technique for structural molecular biology.[96-98] This direct imaging technique requires that the samples are adsorbed to a grid and frozen.[98] The difference in electron density between a protein and the surrounding solution is also often low, which requires staining of the sample with a heavy atom salt that can lead to distortions to the structure.[96]

Small-angle scattering only has a structural resolution of the order of 10 Å, which does not provide information at the sorts of length scales accessible to protein crystallography or NMR. However, it has the significant advantage of allowing rapid protein studies in solution and for membrane protein systems this means native-like environments in the form of aforementioned model systems. Furthermore, the solution properties may easily be varied in a way that allows parametric studies such as those relating to temperature, buffer conditions and pH.[99-101] This is extremely powerful for studies of structural flexibility which is of central importance in protein function, self-assembly and dynamic metabolon formation.

A summary of the available structural techniques and their advantages and limitations with regard to membrane proteins systems is shown in Table 1.1.

Table 1.1 Summary of methods available for structural analysis of membrane proteins.*

Method	Sample requirement	Advantages	Limitations
Crystallography	Crystals	Very high resolution revealing fine detail of atomic structure and active sites (down to 1Å).	Crystals required and not always possible for membrane proteins Flexible portions are not seen. Structure may be influenced by crystal packing forces. Stabilization of membrane proteins in e.g. detergents necessary.
NMR	Dilute solution (~5-10 mg/ml)	High-resolution in solution (down to 2-3 Å).	Not applicable on proteins above ~50 kDa in molecular mass. Membrane protein reconsitution into bilayer mimicks.
Cryo-EM	Frozen dilute solution (<1 mg/ml)	Low amount of material. Direct visualisation of particle shape and sysmmetry.	Low resolution (10 Å). Not applicable for proteins below ~200 kDa in molecular mass. Membrane protein reconsitution into bilayer mimicks.
SAS	Dilute and semi-dilute solution (~1-100 mg/ml)	Analysis of structure, kinetics and interactions in nearly native conditions. Mixture and non-equilibrium system studies. Wide molecular mass range.	Low resolution (10-20 Å). Requires additional information to resolve ambuigity in modelling. Membrane protein reconsitution into bilayer mimicks.
Static and dynamic light scattering	Very dilute solution (<1 mg/ml)	Non destructive. Low amount of material. Simple experiments.	Overall parameters only can be determined. Membrane protein reconsitution into bilayer mimicks.

Small-angle scattering

Over the last decade both small-angle x-ray scattering (SAXS) and small-angle neutron scattering (SANS), have become increasingly important methods in structural studies of water soluble protein systems.[102-105] The developments of both these techniques at synchrotron radiation and neutron beam sources, in combination with sophisticated sample preparation procedures and better, more robust and more general data analysis software tools,[106,107] makes Small-angle scattering (SAS) an increasingly important tool for the study of biomolecular systems. The requirements for sample volumes and sample concentrations have been brought down to about 10-20 µl at a few mg/ml protein concentration for SAXS and 100-300 µl at a similar protein concentration for SANS [102]. This is compatible to what is typically attainable for many membrane protein systems.[108,109] SAS has therefore become an increasingly important technique also for studies of membrane proteins providing valuable information on several membrane protein systems reconstituted in either small unilamellar vesicles[110,111] or detergent systems.[112-122] However two main challenges accompany SAS studies of membrane protein systems: obtaining monodisperse samples of reconstituted membrane proteins in a carrier system and extracting the low-resolution structure of a membrane protein alone from SAS data measured on such a complex multi-component system.

Although small-angle solution scattering is a low-resolution technique it has proven to be a powerful tool for studies of condensed matter and has been applied on a myriad of different materials ranging from metal alloys and synthetic polymers to complex biological assemblies.[123] In studies of biological matter it is often used as a complimentary technique to other structural biology methods such as e.g. protein crystallography in order to validate structural data of proteins in solution and theoretically predicted models.[123] In addition, providing that high-resolution data of individual subunits is available, rigid body refinement of scattering data can be used to construct structural models of more complex assemblies in solution.[123] In small-angle neutron scattering (SANS) the possibility of contrast variation method in combination with sophisticated data analysis tools[124-126] allows for investigations of structures with inherent neutron scattering length density differences such as protein-deuterated protein or protein-nucleic acid complexes, lipid membranes and cellular scaffolding.[127-131]

As a solution technique however the rotational averaging of the molecules in solution limits the resolution of small-angle scattering however the technique can be used

to study oligomerization of proteins in solution or inside a membrane environment, the formation of complexes in solution as well as their shape or conformation.[102,132] It also allows systematic manipulation of parameters such as pH, salt, different ligands and temperature and the effects that this exerts on membrane protein systems,[132] and can lead to important information on interactions between membranes and proteins where high-resolution crystal structures are not available or possible. Many comprehensive introductions to small-angle scattering are available,[133-136] and only a brief description of the essential elements of the technique is given below.

When a sample, such as a protein in solution, is illuminated by a monochromatic plane wave, secondary spherical waves are generated from the interaction of the incoming beam with the individual atoms within the sample. The scattering intensity produced by the interference pattern of the formed spherical waves is recorded on a detector (Fig. 1.6*a*). In x-ray scattering the x-rays interact with the electrons in the sample, while in neutron scattering neutrons interact with the nuclei of the sample. Additionally, in small-angle scattering, only the elastic part of the scattering is regarded.

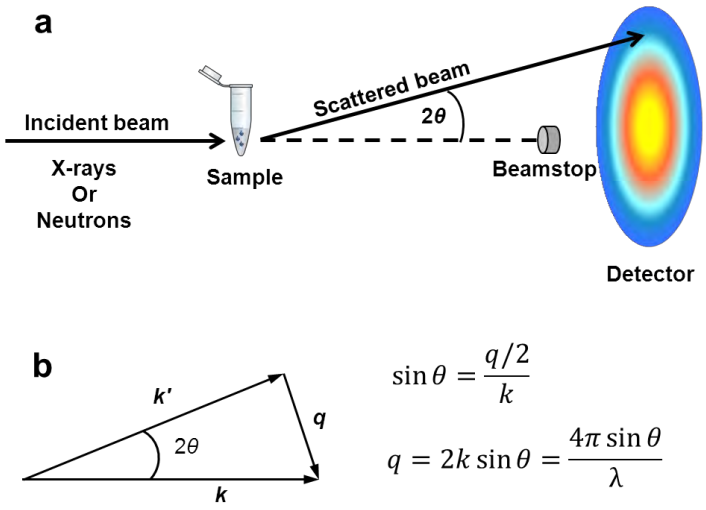

Figure 1.6. (**a**) Schematic representation of a small-angle neutron scattering experimental set up. A highly collimated neutron or X-ray beam illuminates the sample and the scattered radiation is recorded on a 2D detector. The beamstop absorbs the direct beam. (**b**) Scattering triangle for elastic scattering in which the incoming beam is deflected but does not gain or lose energy, $|k'| = |k|$.

The strength of the scattering from a particle is a function of the difference in scattering length density of the particle in relation to the solvent and the size of the particle. This scattering intensity I is measured as a function of the scattering vector q,

$$q = \frac{4\pi \sin\theta}{\lambda} \tag{1.1}$$

where 2θ is the angle between the scattered beam and the incident beam (Fig. 1.6*b*), and λ is the wavelength of the incident radiation.[133,137] Assuming no distance correlation between particles the relationship between a scattering particle in solution and its contribution to the scattering profile can be mathematically expressed by Eq. 1.2:

$$I(q) = n\left\langle \left| \int_V (\rho(\vec{r}) - \rho_s) e^{-i\vec{q}\cdot\vec{r}} d^3r \right|^2 \right\rangle \tag{1.2}$$

where $I(q)$ is the scattered intensity, n is the number of particles per unit volume, $\rho\ r$ is the scattering length density of the particle at position r, ρ_s is the scattering length density of the solvent.[133,137] The integral is taken over the particle volume V and is averaged over time, all orientations and the combination of all structures present in solution during the experiment.[133,137] The difference in scattering length density between the scattering particle and the solvent scattering length density is often termed the contrast and is represented as $\Delta\rho$.[133,137]

The scattering intensity function gives information related to the shape of the molecule in solution and examples of scattering intensity patterns for some typical geometrical shapes of the same size can be seen in Figure 1.7*a*.[123] A general approach when analysing small-angle scattering data however is to Fourier transform the scattering intensity function to obtain the interatomic distance distribution function, $P(r)$, of the scattering particle (Fig. 1.7*b*).[138] This pair distance distribution function holds in principle the same information as the scattering intensity, $I(q)$, but because it is a direct space representation it is more intuitive and allows for the particle shape to be understood visually more easily.[123] As it describes the probable frequency of interatomic vector lengths r within a protein and is sensitive to the symmetry and domain structure within proteins, $P(r)$ can yield information relating to both the shape and volume of a protein or protein complex.[123] Because scattering data can only be measured over a finite q range however $P(r)$ calculations depend on several assumptions, e.g. that $P(r)$ is zero at both $r = 0$ and at the maximum linear dimension, D_{max}. The quality of the scattering data determines the reliability of the D_{max} and in order to enable accurate characterization of

the longest dimensions of the particle the data must be measured to q values $< \pi/D_{max}$, therefore an error to D_{max} cannot be assigned.[139]

The two parameters related to the size and shape of the scattering particle which can be obtained from small-angle scattering data are the radius of gyration (Rg)[137] and the forward scattered intensity at zero angle $(I(0))$.[133] These two parameters provide a rapid and robust way to obtain structural information from scattering data and can be calculated from several different mathematical models. The Rg is the root-mean-squared distance of all elemental scattering volumes from their centre of mass weighted by their scattering length densities.[137] Rg provides information on the size and mass distribution within a particle and objects that have the same volume but differ in shape have different R_g values.[137] $I(0)$ which describes the scattering intensity at zero angle $\theta = 0°$, is not a measureable parameter as it cannot be separated from the radiation of the direct beam and due to the beamstop at $q = 0$.[102] It can however be determined through extrapolation and is related to the number of scattering particles per unit volume (N), the contrast $(\Delta\rho)$ and the particle volume (V) squared[123]

$$I(0) = N(\Delta\rho V)^2 \tag{1.3}$$

The Rg and $I(0)$ can be calculated from the Guinier approximation

$$I(q) = I(0)e^{\frac{-q^2R_g^2}{3}} \tag{1.4}$$

where a linear fit of $ln\ I(q)$ versus q^2 yields Rg from the slope and the $I(0)$ from the y-intercept.[140] Certain constraints exist and for globular proteins e.g. this relationship is true only if qR_g is smaller than 1.3[123] while for elongated shapes the upper limit is increasingly smaller for increasingly extended molecules.[141] The Guinier plot linearity can be used as a quick diagnostic of sample quality.

A particle with a very small internal density fluctuation as compared to the difference between the mean scattering density of the particle ρ_p and that of the solvent ρ_s can be treated as a uniform scattering density object with a mean contrast $\Delta\rho = \rho_p - \rho_s$.[133] The intensity of the small-angle scattering signal from the protein in solution is therefore proportional to the square of this contrast

$$I(q) \propto \Delta\rho^2 \tag{1.5}$$

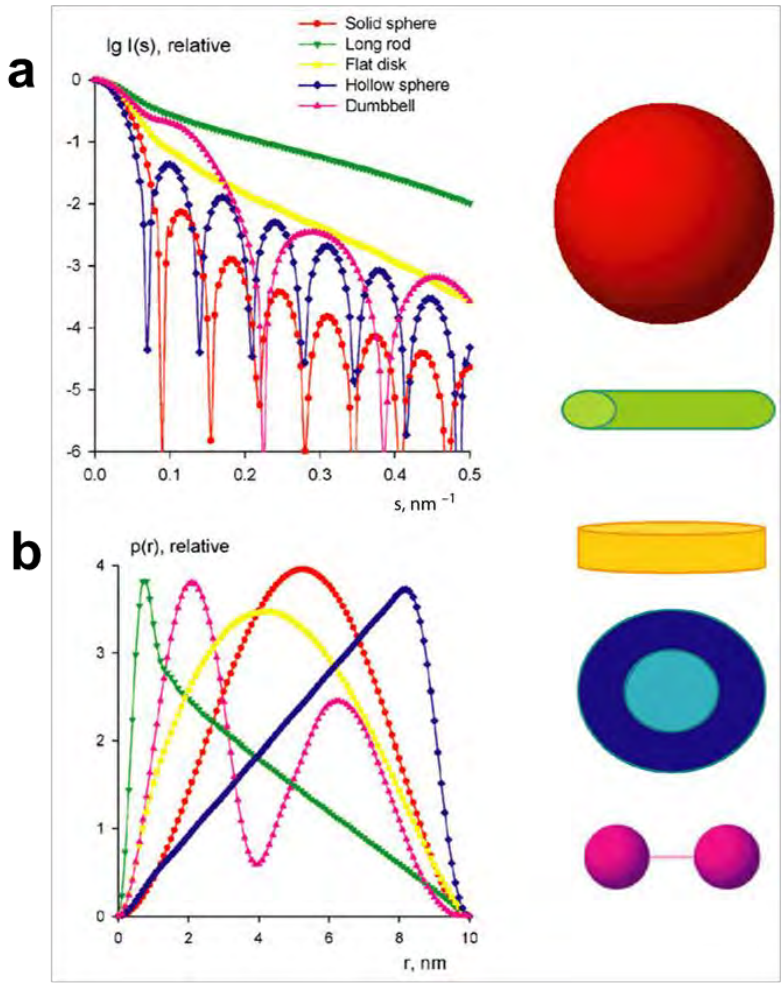

Figure 1.7. Scattering intensities and distance distributions of geometrical bodies according to Svergun and Koch[123] (2003). (**a**) Scattering intensity patterns for some typical geometrical shapes of the same size. (**b**) The pair distance distribution function *P(r)* for the shapes above after Fourier transformation.

where $\Delta\rho$ is readily calculated from the atomic composition of the protein and the solvent and the partial specific molecular volumes.[102] This means that if the average scattering data of the protein is the same as the solvent ($\rho_p - \rho_s = 0$) no scattering signal from the particle is detected and the contributions to the small-angle scattering arising from the internal density fluctuations can be considered negligible.[102,133] This is used in contrast variation experiments on protein complexes and especially in small-angle neutron scattering.[131,133,142,143]

SANS contrast variation

As mentioned above, x-rays interact with the electrons of an atom, while neutrons interact with the nuclei. It turns out that the neutron scattering length varies in a non-systematic manner and depends on both atomic number and the isotope of the atom, while the x-ray scattering length of an atom increases linearly with the number of electrons.[142] Additionally, the magnitude of the coherent neutron scattering lengths of the most common atoms in biological matter and their isotopes are comparable, making visualization of the light atoms easier with neutrons than with x-rays.[133] There is one important exception to this rule. This is between hydrogen and deuterium which also differ in sign and which provides the basis of SANS contrast variation. In many cases, the substitution of deuterium for hydrogen in biological structures only has a limited impact on structure and function.[133] This makes it possible to highlight certain parts of a multiunit system through both contrast variation and the selective deuteration method which makes SANS a very powerful method for investigating complex biological systems which contain intrinsic density fluctuations such as e.g. lipids and proteins.

In the contrast variation method the natural contrast between different biological material such as e.g. protein, DNA and phospholipids can be exploited through manipulation of the H_2O/D_2O ratio of the solvent.[133] Certain "match" points can be reached where the scattering length density of the biological complex or a specific part within it matches that of the solvent background rendering it "neutron invisible".[133] Selective deuteration on the other hand relies on either chemical or biological deuteration to change the scattering length density of the complex in question.[133,142] For a membrane protein system, which consists of both a membrane mimic and a protein, the selective deuteration method offers a means of altering the scattering length density of the different components in order to visualise them separately which can greatly simplify data analysis and provide more information on very complex lipid-protein systems.[133]

Selective deuteration of biomolecules

Partial, selective or full deuteration of biomolecules such as phospholipids and proteins is not only used in neutron scattering but also in other structural techniques such as nuclear magnetic resonance (NMR).[142,144,145] The optimal levels of deuteration differ for different techniques and also depend on the type of experiment that is carried out. In ^{1}H-NMR experiments total deuteration (perdeuteration) is often preferred to improve the

resolution and sensitivity of the method and reduce the overall relaxation rates of the NMR-active nuclei.[144] In neutron scattering experiments however, selective deuteration is required to highlight positions, structure and dynamics of individual components within a complex and the degree of deuteration depends on specific applications.[142,146] Fully deuterated protein crystals e.g. improve the signal-to-noise ratio of neutron diffraction data and enhance the visibility of the molecular structure in neutron protein crystallography.[147] In solution scattering and reflectivity experiments on the other hand partial deuteration of approximately 70% is sufficient to obtain differentiation.[146]

The available approaches for effective production of deuterated biomolecules such as lipids and proteins are chemical synthesis and microbial synthesis/expression or, when obtaining different combinations of deuteration within the molecules is required, a combination of both approaches.[148] For recombinant proteins, microbial expression is the preferred deuteration method – often with *Escherichia coli,* as the expression host.[149] This organism can be adapted to growth in high levels of D_2O,[150] and the use of D_2O can easily be combined with different deuterated carbon sources such as sodium acetate, glycerol, or glucose. This type of approach is now widely used in neutron protein crystallography,[151,152] SANS[153-155] and neutron reflectivity.[156,157] Deuterated phospholipids on the other hand are generally produced by chemical synthesis, which allows for the combination of various fatty acids to obtain many desired mixtures of partially labelled or fully deuterated (perdeuterated) saturated phospholipid species.[148] However, the synthesis of selectively deuterated versions of physiologically relevant unsaturated phosphatidylcholines (PC), the major membrane-forming phospholipids in eukaryotes,[2] still remains difficult.

Thesis objective

Most of the work carried out in this thesis has been done under the cross disciplinary Center for Synthetic Biology at University of Copenhagen where one of the main goals of the Center has been to enable the nanodisc platform for structural and functional analysis of membrane proteins. In this context a great deal of effort has gone into the reconstitution and general handling of membrane proteins using the nanodisc as a carrier as well as laying a foundation for structural and function analysis of such systems.[77-79,158] Procedures have therefore been established to obtain stable well-characterized nanodisc systems[159] and containing functionally active membrane proteins

[158-161] as well as to enable structural analysis of both empty[77,78,162] and membrane carrying discs using small-angle scattering[79] and neutron reflectivity.[158,163,164]

The main objective of this PhD has been the development of a deuterated "stealth" nanodisc system specifically intended for structural studies of membrane proteins using SANS. Reducing the scattering signal of the entire carrier through specific deuteration of the carrier's components, would thus maximize the scattering from an incorporated membrane protein. This neutron-"invisible" carrier would then allow for the low-resolution structural data of a membrane protein to be directly obtained from a single SANS measurement using already available, robust and general data analysis software tools originally developed for soluble proteins.

The protein lipid components of the prototype "stealth" nanodisc were chosen on the basis of successful membrane protein reconstitutions,[74,165] and specifically the use of physiologically relevant specifically phosphatidylcholine species composed of mixed acyl unsaturated fatty acyl residues of 16 to 18 carbons in length was considered important for the bilayer. This was due to their physiological relevance despite the lack of commercial availability[2,148] as these lipids are often the most relevant and therefore most often chosen as model-bilayer lipids for reconstitution of membrane proteins.[2]

A central point to the project was specific deuteration of the nanodisc components that would enable us to reach a match point for the entire nanodisc when it is dispersed into a buffer based on 100% D_2O in order to minimize both the hydrogen incoherent scattering associated with the use of H_2O and the scattering signal from the carrier.[133] Due to natural differences in scattering length density between proteins and phospholipids as well as between the head-groups and the fatty acyl residues of the phospholipid bilayer alone[133,142] selective partial deuteration of three components of the discs was required and the theoretical deuteration levels for the chosen nanodisc system are derived in Chapter 2.

Chapter 3 describes the overexpression of the recombinant membrane scaffold protein in minimal deuterated medium to produce deuterated protein which is invisible in SANS studies under standard buffer conditions. The optimization of the subsequent purification of deuterated MSP with a specific length is also described and which should be applicable to MSPs of various lengths.

The focus of Chapter 4 is the preparation and the subsequent extraction and analysis of PC obtained from genetically modified *Escherichia coli* engineered to produce PC as it major phospholipid. The isolation of PC from mixtures of standard *E. coli* lipids as well

as mixed lipid model membrane systems in the form of nanodiscs is described together with their quantification and characterization procedures which were used in Article I, II and III.

Chapter 5, which is the basis for Article II, presents a new method for selective deuteration of phosphatidiylcholine through biosynthesis in genetically modified strain of *E. coli*. Through careful tuning of the deuteration levels in growth media and varying the deuteration of added carbon sources controlled, site-specific deuteration of three distinct parts for the PC lipid molecule can be achieved. This biosynthetic approach paves the way for the biological synthesis of specifically deuterated physiologically relevant phosphatidylcholine species which can be challenging to obtain through standard chemical synthesis.

In Chapter 6, based on Article III, the self-assembly and the subsequent SANS contrast variation study of specifically deuterated nanodiscs as well as lipid vesicles are presented showing that a match point can be reached at 100% D_2O for these complex lipo-protein particles. This development provides an elegant solution to avoid the intrinsic complexity of SAS data which is associated with the use of carrier-systems and suggests that the "stealth" carriers developed during this thesis can be used as a platform for low-resolution structural studies of membrane proteins using well-established data analysis tools originally developed for soluble proteins. The reconstitution of the first membrane protein into stealth nanodiscs is also discussed.

Finally Chapter 7 focuses on the possibilities and limitations of the developed methods.

Chapter 2

The ‘stealth’ nanodisc model – reaching invisibility

Applied in: Maric, S., Skar-Gislinge, N., Midtgaard, S. R., Thygesen, M. B., Schiller, J., Frielinghaus, H., Moulin, M., Haertlein, M., Forsyth, V. T., Pomorski, T. G., and Arleth, L. 2013. Stealth Carriers for Low-Resolution Structure Determination of Membrane Proteins in Solution, ***Acta Crystallographica Section D70.*** 317-328.

Introduction

The major advantage of SANS in the study of biological matter is the possibility of contrast variation by exchanging between ^{1}H (hydrogen) and ^{2}H (deuterium) in the sample.[131,133,142,143] The difference in contrast arises from the difference in scattering length density (SLD) between the sample and its environment.[133] The strength of the interaction between neutrons and atomic nuclei is characterized by the coherent scattering length of the nucleus.[133] This is dependent on both the atomic species and the isotope of the atom.[142] Scattering lengths for the most abundant elements in biological material are summarized in Table 2.1.[133,142] The very large difference between the scattering length of hydrogen as compared to deuterium and other biologically relevant elements is the very basis of neutron scattering.[133] This can be exploited to highlight certain parts of a multiunit system through both contrast variation method and the selective deuteration method.[133]

In the contrast variation method the natural contrast between different biological material such as e.g. protein, DNA and phospholipids can be exploited through manipulation of the H_2O/D_2O ratio of the solvent.[133] This makes it possible to reach certain "match" points where the SLD of the biological complex or a specific part within it matches that of the solvent background rendering it "neutron invisible".[133] Selective deuteration on the other hand relies on either chemical or biological modification of the deuteration level to change the SLD of the complex in question.[133,142]

The use of H_2O in biological SANS studies is accompanied by a strong background signal due to the large incoherent scattering cross-section of H_2O and SANS experiments on hydrogenated molecules are typically performed in D_2O in order to increase the signal-to-noise ratio.[132,133,142] Selective deuteration of the nanodisc system should therefore be achieved to obtain a match point in a buffer based on 100% D_2O to minimize both the carrier signal and the incoherent scattering associated with the use of H_2O (Fig. 2.1).

Table 2.1. Neutron scattering lengths of hydrogen, deuterium and the most abundant elements found in proteins and lipids.

Element	Scattering length $(\sum b)/10^{-5}$ Å
Hydrogen	-3.74
Deuterium	6.671
Carbon	6.646
Nitrogen	9.36
Oxygen	5.803
Phosphorous	5.13
Sulfur	2.847

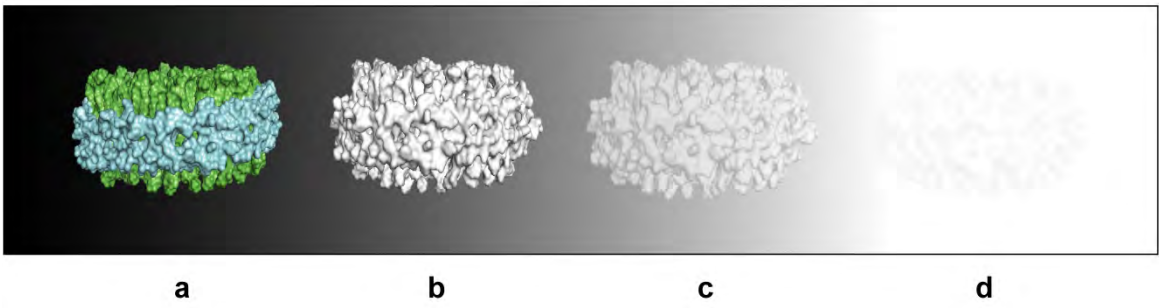

Figure 2.1. Schematic representation of the stealth nanodisc in a buffer solution with a gradually increasing level of D_2O (decreasing grayscale). (**a**) Hydrogenated nanodisc consisting of a phospholipid bilayer (green) and membrane scaffold protein MSP (light blue). (**b**) Stealth nanodisc comprised of deuterated lipid and deuterated MSP at 60% D2O. (**c**) Stealth nanodisc at 80% D_2O. (**d**) Stealth nanodisc at 100% D_2O.

Stealth nanodisc model

Nanodiscs consist of a phospholipid bilayer, typically around 65-80 lipids per leaflet, encircled by two amphipathic membrane scaffold protein (MSP) where the MSP belts interact with the hydrophobic tails of the lipid bilayer to form the defined carrier (Fig. 2.2).[73,74] MSPs are alpha helical proteins derived from the apolipoprotein A-1 (Apo-A1), which is the primary component of high-density lipo-protein (HDL) particles.[75] Structural and functional aspects of Apo-A1 and the modification necessary for preparation of MSPs have been described previously[74,166,167] and currently available constructs are summarized elsewhere.[74] In short, the MSP1 consists of a 43 N-terminus amino acid truncated Apo-A1 which also contains an N-terminal hexahistidine tag and a linker containing a protease site for easy removal of the tag. The main MSP sequence can thus be varied by changing the number of amphipathic helices interspersed by prolines

and glycines which allows for the preparation of different sized nanodiscs, typically between 10 and 12 nm.[74-76] Nanodiscs are formed through a self-assembly process (for more details on their reconstitution see Chapter 6).[74] In addition to the size of the MSP belts the choice of lipid composition and optimal lipid protein stoichiometry can affect the size, shape and the stability of the discs.[74,159]

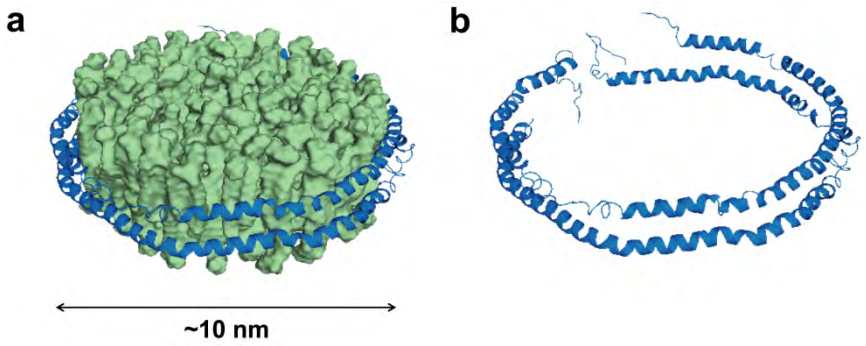

Figure 2.2. Model of the nanodisc based on the double-belt Apo-A1. (**a**) A phospholipid bilayer (POPC) is encircled by two copies of Apo-A1. (**b**) The nanodisc model without the bilayer showing the structure of Apo-A1. Illustration based on Morgan *et al.*[168] The model was built in PyMol (www.pymol.org) using POPC lipids and apo-A1.

The composition of the prototype stealth nanodisc was chosen on the basis of the number of successful membrane protein reconstitutions in hydrogenated conditions.[73-76,92,165] For the phospholipid bilayer 1-palmitoyl-2-oleoyl-*sn*-glycero-3-phosphocholine (POPC) was chosen as it has proven to stabilize many different membrane protein systems[74] and is one of the major components of eukaryotic cell membranes.[2] The his-tagged short membrane scaffold protein MSP1D1 which contains an additional 1-11 N-terminus amino acid deletion as compared to MSP1, and gives nanodiscs with an average size of 10 nm and where significant prior experience in both reconstitution and structural analysis[77] as well as the *Escherichia coli* based expression was present within the UNIK Synthetic Biology project, was the initial choice also for the prototype stealth discs.[75]

Theoretical derivation of nanodisc invisibility

The theoretical deuteration levels required for reaching a match point of the nanodisc system in 100% D_2O differs for the different components of the lipid-protein particle, due to natural differences in SLD between proteins and phospholipids as well as between the head-groups and the fatty acyl residues of the phospholipid bilayer alone.[133,142] The SLD can be calculated through:

$$\rho = \frac{\sum_i^n b_i}{\bar{V}} \tag{2.1}$$

where ρ is the scattering length density, b_i is the scattering length of the relevant atom and is the partial specific molecular volume containing the n atoms.[169] Eq. 2.1 was used to calculate the SLD for hydrogenated lipid head groups and fatty acyl tails as well as their fully deuterated analogues. Figure 2.3*a* shows the calculated scattering length densities for these two components as well as for MSP1D1 as a function of deuterium content in the molecule. The crossing point of each components scattering length density function with the scattering length density of 100% D_2O, is the required match point, and gives the level of deuteration of that particular component where its SLD equals that of D_2O. For the POPC based bilayer this was estimated to 78% deuteration in the head-group and 92% deuteration in the acyl chains (Fig. 2.3*b*). For MSP1D1 encircling the bilayer, the same specific volume as for most other proteins[170] of 1.38 g/cm^3 was assumed as well as the same balance between exchangeable and non-exchangeable hydrogens. Therefore the required level of deuteration should be reached when in average 70% of the non-exchangeable hydrogens are replaced by deuterium (Fig. 2.3*c*).[133,142,171] Due to the exchangeability of the hydrogens bound to oxygen, nitrogen and sulphur atoms, this would lead to an overall level of deuteration of about 75% when the protein is dispersed in 100% D_2O solution.

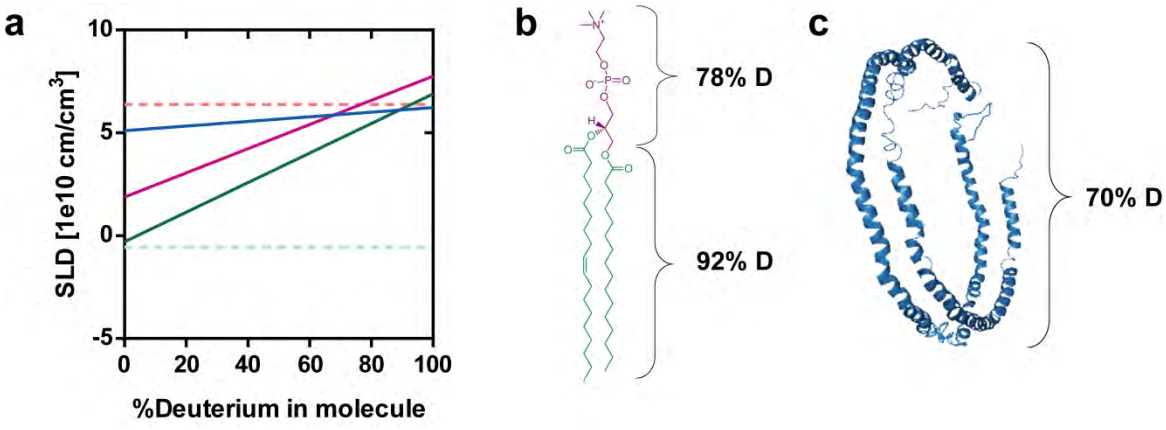

Figure 2.3. (**a**) Scattering length density of the nanodisc components as a function of deuterium level in molecule. H_2O (green dashed line), D_2O (red dashed line), phospholipid head group (purple) and phospholipid tails (green), 70% deuterated protein (blue) reaching 75% deuteration at 100% D_2O after the exchangeable hydrogens bound to oxygen, nitrogen and sulfur atoms have been substituted with deuterium. (**b**) Deuteration levels required for total matching of POPC in 100% D_2O. (**c**) Deuteration level required for total matching of MSP1D1 in 100% D_2O.

An important note here is that the scattering length density of the species to be matched i.e. the phospholipid bilayer and the entire nanodisc, should be as homogenous as possible.[110] Fluctuations in deuteration will result in local deviations from the average excess scattering length density which will then contribute to the overall observed signal at intermediate and large *q*-values.[110] Obtaining uniformelly labelled nanodiscs with a zero excess scattering length density in 100% D_2O at all the SANS relevant length scales is preferable to minimize both the hydrogen incoherent scattering as well as the coherent signal arising from the carrier molecules.

Chapter 3

Deuteration of membrane scaffold protein

Applied in: Maric, S., Skar-Gislinge, N., Midtgaard, S. R., Thygesen, M. B., Schiller, J., Frielinghaus, H., Moulin, M., Haertlein, M., Forsyth, V. T., Pomorski, T. G., and Arleth, L. 2013. Stealth Carriers for Low-Resolution Structure Determination of Membrane Proteins in Solution, ***Acta Crystallographica Section D70*****.** 317-328.

Introduction

In small-angle neutron scattering and reflectivity experiments a match point for a protein in 100% D_2O can be reached when on average 70% of the non-exchangeable hydrogens are replaced by deuterium.[133,142,171] Due to the exchangeability of the hydrogens bound to oxygen, nitrogen and sulphur atoms, this leads to an overall level of deuteration of about 75% when the protein is dispersed in 100% D_2O solution. Partial and fully deuterated (perdeuterated) proteins can be produced through bacterial expression in host systems such as *Escherichia coli* which can readily be adapted to growth in D_2O.[144,145,172] Different types of deuterated media are commercially available but minimal media is most often used when more controlled conditions are required.[144,149] Rich deuterated media is also commercially available or can be prepared "in house" from e.g. algae cell lysates produced in D_2O. In addition to high D_2O media supplementation with selectively or perdeuterated carbon sources such as glucose, glycerol and sodium acetate can be used depending on the desired pattern of deuterium incorporation and the protein of interest.[149] To this hydrogenated amino acids or their precursors can be added to perdeuterated media for preparation of selectively hydrogenated deuterated protein.[172,173]

Adaptation of cells to growth in D_2O can be achieved either by gradual step-wise increase in D_2O concentration or by plating cells on deuterated media of choice and subsequently selecting colonies that perform best for further culture inoculation.[149,174] Scale-up growth and expression can be done in standard shaker flasks or through the use of fermenters similar to hydrogenated protein.[147,175] It should be noted that cell growth is typically slower in deuterated conditions and this longer growth time comes with an increased risk for plasmid loss over time.[149,174] This can be a major problem in deuterated culture leading to lower expression yields. The choice of selection marker is also important and kanamycin resistance is less likely to be prone to leakiness as compared to e.g. ampicillin resistance. Once the target protein has been expressed however, purification can be done using protocols developed for the hydrogenated protein analogue but some optimization is required.[175] The deuteration levels of the final product can be determined by mass spectrometry. [147,149,175]

Membrane scaffold protein expression

Membrane scaffold proteins are efficiently produced by heterologous expression in *Escherichia coli*. This is done using the pET expression vector and a large amount of protein can be produced in a few hours after induction with isopropyl b-D-1-thiogalactopyranoside (IPTG) which induces the expression of the lac operon in *E. coli*.[74] The protein can be susceptible to proteolysis post induction and modifications of the protein can also affect its stability and lower the yield.[74] Both Apo-Al and MSP have however successfully been overexpressed in deuterated media with sufficient yields.[74] This chapter focuses on the preparation of 70% deuterated MSP1D1 (D-MSP1D1) making it invisible in small-angle neutron scattering studies under standard buffer conditions in 100% D_2O solution

Due to the changes in protein stability the isolation of deuterated protein is not always successful using protocols optimized for hydrogenated analogues and therefore the subsequent optimization of the deuteration MSP1D1 purification is also described.

Materials and Methods

Chemicals

All chemicals according to Table 3.1, mineral salts according to Table 3.2 and solvents were obtained in the highest commercially available purity from Sigma-Aldrich Chemie S.a.r.l. (France) and used as supplied unless stated otherwise. Recycled D_2O was obtained from Institut Laue-Langevin Deuteration Facility and D_8-glycerol was from Cambridge Isotope Laboratories.

Table 3.1. Metal salt solution

Medium component	Final concentration [g/l]
$CaCl_2 \cdot 2H_2O$	0.5
$FeCl_3 \cdot 6H_2O$	16.7
$ZnSO_4 \cdot 7H_2O$	0.18
$CuSO_4 \cdot 5H_2O$	0.16
$MnSO_4 \cdot 4H_2O$	0.15
$CoCl_2 \cdot 6H_2O$	0.18
EDTA	20.1

Table 3.2. Minimal media composition*

Medium component	Final concentration [g/l]
$(NH_4)_2SO_4$	6.86
KH_2PO_4	1.56
$Na_2HPO_4 \cdot 2H_2O$	6.48
$(NH_4)_2$-H-citrate	0.49
$MgSO_4$	0.25
Glycerol	5.0

*Including 1ml/l Metal salt solution according to Table 3.1.

Preparation of minimal medium

In order to remove all hydrogens the hydrated metal salts (Table 3.1) were dissolved in D_2O and dried using a rotary evaporator. This process was repeated three times for a complete exchange. The deuterated metal salts were then dissolved in D_2O to a final solution of 1 M. This metal salt solution was added to the 85% D_2O solution containing mineral salts according to Table 3.2. The medium was sterilized by filtration using a vacuum-driven filtration device (Stericup FilterUnits; Millipore) and stored in sealed, dark, glass bottles at room temperature. All of the chemicals required for protein overexpression such as the stock solutions of both kanamycin and IPTG were prepared using D_2O, sterilized by filtration, aliquoted and kept at -20°C.

Membrane scaffold protein expression

A starting culture of BL21 cells previously adapted to minimal deuterated media according to previously described method[175] was thawed from a stock that had been kept at -80 °C. The starting culture was amplified into plastic flasks containing deuterated minimal media and kanamycin (20 µg/ml final concentration) and incubated at 30°C and 37°C respectively until an OD_{600} of ~0.8-1.0 was reached. The cultures were induced with IPTG (1 mM final concentration) and incubated overnight at the respective temperature until an OD_{600} of 3-4 was reached. Cells were harvested by centrifugation (10,000 x g, 20 min, 4°C). The cell paste produced was weighed and stored at -20°C.

Solubility test

A protein solubility test was done by harvesting 10 ml culture by centrifugation (10,000 x g, 5 min, 4°C) and re-suspending the pellet in either 5 ml 20 mM sodium phosphate buffer pH 7.4 containing 1% Triton-X, PMSF or 5 ml of 50 mM Tris-HCl, 500 mM NaCl, pH 8.0. A 1 ml aliquot of each was incubated with 500 µl glass beads (2 mm) and vortexed at 4°C after which a 100 µl aliquot of the respective mix was centrifuged (10,000 x g, 10 min, 4°C) and the supernatant separated from the pellet for analysis on a tricine gel. The solubility test was done for cultures prepared at both 30°C and 37°C.

Membrane scaffold protein purification

After overexpression D-MSP1D1 was first purified according to already established method.[74] Shortly the cell pellet was resuspended in 20 mM sodium phosphate buffer pH 7.4 to which PMSF was added from a stock solution in isopropanol to a final concentration of 1 mM together with Triton X-100 (1% final concentration). This was followed by sonication (5 x 25 s) and the suspension was centrifuged again (12,000 x g, 30 min). The supernatant was incubated with Ni-NTA agarose for 1 h at 4°C and the lysate washed with: (a) 25 ml of 40 mM Tris/HCl, 0.3 M NaCl, 1% TritonX-100, pH 8.0, (b) 25 ml of 40 mM Tris/HCl, 0.3 M NaCl, 50 mM Na-Cholate, 20 mM imidazole pH 8.0, (c) 40 mM Tris/HCl, 0.3 M NaCl, 50 mM imidazole, pH 8.0. D-MSP1D1 was then eluted with 40 mM Tris/HCl, 0.3 M NaCl containing 0.4 M imidazole, pH 8.0 into 1.5 ml fractions. D-MSP1D1 was further purified on a size exclusion column (Superdex 200 10/300 GL, GE Healthcare) equilibrated with 20 mM Tris, 150 mM NaCl, pH 8.0 and analysed on a tricine gel. The final protein concentration was determined after dialysis at 280 nm. Protein concentration was calculated using the extinction coefficient 21,430 and M_W of 24,600.

Subsequent purifications were done by re-suspending the pellet in Tris-HCl, pH 8.0, 1 mM PMSF, 1% Triton X-100 and adding extra washing steps to the Ni-NTA purification procedure while omitting the wash containing 50 mM imidazole.

SAXS structural analysis of D-MSP1D1

D-MSP1D1 was investigated by SAXS using the Bio-SAXS instrument BM29 at European Synchrotron Radiation Facility (ESRF) in Grenoble. All SAXS data were collected at 20°C using the fixed instrument setup also described for the now

disassembled beamline ID14-3,[176] a predecessor to the current beamline. Data processing, including radial averaging, background subtraction and conversion of the data into *I(q)* [cm^2/cm^3] was performed using the ATSAS package.[106] Absolute scale calibration was done with bovine serum albumin as the external reference. Resolution effects were considered negligible due to a very high mono-chromaticity of the incoming beam, a very small beam diameter and a close to perfect collimation.

Results

E. coli strain BL21(DE3) used for the expression of MSP was already adapted to growth in D_2O over a long period of time (Deuteration Laboratory PSB platform within the Life Sciences Group at the Institut Laue-Langevin, ILL, Grenoble, France) facilitating the expression of deuterated MSP according to the already established method for predictable deuteration of proteins (Fig. 3.1).[149] In order to obtain a recombinant MSP deuterated to a level which is suitable for small-angle scattering the expression was done in minimal medium containing 85% D_2O to yield 70% deuterated protein.[149] Mainly recycled 96% D_2O was used in combination with non-deuterated glycerol however when such high concentration of D_2O was not available perdeuterated D_8-glycerol (CIL) was supplemented to the medium to increase the protein degree of deuteration.

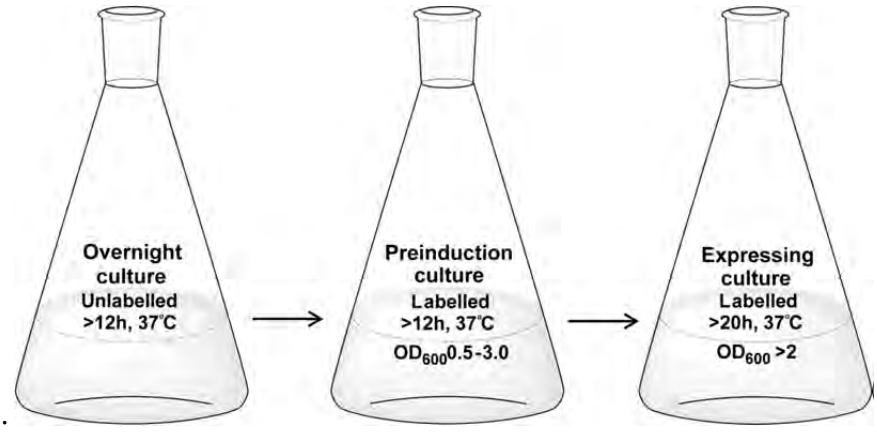

Figure 3.1. Schematic representation of the deuteration protocol for recombinant proteins in *E. coli*. The overnight culture expressed in unlabelled media was amplified into deuterated media followed by induction and overnight expression. Illustration adapted from Leiting *et al*.[149]

Expression of MSP1D1

The first expression of deuterated MSP was done at 37°C according to the established protocol and building on experience from pilot experiments carried out by the structural biophysics group in the D-lab in Grenoble prior to the start of this PhD project (Fig. 3.2*a*).[74] While protein expression time can be longer in D_2O a band at 24 kDa corresponding to the size of MSP1D1 was observed already four hours after induction with IPTG (Fig. 3.2*a lane 2*). Some protein was still left in the supernatant after centrifugation but majority remained in the cell pellet. The biomass yield under standard temperature conditions was determined to 5.4 ± 0.31 g/l D_2O. Change of the expression temperature to 30°C led to a 37% increase in biomass (7.4 ± 0.76 g/l D_2O) but also to reduced solubility in standard phosphate lysis buffer (Fig. 3.2*b*).

MSP1D1 solubility was further tested for both expressions, at 37°C and 30°C, using a different lysis buffer system containing 50 mM Tris-HCl, 500 mM NaCl, pH 8.0 (Fig. 3.2*c*). Analysis of these preparations on a tricine gel showed that the solubility of MSP1D1 at both 37°C and 30°C was better in Tris lysis buffer as compared to phosphate buffer which has been reported as optimal for hydrogenated MSP1D1.[74] This could possibly be due to a slight increase in pH for the Tris-HCl based buffer.

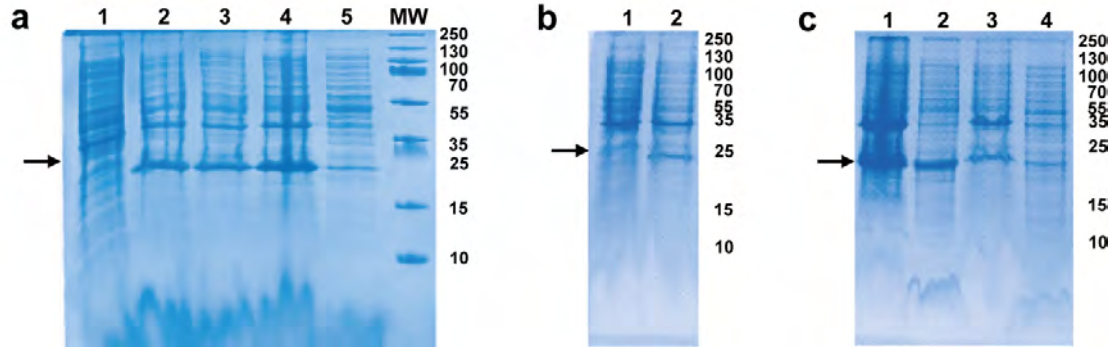

Figure 3.2. Expression of D-MSP1D1 in deuterated medium. (**a**) Commassie stained tricine gel showing MSP1D1 expression at 37°C before induction (*lane 1*), four hours after induction (*lane 2*), overnight expression after induction (*lane 3*), cell pellet (*lane 4*) and the supernatant (*lane 5*). Size of the molecular weight (MW) is given in kDa and indicated on the right. (**b**) Commassie stained tricine gel showing the solubility of MSP1D1 expression before induction at 30°C (*lane 1*), after induction at 30°C (*lane 2*). Size of the molecular weight is given in kDa on the right. Phosphate buffer was used for cell lysis in both preparations. (**c**) Solubility of D-MSP1D1 in 50 mM Tris-HCl, 500 mM NaCl, pH 8.0. Cell pellet from expression at 37°C (*lane 1*), supernatant from expression at 37°C (*lane 2*), cell pellet from expression at 30°C (*lane 3*), supernatant from expression at 30°C (*lane 4*). Molecular weight is given in kDa on the right. Arrows indicate the position of D-MSP1D1.

Optimization of D-MSP1D1 purification

Deuterated MSP1D1, when purified according to purification method already established for hydrogenated MSP,[74] can be seen in Figure 3.3*a*. While some protein was visible in both washes containing Triton-X as well as Na-cholate most D-MSP1D1 eluted using 20 ml of elution buffer containing 0.4 M imidazole. This purification resulted in approximately 6 mg of protein extracted from 5.8 g of cells giving an approximate 1 mg of protein/g of biomass (Fig. 3.3*a* lanes 5-9). Further purification of D-MSP1D1 using size exclusion chromatography as is recommended for hydrogenated MSP did not enhance purity (Fig. 3.3*b*).

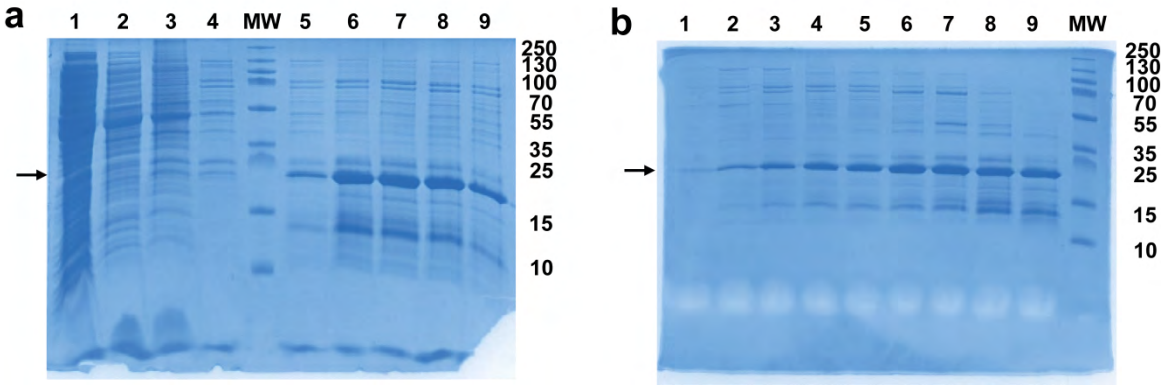

Figure 3.3. Purification of D-MSP1D1. (**a**) Commassie stained tricine gel showing the purification of D-MSP1D1 done according to Ritchie et al (2009) showing the flow through (*lane 1*), wash with Triton X-100 (*lane 2*), wash with Na-Cholate (*lane 3*), wash with 50 mM imidazole (*lane 4)*, eluate 1-5 (*lane 5-9*).), Size of the molecular weight marker (*MW*) given in kDa on the right. (**b**) Commasie stained tricine gel showing the fractions obtained after size exclusion chromatography (Superdex 200 10/300 GL, GE Healthcare). Size of the molecular weight marker (*MW*) given in kDa on the right. Arrows indicate the position of D-MSP1D1.

Additional lysis improves protein yield

An additional lysis of the deuterated cells in 50 mM Tris-HCl, 500 mM NaCl, pH 8.0 recovered additional D-MSP1D1. A purification which included more washing can be seen in Figure 3.4*a*. A significant band corresponding to D-MSP1D1 can be seen in the wash containing 50 mM imidazole as well as in the eluates. The comparison of the purification after size exclusion chromatography, the wash fraction containing 50 mM imidazole from second lysis and eluates from second lysis were analysed on an SDS-PAGE gel (Fig. 3.4*b*). This showed not only that size exclusion did not result in significant improvement of protein purity but also that 50 mM imidazole resulted in

significant elution of D-MSP1D1 and therefore this washing step was omitted from subsequent purifications. The second lysis of the cells (5.8 g) resulted in 4 mg of D-MSP1D1 in the wash fraction and a total of 9.4 mg of protein in the eluate fractions. This was a significant yield improvement as compared to the initial lysis of the same cells resulting in 2.3 mg of protein/g of biomass.

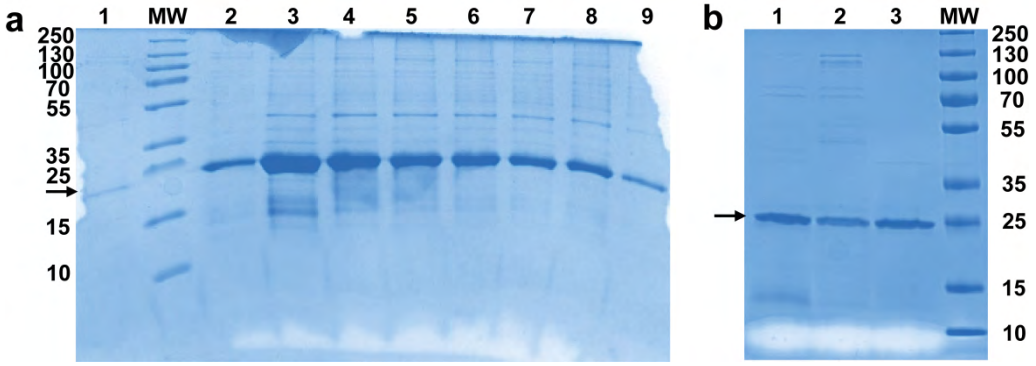

Figure 3.4. (**a**) Additional lysis of deuterated cells cultivated at 37°C. Cells were lysed into 50 mMTris-HCl, 500 mM NaCl, pH 8.0 and D-MSP1D1 purified with 50 ml of each wash buffer. Wash with 50 mM imidazole (*lane 1*), molecular weight marker (*MW*), eluate 1 (*lane 2*), eluate 2 (*lane 3*), eluate 4 (*lane 4*) eluate 6 (*lane 5*), eluate 8 (*lane 6*), eluate 10 (*lane 7*), eluate 12 (*lane 8*), eluate 14 (*lane 9*). Size of the molecular weight marker (*MW*) is given in kDa and indicated on the left. (**b**) SDS-PAGE gel showing the purification after size exclusion (*lane 1*), wash fraction from second lysis (*lane 2*), eluate fractions from second lysis (*lane 3*), molecular weight marker (*MW*) with the size in kDa indicated on the right. Arrows indicate the position of D-MSP1D1.

Purification of D-MSP1D1 from cells cultivated at 30°C

The purification of D-MSP1D1 from 3 g of cells cultivated at 30°C while using more washing with both Triton X-100 and Na-cholate and omitting the wash containing 50 mM imidazole increased protein purity (Fig. 3.5). First lysis of cells in 50 mM Tris-HCl, 500 mM NaCl, pH 8.0 resulted in a total amount of 11.4 mg of protein (3.8 mg of protein/g of biomass) and an additional lysis resulted in 6 mg of protein (2 mg of protein/g of biomass). The average amount of protein which can be obtained from different cultivation conditions are summarized in Table 3.3.

SAXS analysis of D-MSP1D1

SAXS analysis of deuterated MSP1D1 on its own revealed that the purified amphipathic protein-belts formed large disordered aggregates when dissolved in aqueous

solution (data not shown), making any subsequent SANS contrast variation investigations on the isolated protein alone unreliable.

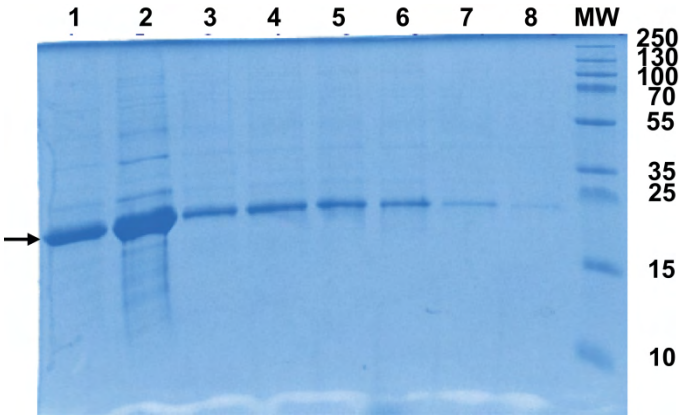

Figure 3.5. Purification of D-MSP1D1 expressed at 30°C after washing with 70 ml wash containing Triton-X and 50 ml wash containing Na-cholate omitting the wash containing 50 mM imidazole and eluting into 1.5 ml fractions. Eluate 1 (*lane 1*), eluate 2 (*lane 2*), eluate 4 (*lane 3*) eluate 6 (*lane 4*), eluate 8 (*lane 5*), eluate 10 (*lane 6*), eluate 12 (*lane 7*), eluate 14 (*lane 8*). Molecular weight marker (*MW*) and the size in kDa are given on the right. Arrow indicates the position of D-MSP1D1.

Table 3.3. Summary of D-MSP1D1 production

Temperature [°C]	Biomass [g]	D_2O [l]	Protein yield/biomass [mg/g]	Protein yield/D_2O [mg/l]
37	43.21	8	3.4	19.6
30	37.06	5	4.3	13.0
Total	80.27	13	3.9	~300

Discussion

Deuterium tolerant bacterial strains are crucial in the production of partial and perdeuterated proteins.[144,147,149,174,175] However even *E. coli* strain BL21(DE3) , which has been well adapted to growth under highly deuterated conditions[147] responds unpredictably to deuteration similar to many other microorganisms.[177,178] Use of minimal media, as well as deuteration effects, lead to significantly longer expression times under deuterated conditions. This can be fatal for proteins that are toxic to bacteria leading to reductions in yield, plasmid loss and elevated mutation rates. While 70% deuterated MSP1D1 can be successfully expressed in *E. coli*, once optimal conditions have been defined under hydrogenated conditions, the final cell density in the minimal media composition is

primarily dependant on the amount of supplemented glycerol.[147] Factors such as temperature as well as pH can also have an effect. For MSP1D1 the biomass yield in minimal deuterated media decreased by a factor of 4 as compared to already established expression under hydrogenated conditions.[74] The optimal expression temperature determined for hydrogenated protein also differed under minimal deuterated conditions and a decrease in expression temperature to 30°C led to a higher yield of biomass and subsequently also of purified protein.

Expression of recombinant proteins under deuterated conditions can also have subtle effects on the physicochemical properties of proteins.[149] In this case this resulted in reduced solubility of deuterated MSP1D1 in buffer systems optimized for its hydrogenated analogue. Re-optimization through systematic change of purification conditions was necessary to reach a similar level of purity as for hydrogenated MSP while at the same time extracting most of the protein out from the deuterated cells. The general protocol for polyhistidine-tagged proteins using Ni-NTA affinity chromatography used for MSPs with additional washing steps and detergent containing buffers were required to obtain D-MSP1D1. However, an increase in the amount of washing, omitting the use of 50 mM imidazole and increasing the pH in the buffer system as compared to purification of non-deuterated MSP lead to a higher protein yield. This systematic approach to optimization of purification conditions for deuterated protein belts should also be applicable on other MSPs with different lengths.

Chapter 4

Isolation and analysis of biosynthesized phosphatidylcholine

Applied in:

Wadsäter, M. H., Maric, S., Simonsen, J. B., Mortensen, K. and Cardenas Gomez, M. 2013, The effect of using binary mixtures of zwitterionic and charged lipids on nanodisc formation and stability, ***Soft Matter*** *9, (7)* 2329-2337.

Maric, S., Thygesen, M. B., Schiller, J., Moulin, M., Marek, M., Haertlein, M., Forsyth, V. T., Arleth, L. and Pomorski, T. G. 2013. Site-specific deuteration of phosphaitdylcholine in *Eshcerichia coli*. ***In preparation for Journal of Lipid Research***.

Maric, S., Skar-Gislinge, N., Midtgaard, S. R., Thygesen, M. B., Schiller, J., Frielinghaus, H., Moulin, M., Haertlein, M., Forsyth, V. T., Pomorski, T. G., and Arleth, L. 2013. Stealth Carriers for Low-Resolution Structure Determination of Membrane Proteins in Solution, ***Acta Crystallographica Section D70.*** 317-328.

Introduction

In addition to D-MSP1D1 the stealth nanodisc model is composed of a phospholipid bilayer. The most commonly used phospholipids in model membrane systems such as nanodiscs and for reconstitution of membrane proteins are phosphatidylcholines, PCs (Fig. 4.1*a*). PC is the main phospholipid in human membranes and accounts for over 50% of total phospholipid in most eukaryotes.[2] Its cylindrical shape allows for spontaneous self-assembly into planar bilayers at a broad range of pH, temperature and ionic strength.[2] Convenient methods, in the preparative sense, for the synthesis of various PC species have been developed including chemical synthesis and extraction from biological tissue.[179] While chemical synthesis is the preferred method for obtaining single PC species extraction from e.g. egg yolk is also used and yields a mixture of PC species called lecithin.[180] Microbial synthesis which has been successfully used for preparation of other phospholipids has for PC been limited to the use of e.g. yeast[181] and certain bacteria while completely lacking from the model-organism *Escherichia coli.* Regardless of this PC has been the most often used phospholipid for the reconstitution of and studies also of bacterial membrane proteins.

This chapter focuses on preparation of physiologically relevant mono-unsaturated PC in a genetically modified strain of *E. coli* engineered to synthesize PC as its major phospholipid.[24] *E. coli* strain AL95 carrying the plasmid pAC-PCSlp-Sp-Gm which allows for expression of PC synthase encoded by the *Legionella pneumophila pcsA* gene was originally developed for the study of the effects PC has on bacterial membrane proteins.[24] However an organism such as the *E. coli* could also be used as a platform for easy preparation of biologically relevant mono-unsaturated PC species as the simplicity of its lipid composition would aid in the subsequent extraction, purification and analysis of the obtained PC species. Most importantly, biological synthesis of PC in *E. coli*, an organism which can be deuterated to a very high degree could pave the way for obtaining also physiologically relevant deuterated PC species which have proven challenging to synthesize through an organic synthesis approach. The methods of extraction, separation and characterization of PC lipids from simple mixtures of *E. coli* lipids as well as lipid mixtures from model systems such as nanodiscs are also described.

Phospholipid composition and biosynthesis in E. coli

The phospholipid bilayer of wild-type *E. coli* is composed of 70-80%, phosphatidylethanolamine (PE), 15-20% phosphatidylglycerol (PG) and 5% or less cardiolipin (CL) (Fig. 4.1*b*).[182] Despite its very simple lipid composition *E. coli* has been one of the most studied model organisms with regard to phospholipid metabolism and has greatly contributed to our knowledge of phospholipid synthesis and function in both prokaryotes and eukaryotes.[182] Mutants of *E. coli* have been developed in which phospholipid composition can be systematically regulated and which lack native or can even synthesize foreign lipids helping define specific roles of individual phospholipids in biological organisms.[182] Figure 4.2 shows the metabolic pathway for the phospholipid synthesis in both wild-type *E. coli* and *E.coli* AL95/pAC-PCSlp-Sp-Gm.[182] In all organisms phospholipid biosynthesis begins with two acylation steps of sn-glycerol-3-P to form phosphatidic acid (PA). PA is in *E. coli* rapidly converted to CDP-diacylglycerol by CDP-diacylglycerol synthase, an enzyme which requires divalent cations for activity and uses CTP as substrate. The CDP-diacylglycerol is then utilised by the two routes which lead to the main membrane phospholipids of wild-type *E. coli*: the zwitterionic PE (Fig. 4.2 *red*) and the negatively charged PG and CL. In *E. coli* strain AL95 the synthesis of PE is supressed by high amount of divalent metal ions while the plasmid pAC-PCSlp-Sp-Gm allows for the expression of PC synthase which is encoded by the *pcsA* gene from *Legionella pneumophila* (Fig. 4.2 *green*) generating an *E. coli* mutant with PC as its major phospholipid.

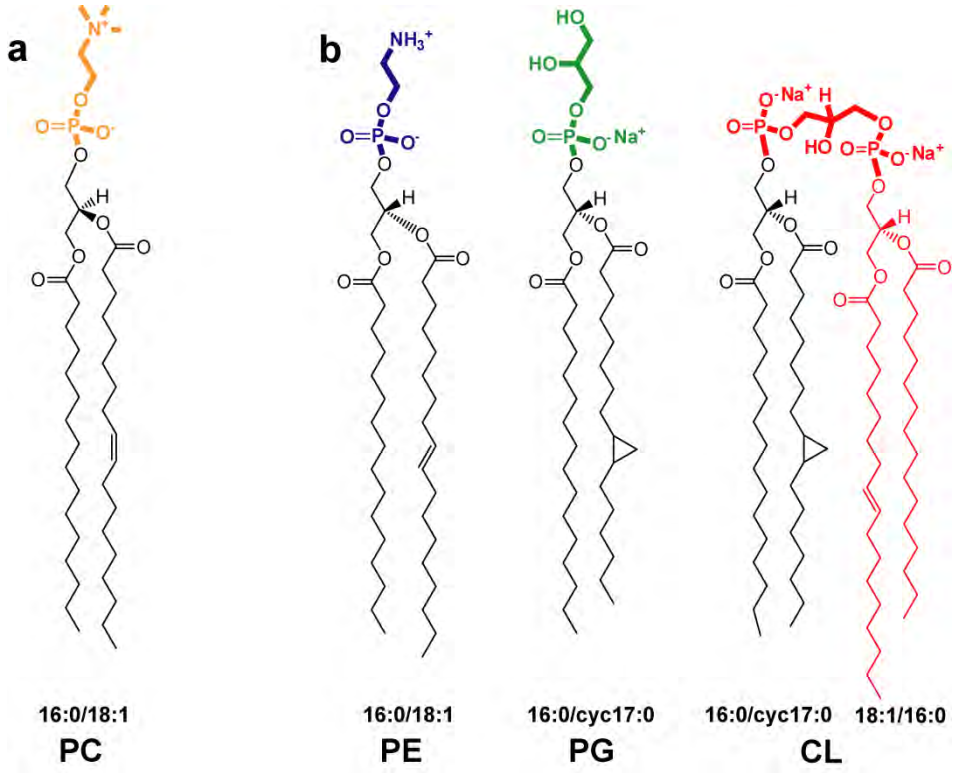

Figure 4.1. (**a**) PC - a major component of eukaryotic membranes (**b**) Major phospholipid species from *E.coli;* phosphatidylethanolamine (PE), phosphatidylglycerol (PG), and cardiolipin (CL). The predominant fatty acyl species are indiciated for each lipid.

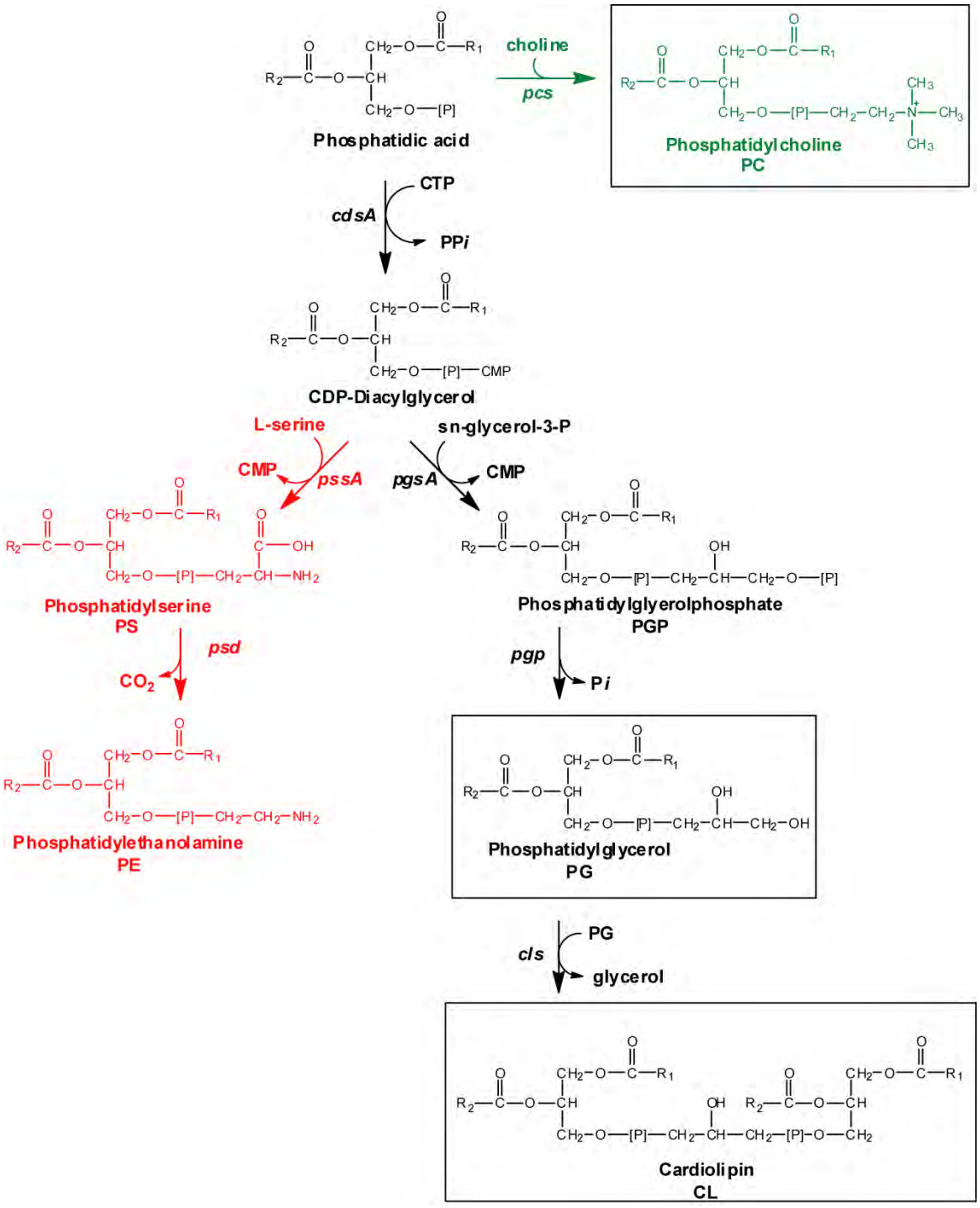

Figure 4.2. Phospholipid synthesis pathways in *E.coli*. The enzymes and their respective genes are: CDP-diacylglycerol synthase (*cdsA*), Phosphatidylserine synthase (*pssA*), Phosphatidylserine decarboxylase (*psd*), Phosphatidylglycerophosphate synthase (*pgsA*), Phosphatidylglycerophosphate phosphatase (*pgp*), Cardiolipin synthase (*cls*). Phosphatidylcholine synthase from *L. pneumophila* (*pcs*) responsible for PC synthesis in AL95 is indicated in green and the supressed PE synthesis pathway is indicated in red.

Isolation of phospholipids from biological tissue

Extraction of total lipid from biological material is done through the use of various organic solvents and the most widely used methods of Folch *et al.*[183] and Bligh and Dyer,[184] both use a chloroform/methanol/water phase system giving a reliable and quantitative isolation. It is important that the solvent mixture is sufficiently polar to disassociate lipids from the cell membranes but not polar enough to dissolve all triacylglycerols and other non-polar lipids.

The Folch extraction method starts with homogenization of the biological tissue with a chloroform-methanol mixture followed by washing the extract with either water or an appropriate salt solution.[183] The resulting mixture is separated into two phases where the lower phase contains the total pure lipid extract.[183] The washing procedure removes essentially all the non-lipid contaminants leading to a small loss (less than 1%) of tissue lipids.[183] This can further be reduced by addition of certain mineral salts which can affect the efficiency of the washing procedure. In the absence of salts substantial amount of acidic lipids e.g. phosphatdic acid (PA) and phosphatidylserine (PS) will remain in the upper phase and will be lost during washing.[183]

In the Bligh and Dyer method which also relies on a chloroform/methanol/water mixture the solvent sample ratio is heavily reduced which is the primary advantage of this method.[184] Here the biological tissue is also homogenized with a chloroform-methanol mixture but in a much smaller ratio and the many washing steps of the crude extracts practiced in the Folch method are omitted.[184] This solvent reduction in the Bligh and Dyer method however does not lead to a significant loss in yield, with a reported recovery of ≥ 95% of total lipid making it both less exhaustive and more cost effective.[184] Due to this the Bligh and Dyer method being was the preferred extraction procedure throughout this work.

Separation of phospholipids from crude extracts

Separation of individual phospholipids from crude extracts according to head-group polarity can be done through column chromatography using silica gel as the stationary phase (Fig. 4.3).[185] The stationary phase adsorbent is placed in a vertical column onto which a mobile phase is added and which can flow through the column by either gravity or applied pressure.[185] The mixture of phospholipids to be separated is loaded on the column after which an eluent is passed through. Due to different interactions of the

individual lipids with the stationary and mobile phase they are carried along the mobile phase with different rates and separation can be achieved using increased polarity of the eluent solvent. The lipids can be collected in different fractions for further analysis.

The polarity of the solvent affects the relative rates at which different phospholipids move across the column and polar solvents can more effectively solvate polar phospholipids.[185] Proper solvent is therefore crucial for successful separation of phospholipids as it will affect their rate of movement and often a series of increasingly polar solvent is used to achieve successful separation. Traditional solvents used for the separation of phospholipids using column chromatography have been mixtures of chloroform and methanol but other solvent systems utilizing hexane, acetone etc. have also been used.[185]

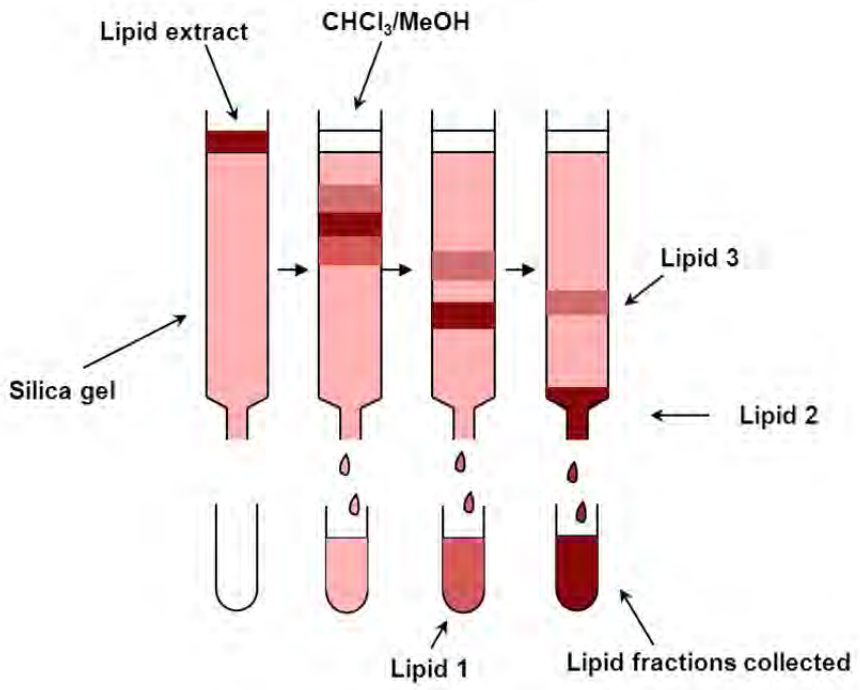

Figure 4.3. Phospholipid separation scheme. Silica gel chromatography set-up for separation of phospholipids according to head-group polarity. For details see text.

Analysis of phospholipids

The available methods for analysis of phospholipids are amongst others thin-layer chromatography, mass spectrometry, NMR spectroscopy and gas-liquid and liquid chromatography. Depending on the application these techniques can be used on both non-deuterated as well as deuterated phospholipids allowing for the monitoring and characterization of the intermediate and final products resulting from lipid synthesis.[148]

Mass spectrometry enables determination of fatty acyl composition and individual lipid species but it can also be used for direct determination of the deuterium content in organic compounds.[186] The isotopic purity and specific deuterium positions however can best be established by ^{1}H-NMR spectroscopy.[148] Here the integral intensity of the ^{1}H-NMR signal which corresponds to hydrogen decreases for the atoms which have been replaced by deuterium. On the other hand in ^{13}C-NMR lipid spectra the incorporation of deuterium leads to a small isotopic upfield shift of the obtained signal.[148] The carbon atom signals when bound to deuterium are readily identified because of the characteristic multiplicity caused by spin-spin interactions with deuterium. This therefore gives a spectrum that shows signals of carbon atoms covalently bound to deuterons and protons simultaneously and thus increases the accuracy of measurements of isotopic purity.[148] Gas-liquid chromatography (GLC) is another method for the analysis of both non-deutertaed and deuterated fatty acids with its possibility of separation of deuterium-enriched and protonated fatty acids exploiting the difference in their retention times.[148]

Materials and methods

Chemicals

All chemicals and solvents were obtained in the highest commercially available purity from Sigma-Aldrich A/S (Copenhagen, Denmark) and used as supplied unless stated otherwise. Phospholipid standards were purchased from Avanti Polar Lipids Inc. (Birmingham, AL, USA) and used as supplied. MALDI matrices used were the acidic 2,5-dihydroxybenzoic acid (DHB) as 0.5 M solution in methanol[187] and basic 9-aminoacridine (9-AA) hemihydrate (Acros Organics, Geel, Belgium) applied as 10 mg/ml solution in 60/40 (v/v) isopropanol/acetonitrile.[188] Thin-layer chromatography (TLC) silica gel 60 plates were from Merck (Darmstadt, Germany) and silica gel 60, 230/400 mesh was from Sigma-Aldrich A/S (Copenhagen, Denmark). Ultrapure water (Ultra Clear Basic, SG, resistivity 18.2 MΩ.cm) was exclusively used in all work.

Biosynthesis of phosphatidylcholine

E. coli strain AL95 carrying the plasmid pAC-PCSlp-Sp-Gm which allows for the expression of PC synthase encoded by the *Legionella pneumophila pcsA* gene under control of an arabinose inducible promotor was used for the PC synthesis as previously

described.[189] For deuterated PC species this was modified to growth in minimal media according to established protocols.[175] Briefly, a fresh overnight culture of AL95 grown in Luria-Bertani broth (LB) with 50 mM $MgCl_2$ was diluted to an initial cell density of 0.95 (OD_{600}) into flasks containing: 6.86 g/l $(NH_4)_2SO_4$, 1.56 g/l KH_2PO_4, 6.48 g/l $Na_2HPO_4{\cdot}2H_2O$, 0.49 g/l $(NH_4)_2$-H-citrate, 0.25 g/l $MgSO_4{\cdot}7H_2O$, 1.0 ml/l of a salt mix (0.5 g/l $CaCl_2{\cdot}2H_2O$, 16.7 g/l $FeCl_3{\cdot}6H_2O$, 0.18 g/l $ZnSO_4{\cdot}7H_2O$, 0.16 g/l $CuSO_4{\cdot}5H_2O$, 0.15 g/l $MnSO_4{\cdot}4H_2O$, 0.18 g/l $CoCl_2{\cdot}6H_2O$, 20.1 g/l EDTA), with 5 g/l glycerol and 10 mg/l gentamicin all in H_2O and incubated overnight at 37°C. The adapted culture was amplified in minimal deuterated media containing 5% of either hydrogenated (Sigma Aldrich) or deuterated (1,1,2,3,3-D5, 99%, Eurisotop) glycerol and the cells induced with 0.2% arabinose (Sigma Aldrich), and 2 mM choline chloride as previously described.[189] After incubation at 37˚C for 24 h the cells were harvested by centrifugation (10,000 x g, 20 min, 4°C), and washed with MiliQ water.

Phospholipid extraction and purification

Total lipid fractions of the cells were extracted through a modified method of Bligh and Dyer.[184] In short, after centrifugation and washing of the cell pellet, the cells were resuspended in H_2O (5 ml H_2O/g of cell paste) and cells broken by sonication (10 x 2 s pulses at about 20% power using a Branson Sonifier® 450 Sonicator). Methanol (2.2 ml) and chloroform (1 ml) were added per 1-ml cell suspension aliquot. After 30 min at 25°C phase separation was induced by addition of chloroform (1 ml) and H_2O (1 ml) followed by centrifugation (800 x g, 10 min, 4°C). The chloroform phase was collected and the process repeated two more times. The chloroform phase was stored at -20°C overnight upon which the last remaining of water phase was removed. The final chloroform phase was dried using a stream of nitrogen, and lipid extracts stored at -20°C.

Column chromatography

A silica gel column was prepared using a long thin glass column (1.2 x 30 cm) with a glass frit and a tap on the bottom into which silica powder (Silica Gel 60, 230/400 mesh, 6 g) soaked in chloroform was carefully poured to avoid the formation of bubbles. The column was washed with several bed-volumes of chloroform prior to loading of the lipid extract. After equilibration of the lipid extract with the stationary silica gel phase the individual phospholipids were separated through a serial elution using solvent consisting

of chloroform with an increasing level of methanol. The separated lipids were collected in fractions and further analysed by TLC. All separations were done at room temperature.

Characterization and quantification of phosphatidylcholine

The phospholipid species were characterized after separation on one-dimensional TLC plates and developed in either chloroform/methanol/water (60/25/4, v/v/v), chloroform/acetone/ methanol/ acetic acid/water (50/20/10/10/5, v/v/v/v/v) or chloroform/ethanol/water/triethylamine (30/35/7/35, v/v/v/v) and identified through comparison with known standards for PC, PG, PE and CL. The lipids were visualized by staining with primuline solution (5 mg primuline in 100 ml acetone/water, 80/20, v/v) which shows the presence of lipids through to the non-covalent binding of the dye to the fatty acyl residues.[190] Upon illumination with UV light at 366 nm, individual lipid classes were detected as coloured spots and scraped off using a razorblade. Total phospholipid content was determined by digesting the lipids in deionized water and perchloric acid for 1 h at 180°C followed by addition of ammonium molybdate and ascorbic acid. After further heating to 80°C for 10 min, the sample was cooled and the absorbance was read at 812 nm to quantify total lipid phosphorus as previously described.[191]

MALDI-TOF mass spectrometry

For MS analysis, lipid spots from primuline stained TLC were scraped off and extracted three times with 100 µl of a mixture of chloroform, methanol and 0.9 % aqueous NaCl (1:1:1, v/v/v). The obtained lipid fractions (concentrated to a volume of 10 µl) as well as total extracts (10 µl) were independently pre-mixed 1:1 (v/v) with the different matrix compounds (DHB and 9-AA) prior to deposition onto the MALDI target and investigated by positive and negative ion-mode MALDI-TOF MS. MALDI-TOF mass spectra were acquired on a Bruker Autoflex mass spectrometer (Bruker Daltonics) which utilizes a pulsed nitrogen laser, emitting at 337 nm. The extraction voltage was 20 kV and gated matrix suppression was applied to prevent the saturation of the detector by matrix ions.[192] For each mass spectrum, 100 single laser shots were averaged. In order to enhance the resolution, all spectra were acquired in the reflector mode using delayed extraction conditions. A more detailed methodological description of MALDI-TOF MS with the focus on lipid analysis is available for further reading.[193,194] All data were processed with the software "Flex Analysis" version 2.2 (Bruker Daltonics). The lipids

were also analysed subsequent to PLA_2 digestion in order to determine the fatty acid composition as previously described.[193] This data collection and analysis was done in collaboration with Dr. Jürgen Schiller from the University of Leipzig.

NMR spectroscopy

The purified PC was analysed by H^1-NMR through and compared to commercially available PC as well as deuterated PC analogues synthesized in *E. coli.* All lipids were dissolved in chloroform-d (99.96%, 0.03% (v/v) TMS) and all spectra were recorded with a Bruker Avance 300 MHz instrument. Assignments were aided by $^1H–^1H$ COSY. This data collection and analysis was done in collaboration with Dr. Mikkel B. Thygesen from the Chemistry Department at KU.

Separation of phospholipids from phospholipid mixtures in nanodiscs

Nanodisc containing mixtures of 1,2-dimyristoyl-*sn*-glycero-3-phosphocholine (DMPC) and 1,2-dimyristoyl-*sn*-glycero-3-phospho-(1'-*rac*-glycerol) (DMPG) were prepared according to established protocols described elsewhere.[75,159] To estimate the overall composition of lipids in the discs, the lipids were extracted after nanodiscs formation according to the method of Bligh and Dyer.[184] Shortly this was done by three repeating rounds of 1) adding chloroform, methanol and water to the nanodisc sample and 2) extracting the lipid containing chloroform phase upon phase separation. DMPC and DMPG were then separated on TLC plates developed in chloroform/acetone/methanol/acetic acid/water (30:40:10:10:5 v/v/v/v/v). Approximately 100 nmol lipids were loaded to a TLC plate (silica gel 60 F_{254}, Merck) and the lipids were visualized in UV-light after spraying with primuline solution (5 mg primuline in 100 ml acetone/water, 80/20, v/v). The separated spots were compared to reference DMPC and DMPG spots and scraped off using a razor blade.

The lipid concentration of the extracted nanodisc lipids in each of the spots recovered from the TLC plate was determined by analysis of the phosphoric amount in the sample as described above.

Results

Phospholipids prepared in *E. coli* AL95 cells carrying the pAC-PCSlp-Sp-Gm from *L. pneumophila* cultivated under normal previously described conditions[189] as well as after deuteration were easily extracted through a modified method of Bligh and Dyer.[184] Here the additional washing steps of the lipid-containing chloroform phase were omitted and the cell pellet was instead extracted two times which showed to improve the lipid yields. Suspension of cell pellet in 0.1 M NaCl instead of H_2O under the extraction procedure also improved the yield of the obtained phospholipids (data not shown) indicating that less lipid remained in the water phase when a salt solution was used instead of pure H_2O. The lipid extracts dried either under vacuum or by using a stream of nitrogen at room temperature were stable up to 1.5 years when stored at -20°C.

Characterization of the obtained phospholipids using thin-layer chromatography through comparison with known lipid standards was dependant on the solvent used for TLC development (Fig. 4.4). Neutral solvent consisting of chloroform/methanol/water (60/25/4, v/v/v) unfortunately gave no clear separation of PC and PG (data not shown) but a clear separation of PC could be achieved by using acidic solvent system consisting of chloroform/acetone/methanol/acetic acid/water (50/20/10/10/5, v/v/v/v/v) (Fig. 4.4*a*). This however did not result in significant separation of the phospholipids PE and PG. For a better separation of these two lipids and also PC the TLC plates were developed using a solvent consisting of chloroform/ethanol/water/triethylamine (30/35/7/35, v/v/v/v) (Fig. 4.4*b*). However this solvent system resulted in the co-migration of PG and CL which were difficult to resolve and care should be taken in choosing appropriate solvent based on the lipid to be separated.

This analysis also revealed differences in phospholipid composition between *E. coli* AL95/ pAC-PCSlp-Sp-Gm before and after adaptation to D_2O which are described in more detail in Chapter 5.

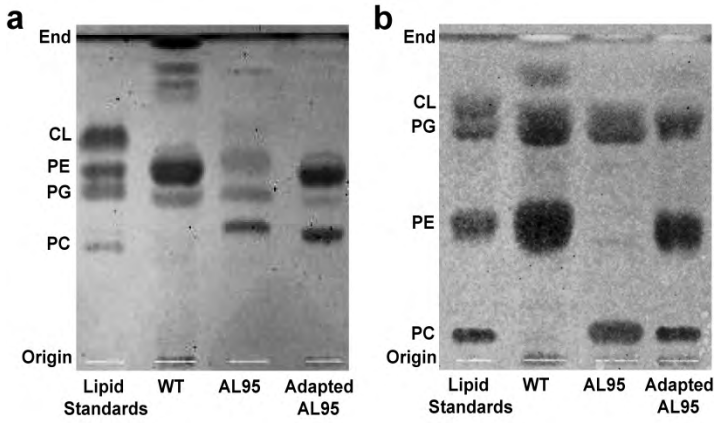

Figure 4.4. Solvent dependent TLC separation of total lipid extracts**.** Lipid standards with phosphatidylcholine (PC), phosphatidylglycerol (PG), phosphatidylethanolamine (PE), cardiolipin (CL) indicated on the left. Wild type E. coli (WT), AL95/pAC-PCSlp-Sp-Gm before (AL95) and after D_2O adaptation (Adapted AL95) separated on a TLC developed in **(a)** acidic solvent system consisting of chloroform/ acetone/ methanol/ acetic acid/ water (50/20/10/10/5, v/v/v/v/v) and **(b)** chloroform/ ethanol/ water/ triethylamine (30/35/7/35, v/v/v/v). Lipids were visualised by primuline staining.

Phospholipid separation

For preparative large-scale phospholipid separation silica gel column chromatography was used according to the scheme in Figure 4.3 enabling separation according to head-group polarity. PC could easily be isolated from the other *E. coli* lipids using a mobile phase consisting of chloroform with a gradually increased concentration of methanol in a serial elution. A fractionation of phospholipids obtained from AL95 before adaptation to D_2O can be seen Figure 4.5 where the collecting of small (10 ml) eluted fractions showed that CL and PG lipids started eluting already at small concentrations of methanol (Fig. 4.5 *lane 9-10*) where for CL elution started already at a chloroform/methanol (70/30, v/v) mixture, while PG started eluting at chloroform/methanol (50/50, v/v (Fig. 4.5 *lane 14-17*). PC on the other hand required very high concentrations of methanol and began eluting only when a methanol concentration of 90% was used (chloroform/methanol, 10/90, v/v) (Fig. 4.5 *lane 20*).

Phospholipid separation through silica gel chromatography was further optimized for deuterated preparations of adapted AL95 which contained a mixture of four lipids (CL, PG, PE and PC). Constant pressure was used in order to control and increase the rate of elution as PC had a tendency to hydrolyse after more than six hours on the column. Similarly to preparations of hydrogenated lipid mixtures consisting of PC, PG and CL it

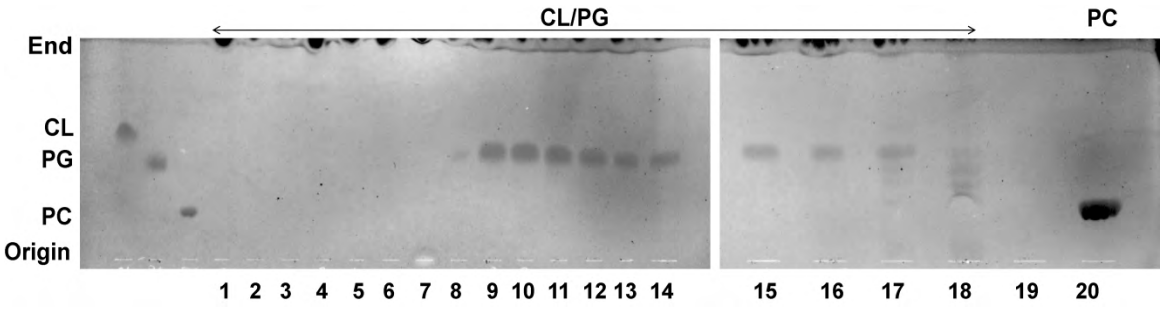

Figure 4.5. Thin-layer chromatography analysis of *E.coli* lipids eluted through a silica gel column and collected in 10 ml fractions. Elution with chloroform/methanol (90/10, v/v) (*lane 1-5*), (80/20, v/v) (*lane 6-7*), (70/30, v/v) (*lane 8-9*), (60/40, v/v) (*lane 10-11*), (50/50, v/v) (*lane 12-13*), (40/60, v/v) (*lane 14-15*), (30/70, v/v) (*lane 16-17*), (20/80, v/v) (*lane 18-19*) and (10/90, v/v) (*lane 20*). The TLC plate was developed using chloroform/acetone/methanol/acetic acid/water (50/20/10/10/5, v/v/v/v/v) and lipids visualised by primuline staining. Phosphatidylcholine (PC), phosphatidylglycerol (PG), cardiolipin (CL) are indicated on the left.

was possible to separate PC out of deuterated lipid mixtures containing also the native *E. coli* lipid PE. Here CL, PG and PE were eluted first using chloroform/methanol (90/10, v/v), (80/20, v/v), and (70/30, v/v), while PC again with the longest retention time was eluted last from the column (Fig. 4.6). However with increased pressure PC could be eluted already at 50% methanol minimizing the retention time and thus hydrolysis of PC at room temperature (Fig. 4.6). It should be noted that elution times and lipid retention times varied with both temperature and humidity which were not possible to control in the laboratory and controlled collection of smaller elution fractions is therefore recommended to avoid incomplete separation.

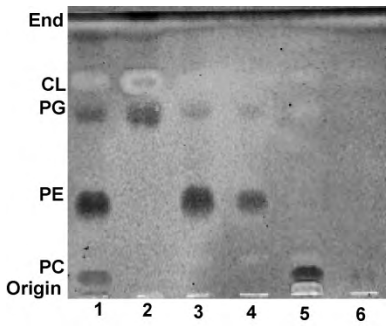

Figure 4.6. Thin-layer chromatography of *E. coli* lipids extracted from adapted AL95, eluted through a silica gel column and collected in 50 ml fractions (*lane 1*) total extract, (*lane 2*) (90/10, v/v), (*lane 3*) (80/20, v/v), (*lane 4*) (70/30, v/v), (*lane 5*) (50/50, v/v), and (*lane 6*) (30/70, v/v). The TLC was developed in chloroform/ethanol/water/triethylamine (30/35/7/35, v/v/v/v) and lipids were visualised by primuline staining. Phosphatidylcholine (PC), phosphatidylglycerol (PG), phosphatidylethanolamine (PE), cardiolipin (CL) are indicated on the left.

E. coli phosphatidylcholine characterization

The PC species obtained from AL95/pAC-PCSlp-Sp-Gm, were analysed by MALDI-TOF analysis.[195] The positive ion MALDI-TOF spectra for isolated PC lipids showed predominantly two PC lipids species extracted from AL95 cells before adaptation to D_2O which were harvested in stationary growth phase (Fig. 4.7*a*). The peaks at *m/z* 732.6 and 754.6 corresponded to the respective proton and sodium adducts of this 1-palmitoyl-2-palmitoleoyl-*sn*-glycero-3-phosphocholine (16:0/16:1 PC) while the peaks at *m/z* 746.6 and 768.6 corresponded to the proton and sodium adducts of -palmitoyl-2-palmitoleoyl-*sn*-glycero-3-phosphocholine with a cyclopropane modified fatty acyl residue (16:0/17:0cyc PC). These cyclopropanated fatty acyl residues are typical of *E. coli* lipids harvested in stationary growth phase and appear to improve lipid stability as these are less reactive to oxidative modifications than their corresponding unsaturated fatty acyl residues while they keep the overall membrane fluidity unchanged.[196-198] These results showed a slight change in fatty acid composition in AL95 lipids extracted from cells harvested in stationary growth phase as compared to the previously reported lipids obtained in the exponential growth phase where a larger variety of fatty acyl length ranging from 14 to 18 carbons and most abundantly 16:0/16:1 and 16:0/18:1 PC was shown.[189] These results indicated that the carbon chain length and the degree of saturation of PC can be regulated during the bacterial growth cycle similar to that of other *E. coli* phospholipids.[198] Positive ion MALDI-TOF analysis of PC lipids obtained from deuterated *E. coli* cultures was also used to determine the degree of PC deuteration while also giving insights into the lipid biosynthesis pathways for the individual lipids (Chapter 5).

The *E. coli* produced PC lipids were also analysed by ^{1}H-NMR where the peak at 0.5 ppm confirmed the presence of cyclopropanated fatty acyl chains (Fig. 4.7*b*). The peaks at 3.4 ppm 3.8 ppm and 4.4 ppm corresponding to the methyl and ethylene moieties of the choline head-group, 3.9 and 4.1 ppm corresponding to the glycerol back-bone and 1.2 ppm corresponding to the fatty acyl chains were used as reference for the investigation of deuterated PC lipids where the reduction in integral ^{1}H signal intensity showed the level of deuteration for these parts of the PC molecule. Not only enabling rapid monitoring of deuteration levels ^{1}H-NMR was used a means of establishing phospholipid purity after column chromatography before their use in the assembly of model membrane systems.

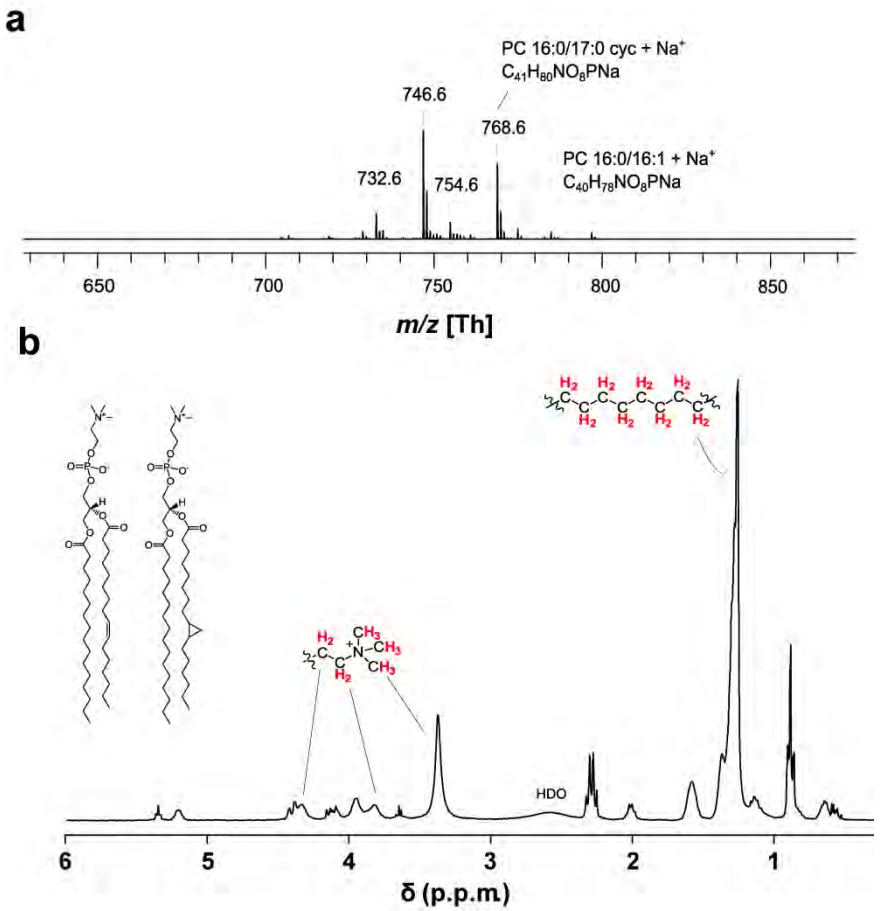

Figure 4.7. Identification of phosphatidylcholine (PC) species produced in genetically modified *E. coli*. Positive-ion (**a**) MALDI-TOF spectra of purified phosphatidylcholine PC obtained from *E. coli* strain AL95/pAC-PCSlp-Sp-Gm grown in hydrogenated media. Peaks are marked with their *m/z* values and assignments are indicated. (**b**) ^{1}H-NMR analysis of PC produced in *E. coli* AL95. The peaks representing the choline head group as well as fatty acyl protons are indicated in red. Molecular structures of the two major PC species from AL95 grown until stationary growth phase are shown in inset and hydrogens corresponding to specific peaks are indicated.

Separation of phospholipids from nanodisc samples

Same extraction procedure which was used on total *E. coli* cells could also be applied on high density lipoprotein particles such as the nanodiscs composed of a mixture of 1,2-dimyristoyl-*sn*-glycero-3-phosphocholine (DMPC) and 1,2-dimyristoyl-*sn*-glycero-3-phosphoglycerol (DMPG). These were extracted from the MSP-lipid mixtures by the modified method of Bligh and Dyer and further separated according to head-group polarity on TLC plates developed in acidic solvent system (Fig. 4.8). Total phosphorous was then determined for the individual spots after scraping off the silica yielding the fractions of the individual lipids incorporated in nanodiscs (Table 4.1). The measured

fractions of DMPG in extracted lipids from nanodiscs typically showed an error of less than ±5% units among separate nanodisc preparations and analyses.

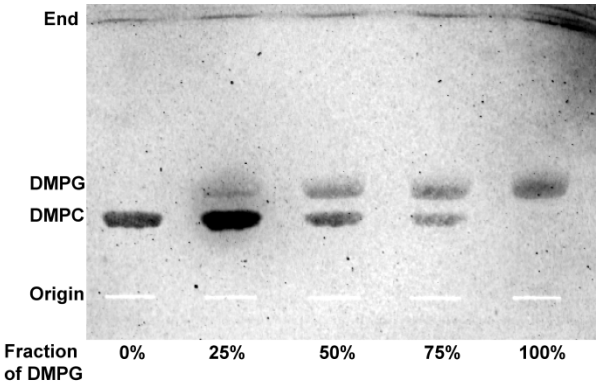

Figure 4.8. Separation of zwitterionic and charged lipids from nanodisc samples. After extraction lipids were separated on a TLC plate developed in chloroform/acetone/methanol/acetic acid/water (30:40:10:10:5 v/v/v/v/v). Lipids were visualised by primuline staining with 1,2-dimyristoyl-*sn*-glycero-3-phosphocholine (DMPC) and 1,2-dimyristoyl-*sn*-glycero-3-phosphoglycerol (DMPG) indicated on the left.

Table 4.1. Measured lipid/protein stoichiometry and lipid composition in the nanodiscs[a]

Fraction of DMPG in assembly mixture	Lipids/MSP1D1	Fraction of DMPG in nanodiscs
0	90 ± 5	NA[b]
0.25	88 ± 1	0.26
0.5	91 ± 1	0.50
0.75	92 ± 1	0.78
1.0	91 ± 6	NA[b]

a Typically the measured fraction of DMPG in extracted lipids from nanodiscs varied by less than ±5% units among separate nanodisc preparations and analyses.*b* Not applicable.

Discussion

Lipids from genetically modified AL95 cultivated under both non-deuterated and deuterated conditions were easily extracted using the Bligh and Dyer method. However including salt in the extraction procedure was necessary to reduce the number of extraction cycles indicating the lipids had a tendency to adhere to the water phase.

The purification of both deuterated and non-deuterated PC using silica gel chromatography and a simple solvent consisting of chloroform and methanol as the mobile phase resulted in the separation of PC from the other E. coli lipids PE, PG and CL.

Unfortunately this purification system did not offer a successful separation of PG from CL which had a tendency to co-migrate. However inclusion of a small amount of acidic solution to the elution solvent together with additional washing steps and collecting of smaller fractions could be a means to obtain a better separation of these two lipids. While silica gel chromatography in combination with a chloroform/methanol solvent system enabled a successful purification of PC at room temperature the rate of elution was in the order of tens of hours resulting in a significant amount of degradation and lysoPC. Another disadvantage of this purification set-up was the large amount of organic solvent used per purification consisting of up to 300 ml of solvent mixture. Optimizing the purification procedure through the use of preparative HPLC systems in combination with other possibly more optimal solvent systems as the mobile phase should be the next step in automatizing the large-scale purification for this very simple phospholipid composition.

The yields of PC both non-deuterated and deuterated that could be obtained through the microbial approach are in the range of 50 mg/l for flask cultures and up to 200 mg/l from a pilot fermentation. While this is 100 and even 1000-fold smaller quantities than what is possible for synthetic PC the microbial approach could offer easy access to partially and perdeuterated monounsaturated versions of physiologically relevant PC species.

The fatty acyl distribution of the phospholipids obtained from AL95/pAC-PCSlp-Sp-Gm, was slightly different when the AL95 lipids were extracted from cells harvested in stationary growth phase as compared to the previously reported lipids obtained in the exponential growth phase.[24] Both a reduced variety in fatty acyl length and cyclopropane modified fatty acyl residues typical of *E. coli* lipids harvested in stationary growth phase were observed. While these are thought to improve lipid stability due to being less reactive to oxidative modifications than their corresponding unsaturated fatty acyl residues[196-198] this change in fatty acyl composition indicated that the carbon chain length and the degree of saturation of PC could be regulated during the bacterial growth cycle similar to that of other *E. coli* phospholipids.[198] The large head-group difference between PC and the other *E. coli* lipids eased the MALDI-TOF analysis as PC species were the dominant signals in positive ion mode and this lipid mass range giving a quick way of lipid characterization for both deuterated and non-deuterated species. ^{1}H-NMR which was

used throughout this work to localize deuterium positions within the PC molecules could also be used for purity assessment prior to the assembly of model membrane systems.

The same phospholipid separation procedures used for the isolation of PC from native *E. coli* lipids could also be used to separate lipids from mixtures in model-membrane systems such as nanodiscs. In this example mixtures of DMPC and DMPG could easily be separated on TLCs developed in an acidic solvent system and the amount of each lipid determined to very high accuracy through measurements of the total amount of phosphorous in the samples.

Chapter 5

Preparation of selectively deuterated phosphatidylcholine in genetically engineered *Escherichia coli*

Applied in:

Maric, S., Thygesen, M. B., Schiller, J., Moulin, M., Marek, M., Haertlein, M., Forsyth, V. T., Arleth, L. and Pomorski, T. G. 2013. Biosynthetic preparation of selectively deuterated phosphatidylcholine in genetically modified *Escherichia coli*. ***In preparation for Journal of Lipid Research.***

Maric, S., Skar-Gislinge, N., Midtgaard, S. R., Thygesen, M. B., Schiller, J., Frielinghaus, H., Moulin, M., Haertlein, M., Forsyth, V. T., Pomorski, T. G., and Arleth, L. 2014. Stealth Carriers for Low-Resolution Structure Determination of Membrane Proteins in Solution, ***Acta Crystallographica Section D70.*** 317-328.

Introduction

Deuterium-labelled lipids were originally employed in mass spectrometry and the analysis of lipid pathways. The development of NMR and neutron diffraction methods, where large sample quantities are required, has pushed the development of deuterium-labelled lipids towards more convenient preparation methods.[148] The available labelling approaches today are either through chemical synthesis, microbial synthesis or, when obtaining different combinations of deuteration within the lipid head-groups as opposed to the fatty acyl chains is required, a combination of the two.[148]

A thorough review of the methods available for the synthesis of phospholipids and their chemical precursors is already available[179] and the use of commercially available deuterium-enriched chemical reagents and the approaches possible for achievement of deuteration in various functional groups of the lipid molecules are described.[148] Many versions of fully or partially deuterated but saturated phospholipid species have been prepared in the ways previously described and are commercially available from Avanti Polar Lipids where fully deuterated versions of certain phosphatidylcholine species can also be synthesized on request (Table 5.1). Synthetic lipids can be deuterated in either the head-groups, the fatty acyl residues or both. Synthetic phospholipids can have saturated acyl chains or partially saturated acyl chains but their deuteration is a challenge due to possible oxidation during deuteration procedures.[179,199-201]

When chemical synthesis of deuterium-labelled lipids has proven difficult, or when uniformly labelled or perdeuterated lipids are required, microbial synthesis can be applied. Special bacterial strains of e.g. *Escherichia coli* adapted to tolerate the presence of D_2O have been used as non-specific deuteration of phospholipids can be achieved simply by growing the organism in culture media where D_2O is used instead of H_2O.[202] The incorporation of specifically deuterated components such as e.g. glycerol into phospholipids has be achieved by growing *E. coli* cells on culture media containing deuterated glycerol[203] and the same approach can be used with other phospholipid precursors. Microbiological approach is also often used as a tool to obtain perdeuterated fatty acids through culturing of cells on 100% D_2O culture medium. In the case of deuterated lipids produced through microbial synthesis these can easily be isolated from culture mass by conventional methods, including cell disruption, lipid extraction and subsequent chromatographic purification allowing for significant modifications to be

done after lipid separation.[204] The resulting phospholipid preparations are mixtures of homologues which differ in fatty acid length and degree of unsaturation. For deuterated protein microbial deuteration is the preferred and very well-established method, and using alternative carbon sources for large-scale preparations through fermentation has proven very successful.[149] Microbial deuteration which most often is done in *E. coli* as host systems offers a few challenges with regard to lipid deuteration with the major disadvantage being the limiting selection of native phospholipids that can be obtained in this way. Other organisms such as yeast have therefore also been used for preparation of certain phospholipids but have led to more challenging growth and purification conditions that accompany the higher organisms. Another disadvantage is the severe impairment of microbial growth in highly deuterated media which leads to lower yields and reduced biological mass activities.[149]

Finally the deuterium-enriched lipid fragments which are obtained through either chemical and/or microbial approaches can be assembled into phospholipids with any desired deuterium combination by means of organic synthesis and traditional methods employed in lipid chemistry.[148]

Table 5.1. Commercially available deuterated phospholipids (Avanti Polar Lipids)

Deuterium localization	**Phospholipid species**					
	PC[a]	**PE**	**PG**	**PA**	**PS**	**PI**
Head group	(14:0), (16:0) (18:0)					
Fatty acid (single)	(14:0), (16:0) (18:0) (16:0/18:1)	(16:0/18:1)	(16:0/18:1)	(16:0/18:1)	(16:0/18:1)	(16:0/18:1)
Fatty acid (both)	(6:0), (14:0) (16:0), (18:0) (16:0/18:1)	(14:0) (16:0) (18:0)	(14:0) (16:0) (18:0)	(14:0) (16:0) (18:0)	(14:0) (16:0) (18:0)	
Complete deuteration	(6:0), (14:0) (16:0),(18:0)					

[a]Abbreviations used are phosphatidylcholine (PC), phosphatidylethanolamine (PE), phosphatidylglycerol (PG), phosphatidic acid (PA), phosphatidylserine (PS) and phosphatidylinositol (PI).

Deuteration of phosphatidylcholine

Phosphatidylcholine, PC, is one of the most widely used phospholipids for the studies of structural organisation and the functioning of biological membranes and a major component of the eukaryotic cell membranes.[2] It is therefore one of the most commonly used phospholipids for reconstitution of membrane proteins into model membrane systems such as lipid vesicles, micelles and nanodiscs. Selectively deuterated versions of this phospholipid are highly sought after and can be exploited in structural techniques such as NMR, neutron reflectivity and small-angle neutron scattering.

The most convenient preparation method for deuterium-labelled phosphatidylcholines is through acylation of glycerophosphate derivatives instead of total chemical synthesis.[148] A choline head-group obtained through either chemical synthesis or in most cases through hydrolysis of natural e.g. egg-PC (lecithin) is modified according to the desired functional group deuteration.[205-207] The desired deuterated fatty acids are usually incorporated into the lipid molecules at the final stages of the synthesis due to their relatively high cost.[148] This approach allows the combining of various fatty acids to obtain many desired mixtures of deuterium-labelled and also perdeuterated PC species. Figure 5.1 shows the PC species available through Avanti Polar Lipids with a 16 carbon fatty acyl length. For the choline head-group it is possible to obtain such species where either the methyl and/or ethyl groups are deuterated while the glycerol is kept non-deuterated (Fig. 5.1*a*). PC lipids where one or both fatty acids are deuterated can be achieved for saturated species (Fig. 5.1*b*) while selectively deuterated choline moieties in combination with perdeuterated fatty acyl chains are also available for saturated species (Fig. 5.1*c*).

While PC has long been regarded as a typically eukaryotic phospholipid and thought only to occur in a few specialized photosynthetic bacteria it has now been found in approximately 15% of all bacteria.[208] It is typically synthesized through the methylation pathway or the CDP-choline pathway in eukaryotes while the N-methylation pathway and the phosphatidylcholine synthase pathway (Pcs) are the predominant synthesis methods in bacteria.[208] Nonetheless microbial deuteration of PC has not yet been fully exploited mainly due to *E. coli*, the most widely used organism for random deuteration biomolecules, being completely devoid of PC.[209]

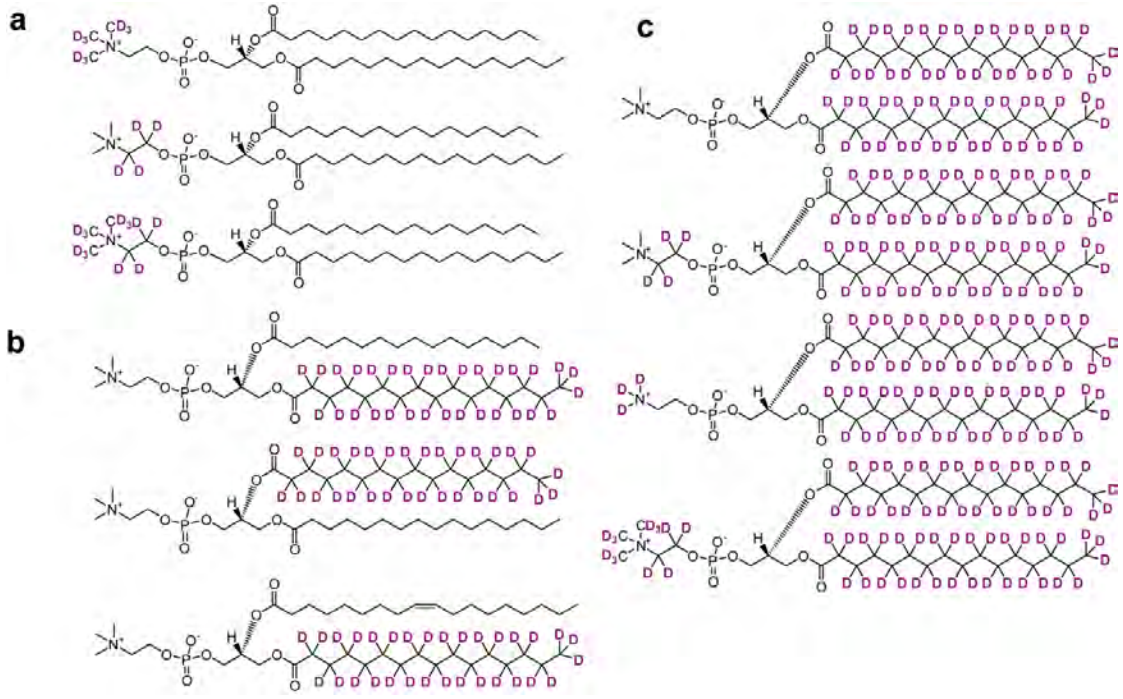

Figure 5.1. Commercially available deuterated 16-carbon PC species**. (a)** Head-group deuteration, **(b)** fatty-acyl deuteration and **(c)** over-all PC deuteration.

E. coli AL95, a mutant which can synthesize PC while completely lacking PE was recently engineered in order to study the effects of these most often used model-lipids on bacterial membrane proteins.[24] The strain, when carrying the plasmid pAC-PCSlp-Sp-Gm from *Legionella pneumophila* which codes for the phosphatidylcholine synthase (Pcs) gene, gives phospholipids which consist primarily of phosphatidylcholine (PC), phosphatidylglycerol (PG) and cardiolipin (CL) with mixed acyl unsaturated fatty acyl residues of 14 to 18 carbons in length.[24] This very simple lipid composition as compared to, for example, yeast,[210] in combination with an *E. coli* host, which usually can be deuterated to a very high degree,[174] makes this development a promising new vehicle also for the deuteration of physiological relevant PC facilitating both biosynthesis and the subsequent extraction and lipid isolation. This chapter focuses on the adaptation of AL95 and impact of cell growth in D_2O, characterization of the obtained PC and the accompanying *E. coli* lipids as well as the controlled, site-specific deuteration of three distinct parts; lipid head group, glycerol backbone and fatty acyl tail of the PC lipid molecule.

Materials and methods

Chemicals

All chemicals and solvents were obtained in the highest commercially available purity from Sigma-Aldrich A/S (Copenhagen, Denmark) and used as supplied unless stated otherwise. Deuterated glycerol (1,1,2,3,3-D5, 99%) and deuterated choline chloride (Trimethyl-D9, 98%) were from Eurisotop (ST-Aubin Cedex, France) and Silantes was purchased from Silantes GmbH (München, Germany). Phospholipid standards were purchased from Avanti Polar Lipids Inc. (Birmingham, AL, USA) and used as supplied. MALDI matrices used were the acidic 2,5-dihydroxybenzoic acid (DHB) as 0.5 M solution in methanol[187] and basic 9-aminoacridine (9-AA) hemihydrate (Acros Organics, Geel, Belgium) applied as 10 mg/ml solution in 60/40 (v/v) isopropanol/acetonitrile.[188] Thin-layer chromatography (TLC) silica gel 60 plates were from Merck (Darmstadt, Germany). Ultrapure water (Ultra Clear Basic, SG, resistivity 18.2 MΩ.cm) was exclusively used in all work.

Adaptation of AL95/pAC-PCSlp-Sp-Gm to minimal media

E. coli strain AL95 carrying the plasmid pAC-PCSlp-Sp-Gm which allows for the expression of PC synthase encoded by the *Legionella pneumophila pcsA* gene under control of an arabinose inducible promotor [189] was adapted to minimal deuterated medium after a multi-stage adaptation process according to a modified method by Artero *et al.* [175]. Briefly, a fresh overnight culture of AL95 strain carrying the plasmid and grown in Luria-Bertani broth (LB) supplemented with 50 mM $MgCl_2$ was diluted to an initial cell density of 0.95 (A_{600}) into flasks containing: 6.86 g/l $(NH_4)_2SO_4$, 1.56 g/l KH_2PO_4, 6.48 g/l $Na_2HPO_4{\cdot}2H_2O$, 0.49 g/l diammoniumhydrogen-citrate, 0.25 g/l $MgSO_4{\cdot}7H_2O$, 1.0 ml/l of a salt mix (0.5 g/l $CaCl_2{\cdot}2H_2O$, 16.7 g/l $FeCl_3{\cdot}6H_2O$, 0.18 g/l, $ZnSO_4{\cdot}7H_2O$, 0.16 g/l $CuSO_4{\cdot}5H_2O$, 0.15 g/l $MnSO_4{\cdot}4H_2O$, 0.18 g/l $CoCl_2{\cdot}6H_2O$, 20.1 g/l EDTA), with 5 g/l glycerol and 10 µg/ml gentamicin in H_2O. To ensure initial growth divalent metal ions in the form of 50 mM $MgSO_4$ solution were added to the flask cultures in addition to 10% Silantes rich medium. After overnight incubation at 37°C this process was repeated daily over a course of three weeks. After adaptation to non-deuterated minimal medium the cells were amplified (1 in 10) in minimal medium based on D_2O also containing 50 mM

$MgSO_4$ solution and 10% deuterated Silantes® rich medium. This process was then repeated for one week.

Preparation of deuterated phosphatidylcholine

The adapted starting cultures were amplified in minimal media containing different levels of D_2O (50-100%) in media [175] with 5% of either non-deuterated (Sigma Aldrich) or deuterated (1,1,2,3,3-D5, 99%, Eurisotop) glycerol. The cells were induced with 0.2% arabinose (Sigma Aldrich), and 2 mM deuterated choline chloride (trimethyl-D9, 98%, Eurisotop) as previously described.[189] After incubation at 37˚C for 24 h the cells were harvested by centrifugation (10,000 x g, 20 min, 4°C), and washed with MiliQ water.

The phospholipids were extracted and separated by silica gel chromatography as previously described (Chapter 5). The purified PC was analysed by MALDI-TOF mass spectrometry subsequent to PLA_2 digestion in order to determine the fatty acid composition as described in Chapter 5[193] and the data collection and analysis was done in collaboration with Dr. Jürgen Schiller from the University of Leipzig.

Deuteration level determination

The level of deuteration for the lipid species obtained from adapted AL95 preparations with varying level of D_2O were determined through comparison of the lipid species actual mass with calculated theoretical mass for its fully deuterated analogue and calculated using:

$$X_D = \frac{m_{DPC} - m_{HPC}}{m_{100\%\,DPC} - m_{HPC}} \tag{5.1}$$

Where m_{DPC} is the average mass obtained for the deuterated species, m_{HPC} is the mass of non-deuterated PC and $m_{100\%\,DPC}$ is the theoretical mass of fully deuterated PC.

NMR spectroscopy

The purified PC was analysed by H^1-NMR through and compared to commercially available PC as well as deuterated PC analogues synthesized in *E. coli.* All lipids were dissolved in chloroform-d (99.96%, 0.03 % (v/v) TMS) and all spectra were recorded with a Bruker Avance 300 MHz instrument. Assignments were aided by ^1H–^1H COSY. This data collection and analysis was done in collaboration with Dr. Mikkel B. Thygesen from the Chemistry Department at KU.

Results

Growing *E. coli* AL95/pAC-PCSlp-Sp-Gm bacteria in a deuterated medium required a process of adaptation.[177] Initial amplification of the strain in minimal medium according to the method of Artero *et al.*[175] (Fig. 5.2) resulted in no significant cell growth neither in non-deuterated nor deuterated conditions (data not shown). This result was expected as the auxotroph strain requires most amino acids and high amounts of divalent metal ions for growth.[189,211] Supplementation with 10% rich medium (Silantes®) was necessary to reach a cell density (OD_{600}) of two upon overnight growth (Fig. 5.3a black squares). After a three week long adaptation period of daily culture amplification using Silantes® medium in all preparations a significant increase in bacterial cell growth was observed resulting in cell densities (OD_{600}) of 9 for the adapted AL95 strain (Fig. 5.3a grey circles). After the initial adaptation phase the strain was able to grow on minimal medium without any kind of supplementation.

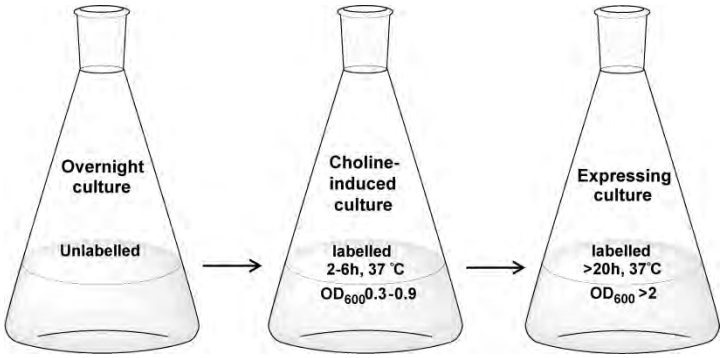

Figure 5.2. Schematic for the adaptation of AL95/pAC-PCSlp-Sp-Gm to deuterated minimal media. The overnight culture expressed in unlabelled media was amplified into labelled media containing choline as inducer followed by an overnight incubation period.

The adaptation to minimal medium led to substantial changes in the lipid composition of the strain. While AL95/pAC-PCSlp-Sp-Gm produced predominantly PC, PG and CL, with only a negligible contribution of PE, a clear reversion to high amounts of PE was detected in the adapted AL95 strain (Fig. 5.3*b*). It has previously been shown that magnesium is a requirement for PE suppression and that growth of the cells in the absence of high levels of divalent metal ions leads to increased levels of PE.[189,211] Therefore it is most likely that the relapse to a more wild type-like lipid composition in adapted AL95 was not due only to the deuterium isotope effect on the organism but was a result of the lower concentration of divalent metal ions used in the preparations.

Figure 5.3*c* shows the proportion of the four individual phospholipid classes in wild-type *E. coli* (WT), AL95/pAC-PCSlp-Sp-Gm before adaptation (AL95) and AL95/pAC-PCSlp-Sp-Gm after adaptation (Adapted AL95). Before adaptation the lipid composition of the PC producing strain consisted of up to 60% PC together with 40% CL and a small contribution (less than 1.5%) of PG. The well-adapted strain however showed more than 50% PE together with almost equal amounts of PC and PG, 22% and 23% respectively, and a small contribution (less than 1%) of CL. Even under conditions of the reversion to a more wild type-like lipid composition for the well-adapted strain the ability to synthesize PC was obvious, leading to a, for *E. coli*, new lipid composition of four phospholipids. This might explain the improved bacterial growth in minimal conditions as compared to AL95/pAC-PCSlp-Sp-Gm bacteria before adaptation and wild-type *E. coli*.

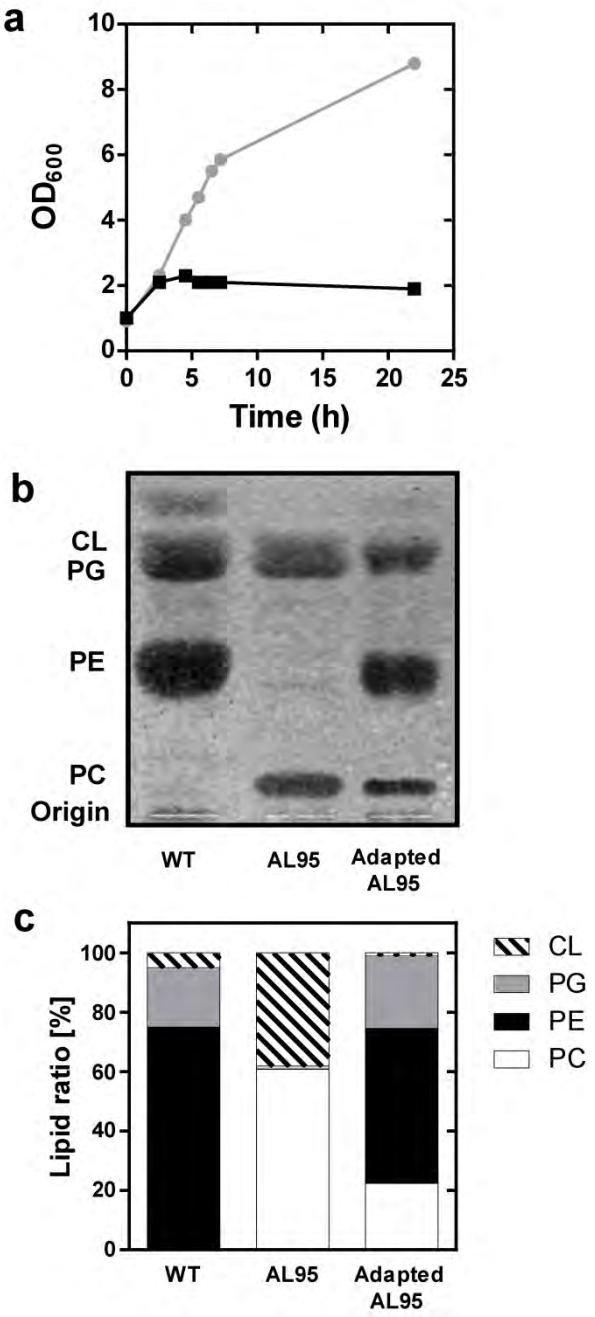

Figure 5.3. Adaptation of *E. coli* AL95/pAC-PCSlp-Sp-Gm to D_2O. (**a**) AL95 carrying the plasmid pAC-PCSlp-Sp-Gm growth curves in minimal deuterated medium with 10% Silantes® supplementation (black squares) and adapted AL95 in minimal medium without any supplementation (grey circles). Results are the means from two independent experiments; the S.D. is less than 5% of the mean for all data shown. (**b**) Total lipid extracts separated by thin-layer chromatography from wild -type *E. coli* (1), AL95 before adaptation to minimal medium (AL95) and after D_2O adaptation (Adapted AL95). Lipids were visualized by primuline staining. (**c**) Phospholipid composition of wild type *E. coli* (WT) and AL95 before adaptation (AL95) and after D_2O adaptation (Adapted AL95). Phosphatidylethanolamine, PE, (black), posphatidylcholine, PC, (white), phosphatidylglycerol, PG, (striped) and cardiolipin, CL, (grey). Results are the means from four independent experiments; the S.D. is less than 3% of the mean for all data shown.

Fatty acyl distribution of deuterated phospholipids from adapted E. coli AL95

After the initial adaptation process the adapted *E.coli* AL95 was cultured in deuterated medium and the phospholipids were extracted, purified using silica columns and characterized by mass spectrometry. For a preparation of Adapted AL95 where 100% D_2O was used together with deuterated glycerol as carbon source this gave a narrow distribution of highly deuterated phospholipid species enabling the determination of their fatty acyl composition (Fig. 5.4). Lipids extracted from the cells harvested in the stationary phase showed predominantly 1-palmitoyl-2-palmitoleoyl (16:0/16:1) PC and its cyclopropane modified analogue (16:0/17:0cyc) (Fig 5.5*a*).[212]

The species containing the cyclopropane residue was the most abundant as is usually the case with *E. coli* lipids, and was further analysed (Fig. 5.4). The peak maximum at *m/z* 810 (H^+ adduct) corresponded to the PC species where 63 hydrogen atoms are replaced by deuterium. This assignment could be made because it is known that 9-AA results primarily in H^+ adduct formation while the generation of Na^+ adducts (*m/z* 832) plays only a minor role.[188] In contrast to PC which is preferentially detected as positive ion, all other phospholipids of interest were more easily detectable in the negative ion mode. PE 16:0/17:0cyc and PG 16:0/17:0cyc were detected at *m/z* 769 and 802, respectively, which indicated the incorporation of either 66 or 68 deuterium atoms and, thus, gave data comparable to PC. Remarkably, there was in all cases a signal with a marked isotope pattern at *m/z* 769 (PC), 728 (PE) and 761 (PG). These signals could not be assigned so far. However, the mass difference in comparison to the most intense signals was always 41 mass units. This made an assignment even more difficult because the head-groups of all discussed phospholipids are different and, thus, the generation of fragment ions during the MS process was very unlikely. Although we were also able to detect some deuterated cardiolipin (CL) species, these particular species are not discussed here due to poor signal-to-noise ratio in accordance with a previous study on CL detection[213] and in particular since deuteration leads to an additional decrease of sensitivity.

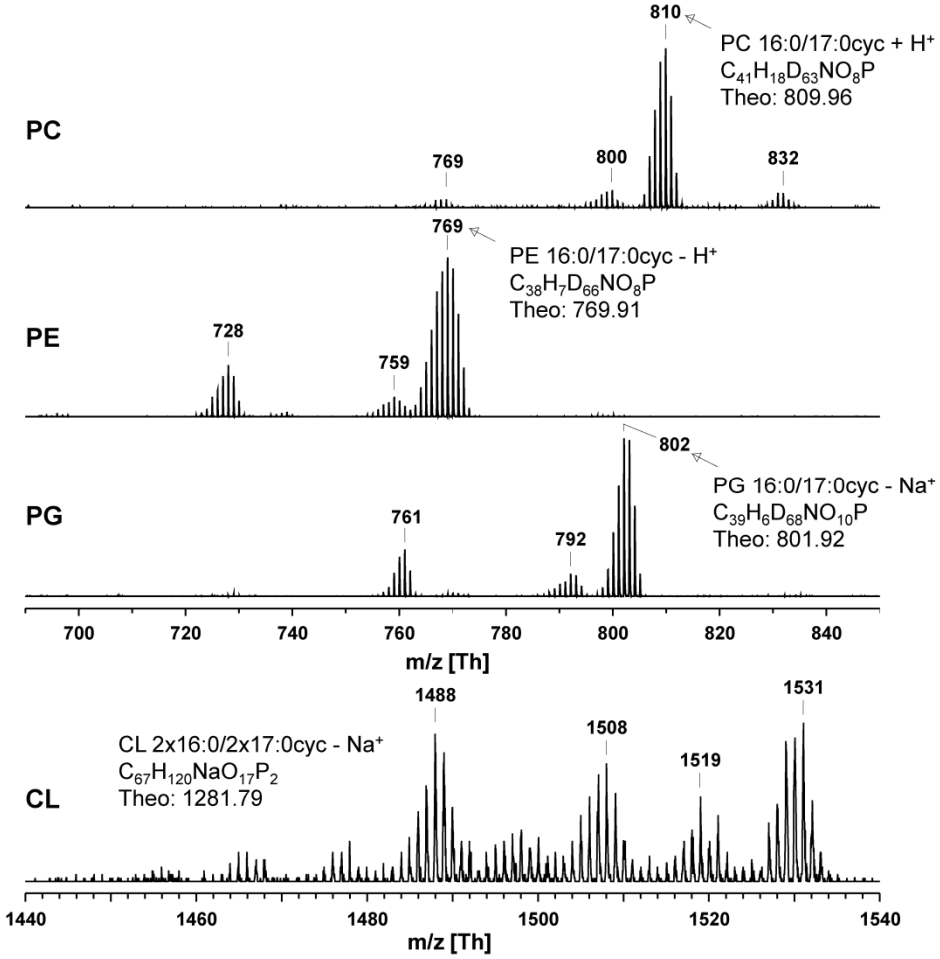

Figure 5.4. Positive phosphatidylcholine (PC) and negative ion (all other phospholipids) MALDI-TOF mass spectra of phospholipid species extracted from adapted AL95 grown in ~100% D_2O supplemented with deuterated glycerol and non-deuterated choline. Spectra were recorded in the presence of 9-aminacridine as the matrix and only the most abundant species 16:0/17:0cyc were investigated in more detail and compositional details are given exclusively for this species. Abbreviations: phosphatidylcholine (PC), phosphatidylethanolamine (PE), phosphatidylglycerol (PG), cardiolipin (CL). Although CL species were detectable, they were not investigated in more detail due to the poor signal-to-noise ratio.

Deuteration levels of phosphatidylcholine in adapted E. coli AL95

Adapted AL95 was cultivated in an increasing level of D_2O in order to monitor the effects of D_2O on the obtained PC species (Fig. 5.5*a*) where deuterated minimal medium ranged from 50% to 100% D_2O. This was done in presence of both deuterated and non-deuterated glycerol while the choline carbon source, used for induction, was kept non-deuterated.

The deuteration level for the resulting PC species was determined through comparison of the actual average mass with that of the theoretical mass of fully

deuterated species according to Equation 5.1. This calculation assumes that no major changes in the fatty acyl composition are present as a result of deuteration, as it was shown by comparing the highly deuterated species produced in 100% D_2O with the analogous lipids produced in H_2O (Fig. 5.4). As expected, the increased level of D_2O in the growth medium resulted in increased deuteration of PC for preparations with non-deuterated as well as deuterated glycerol (Fig. 5.5*b* black and red respectively). It was observed that the PC lipids biosynthesized in both 50% and 75% D_2O displayed a very broad *m/z* distribution when analysed by mass spectrometry. This was most likely a result of random deuterium incorporation in the lipid molecules leading to different species of partially deuterated PC and making the fatty acyl analysis challenging. Assuming 80 possible deuterium atoms for fully deuterated 16:0/17:0cyc PC it can be seen that with non-deuterated glycerol as carbon source the deuteration of the most abundant PC species increased from 21% to 83% (Fig. 5.5*b* black) while for the preparations with deuterated glycerol the deuteration of PC naturally increased from 43% to 90% (Fig. 5.5*b* red). Full deuteration was not observed for any of the species indicating that the non-deuterated choline chloride used for induction was also incorporated into the lipid molecules and lowered the overall deuteration levels.

NMR analysis of the PC extracted and purified from preparations grown in an increasing level of D_2O showed a gradual decrease of the ^{1}H-signal (Fig. 5.5*c*). This was most obvious for the large signal at 1.2 ppm corresponding to the hydrogens of the fatty acyl tails and which become increasingly deuterated with increasing level of D_2O in growth medium. The signals at 3.9 ppm and 4.4 ppm belonging to the ethylene hydrogens and the signal at 3.4 ppm corresponding to the methyl groups all belonging to the choline head-group were observed in all preparations where the supplemented choline was non-deuterated. The glycerol signals on the other hand at 4.0 ppm 4.2 ppm and 5.2 ppm were not observed in the preparations where deuterated glycerol was used as a supplement. These data indicated that the carbon source had an effect on the PC head-group deuteration while the increasing fatty acyl residue deuteration depended mainly on the total amount of D_2O. This is consistent with previous studies where fatty acyl residues obtained from *E .coli* cells grown in D_2O showed replacement of almost every hydrogen by deuterium without supplementation of deuterated carbon sources.[202]

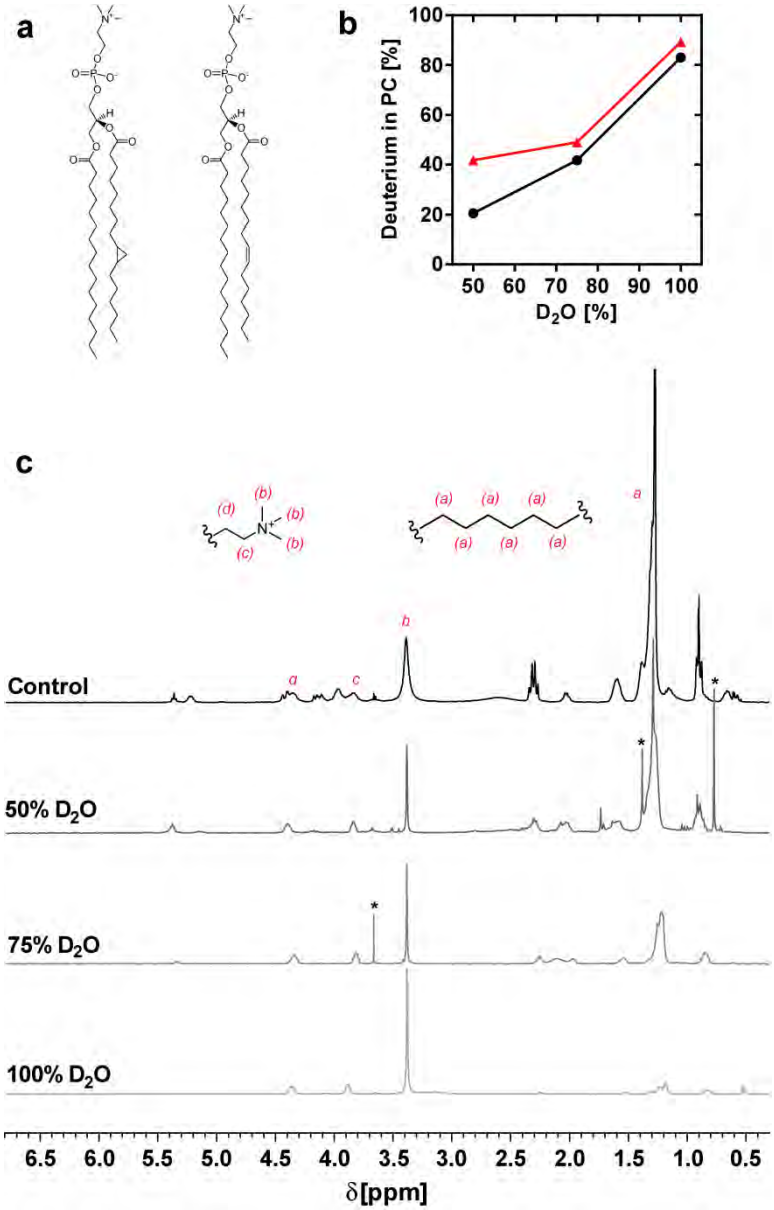

Figure 5.5. Increased levels of D_2O lead to increasingly deuterated phosphatidylcholine PC. (**a**) Most abundant PC species from adapted AL95 cultivated in non-deuterated medium and harvested in the stationary phase. (b) Level of deuteration in the PC molecule as a function of the D_2O level in the growth medium containing non-deuterated glycerol (black) and deuterated glycerol (red). Deuteration levels were calculated from mass spectrometry data through comparison of the average mass obtained with the calculated theoretical mass of fully deuterated species. (**c**) ^{1}H-NMR spectra of increasingly deuterated PC normalized to the intensity of choline ethylene resonance. From top to bottom: PC synthesized in AL95 under non-deuterated conditions (Control), PC produced in adapted AL95 cultivated in 50% D_2O (50% D_2O), PC produced in adapted AL95 cultivated in 75% D_2O (75% D_2O) and PC produced in adapted AL95 cultivated in 100% D_2O (100% D_2O) with deuterated glycerol and non-deuterated choline in the three preparations. *Insert:* hydrogen positions and the corresponding peaks are indicated with red letters for aliphatic methylene groups from increasingly deuterated medium and for choline methyl and ethylene groups from non-deuterated supplementation. The asterisks indicate signals of minor contaminants present in two of the samples.

Head-group deuteration of PC synthesized in adapted AL95

To determine the effect of deuteration for both glycerol and choline moiety of the PC head-group the adapted AL95 was cultivated in growth medium supplemented with deuterated glycerol (Fig. 5.6*a*) and deuterated choline (Fig. 5.6*b*) and their non-deuterated analogues according to Table 5.2.

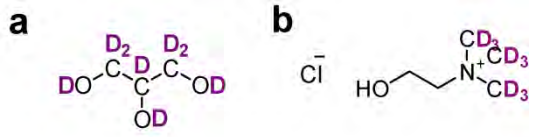

Figure 5.6. Deuterium-enriched carbon source supplementation to growth medium. (**a**) Glycerol $C_3D_8O_3$ and (**b**) choline chloride $C_5H_5D_9ClNO$.

Table 5.2. Deuterium variation in bacterial growth media

Growth media preparation	Carbon source isotope	
	Glycerol	Choline
$D_{gly}D_{cho}$	$C_3\mathbf{D}_8O_3$	$C_5H_5\mathbf{D}_9ClNO$
$D_{gly}H_{cho}$	$C_3\mathbf{D}_8O_3$	$C_5H_{14}ClNO$
$H_{gly}D_{cho}$	$C_3H_8O_3$	$C_5H_5\mathbf{D}_9ClNO$
$H_{gly}H_{cho}$	$C_3H_8O_3$	$C_5H_{14}ClNO$

The positive ion MALDI-TOF mass spectra of PC lipids synthesized in deuterated media at ~100% D_2O while varying the deuteration of both, the glycerol and the choline moiety, is shown in Figure 5.7. The PC species were compared to commercially available hydrogenated POPC and D_{31}-POPC (Avanti Polar Lipids) after digestion with phospholipase PLA_2 (that is known to cleave exclusively the fatty acyl chain in *sn*-2 position) to yield LPC 16:0 which helps to obtain a more accurate differentiation of both fatty acyl residues. This method was chosen because our MALDI MS does not possess a dedicated collision cell. The peaks at *m/z* 526.5 and 549.5 correspond to the respective proton and sodium adducts of 16:0 LPC with fully deuterated fatty acyl residues and a hydrogenated head. LPC was obtained from D_{31}-POPC after digestion with PLA_2 and showed a rather narrow mass distribution due to the lacking possibility of exchange reactions with the solvent. A similar mass distribution was also observed for highly deuterated preparations of PC obtained through *E. coli* biosynthesis. PC extracted from

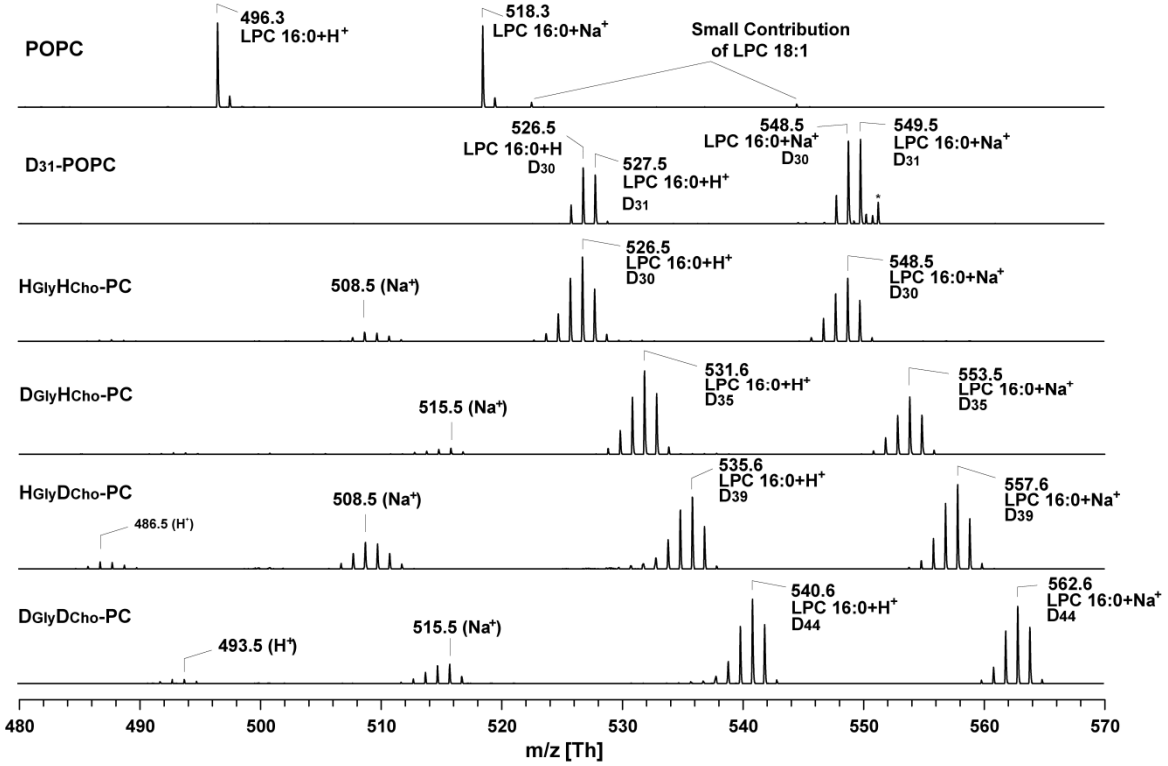

Figure 5.7. Positive ion MALDI-TOF spectra of the different species of purified PC extracted from adapted AL95 cultivated in deuterated media and varying carbon source deuteration subsequent to digestion with phospholipase PLA_2 shows selective deuteration. From top to bottom: synthetic hydrogenated LPC (POPC), synthetic LPC with hydrogenated head-group and deuterated fatty acyl chain (D_{31}-POPC), PC synthesized in 100% D_2O supplemented with H-glycerol ($C_3H_8O_2$) and H-choline ($C_5H_{14}ClNO$) ($H_{gly}H_{cho}$-PC), PC synthesized in 100% D_2O supplemented with D-glycerol ($C_3D_8O_2$) and H-choline ($C_5H_{14}ClNO$) ($D_{gly}H_{cho}$-PC), PC synthesized in 100% D_2O supplemented with H-glycerol ($C_3H_8O_2$) and D-choline ($C_5H_5D_9ClNO$) ($H_{gly}D_{cho}$-PC), PC synthesized in 100% D_2O supplemented with D-glycerol ($C_3D_8O_2$) and D-choline ($C_5H_5D_9ClNO$) ($D_{gly}D_{cho}$-PC). Peaks are marked with their *m/z* values and assignments are indicated.

cells cultivated with non-deuterated carbon sources ($H_{gly}H_{cho}$-PC) showed an almost identical profile as that of D31-POPC with major peaks at *m/z* 526.5 and 548.5 corresponding to the proton and sodium adduct of LPC 16:0, respectively. Deuterated PC extracted from cells cultivated with deuterated glycerol ($D_{gly}H_{cho}$-PC) showed an increase of exactly five amu as compared with $H_{gly}H_{cho}$-PC resulting in peaks at *m/z* 531.5 and 553.5. This favourably agrees with the mass of five deuterium atoms of the glycerol moiety in the lipid molecule. In contrast to this, the preparation of PC where deuterated choline was used together with non-deuterated glycerol ($H_{gly}D_{cho}$-PC) resulted in a mass difference of exactly nine amu (*m/z* 535.6 and 557.6) corresponding favourably to the nine available deuterium atoms from the supplemented choline. The $D_{gly}D_{cho}$-PC

preparation, where both carbon sources were deuterated showed peaks at *m/z* 540.6 and 562.6, i.e. an increase of 14 amu when compared to both $H_{gly}H_{cho}$-PC and D_{31}-POPC. This mass difference agrees well with the difference between the protonated and deuterated carbon sources added to the media with choline possessing nine and glycerol with five hydrogen atoms.

The extent of deuteration of the remaining cellular lipids from adapted AL95 preparations with varying deuterated carbon source (Table 5.2) was also determined by MALDI-TOF MS and the masses of the most abundant phospholipid species are summarized in Table 5.3. While deuterium enriched glycerol and choline had an effect on the deuteration of the obtained PC the remaining lipids were affected solely by glycerol. These data showed that choline was not metabolized into the WT *E. coli* lipids and confirmed the lipid synthesis pathways as suggested by Dowhan.[182]

Table 5.3. *m/z* values (determined by MALDI-TOF MS) of major lipid species from AL95 after deuterium variation in bacterial growth media

		Mass			
Lipid species		**$D_{gly}D_{cho}$**	**$D_{gly}H_{cho}$**	**$H_{gly}D_{cho}$**	**$H_{gly}H_{cho}$**
PC	16:0/17cyc	818	810	813	804
PE	16:0/17cyc	774	769	763	763
PG	16:0/17cyc	806	802	792	792

Deuterium localization in PC synthesized in adapted AL95

For PC species obtained from preparations of adapted AL95 cultivated in deuterated media and varying deuterated carbon sources (according to Table 5.2) the localization of the deuterium atoms within the head-group was investigated by ^{1}H-NMR (Fig. 5.8). The preparation of PC in the presence of non-deuterated carbon sources ($H_{gly}H_{cho}$-PC) showed a head-group identical to that of non-deuterated PC. The two signals seen at 4.04 ppm and 4.50 ppm in the $D_{gly}D_{cho}$-PC preparation (Fig. 5.8, $D_{gly}D_{cho}$-PC) were in agreement with the ethylene hydrogens of the choline head-group (Fig. 5.6). Although the deuterated species gave a chemical shift slightly downfield-shifted in comparison to the hydrogenated sample, these signals were present in all preparations and this could also be confirmed by ^{13}C-NMR (data not shown). The signal at 3.4 ppm assigned to the methyl groups of the choline moiety was present in both preparations of PC where non-deuterated choline was used ($H_{gly}H_{cho}$-PC and $D_{gly}H_{cho}$-PC). However this signal was

completely lacking in preparations where deuterated choline was used ($H_{gly}D_{cho}$-PC and $D_{gly}D_{cho}$-PC) confirming the direct choline incorporation into the PC head-group. Similarly, the ^{1}H signals at 4.0 ppm and 4.2 ppm as well as 5.2 ppm (corresponding to the glycerol backbone of the PC) were absent in preparations where deuterated glycerol was used ($D_{gly}H_{cho}$-PC and $D_{gly}D_{cho}$-PC) but were still present in PC obtained from preparations where the growth medium was supplemented with non-deuterated glycerol. The many small signals seen in NMR for the deuterated analogues (Fig. 5.5*c*) were associated with the acyl residues and indicated that the remaining hydrogens were randomly distributed throughout the fatty acyl chains.

The combined ^{1}H-NMR and MALDI-TOF data showed that both glycerol and choline were taken up by adapted AL95 and incorporated directly into the PC head-groups without modifications. The data presented clearly indicate that head-group deuteration of PC can be controlled by carbon source supplementation while the degree of deuteration for the fatty acyl chains is dependent on the total amount of D_2O in the media. Therefore, it should also be possible to prepare PC species with selective head-group deuteration while the fatty acyl chains are kept non-deuterated. Examples of the selectively deuterated PC species obtained at ~100% D_2O are illustrated in Figure 5.9.

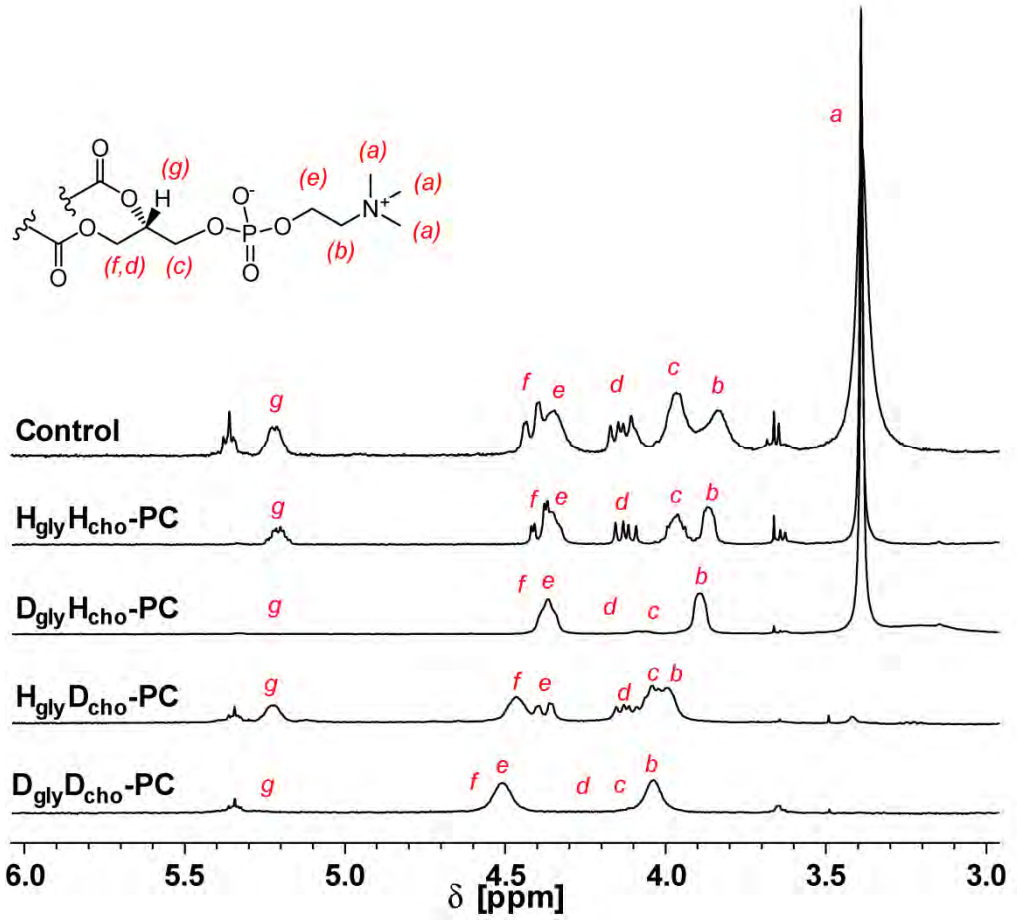

Figure 5.8. Selective head-group deuteration of phosphatidylcholine (PC) can be monitored through ^{1}H-NMR. From top to bottom: PC synthesized in AL95 under non-deuterated conditions (Control), PC synthesized in deuterated media containing hydrogenated glycerol and hydrogenated choline ($H_{gly}H_{cho}$-PC), PC synthesized in deuterated media containing deuterated glycerol and non-deuterated choline ($D_{gly}H_{cho}$-PC), PC synthesized in deuterated media supplemented with non-deuterated glycerol and deuterated choline ($H_{gly}D_{cho}$-PC) and PC synthesized in deuterated media with deuterated glycerol and deuterated choline ($D_{gly}D_{cho}$-PC). Spectrum intensities are normalized to the choline ethylene signals. Signals at 3.55 ppm originate from alkene protons. *Insert* PC head-group with hydrogen positions and their corresponding protons indicated by red letters.

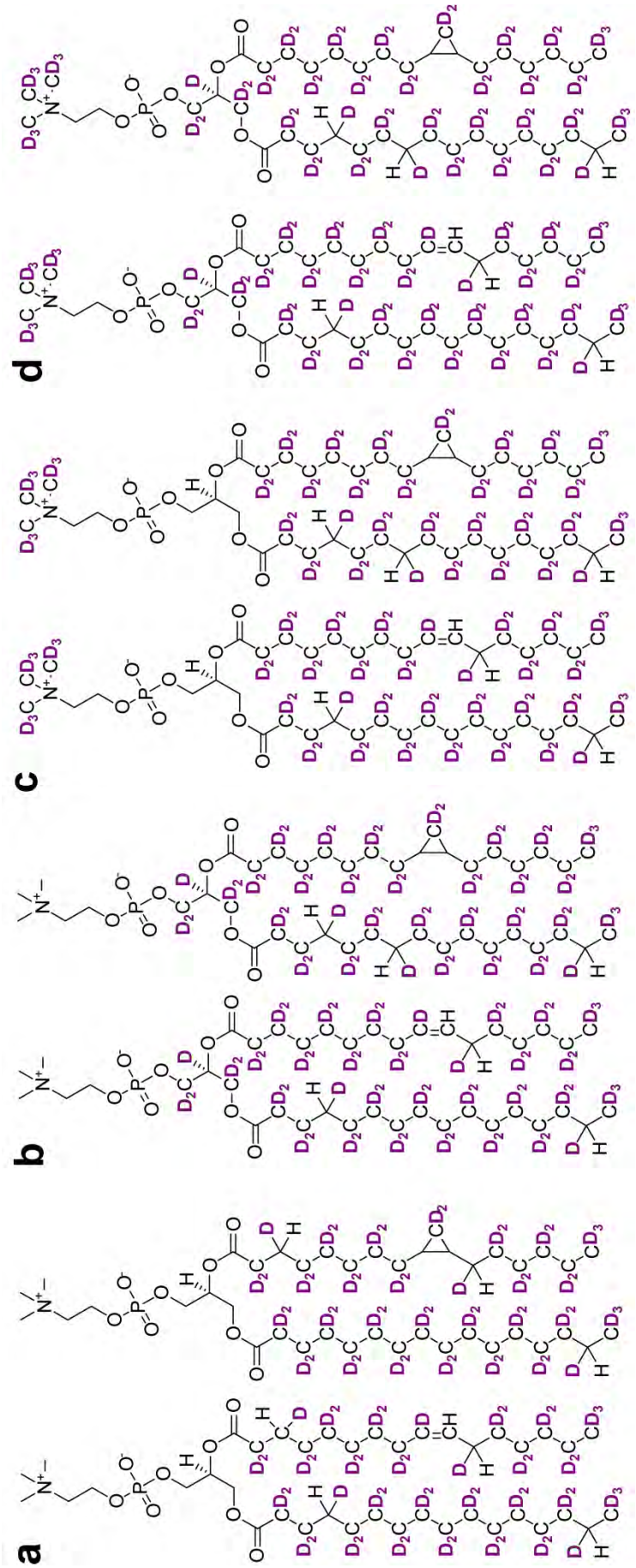

Figure 5.9. Molecular structures of the *E. coli* synthesized PC according to deuteration. Examples of main species for (**a**) PC synthesized in deuterated media containing both non-deuterated glycerol and non-deuterated choline ($H_{Gly}H_{Cho}$-PC). (**b**) PC synthesized in deuterated media supplemented with D_8-glycerol and non-deuterated choline ($D_{Gly}H_{Cho}$-PC). (**c**) PC synthesized in deuterated media containing non-deuterated glycerol and D_9-choline ($H_{Gly}D_{Cho}$-PC). (**d**) PC synthesized in adapted AL95 grown in deuterated media supplemented with D_8-glycerol and D_9-choline ($D_{Gly}D_{Cho}$-PC).

Discussion

Adaptation to deuterated conditions is harsh for any organism and in most cases is only possible at low levels of deuteration. Microorganisms appear to have considerable difficulty adapting to growth in D_2O as compared to adjusting to a single deuterated carbon source only.[177] For bacteria such as *E. coli*, the deuterium adaptation process, when successful, has been shown to lead to many unusual features.[177] In this work it was shown that the *E. coli* strain AL95/pAC-PCSlp-Sp-Gm, designed so that phosphatidylcholine (PC) replaces the native phospholipid phosphatidylethanolamine (PE), could be adapted to grow under fully deuterated minimal conditions. This was, however, accompanied by severe metabolic modifications of the strain as a function of the growth medium. The austerity of the adaptation process and the limiting choice of deuterated supplements, led to changes in both, auxotrophy and lipid composition, of the strain. A clear reversion towards the production of high amounts of PE was observed after the adaptation process as had previously been observed for preparations with insufficient Mg^{2+} concentration in the growth media.[189,211] While the adapted strain continued to produce PC, the adaptation process resulted in a novel lipid composition which was associated by an enhanced biomass production.

The yields of deuterated PC that could be obtained through the biosynthetic approach are in the range of 50 mg/l for flask cultures - clearly sufficient for use in techniques such as NMR, SANS and neutron reflectivity. Based on the amount of cell paste obtained in a pilot fermentation study, it is also possible to scale the production up to over 200 mg/l. While this is 100-fold lower in comparison to partial or perdeuterated synthetic PC, the approach allows access to partially and perdeuterated versions of the physiologically relevant PC lipids. The PC lipids can easily be extracted and purified in high yields using established methods. However, enabling purification procedures by means of preparative high-performance liquid chromatography (HPLC) may be preferable for large-scale preparations.

Mass spectrometry showed no major difference in fatty acyl length or degree of saturation for the biosynthetically deuterated PC species when compared to their hydrogenated analogues with possibilities for regulation of the fatty acyl composition during biosynthesis. The cyclopropenated residues are typical of *E. coli* lipids from cells harvested in the stationary growth phase[198] and have been shown to improve stability while maintaining the overall membrane fluidity[196,197] The fatty acyl distribution can be

regulated during the bacterial growth cycle [198] but harvesting cells in stationary growth phase is recommended if the highest biomass and therefore the highest yield of phospholipid is of interest for the lowest cost of deuterated medium.

The biologically produced PC lipids can be deuterated to a very high extent and the level of deuteration can be easily controlled by adjusting the total level of D_2O in the growth medium. Direct carbon source incorporation into the PC head groups provides additional control to selectively deuterate this part of the molecule through supplementation of selectively deuterated carbon sources to the growth media. While the *E. coli* strain AL95/pAC-PCSlp-Sp-Gm was originally engineered to test the effects of the eukaryotic model lipids on bacterial membrane proteins, this project showed that it can also be used as a production platform for physiologically relevant deuterium-labelled phosphatidylcholines and that this approach is also applicable for the deuteration of other physiologically relevant phospholipids and membrane components.

Chapter 6

Stealth carriers for low-resolution structure determination of membrane proteins in solution

Based on: Maric, S., Skar-Gislinge, N., Midtgaard, S. R., Thygesen, M. B., Schiller, J., Frielinghaus, H., Moulin, M., Haertlein, M., Forsyth, V. T., Pomorski, T. G., and Arleth, L. 2013. Stealth Carriers for Low-Resolution Structure Determination of Membrane Proteins in Solution, ***Acta Crystallographica Section D70.*** 317-328.

Introduction

Solution scattering studies of membrane associated proteins are accompanied with two major challenges today; obtaining the protein in a functionally active, soluble and structurally well-defined and relevant state and deriving the structural information from the very complex scattering data arising from the membrane protein and carrier system. Many model membrane systems such as detergent micelles, liposomes and nanodiscs have been developed for use as mimics to the native membrane environment and reconstitution of membrane proteins into such systems greatly aids their structural and functional studies.[31,71,72] Each of the so far established systems has different advantages as well as important limitations and care should be taken in choosing the most appropriate carrier for the application. The main focus of this study has been the well-tested and structurally well-defined nanodisc system,[74-76] where its defined carrier size makes it a promising new platform for structural studies of membrane proteins using solution scattering. However in cases of very large membrane protein complexes, where reconstitution into nanodiscs is not appropriate or where a more cell-like environment is desired, e.g. in electrolyte or pH gradient studies, lipid vesicles can be a better alternative and are therefore also discussed.

The Nanodisc Platform

Nanodiscs have proven excellent membrane-mimicking systems for studies of membrane anchored and integral membrane proteins under defined experimental conditions.[73,74] Their self-assembly is initiated when Bio-Beads are added to a mixture of MSP in aqueous suspension incubated with a phospholipid detergent mixture (Fig. 6.1).[92] After the removal of detergents by the Bio-Beads the self-assembled nanodiscs are purified using size-exclusion chromatography. In membrane protein reconstitution into nanodiscs the membrane protein of interest, also solubilized in detergent, is incubated with the initial mixture of MSP and phospholipids.[92] This is then followed by an additional affinity purification step for the separation of empty and membrane protein containing discs.[92] This self-assembly process has been optimized for several different phospholipid compositions and sizes. [74] The choice of detergents as well as optimal lipid-protein stoichiometry is important to obtain uniform discs while it is the length of the MSP that determines the nanodisc size.[74] Both reconstitution detergent as well final

nanodisc lipid composition should be chosen on the basis of the membrane protein of study, and have been shown to affect both membrane protein and the nanodisc stability.[73-75,159,214]

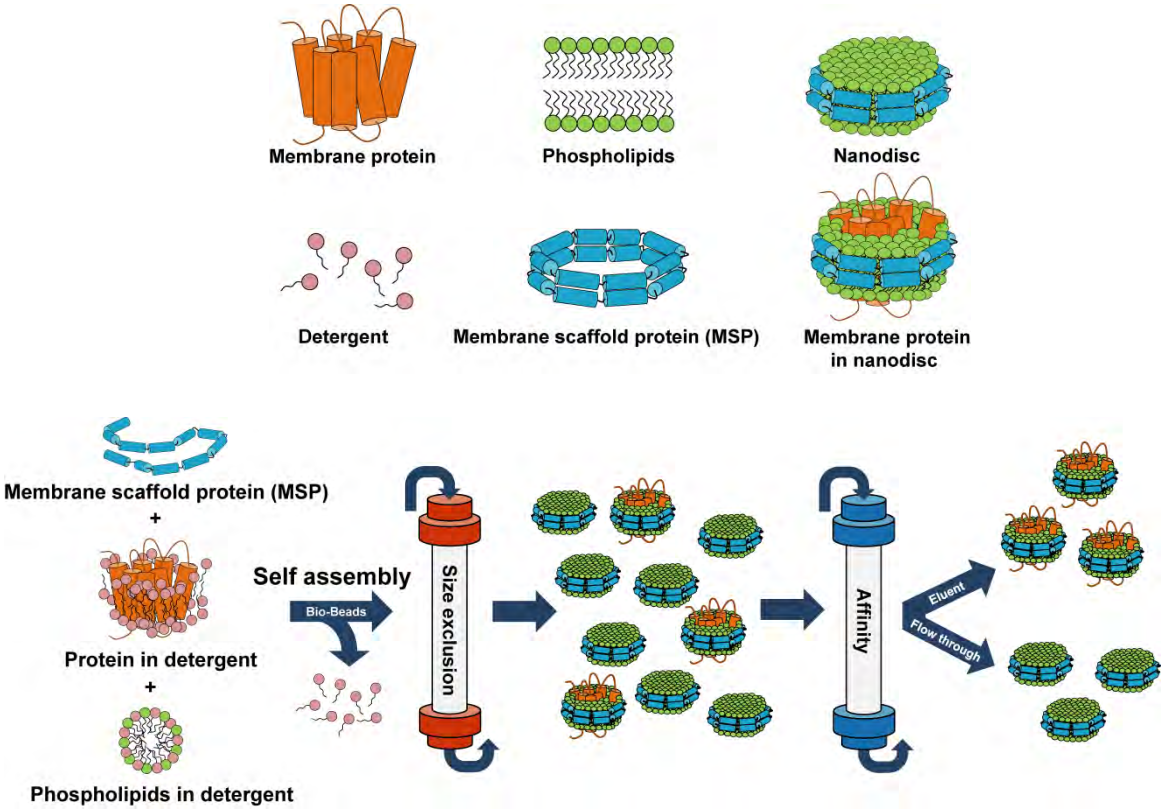

Figure 6.1. Nanodisc self-assembly process. For empty nanodisc assembly a mixture of membrane scaffold protein (MSP) in aqueous suspension is incubated with phospholipid detergent mixture. Upon addition of Bio-Beads detergent is removed which initiates the self-assembly process. After removal of detergents the nanodiscs are purified using size-exclusion chromatography. For membrane protein reconstitution the membrane protein of interest solubilized in detergent is incubated with the initial mixture of MSP and phospholipids and subsequently an additional affinity purification step is added for the separation of empty and full discs. Illustration based on Baas *et al.*[92]

The main advantage of the use of nanodiscs in membrane protein reconsitution is keeping the protein in a native-like environment that is soluble, stable and detergent-free. Proteins can in this way be isolated as individual particles in a monomeric or oligomeric state for analysis with a range of different functional and structural techniques. Since its first development in 2003 more than 100 membrane proteins ranging from transporters to different signaling receptors have succesffully been reconstituted into this system.[73]

Phospholipid vesicles

Unilamellar phospholipid vesicles are closed, spherical phospholipid structures consisting of a curved bilayer which enclose a part of the surrounding solvent inside their interior. They offer both a native-like membrane environment as well as compartmentalization and are more relevant when membrane transport through ion pumps and channels is studied. Unilamellar vesicles can be prepared in different sizes ranging from 30 nm to 150 nm or even in micrometre size, then termed giant unilamellar vesicles, which are easily observable using microscopy. These can be investigated using pipettes, optical tweezers and atomic force microscopy. Reconstitution of membrane proteins into lipid vesicles can be done through various methods but detergent intermediated reconstitution is usually preferred as it offers the most gentle and quick approach and many different detergent systems and detergent removal procedures tailored to particular proteins are available. One of the major limitations when it comes to solution scattering studies of membrane proteins using phospholipid vesicles is the overall concentration of membrane proteins that can be achieved in this system and difficulties in obtaining sufficiently large membrane protein to lipid ratio. However in cases of very large membrane protein complexes, where reconstitution into nanodiscs is not appropriate or where a more cell-like environment is desired, e.g. in electrolyte or pH gradient studies, phospholipid vesicles can still be a better alternative and development of stealth vesicle systems would greatly simplify the SANS data analysis also for these membrane mimics.

Phospholipid vesicles are formed when a thin lipid film is hydrated and the lipid bilayer self-closes. This prevents the water interacting with the hydrophobic fatty acyl chains of the lipid molecules leaving the hydrophilic head-groups facing the aqueous exterior to interact with the water molecules (Fig. 6.2). Once the multilamellar vesicles are formed several different methods have been developed to reduce the phospholipid vesicle size such as sonication or extrusion.

Reconstitution of membrane proteins into phospholipid vesicles can be achieved by combining a suspension of vesicles obtained by sonication or extrusion in aqueous medium with an isolated and detergent solubilized membrane protein. Upon removal of the detergent by either dialysis or Bio-Beads, spontaneous incorporation of the protein into the phospholipid bilayer will occur.

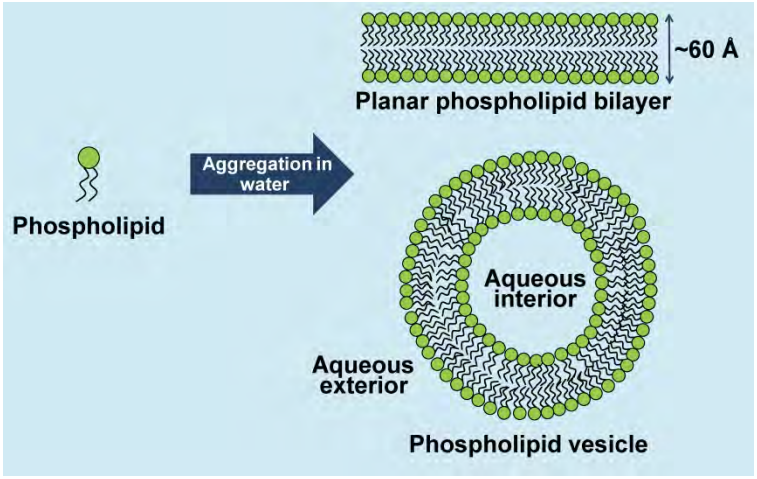

Figure 6.2. Phospholipid vesicle formation in water. Many phospholipids including phosphatidylcholines spontaneously form lipid bilayers when places in aqueous solution. The hydrophobic fatty acyl tails face each other to avoid the water while the hydrophilic head-groups face the outside environment and interact with the water molecules.

This chapter focuses on the assembly of specifically deuterated nanodiscs as well as vesicles, the subsequent SANS contrast variation study determining the match point that can be reached for these complex lipo-protein particle as well as the reconstituion of membrane proteins into the invisible discs.

Materials and Methods

Stealth Nanodisc Preparation

Selective deuteration of PC with the relevant scattering length density was described in Chapter 5. In short, to obtain PC with 78% deuteration in head-group and 93% in the fatty acyl residues adapted AL95 was cultivated in ~100% deuterated minimal media[175] containing 0.2% arabinose (Sigma Aldrich), 5% deuterated glycerol (1,1,2,3,3-D5, 99%, Eurisotop) and 2 mM deuterated choline chloride (trimethyl-D9, 98%, Eurisotop). After cultivation at 37˚C for 24 h the cells were harvested by centrifugation and PC extracted and purified as described elsewhere (Chapter 4).

Stealth nanodiscs were reconstituted using the deuterated version of MSP1D1 (Chapter 3) together with the deuterated stealth PC lipids through the previously described self-assembly based procedure.[74] All SAXS measurements were done in H_2O based buffer. Prior to the SANS measurements, the H_2O-based buffer used in the initial nanodisc preparation was substituted for a 100% D_2O based buffer solution using

centrifugal spin-filters with a cut-off of 50 kDa (Millipore). To achieve the H_2O/D_2O ratios required for the subsequent SANS measurements (60%-100% D_2O) the nanodisc stock solution in 100% D_2O was diluted with an adequate amount of H_2O buffer solution.

Stealth Liposome Preparation

Liposomes were prepared by extrusion of the stealth PC lipids in D_2O buffer solution (20 mM Tris-HCl, 100 mM NaCl, pH 7.5) through 100 nm polycarbonate filters (Avanti Polar Lipids Inc). Liposomes at different D_2O/H_2O ratios were achieved through dilution of the D_2O based liposome stock preparation with adequate amount of H_2O buffer solution (20 mM Tris-HCl, 100 mM NaCl, pH 7.5). This allowed for obtaining liposomes at 60%-100% D_2O for the subsequent SANS measurements. The liposome size was confirmed through dynamic light scattering on a BI-200SM System (Brookhaven Instruments).

SAXS Structural Analysis

The nanodiscs were characterized by SAXS using the Bio-SAXS instrument BM29 at European Synchrotron Radiation Facility (ESRF) in Grenoble as described in Chapter 3 for MSP1D1. All SAXS data were collected at 20°C a *q*-values ranging from 0.0040 1/Å to 0.45 1/Å with $q = 4\pi\sin\theta/\lambda$ using the fixed instrument setup[176] and the data were analysed using an already established approach for the nanodisc system.[77,78]

SANS Contrast Variation

All reported contrast variation SANS data were collected at 25°C at the KWS1 instrument at the Forschungs-Neutronenquelle Heinz Maier-Leibnitz (FRMII) in Munich while initial pilot data as well as the data from the nanodiscs prepared with commercially available POPC (Avanti Polar Lipids Inc) had been obtained at the D11 instrument at the Institut Laue-Langevin (ILL) Grenoble. All reported measurements from FRMII were performed with 4.5 Å neutrons with a wavelength spread $\Delta\lambda/\lambda$ of 10% FWHM. A combination of two to three instrumental settings were used to obtain a sufficiently wide *q*-range: High *q*-values (0.035 1/Å to 0.45 1/Å) were covered with a sample-detector distance of 1.5 m and a collimation length of 4 m. Intermediate *q*-values (0.0057 1/Å to 0.077 1/Å) were covered with a sample-detector distance of 8 m and a collimation length of 8 m. Low *q*-values (0.0022 1/Å to 0.03 1/Å) were covered with a sample-detector

distance of 20 m and a collimation length of 20 m. Due to the small size of the nanodiscs, these were only measured at high and intermediate *q*-values, while the liposomes, which have structural features ranging from the ~40 Å bilayer thickness to the ~1200 Å liposome diameter, had to be measured at all three settings. Absolute scale calibration was performed using a calibrated Plexiglas-sample as external reference and following the standard procedures at the facility. Radial averaging, background subtraction and absolute scale calibration to convert the data into scattering intensity, *I(q)* in units of cm^{-1} as a function of momentum transfer $q = 4\pi\sin\theta/\lambda$ (where θ is the half scattering angle and λ is the wavelength of the incoming beam) was carried out using the software QtiKWS.[215] This data reduction was done in collaboration with Søren Kynde from the Structural Biophysics group at NBI, KU. Small resolution effects were present in the SANS data, mainly due to the non-negligible wave-length spread of the incoming neutrons. These were taken into account in the subsequent model based data analysis by smearing of the fit-function with the calculated resolution function.[216] All samples were measured in flat rectangular Hellma quartz cells. The samples in 85% - 100% D_2O were measured in cells with a path length of 2 mm, whereas the samples in 60% - 80% D_2O were measured in cells with a path length of 1 mm in order to optimize signal-to-noise and minimize incoherent background and multiple-scattering effects.

Determination of Forward Scattering Intensity I(0)

For each contrast measurement the forward scattering was estimated by the indirect Fourier transform method with overlap optimization and background correction[138,217] and by taking the resolution effects into account.[216] The absolute scaled data for the liposome and nanodisc samples were normalized by sample concentration and the match points derived the standard way[218] by fitting a second order polynomial to the forward scattering plotted as a function of volume fraction of D_2O in the buffer solution. This forward scattering analysis was done in collaboration with Nicholas Skar-Gislinge from the Structural Biophysics group at NBI, KU.

Model Calculation of Liposomes

The theoretical scattering signal for D_{64}-POPC liposomes was calculated using the same approach and Fortran77 implementation of the analytical model as previously described.[219] However, to adapt the calculations to the D_{64}-POPC-case, the following total

lipid scattering lengths, *b*, and partial specific molecular volumes were applied: PC head group: $b = 6.0 \times 10^{-12}$ cm, $\upsilon = 319$ Å^3 and PO tail group: $b = 6.4 \times 10^{-11}$ cm, $\upsilon = 927$ Å^3. The model calculations assume that the liposomes are measured on a background of 100% D2O with a scattering length density of 6.38×10^{10} 1/cm^2. An average liposome radius of 500 Å in a Gauss-distribution with $\Delta\sigma/\sigma = 0.25$ was assumed, with a liposome bilayer thickness of 40 Å. This is an idealized model calculation which does not take into account incoherent background effects or other small effects that are typically present in the experimental situation and that contribute to the overall observed scattering.

Model Calculation of Protein Scattering Signal

The theoretical scattering signal for the epidermal growth factor receptor, EGFR, was based on a combination of available crystal structures Protein Data Bank (PDB) accession codes 1IVO, 1NQL, 2JWA, 1EGF and 2GS6 which were assembled manually using PyMOL [220] based on available structural information for the system.[221-225] Assuming one active dimer per nanodisc, the scattering data were then calculated using the program CRYSON.[226] The theoretical scattering signal for the CorA (PDB accession code 2BBJ)[227] were calculated using CRYSON assuming one pentameric complex per disc. The data were normalized in relation to the to nanodisc data by exploiting that the absolute forward scattering intensity for a dilute system of particles in solution can be calculated as $I(0)=nV^2(\Delta\rho)^2$ where n is the concentration (mol/l), V is the partial specific molecular volume of the protein, which is 1.35 g/cm^3,[170] and $\Delta\rho$ is the excess scattering length density of the (non-deuterated) protein in D_2O, which is $3 \cdot 10^{10}$ 1/cm^2.[133]

Results

Stealth Nanodisc Assembly

As previously explained, SAXS analysis of deuterated MSP1D1 on its own showed large disordered aggregates when dissolved in aqueous solution (data not shown), making subsequent SANS contrast variation investigations unreliable. However, by combining deuterated MSP1D1 (Fig. 6.3*a*) and the produced $D_{gly}D_{cho}$-PC (Fig. 6.3*b*) using the standard nanodisc preparation procedures,[74] a successful assembly of nanodiscs was achieved. Size exclusion chromatography showed an elution profile (Fig. 6.4*a*) commonly seen for hydrogenated nanodiscs.[74] A small shoulder seen on the

chromatogram indicated that the ratio of phospholipid to membrane scaffold protein was not at the optimal level for reconstitution. Non-optimal ratios can be due to slight discrepancies in concentration measurements when dealing with deuterated versions of the phospholipids and MSP and would lead to fractions of slightly larger lipid-protein aggregates. Therefore only the fractions thought to contain the typical size of nanodisc were used for further analysis (Fig. 6.4*a* green).

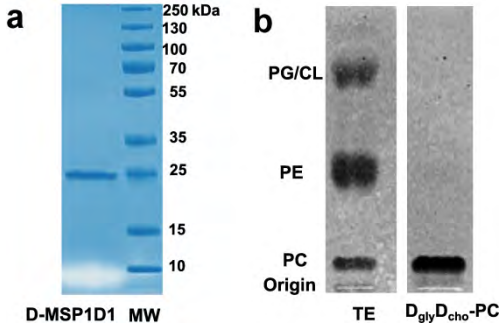

Figure 6.3. Deuterated nanodisc components (**a**) Commassie stained SDS-PAGE showing deuterated membrane scaffold protein D-MSP1D1used in the preparation of the stealth nanodiscs next to a molecular weight marker (Fermentas). (**b**) Thin layer chromatography of a total lipid extract (TE) obtained from a genetically modified *E. coli* strain (grown in deuterated media at ~100% D_2O in the presence of deuterated glycerol and partially deuterated choline) and of purified deuterated phosphatidylcholine PC ($D_{gly}D_{cho}$-PC). Cardiolipin (CL), phosphatidylglycerol (PG), phosphatidylethanolamine (PE) and PC. Lipids were visualised by primuline staining.

Successful nanodisc assembly was supported through SAXS analysis. The very distinct SAXS curve characteristic of the nanodisc system (Fig. 6.4*b* green) gave a *p(r)* function that indicated a maximum size of approximately 12 nm for the discs (Fig. 6.4*c*). This was consistent with the previously observed size of nanodiscs with attached his-tags which was also the case in this preparation.[77] Finally, a recently derived mathematical model for the nanodisc,[77,78] was fitted to the experimental data (Fig. 6.4*b* black) and confirmed that the SAXS data were fully consistent with nanodiscs having approximately the same structure as has previously been observed in our group.[77,78]

The SANS contrast variation study of the stealth nanodisc showed a systematic decrease in scattering intensity with an increasing level of deuterium in the solvent and revealed a clear minimum in the overall scattering intensity at 100% D_2O (Fig. 6.5*a*-*b*). This initial preparation of the stealth carriers did result in a small, residual signal for the nanodiscs which could be due to the aforementioned statistical fluctuations in deuteration of the lipids and the MSP1D1. The observed intensity decreased to a level only slightly

above that of the experimental background and was therefore difficult to measure accurately.

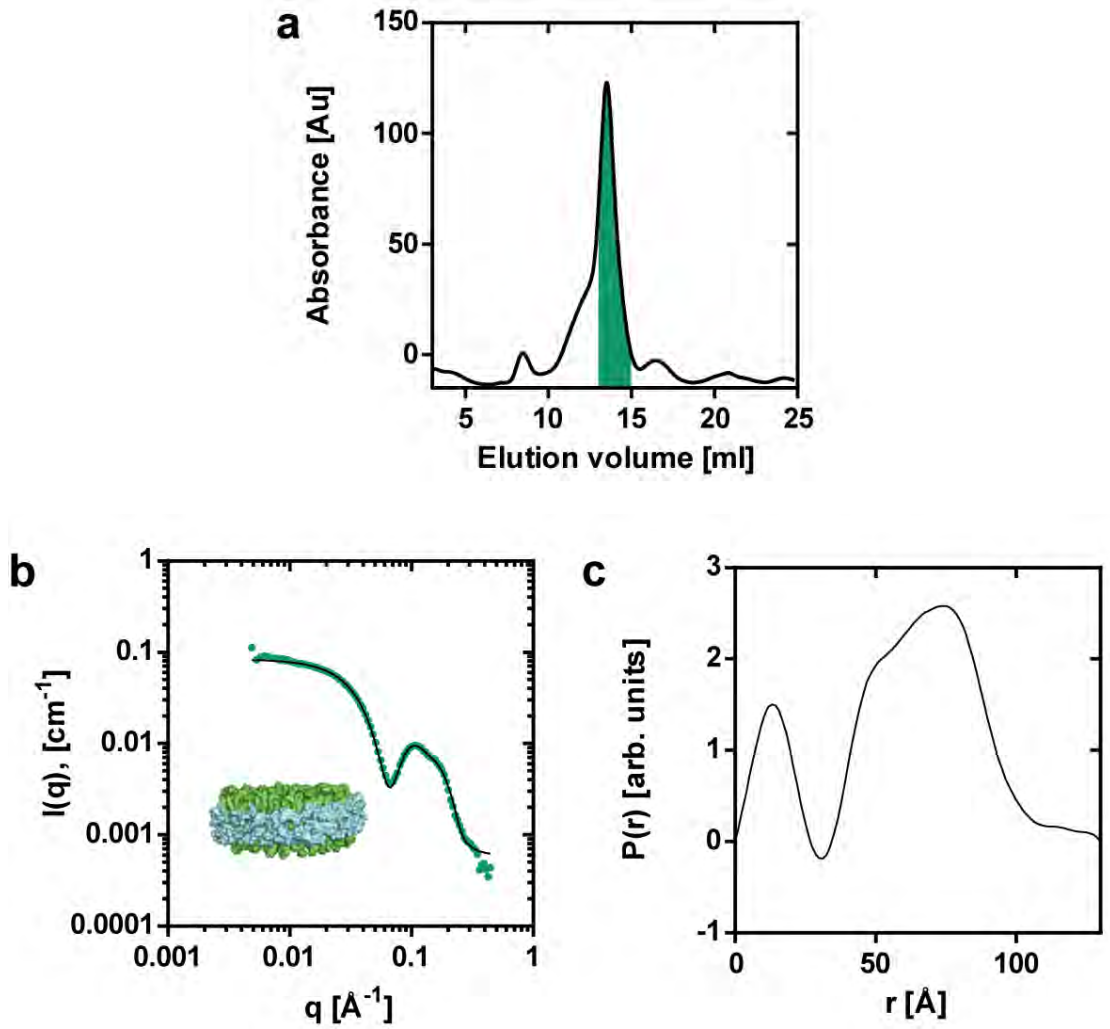

Figure 6.4. Assembly of deuterated stealth nanodiscs. (**a**) Size exclusion chromatogram (Superdex 200 10/300 GL, GE Healthcare) of the nanodisc assembled with $D_{glycerol}D_{choline}$-PC and D-MSP1D1 with the fractions used for further analysis marked in green. Absorption is monitored at 280 nm and displayed in arbitrary units (a.u.). (**b**) Small-angle x-ray scattering data from nanodiscs in H_2O (green) shown together with the fitted structural model (black). *Insert* shows a pdb of the nanodisc assembled in PyMol. (**c**) The pair distance distribution function for the stealth discs with information about the disc size.

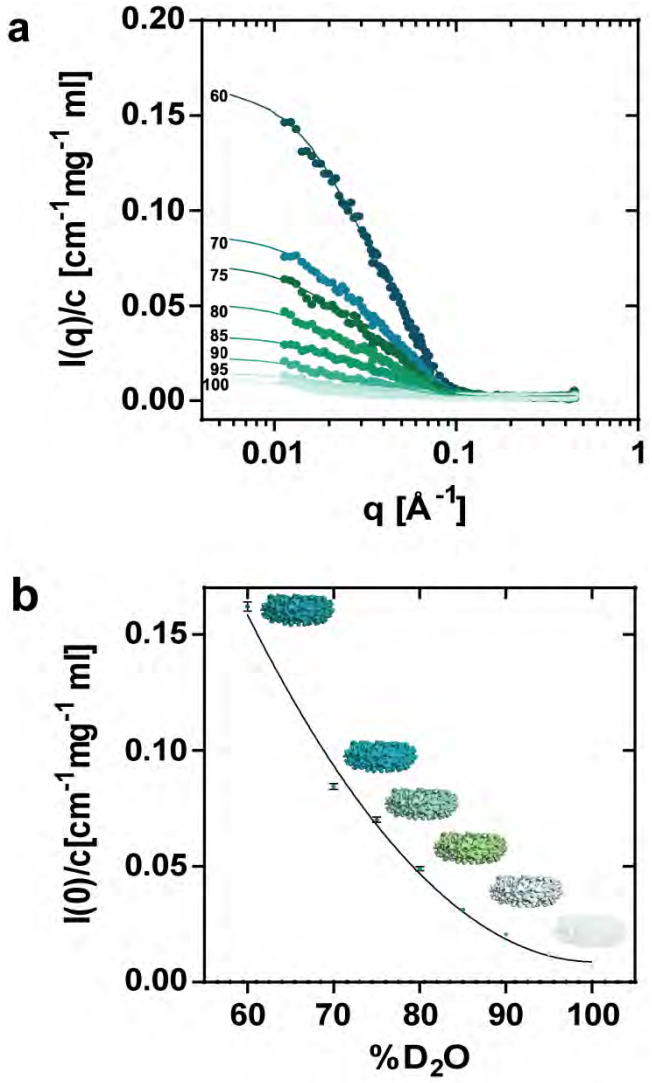

Figure 6.5. Stealth nanodisc SANS contrast variation**.** (**a**) SANS data together with IFT fits showing the decrease in scattering intensity from the stealth nanodiscs with the indicated increasing buffer contents of D_2O in solution. (**b**) SANS forward scattering as a function of the D_2O contents of the buffer.

Stealth Nanodisc Performance

In Figure 6.6*a* we compare the residual nanodisc signal to a SANS signal of a nanodisc assembled with D-MSP1D1 in combination with commercially available, chemically synthesized D_{64}-POPC (Avanti Polar Lipids) containing fully deuterated fatty acyl chains and protonated head-groups. These data were obtained at the D11 SANS instrument at ILL by Søren Roi Midtgaard from the Structural Biophysics Group at NBI, KU. While the forward scattering signals from both of the deuterated nanodisc samples are over ~150 fold lower than that of a protonated nanodisc (Fig. 6.6*b*) the biosynthesized

stealth nanodisc clearly shows an improvement in lowering the scattering intensity in the entire *q*-range when compared to the chemically synthesized version of the disc. An even better match-out could potentially be achievable through further optimization of the deuteration levels for both the lipid bilayer and the membrane scaffold protein.

In order to obtain insight into the potential performance of the developed stealth nanodiscs, a comparison of the residual stealth nanodisc signal was done with a range of possible protein targets of different sizes (Fig. 6.6*c*), where the theoretical scattering intensity was generated using the program CRYSON.[226] For the epidermal growth factor receptor (EGFR), where the complete structure is yet to be resolved, the scattering data were based on a manual assembly of the available structural parts[221-225] while for the other proteins the curves were generated using already available structural information.[86,228-231] For larger protein complexes such as the EGFR in one active dimer per nanodisc, a ~120 fold larger forward scattering intensity can be seen for the protein as compared to the stealth nanodisc carrier while for the CorA pentameric complex[227] the signal is ~45 fold larger than that of the stealth nanodisc. In such cases the signal from the nanodisc can to the first order be ignored, allowing for the use of the stealth nanodisc system in combination with already tested bead modelling and rigid-body approaches[232,233] to obtain a good low-resolution determination of the membrane protein structure.

In the case of smaller membrane protein systems, it would be beneficial to include a primitive model for the weakly scattering stealth nanodisc in order to resolve the membrane protein signal. In all cases, combining the bead modelling approach with an approximate model for the weakly scattering stealth nanodisc, should make it possible to further improve the structural resolution of the membrane protein towards the standard ~10Å resolution typically achievable from small-angle scattering data.

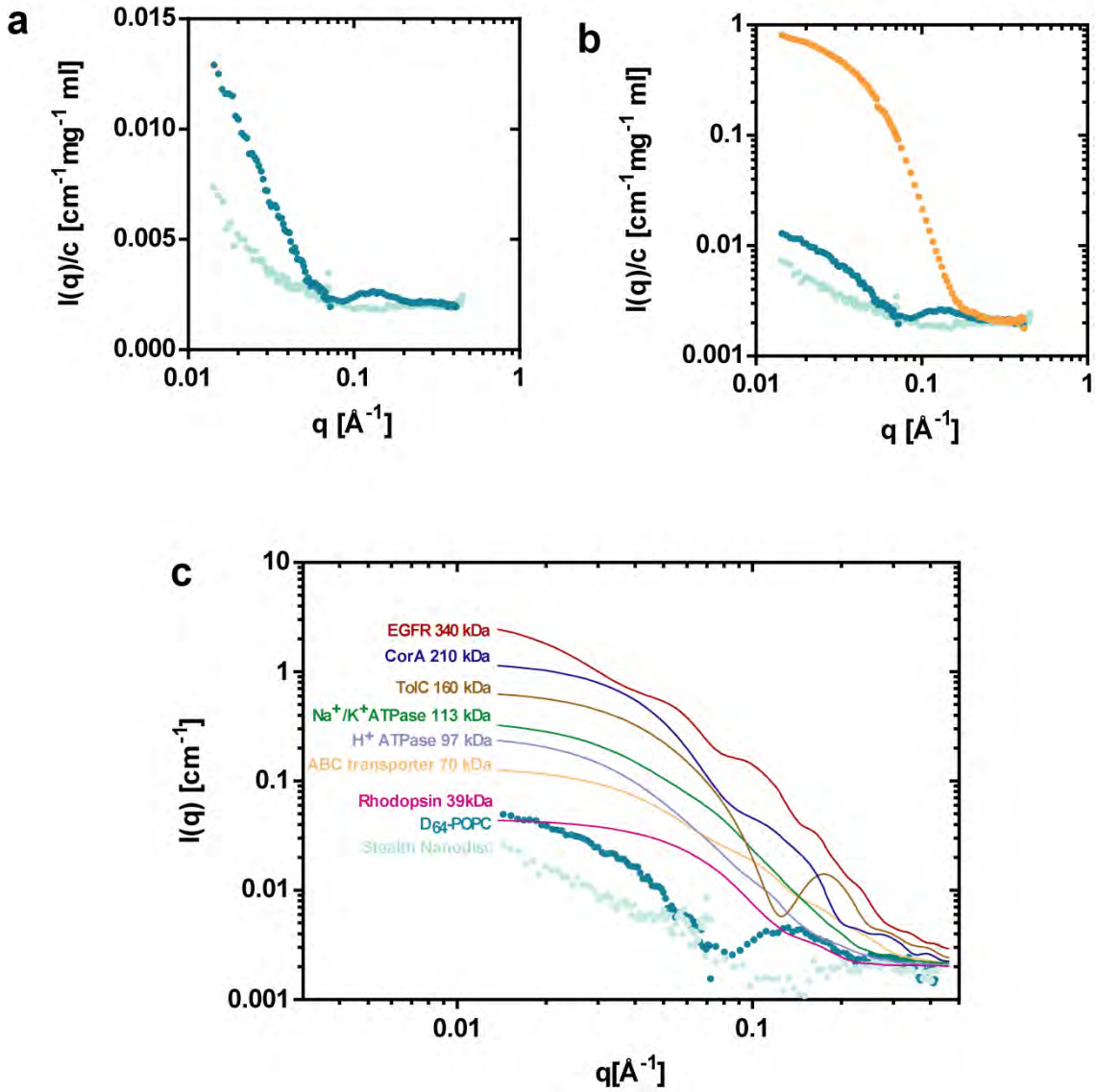

Figure 6.6. Comparison of stealth nanodisc SANS signal with synthetic lipids and model proteins. (**a**) Stealth nanodisc SANS data (light green) and SANS data measured for nanodisc assembled with D-MSP1D1 and commercially available D_{64}-POPC (Avanti Polar Lipids) (petrol). (**b**) shows a comparison of the two versions of deuterated discs (light green and blue) with protonated version of the nanodisc (orange) on a logarithmic scale. (**c**) SANS data from stealth nanodiscs in 100% D_2O (green) and D_{64}-POPC nanodiscs (petrol) shown together with the theoretical scattering signals for bovine rhodopsin in purple, ATP-binding cassette transporter (ABCB10) in orange, H^+-ATPase in light blue, Na^+/K^+ ATPase in green, trimeric TolC protein of *E. coli* in brown, bacterial magnesium transporter CorA in dark blue and the epidermal growth factor receptor EGFR in dark red. All scattering curves were generated using Cryson and pdb accession codes available for each protein (1F88, 4AYW, 3B8C, 2ZXE, 1TQQ, 2BBJ) while the EGFR structure was combined in PyMOL (http://www.pymol.org) using PDB accession codes: 1IVO, 1NQL, 2JWA, 2GS6 and 1EGF.

Stealth Liposome Assembly and Performance

Small unilamellar liposomes were prepared from the purified $D_{gly}D_{cho}$-PC (Fig. 6.3*b*). These stealth liposomes showed an average diameter of 110 nm when probed with dynamic light scattering. The liposome size was also confirmed through SANS, where model fitting[234] and the pair distance distribution function, *p(r)*, obtained by indirect Fourier transformation gave a maximum dimension of 120 nm Å (Fig. 6.7*a* insert). Contrast variation SANS data, collected over a broad *q*-range for the prepared liposomes at increasing D_2O contents in the buffer, showed a systematic decrease in scattering intensity with increasing level of D_2O (Fig. 6.7*a*). The minimum in scattering intensity for the liposomes derived from the SANS forward scattering as a function of D_2O contents is observed to be close to 100% D_2O (Fig. 6.7*b*).

A comparison of the scattering from the stealth liposomes to the theoretically expected results for the commercially available D_{64}-POPC deuterated lipids in 100% D_2O is provided in Figure 6.8. The plot shows that the forward scattering of the liposomes is minimized in the stealth lipid system. This is expected as the commercially available D_{64}-POPC-lipids are not matched out at 100% D_2O, which is the optimal contrast in order to maximize the signal-to-noise ratio of an inserted membrane protein. However, and more importantly, the oscillation at intermediate to high-*q*, present in the commercial system due to the different internal scattering length densities in the lipids, is much less visible in the stealth lipids. Since the scattering signal from a typical membrane protein is expected to be present in this region (Fig. 6.8*b*) this is an important result. Figure 6.8 also shows that while the biosynthetically produced lipids minimize the scattering from the liposomes, even though the scattering intensity at 100% D_2O is unfortunately not zero. A complete $I(q)=0$ is impossible to obtain due to internal deuteration-fluctuations within the single lipids. But the data indicates that an even better match-out could potentially be achieved through further fine-tuning of the growth conditions, which will be pursued in future work.

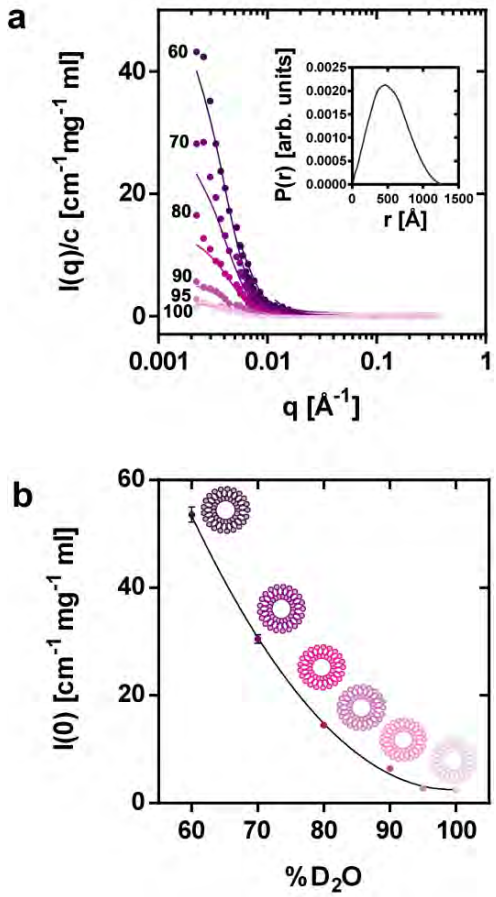

Figure 6.7. Stealth liposome SANS contrast variation. (**a**) SANS data together with IFT fits showing the decrease in scattering intensity from the stealth liposomes with the indicated increasing levels of D_2O in the buffer. *Insert* shows pair distance distribution function for stealth liposomes at 60% D_2O. (**b**) SANS forward scattering as a function of the D_2O contents of the buffer. Insert: a schematic representation of stealth liposomes with decreasing contrast in D_2O.

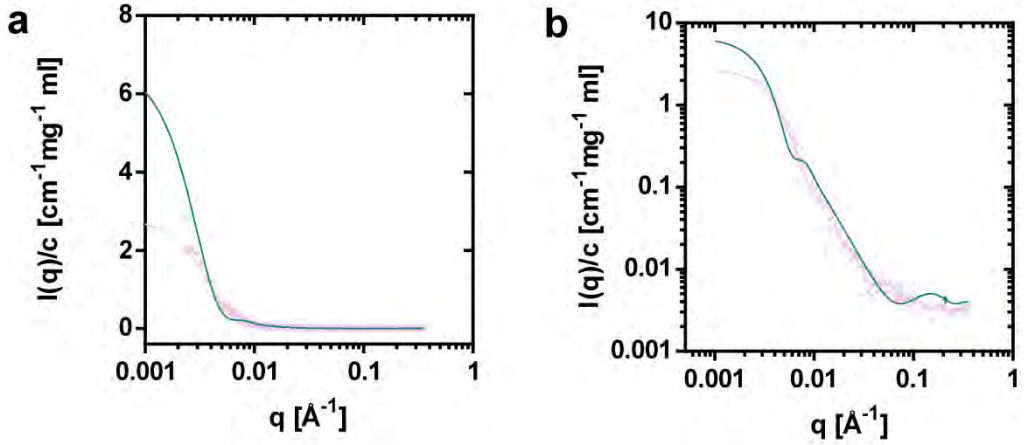

Figure 6.8. Stealth Liposome Performance. (**a**) Stealth liposome SANS data (light purple) and theoretical SANS data calculated for liposomes with commercially available D_{64}-POPC (Avanti Polar Lipids) (petrol). (**b**) A comparison of the two versions of deuterated liposomes (light purple and dark cyan) on a logarithmic scale.

Reconstitution of membrane proteins into stealth nanodiscs

As part of this thesis the first membrane protein was incorporated into selectively deuterated "stealth" nanodiscs and analysed by SAXS. Purified sensory rhodopsin II (SRII), provided by PhD student Pie Huda from the Structural Biophysics Group at NBI, KU, was reconstituted into stealth nanodiscs according to already available protocols.[74] Even though this is a small protein of ~25kDa in size it was chosen as a first assessment of protein incorporation and behaviour in the deuterated discs due to its availability, previously reported stability and a known structure obtained through crystallography.

SAXS data collected at the beamline BM29 at the European Synchrotron Radiation Facility (ESRF) are shown in Figure 6.9. SRII loaded nanodiscs showed an oscillatory behaviour similar to empty stealth nanodiscs (Fig. 6.4) however the specific shape of the scattering curve differs for the SRII as compared to empty discs (Fig. 6.9*a*). The oscillatory behaviour of both systems is characteristic of a lipid bilayer and is due to its mixture of positive and negative excess scattering length densities. The small tail which can be seen from the pair distance distribution function shows that there is a small percentage of aggregation in the sample (Fig. 6.9*b*). This gives a larger maximum size for the SRII containing discs as compared to empty discs (Fig. 6.4) which can be due to a small percentage of protein aggregates in the sample. There is also a possibility of dimerization of the SRII in a lipid environment as has been reported for the structures obtained through crystallography studies. However an additional contrast situation from SANS and modelling of the data is necessary to extract more information on the system.

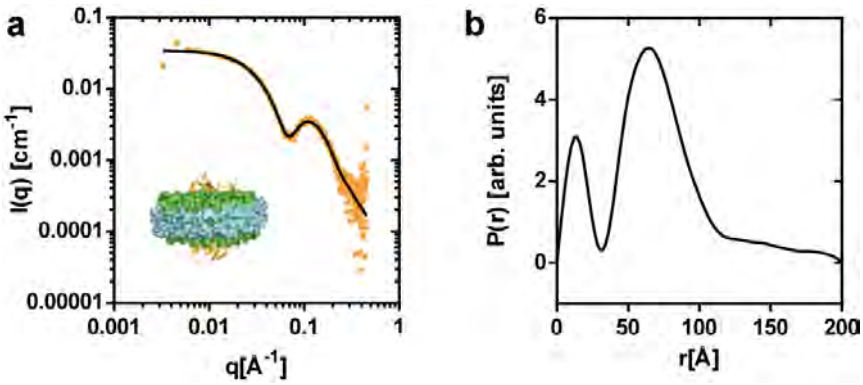

Figure 6.9. Reconstitution of sensoryrhodopsin II in stealth nanodisc. (**a**) SAXS experimental data for selectively deuterated nanodiscs with incorporated sensoryrhodopsin II (orange), Indirect Fourier Transform fit (black), *insert* pdb of nanodisc together with structure of sensory rhodopsin II combined in PyMOL (http://www.pymol.org) using PDB accession code 1h68. (**b**) Pair distance distribution function of sensoryrhodopsin II reconstituted in specifically deuterated discs. Indirect transform fit and pair distance distribution function were obtained using GNOM.

Discussion

The deuteration levels of physiologically relevant PC can be separately controlled for headgroups and tails via a biosynthetic pathway (Chapter 5). This includes targeted substitution of hydrogen by deuterium in the different parts of the phospholipid molecule through systematic addition of deuterated nutrients. Exploiting this development to prepare carrier systems for membrane proteins that become "invisible" to neutrons in 100% D_2O-based buffers offers a general approach to determine the low resolution structure of membrane proteins and their complexes in solution using already established SAXS/SANS data analysis methods.[103,104] These deuterated stealth carriers can be produced in sufficiently large amounts to facilititate SANS based structural studies of membrane proteins that are generally only available in small quantities.[108,109]

The SAXS analysis of the prepared nanodiscs showed that the overall disc structure did not change as compared to POPC nanodiscs that have previously been described.[77,78] This confirmed that the cyclopropane substitution of some of the double bonds on the PC unsaturated fatty acyl chain that occurs in *E. coli* during the stationary growth phase[198] and which should not affect the bilayer fluidity,[197] also did not affect nanodisc formation. Harvesting cells in this growth phase is therefore recommended as it leads to the highest biomass and consequently the highest yield of phospholipid for the lowest cost of deuterated media (Chapter 6). The fatty acyl distribution can also be regulated during the bacterial growth cycle[198] creating additional opportunities for the development of the stealth lipids.

In the case of the reported stealth nanodiscs and liposomes a residual signal is visible for both carriers when investigated with SANS in 100% D_2O. This signal is negligible by comparison with that of a possible protein signal in 100% D_2O as shown in the comparison of the nanodisc carrier with a range of model membrane protein signals. In these examples, the signal caused by the nanodisc can to a good approximation be ignored when reconstructing the low-resolution membrane protein structure from SANS data. For studies of small membrane proteins however with a size of ~50 kDa, where the membrane protein signal is also relatively weak in 100% D_2O, the residual nanodisc signal needs either to be incorporated in the data analysis or needs further reduction to achieve the same negligibility.

Stealth liposomes naturally give a larger residual signal than the nanodiscs, due to the much larger size of the particles. However, they can be used as an alternative carrier for larger membrane protein systems where reconstitution into nanodiscs is not appropriate or where a more cell-like environment is desired, e.g. in electrolyte or pH gradient studies.

For accurate and reliable data interpretation in terms of the structural parameters, the scattering data should be obtained from a pure and well-defined sample as with any other systems when studied by SAS. As with regular nanodiscs the reconstitution conditions should be optimized for each membrane protein under study.[74] Based on the initial stealth nanodisc assembly shown in this study, we do not foresee that the reconstitution conditions will differ significantly for these specifically deuterated nanodiscs. The use of D_2O based buffer in SANS has in unfavourable cases given rise to greater protein instability[235] which has compromised the data quality obtained from SANS measurements.

Nevertheless, for membrane protein complexes, the nanodisc-based approach of "mimicked-solubility" has already led to an improved understanding of membrane protein function in a more native-like environment [74] as well as structure, using e.g. NMR.[236] It is therefore anticipated that both the stealth nanodiscs as well as stealth liposomes will be a great advantage as "neutron-invisible" carriers to be used as a platform for SANS structural studies of membrane proteins in solution. Combined with the advancement of *ab-initio* and rigid-body modelling programs for structural data analysis and development of powerful, next generation neutron sources, data obtained through this development can lead to further insights into the dynamics, protein-ligand binding and conformational changes of membrane proteins in a solution environment. Collectively, this approach establishes the experimental basis for using the system for low-resolution structural studies of membrane proteins with the same data analysis tools already available for soluble proteins in solution.[103,104,106]

While the preliminary SAXS data of a membrane protein incorporated into stealth nanodiscs in the form of SRII show the possibility of incorporation of integral membrane proteins in deuterated discs for this protein system unfortunately the amount of SRII in stealth nanodiscs in this first reconstitution was insufficient for a reliable SANS analysis which requires a much higher sample amounts than SAXS. Further experiments are necessary to show the SANS scattering profile of an integral membrane protein in

invisible discs and experimentally prove the principle of this method. However reconstitution of a larger membrane protein system is then advisable to fully exploit this development.

Chapter 7

Conclusions and outlook

Due to its uniformity and well defined shape the nanodisc system shows great potential as a platform for small-angle scattering studies of membrane proteins. However at the moment there are two important limitations to this approach; obtaining pure and well defined samples of reconstituted membrane proteins in nanodiscs in sufficient amounts for both SAXS and SANS analysis and extracting the low resolution structural information on membrane proteins alone from data measured on complex multi-component systems. The first challenge probably has to be solved on a system to system basis while the latter has in principle been solved recently[79] but has thus far only resulted in the full modelling of a single system, namely the model-system bacteriorhodopsin in nanaodiscs using small-angle scattering.[79]

This thesis presents the development of a specifically deuterated, stealth nanodisc system which is optimised for SANS structural analysis of membrane proteins in solution. In combination with the D_2O/H_2O-based contrast variation method[133] it is demonstrated that it is possible to prepare specifically deuterated analogues of the nanodisc, which give minimal contribution to the neutron scattering data when used in 100% D_2O (Chapter 6). The stealth discs produced in this way should be generally usable in low-resolution structural studes of many membrane proteins and their complexes in solution as the analysis of SANS data for this platform is greatly simplified and allows for the application of existing data analysis tools already available for soluble proteins.

The reported prototype stealth carriers show a residual signal when investigated with SANS in 100% D_2O (see Chapter 6. Fig. 6.5). This signal is small by comparison with that of a possible protein signal in 100% D_2O as shown in the comparison of the nanodisc carrier with a range of model membrane protein signals and can for medium to large sized membrane proteins to a good approximation be ignored when reconstructing the low-resolution membrane protein structure from SANS data (see Chapter 6. Fig. 6). For studies of small membrane proteins with a size of ~50 kDa or less, where the membrane protein signal is also relatively weak in 100% D_2O, the residual nanodisc signal needs either to be incorporated in the data analysis or needs further reduction to achieve the same negligibility.

The possibility of incorporation of integral membrane proteins into the deuterated stealth discs was shown by SAXS analysis for sensory rhodopsin II (SRII) (Chapter 6. Fig. 6.9). However the first reconstitution resulted in sample amounts insufficient for a full and reliable SANS analysis which requires much higher sample amounts than SAXS.

Further experiments are therefore necessary to show the SANS scattering profile of an integral membrane protein in invisible discs and experimentally prove the principle of this method. However reconstitution of a larger membrane protein system is then advisable to fully exploit this development.

Selective deuteration of the nanodisc components

An important achievement during this thesis was obtaining selective partial deuteration of the nanodisc system necessary for the total matching at 100% D_2O, through an *E. coli* based biosynthesis for both deuterated phosphatidylcholines as well as membrane scaffolding protein. To obtain physiologically relevant deuterated phosphatidylcholine (PC) species with the required scattering length density a novel method for deuteration of PC was developed to separately control the deuteration levels of three different parts of the phospholipid molecule: the lipid head-group, glycerol-backbone and fatty-acyl tails (Chapter 5). This could be achieved via a biosynthetic pathway in a genetically modified *E. coli* strain adapted to growth in D_2O in combination with a systematic supplementation with deuterated nutrients.

The specifically deuterated lipids developed in this work could be suitable for studies of phospholipid packing and distribution inside the nanodisc system. For the nanodisc system it has been shown that mixing of different lipids such as the zwitterionic PC lipids with negatively charged phospholipids such as phosphatidylglycerol (PG) increases the stability of empty discs[159] (Article 1.) as well as membrane protein containing discs.[79] Theoretical calculations show that SANS studies of mixed lipid systems where one of the components is deuterated while the other is kept hydrogenated should yield sufficiently large difference in their scattering profiles to distinguish if there is a preference for the way the lipids pack inside the discs (Fig. 7.1), i.e. if the negatively charged lipids prefer to pack around the rim of the belts (Fig. 7.1*a*), in the centre of the discs or if the lipids are randomly distributed within the bilayer (Fig. 7.1*b*).

Same approach should be applicable on mixtures of PC lipids with different fatty acyl length. Specific deuteration of one type of lipid while the other is kept hydrogenated could give insights into the shape of nanodiscs composed of deuterated PC containing long fatty acyl chains (16:0/16:1 PC) and hydrogenated PC with shorter tails (12:0 PC) or vice versa. These should yield different scattering patterns when measured using SANS based on their distribution within the discs and the clustering of deuterated lipids

within the disc centre should yield a scattering pattern for hollow discs while the opposite should result in a scattering profile corresponding to smaller sized discs (Fig. 7.1*c*-*d*).

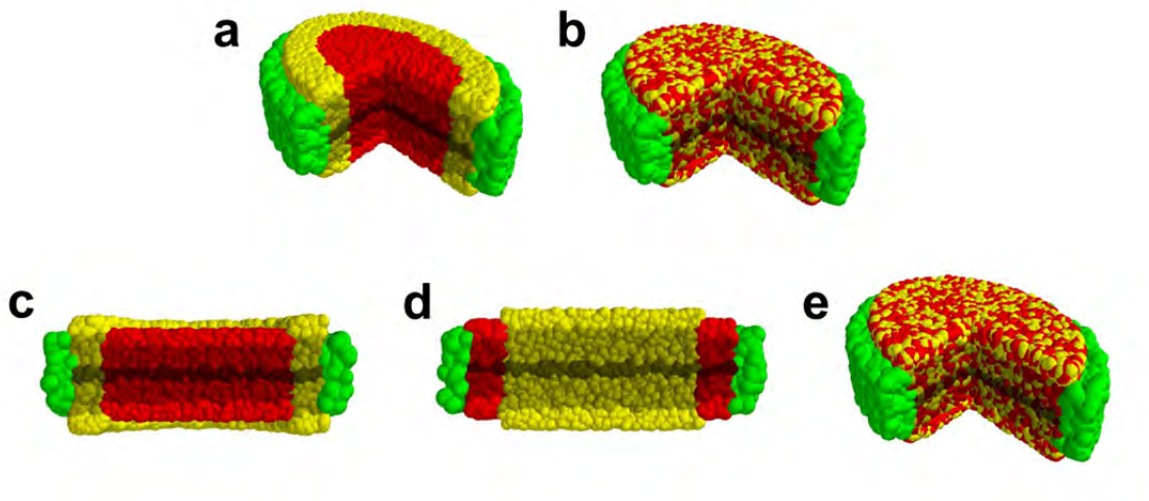

Figure 7.1. Nanodisc models composed of MSP (green) and mixtures of phopsholipids. (**a**) 50% phosphatidylglycerol (PG) (yellow) and 50% phosphatidylcholine (PC) (red) where PG is localized around the rim of the MSP and PC lipids are localized in the centre of the disc. (**b**) PG and PC are randomly distributed within the bilayer. (**c**) Nanodisc model composed of MSP (green) and mixture of 50% 1-palmitoyl-2-palmitoleoyl -*sn*-glycero-3-phosphocholine (16:0/16:1 PC) (yellow) and 50% 1,2-didodecanoyl-*sn*-glycero-3-phosphocholine (12:0 PC) (red) and 50% PC (yellow). Long chain lipids are localized around the rim of the nanodisc belts, (**d**) long chain lipids are localized in the centre of the disc and (**e**) both lipid types are randomly distributed inside the discs. Theoretical calcualtions and models were prepared by PhD student Martin Cramer Pedersen (Niels Bohr Institute).

The deuteration approach through biosynthesis allows the production of different types of specifically deuterated physiologically-relevant lipid species that can be exploitable using other structural techniques such as NMR and neutron reflectometry. In NMR studies of complex protein-lipid systems a complete cancelling of the ^{1}H signal through the use of fully deuterated PC leads to significant simplification in data analysis[236] while physiologically relevant PC may provide better stability for the incorporated membrane protein.[2] In neutron reflectometry, on the other hand, the advantages lie in obtaining different contrasts in different parts of the lipid bilayer which can be controlled through different deuteration levels thus highlighting specific parts.[237] This can then be exploited in studies of not only the effect of the lipid environment on membrane protein systems but also for studies of various ligands and potential drugs and their interactions with the membrane.[238] In this context, using the lipids for understanding

e.g. the interactions of antimicrobial peptides with bacterial membranes could lead to novel insights crucial for solving the increasing problem of antibiotic resistance of more and more bacterial strains.[239]

Specifically deuterated physiologically relevant phospholipids have many applications however the microbial approach for the synthesis of such lipids, resulted in yields sufficient for SANS based structural studies of membrane proteins that are generally only available in small quantities.[108,109] Further optimization of the phospholipid synthesis and isolation is necessary if large-scale preparation of deuterated lipids is of interest. For preparation of other phospholipids using the same approach such as for example phosphatidylserine (PS) the use of an autotroph strain is recommended as the amplification of the auxotroph *E. coli* strain AL95 in minimal media according to the method of Artero *et al*[175] resulted in substantial changes of the lipid composition. Also the purification set-up used throughout this work resulted in smearing of lipids of similar polarity such as PG and cardiolipin (CL), significant amounts of lysoPC following the long purification times at room temperature and the use of large amounts of organic solvent mixtures. Automation through preparative HPLC systems in combination with other possibly more optimal and less toxic solvent systems is therefore recommended as the next step.

References

1 Vance, D. E. & Vance, J. E. *Biochemistry of lipids, lipoproteins, and membranes*. 4th edn, (Elsevier, 2002).

2 van Meer, G., Voelker, D. R. & Feigenson, G. W. Membrane lipids: where they are and how they behave. *Nature reviews. Molecular cell biology* **9**, 112-124, (2008).

3 van Meer, G. & de Kroon, A. I. Lipid map of the mammalian cell. *Journal of cell science* **124**, 5-8, (2011).

4 Dowhan, W. Molecular basis for membrane phospholipid diversity: why are there so many lipids? *Annu Rev Biochem* **66**, 199-232, (1997).

5 Gorter, E. & Grendel, F. On Bimolecular Layers of Lipoids on the Chromocytes of the Blood. *The Journal of experimental medicine* **41**, 439-443, (1925).

6 Danielli, J. F. & Davson, H. A contribution to the theory of permeability of thin films. *J Cell Compar Physl* **5**, 495-508, (1935).

7 Singer, S. J. & Nicolson, G. L. The fluid mosaic model of the structure of cell membranes. *Science* **175**, 720-731, (1972).

8 Lee, A. G. How lipids affect the activities of integral membrane proteins. *Bba-Biomembranes* **1666**, 62-87, (2004).

9 Jensen, M. O. & Mouritsen, O. G. Lipids do influence protein function - the hydrophobic matching hypothesis revisited. *Bba-Biomembranes* **1666**, 205-226, (2004).

10 Andersen, O. S. & Koeppe, R. E. Bilayer thickness and membrane protein function: An energetic perspective. *Annu Rev Bioph Biom* **36**, 107-130, (2007).

11 Marsh, D. Protein modulation of lipids, and vice-versa, in membranes. *Bba-Biomembranes* **1778**, 1545-1575, (2008).

12 Engelman, D. M. Membranes are more mosaic than fluid. *Nature* **438**, 578-580, (2005).

13 McMahon, H. T. & Gallop, J. L. Membrane curvature and mechanisms of dynamic cell membrane remodelling. *Nature* **438**, 590-596, (2005).

14 Zimmerberg, J. & Kozlov, M. M. How proteins produce cellular membrane curvature. *Nature reviews. Molecular cell biology* **7**, 9-19, (2006).

15 Zimmerberg, J. & Gawrisch, K. The physical chemistry of biological membranes. *Nature chemical biology* **2**, 564-567, (2006).

16 Phillips, R., Ursell, T., Wiggins, P. & Sens, P. Emerging roles for lipids in shaping membrane-protein function. *Nature* **459**, 379-385, (2009).

17 Epand, R. M. Lipid polymorphism and protein-lipid interactions. *Bba-Rev Biomembranes* **1376**, 353-368, (1998).

18 Soubias, O., Teague, W. E., Hines, K. G., Mitchell, D. C. & Gawrisch, K. Contribution of Membrane Elastic Energy to Rhodopsin Function. *Biophysical journal* **99**, 817-824, (2010).

19 Perozo, E., Kloda, A., Cortes, D. M. & Martinac, B. Physical principles underlying the transduction of bilayer deformation forces during mechanosensitive channel gating. *Nature structural biology* **9**, 696-703, (2002).

20 Gibson, N. J. & Brown, M. F. Membrane lipid influences on the energetics of the metarhodopsin I and metarhodopsin II conformational states of rhodopsin probed by flash photolysis. *Photochemistry and photobiology* **54**, 985-992, (1991).

21 Gibson, N. J. & Brown, M. F. Lipid headgroup and acyl chain composition modulate the MI-MII equilibrium of rhodopsin in recombinant membranes. *Biochemistry* **32**, 2438-2454, (1993).

22 Mitchell, D. C. & Litman, B. J. Effect of protein hydration on receptor conformation: decreased levels of bound water promote metarhodopsin II formation. *Biochemistry* **38**, 7617-7623, (1999).

23 van den Brink-van der Laan, E., Killian, J. A. & de Kruijff, B. Nonbilayer lipids affect peripheral and integral membrane proteins via changes in the lateral pressure profile. *Biochimica et biophysica acta* **1666**, 275-288, (2004).

24 Bogdanov, M., Heacock, P., Guan, Z. & Dowhan, W. Plasticity of lipid-protein interactions in the function and topogenesis of the membrane protein lactose permease from Escherichia coli. *Proceedings of the National Academy of Sciences of the United States of America* **107**, 15057-15062, (2010).

25 Phillips, M. C., Ladbrooke, B. D. & Chapman, D. Molecular interactions in mixed lecithin systems. *Biochimica et biophysica acta* **196**, 35-44, (1970).

26 Shimshick, E. J. & McConnell, H. M. Lateral phase separation in phospholipid membranes. *Biochemistry* **12**, 2351-2360, (1973).

27 Jain, M. K. & White, H. B., 3rd. Long-range order in biomembranes. *Advances in lipid research* **15**, 1-60, (1977).

28 Israelachvili, J. N. Refinement of the fluid-mosaic model of membrane structure. *Biochimica et biophysica acta* **469**, 221-225, (1977).

29 Mouritsen, O. G. & Bloom, M. Mattress model of lipid-protein interactions in membranes. *Biophysical journal* **46**, 141-153, (1984).

30 Simons, K. & van Meer, G. Lipid sorting in epithelial cells. *Biochemistry* **27**, 6197-6202, (1988).

31 Pomorski, T. G., Nylander, T. & Cardenas, M. Model cell membranes: Discerning lipid and protein contributions in shaping the cell. *Advances in colloid and interface science*, (2013).

32 Brown, M. F. Modulation of rhodopsin function by properties of the membrane bilayer. *Chemistry and physics of lipids* **73**, 159-180, (1994).

33 Fersht, A. *Structure and mechanism in protein science : a guide to enzyme catalysis and protein folding*. (W.H. Freeman, 1999).

34 Brown, M. F. Curvature forces in membrane lipid-protein interactions. *Biochemistry* **51**, 9782-9795, (2012).

35 Terstappen, G. C. & Reggiani, A. In silico research in drug discovery. *Trends in pharmacological sciences* **22**, 23-26, (2001).

36 Fagerberg, L., Jonasson, K., von Heijne, G., Uhlen, M. & Berglund, L. Prediction of the human membrane proteome. *Proteomics* **10**, 1141-1149, (2010).

37 Baker, M. Structural biology: The gatekeepers revealed. *Nature* **465**, 823-826, (2010).

38 Bhattacharya, A. Protein structures: Structures of desire. *Nature* **459**, 24-27, (2009).

39 White, S. H. Biophysical dissection of membrane proteins. *Nature* **459**, 344-346, (2009).

40 Singer, S. J. The molecular organization of membranes. *Annu Rev Biochem* **43**, 805-833, (1974).

41 Singer, S. J. The structure and insertion of integral proteins in membranes. *Annual review of cell biology* **6**, 247-296, (1990).

42 Vonheijne, G. Transcending the Impenetrable - How Proteins Come to Terms with Membranes. *Biochimica et biophysica acta* **947**, 307-333, (1988).

43 von Heijne, G. Membrane-protein topology. *Nature reviews. Molecular cell biology* **7**, 909-918, (2006).

44 von Heijne, G. & Rees, D. Membranes: reading between the lines. *Curr Opin Struct Biol* **18**, 403-405, (2008).

45 Brown, M. F. Influence of nonlamellar-forming lipids on rhodopsin. *Curr Top Membr* **44**, 285-356, (1997).

46 White, S. H. & Wimley, W. C. Membrane protein folding and stability: Physical principles. *Annu Rev Bioph Biom* **28**, 319-365, (1999).

47 Kusnetzow, A. K., Altenbach, C. & Hubbell, W. L. Conformational states and dynamics of rhodopsin in micelles and bilayers. *Biochemistry* **45**, 5538-5550, (2006).

48 Khelashvili, G., Albornoz, P. B. C., Johner, N., Mondal, S., Caffrey, M. & Weinstein, H. Why GPCRs behave differently in cubic and lamellar lipidic mesophases. *Journal of the American Chemical Society* **134**, 15858-15868, (2012).

49 Lee, A. G. How lipids interact with an intrinsic membrane protein: the case of the calcium pump. *Bba-Rev Biomembranes* **1376**, 381-390, (1998).

50 Olesen, C., Picard, M., Winther, A. M. L., Gyrup, C., Morth, J. P., Oxvig, C., Moller, J. V. & Nissen, P. The structural basis of calcium transport by the calcium pump. *Nature* **450**, 1036-U1035, (2007).

51 Kobilka, B. & Schertler, G. F. X. New G-protein-coupled receptor crystal structures: insights and limitations. *Trends in pharmacological sciences* **29**, 79-83, (2008).

52 Hirai, T., Subramaniam, S. & Lanyi, J. K. Structural snapshots of conformational changes in a seven-helix membrane protein: lessons from bacteriorhodopsin. *Curr Opin Struc Biol* **19**, 433-439, (2009).

53 Choe, H. W., Kim, Y. J., Park, J. H., Morizumi, T., Pai, E. F., Krauss, N., Hofmann, K. P., Scheerer, P. & Ernst, O. P. Crystal structure of metarhodopsin II. *Nature* **471**, 651-U137, (2011).

54 Standfuss, J., Edwards, P. C., D'Antona, A., Fransen, M., Xie, G. F., Oprian, D. D. & Schertler, G. F. X. The structural basis of agonist-induced activation in constitutively active rhodopsin. *Nature* **471**, 656-660, (2011).

55 Rosenbaum, D. M., Zhang, C., Lyons, J. A., Holl, R., Aragao, D., Arlow, D. H., Rasmussen, S. G. F., Choi, H. J., DeVree, B. T., Sunahara, R. K., Chae, P. S., Gellman, S. H., Dror, R. O., Shaw, D. E., Weis, W. I., Caffrey, M., Gmeiner, P. & Kobilka, B. K. Structure and function of an irreversible agonist-beta(2) adrenoceptor complex. *Nature* **469**, 236-240, (2011).

56 Fromme, P. & Spence, J. C. H. Femtosecond nanocrystallography using X-ray lasers for membrane protein structure determination. *Curr Opin Struc Biol* **21**, 509-516, (2011).

57 Chaptal, V., Kwon, S., Sawaya, M. R., Guan, L., Kaback, H. R. & Abramson, J. Crystal structure of lactose permease in complex with an affinity inactivator yields unique insight into sugar recognition. *Proceedings of the National Academy of Sciences of the United States of America* **108**, 9361-9366, (2011).

58 Katritch, V., Cherezov, V. & Stevens, R. C. Diversity and modularity of G protein-coupled receptor structures. *Trends in pharmacological sciences* **33**, 17-27, (2012).

59 Rasmussen, S. G., Choi, H. J., Rosenbaum, D. M., Kobilka, T. S., Thian, F. S., Edwards, P. C., Burghammer, M., Ratnala, V. R., Sanishvili, R., Fischetti, R. F., Schertler, G. F., Weis, W. I. & Kobilka, B. K. Crystal structure of the human beta2 adrenergic G-protein-coupled receptor. *Nature* **450**, 383-387, (2007).

60 Cherezov, V., Rosenbaum, D. M., Hanson, M. A., Rasmussen, S. G., Thian, F. S., Kobilka, T. S., Choi, H. J., Kuhn, P., Weis, W. I., Kobilka, B. K. & Stevens, R. C. High-

resolution crystal structure of an engineered human beta2-adrenergic G protein-coupled receptor. *Science* **318**, 1258-1265, (2007).

61 Rosenbaum, D. M., Cherezov, V., Hanson, M. A., Rasmussen, S. G., Thian, F. S., Kobilka, T. S., Choi, H. J., Yao, X. J., Weis, W. I., Stevens, R. C. & Kobilka, B. K. GPCR engineering yields high-resolution structural insights into beta2-adrenergic receptor function. *Science* **318**, 1266-1273, (2007).

62 Rasmussen, S. G., Choi, H. J., Fung, J. J., Pardon, E., Casarosa, P., Chae, P. S., Devree, B. T., Rosenbaum, D. M., Thian, F. S., Kobilka, T. S., Schnapp, A., Konetzki, I., Sunahara, R. K., Gellman, S. H., Pautsch, A., Steyaert, J., Weis, W. I. & Kobilka, B. K. Structure of a nanobody-stabilized active state of the beta(2) adrenoceptor. *Nature* **469**, 175-180, (2011).

63 Rasmussen, S. G., DeVree, B. T., Zou, Y., Kruse, A. C., Chung, K. Y., Kobilka, T. S., Thian, F. S., Chae, P. S., Pardon, E., Calinski, D., Mathiesen, J. M., Shah, S. T., Lyons, J. A., Caffrey, M., Gellman, S. H., Steyaert, J., Skiniotis, G., Weis, W. I., Sunahara, R. K. & Kobilka, B. K. Crystal structure of the beta2 adrenergic receptor-Gs protein complex. *Nature* **477**, 549-555, (2011).

64 Roth, B. L. & Marshall, F. H. NOBEL 2012 Chemistry: Studies of a ubiquitous receptor family. *Nature* **492**, 57, (2012).

65 Bloom, M., Evans, E. & Mouritsen, O. G. Physical-Properties of the Fluid Lipid-Bilayer Component of Cell-Membranes - a Perspective. *Quarterly reviews of biophysics* **24**, 293-397, (1991).

66 Singer, S. J. Some early history of membrane molecular biology. *Annu Rev Physiol* **66**, 1-27, (2004).

67 Sachs, J. N. & Engelman, D. M. Introduction to the membrane protein reviews: The interplay of structure, dynamics, and environment in membrane protein function. *Annu Rev Biochem* **75**, 707-712, (2006).

68 Leftin, A. & Brown, M. F. An NMR database for simulations of membrane dynamics. *Bba-Biomembranes* **1808**, 818-839, (2011).

69 Antonny, B. Mechanisms of Membrane Curvature Sensing. *Annual Review of Biochemistry, Vol 80* **80**, 101-123, (2011).

70 Lyman, E., Cui, H. S. & Voth, G. A. Reconstructing protein remodeled membranes in molecular detail from mesoscopic models. *Physical Chemistry Chemical Physics* **13**, 10430-10436, (2011).

71 Seddon, A. M., Curnow, P. & Booth, P. J. Membrane proteins, lipids and detergents: not just a soap opera. *Biochimica et biophysica acta* **1666**, 105-117, (2004).

72 Chan, Y. H. & Boxer, S. G. Model membrane systems and their applications. *Current opinion in chemical biology* **11**, 581-587, (2007).

73 Bayburt, T. H. & Sligar, S. G. Membrane protein assembly into Nanodiscs. *FEBS letters* **584**, 1721-1727, (2010).

74 Ritchie, T. K., Grinkova, Y. V., Bayburt, T. H., Denisov, I. G., Zolnerciks, J. K., Atkins, W. M. & Sligar, S. G. Chapter 11 - Reconstitution of membrane proteins in phospholipid bilayer nanodiscs. *Methods in enzymology* **464**, 211-231, (2009).

75 Bayburt, T. H., Grinkova, Y. V. & Sligar, S. G. Self-assembly of discoidal phospholipid bilayer nanoparticles with membrane scaffold proteins. *Nano Letters* **2**, 853-856, (2002).

76 Nath, A., Atkins, W. M. & Sligar, S. G. Applications of phospholipid bilayer nanodiscs in the study of membranes and membrane proteins. *Biochemistry* **46**, 2059-2069, (2007).

77 Skar-Gislinge, N., Simonsen, J. B., Mortensen, K., Feidenhans'l, R., Sligar, S. G., Lindberg Moller, B., Bjornholm, T. & Arleth, L. Elliptical structure of phospholipid bilayer nanodiscs encapsulated by scaffold proteins: casting the roles of the lipids and the protein. *Journal of the American Chemical Society* **132**, 13713-13722, (2010).

78 Skar-Gislinge, N. & Arleth, L. Small-angle scattering from phospholipid nanodiscs: derivation and refinement of a molecular constrained analytical model form factor. *Physical chemistry chemical physics : PCCP* **13**, 3161-3170, (2011).

79 Kynde, S. A. R., Skar-Gislinge, N., Pedersen, M. C., Midtgaard, S. R., Simonsen, J. B., Schweins, R., Mortensen, K. & Arleth, L. Small-angle scattering gives direct structural information about a membrane protein inside a lipid environment. *Acta Crystallographica Section D* **70**, 371-383, (2014).

80 Carpenter, E. P., Beis, K., Cameron, A. D. & Iwata, S. Overcoming the challenges of membrane protein crystallography. *Curr Opin Struct Biol* **18**, 581-586, (2008).

81 Newstead, S., Hobbs, J., Jordan, D., Carpenter, E. P. & Iwata, S. Insights into outer membrane protein crystallization. *Molecular membrane biology* **25**, 631-638, (2008).

82 Newstead, S., Ferrandon, S. & Iwata, S. Rationalizing alpha-helical membrane protein crystallization. *Protein science : a publication of the Protein Society* **17**, 466-472, (2008).

83 Newby, Z. E., O'Connell, J. D., 3rd, Gruswitz, F., Hays, F. A., Harries, W. E., Harwood, I. M., Ho, J. D., Lee, J. K., Savage, D. F., Miercke, L. J. & Stroud, R. M. A general protocol for the crystallization of membrane proteins for X-ray structural investigation. *Nature protocols* **4**, 619-637, (2009).

84 Bill, R. M., Henderson, P. J., Iwata, S., Kunji, E. R., Michel, H., Neutze, R., Newstead, S., Poolman, B., Tate, C. G. & Vogel, H. Overcoming barriers to membrane protein structure determination. *Nature biotechnology* **29**, 335-340, (2011).

85 Kang, H. J., Lee, C. & Drew, D. Breaking the barriers in membrane protein crystallography. *The international journal of biochemistry & cell biology* **45**, 636-644, (2013).

86 Pedersen, B. P., Buch-Pedersen, M. J., Morth, J. P., Palmgren, M. G. & Nissen, P. Crystal structure of the plasma membrane proton pump. *Nature* **450**, 1111-1114, (2007).

87 Morth, J. P., Pedersen, B. P., Toustrup-Jensen, M. S., Sorensen, T. L., Petersen, J., Andersen, J. P., Vilsen, B. & Nissen, P. Crystal structure of the sodium-potassium pump. *Nature* **450**, 1043-1049, (2007).

88 Morth, J. P., Pedersen, B. P., Buch-Pedersen, M. J., Andersen, J. P., Vilsen, B., Palmgren, M. G. & Nissen, P. A structural overview of the plasma membrane Na+,K+-ATPase and H+-ATPase ion pumps. *Nature reviews. Molecular cell biology* **12**, 60-70, (2011).

89 Baker, M. Making membrane proteins for structures: a trillion tiny tweaks. *Nature methods* **7**, 429-434, (2010).

90 Ferguson, K. M. Structure-based view of epidermal growth factor receptor regulation. *Annual review of biophysics* **37**, 353-373, (2008).

91 Herbst, R. S. Review of epidermal growth factor receptor biology. *International journal of radiation oncology, biology, physics* **59**, 21-26, (2004).

92 Baas, B. J., Denisov, I. G. & Sligar, S. G. Homotropic cooperativity of monomeric cytochrome P450 3A4 in a nanoscale native bilayer environment. *Archives of biochemistry and biophysics* **430**, 218-228, (2004).

93 Sanders, C. R. & Sonnichsen, F. Solution NMR of membrane proteins: practice and challenges. *Magnetic resonance in chemistry : MRC* **44 Spec No**, S24-40, (2006).

94 Hong, M., Zhang, Y. & Hu, F. Membrane protein structure and dynamics from NMR spectroscopy. *Annual review of physical chemistry* **63**, 1-24, (2012).

95 Opella, S. J. Structure determination of membrane proteins by nuclear magnetic resonance spectroscopy. *Annual review of analytical chemistry* **6**, 305-328, (2013).

96 Rubinstein, J. L. Structural analysis of membrane protein complexes by single particle electron microscopy. *Methods* **41**, 409-416, (2007).

97 Bartesaghi, A. & Subramaniam, S. Membrane protein structure determination using cryo-electron tomography and 3D image averaging. *Curr Opin Struct Biol* **19**, 402-407, (2009).

98 Goldie, K., Abeyrathne, P., Kebbel, F., Chami, M., Ringler, P. & Stahlberg, H. in *Electron Microscopy* Vol. 1117 *Methods in Molecular Biology* (ed John Kuo) Ch. 15, 325-341 (Humana Press, 2014).

99 Round, A. R., Franke, D., Moritz, S., Huchler, R., Fritsche, M., Malthan, D., Klaering, R., Svergun, D. I. & Roessle, M. Automated sample-changing robot for solution scattering experiments at the EMBL Hamburg SAXS station X33. *Journal of Applied Crystallography* **41**, 913-917, (2008).

100 Toft, K. N., Vestergaard, B., Nielsen, S. S., Snakenborg, D., Jeppesen, M. G., Jacobsen, J. K., Arleth, L. & Kutter, J. P. High-throughput Small Angle X-ray Scattering from proteins in solution using a microfluidic front-end. *Analytical chemistry* **80**, 3648-3654, (2008).

101 Hura, G. L., Menon, A. L., Hammel, M., Rambo, R. P., Poole, F. L., 2nd, Tsutakawa, S. E., Jenney, F. E., Jr., Classen, S., Frankel, K. A., Hopkins, R. C., Yang, S. J., Scott, J. W., Dillard, B. D., Adams, M. W. & Tainer, J. A. Robust, high-throughput solution structural analyses by small angle X-ray scattering (SAXS). *Nature methods* **6**, 606-612, (2009).

102 Jacques, D. A. & Trewhella, J. Small-angle scattering for structural biology--expanding the frontier while avoiding the pitfalls. *Protein science : a publication of the Protein Society* **19**, 642-657, (2010).

103 Petoukhov, M. V. & Svergun, D. I. Applications of small-angle X-ray scattering to biomacromolecular solutions. *The international journal of biochemistry & cell biology* **45**, 429-437, (2012).

104 Blanchet, C. E. & Svergun, D. I. Small-Angle X-Ray Scattering on Biological Macromolecules and Nanocomposites in Solution. *Annual review of physical chemistry*, (2012).

105 Rambo, R. P. & Tainer, J. A. Super-resolution in solution X-ray scattering and its applications to structural systems biology. *Annual review of biophysics* **42**, 415-441, (2013).

106 Konarev, P. V., Petoukhov, M. V., Volkov, V. V. & Svergun, D. I. *Atsas* 2.1, a program package for small-angle scattering data analysis. *Journal of Applied Crystallography* **39**, 277-286, (2006).

107 Jacques, D. A., Guss, J. M., Svergun, D. I. & Trewhella, J. Publication guidelines for structural modelling of small-angle scattering data from biomolecules in solution. *Acta crystallographica. Section D, Biological crystallography* **68**, 620-626, (2012).

108 Midgett, C. R. & Madden, D. R. Breaking the bottleneck: eukaryotic membrane protein expression for high-resolution structural studies. *Journal of structural biology* **160**, 265-274, (2007).

109 Tate, C. G. Practical considerations of membrane protein instability during purification and crystallisation. *Methods in molecular biology* **601**, 187-203, (2010).

110 Hunt, J. F., McCrea, P. D., Zaccai, G. & Engelman, D. M. Assessment of the aggregation state of integral membrane proteins in reconstituted phospholipid vesicles using small angle neutron scattering. *Journal of molecular biology* **273**, 1004-1019, (1997).

111 Bu, Z., Wang, L. & Kendall, D. A. Nucleotide binding induces changes in the oligomeric state and conformation of Sec A in a lipid environment: a small-angle neutron-scattering study. *Journal of molecular biology* **332**, 23-30, (2003).

112 Zimmer, J., Doyle, D. A. & Grossmann, J. G. Structural characterization and pH-induced conformational transition of full-length KcsA. *Biophysical journal* **90**, 1752-1766, (2006).

113 Johs, A., Hammel, M., Waldner, I., May, R. P., Laggner, P. & Prassl, R. Modular structure of solubilized human apolipoprotein B-100. Low resolution model revealed by small angle neutron scattering. *The Journal of biological chemistry* **281**, 19732-19739, (2006).

114 Cardoso, M. B., Smolensky, D., Heller, W. T. & O'Neill, H. Insight into the structure of light-harvesting complex II and its stabilization in detergent solution. *The journal of physical chemistry. B* **113**, 16377-16383, (2009).

115 Tang, K. H., Urban, V. S., Wen, J., Xin, Y. & Blankenship, R. E. SANS investigation of the photosynthetic machinery of Chloroflexus aurantiacus. *Biophysical journal* **99**, 2398-2407, (2010).

116 Nogales, A., Garcia, C., Perez, J., Callow, P., Ezquerra, T. A. & Gonzalez-Rodriguez, J. Three-dimensional model of human platelet integrin alphaIIb beta3 in solution obtained by small angle neutron scattering. *The Journal of biological chemistry* **285**, 1023-1031, (2010).

117 Compton, E. L., Karinou, E., Naismith, J. H., Gabel, F. & Javelle, A. Low resolution structure of a bacterial SLC26 transporter reveals dimeric stoichiometry and mobile intracellular domains. *The Journal of biological chemistry* **286**, 27058-27067, (2011).

118 Wu, Z., Gogonea, V., Lee, X., Wagner, M. A., Li, X. M., Huang, Y., Undurti, A., May, R. P., Haertlein, M., Moulin, M., Gutsche, I., Zaccai, G., Didonato, J. A. & Hazen, S. L. Double superhelix model of high density lipoprotein. *The Journal of biological chemistry* **284**, 36605-36619, (2009).

119 Clifton, L. A., Johnson, C. L., Solovyova, A. S., Callow, P., Weiss, K. L., Ridley, H., Le Brun, A. P., Kinane, C. J., Webster, J. R., Holt, S. A. & Lakey, J. H. Low resolution structure and dynamics of a colicin-receptor complex determined by neutron scattering. *The Journal of biological chemistry* **287**, 337-346, (2012).

120 Berthaud, A., Manzi, J., Perez, J. & Mangenot, S. Modeling detergent organization around aquaporin-0 using small-angle X-ray scattering. *Journal of the American Chemical Society* **134**, 10080-10088, (2012).

121 Clantin, B., Hodak, H., Willery, E., Locht, C., Jacob-Dubuisson, F. & Villeret, V. The crystal structure of filamentous hemagglutinin secretion domain and its implications for the two-partner secretion pathway. *Proceedings of the National Academy of Sciences of the United States of America* **101**, 6194-6199, (2004).

122 Calcutta, A., Jessen, C. M., Behrens, M. A., Oliveira, C. L., Renart, M. L., Gonzalez-Ros, J. M., Otzen, D. E., Pedersen, J. S., Malmendal, A. & Nielsen, N. C. Mapping of unfolding states of integral helical membrane proteins by GPS-NMR and scattering techniques: TFE-induced unfolding of KcsA in DDM surfactant. *Biochimica et biophysica acta* **1818**, 2290-2301, (2012).

123 Svergun, D. I. & Koch, M. H. J. Small-angle scattering studies of biological macromolecules in solution. *Reports on Progress in Physics* **66**, 1735-1782, (2003).
124 Petoukhov, M. V. & Svergun, D. I. Analysis of X-ray and neutron scattering from biomacromolecular solutions. *Curr Opin Struc Biol* **17**, 562-571, (2007).
125 Neylon, C. Small angle neutron and X-ray scattering in structural biology: recent examples from the literature. *Eur Biophys J Biophy* **37**, 531-541, (2008).
126 Madl, T., Gabel, F. & Sattler, M. NMR and small-angle scattering-based structural analysis of protein complexes in solution. *Journal of structural biology* **173**, 472-482, (2011).
127 Niemann, H. H., Petoukhov, M. V., Hartlein, M., Moulin, M., Gherardi, E., Timmins, P., Heinz, D. W. & Svergun, D. I. X-ray and neutron small-angle scattering analysis of the complex formed by the met receptor and the Listeria monocytogenes invasion protein InlB. *Journal of molecular biology* **377**, 489-500, (2008).
128 Li, J. Q., Callaway, D. J. E. & Bu, Z. M. Ezrin Induces Long-Range Interdomain Allostery in the Scaffolding Protein NHERF1. *Journal of molecular biology* **392**, 166-180, (2009).
129 Chaudhuri, B. N., Gupta, S., Urban, V. S., Chance, M. R., D'Mello, R., Smith, L., Lyons, K. & Gee, J. A combined global and local approach to elucidate spatial organization of the Mycobacterial ParB-parS partition assembly. *Biochemistry* **50**, 1799-1807, (2011).
130 Christie, M. P., Whitten, A. E., King, G. J., Hu, S. H., Jarrott, R. J., Chen, K. E., Duff, A. P., Callow, P., Collins, B. M., James, D. E. & Martin, J. L. Low-resolution solution structures of Munc18:Syntaxin protein complexes indicate an open binding mode driven by the Syntaxin N-peptide. *Proceedings of the National Academy of Sciences of the United States of America* **109**, 9816-9821, (2012).
131 Heller, W. T. & Littrell, K. C. Small-angle neutron scattering for molecular biology: basics and instrumentation. *Methods in molecular biology* **544**, 293-305, (2009).
132 Breyton, C., Gabel, F., Lethier, M., Flayhan, A., Durand, G., Jault, J. M., Juillan-Binard, C., Imbert, L., Moulin, M., Ravaud, S., Hartlein, M. & Ebel, C. Small angle neutron scattering for the study of solubilised membrane proteins. *The European physical journal. E, Soft matter* **36**, 71, (2013).
133 Jacrot, B. The study of biological structures by neutron scattering from solution. *Reports on Progress in Physics* **39**, 911-953, (1976).
134 Jacrot, B. & Zaccai, G. Determination of Molecular-Weight by Neutron-Scattering. *Biopolymers* **20**, 2413-2426, (1981).
135 Zaccai, G. & Jacrot, B. Small-Angle Neutron-Scattering. *Annual review of biophysics and bioengineering* **12**, 139-157, (1983).
136 Koch, M. H. J., Vachette, P. & Svergun, D. I. Small-angle scattering: a view on the properties, structures and structural changes of biological macromolecules in solution. *Quarterly reviews of biophysics* **36**, 147-227, (2003).
137 Guinier, A. & Fournet, G. r. *Small-angle scattering of X-rays*. (Wiley, 1955).
138 Glatter, O. A new method for the evaluation of small-angle scattering data. *Journal of Applied Crystallography* **10**, 415-421, (1977).
139 Moore, P. B. Small-Angle Scattering - Information-Content and Error Analysis. *Journal of Applied Crystallography* **13**, 168-175, (1980).
140 Guinier, A. The diffusion of x-rays under the extremely weak angles applied to the study of fine particles and colloidal suspension. *Cr Hebd Acad Sci* **206**, 1374-1376, (1938).

141 Hjelm, R. P. The Small-Angle Approximation of X-Ray and Neutron Scatter from Rigid Rods of Non-Uniform Cross-Section and Finite Length. *Journal of Applied Crystallography* **18**, 452-460, (1985).

142 Engelman, D. M. & Moore, P. B. Determination of quaternary structure by small angle neutron scattering. *Annual review of biophysics and bioengineering* **4**, 219-241, (1975).

143 Heller, W. T. Small-angle neutron scattering and contrast variation: a powerful combination for studying biological structures. *Acta crystallographica. Section D, Biological crystallography* **66**, 1213-1217, (2010).

144 Lian, L. Y. & Middleton, D. A. Labelling approaches for protein structural studies by solution-state and solid-state NMR. *Prog Nucl Mag Res Sp* **39**, 171-190, (2001).

145 Venters, R. A., Huang, C. C., Farmer, B. T., 2nd, Trolard, R., Spicer, L. D. & Fierke, C. A. High-level 2H/13C/15N labeling of proteins for NMR studies. *Journal of biomolecular NMR* **5**, 339-344, (1995).

146 Clifton, L. A., Neylon, C. & Lakey, J. H. Examining protein-lipid complexes using neutron scattering. *Methods in molecular biology* **974**, 119-150, (2013).

147 Meilleur, F., Dauvergne, M. T., Schlichting, I. & Myles, D. A. Production and X-ray crystallographic analysis of fully deuterated cytochrome P450cam. *Acta crystallographica. Section D, Biological crystallography* **61**, 539-544, (2005).

148 Bragina, N. A. & Chupin, V. V. Methods of synthesis of deuterium-labelled lipids. *Russian Chemical Reviews* **66**, 975-986, (1997).

149 Leiting, B., Marsilio, F. & O'Connell, J. F. Predictable deuteration of recombinant proteins expressed in Escherichia coli. *Anal Biochem* **265**, 351-355, (1998).

150 Barbara Leiting, F. M., and John F. O'Connell. Predictable Deuteration of REcombinant Proteins Expressed in *Escherichia coli*. *Analytical Biochemistry* **265**, 351-355, (1998).

151 Howard, E. I., Blakeley, M. P., Haertlein, M., Petit-Haertlein, I., Mitschler, A., Fisher, S. J., Cousido-Siah, A., Salvay, A. G., Popov, A., Muller-Dieckmann, C., Petrova, T. & Podjarny, A. Neutron structure of type-III antifreeze protein allows the reconstruction of AFP-ice interface. *Journal of molecular recognition : JMR* **24**, 724-732, (2011).

152 Cuypers, M. G., Mason, S. A., Blakeley, M. P., Mitchell, E. P., Haertlein, M. & Forsyth, V. T. Near-atomic resolution neutron crystallography on perdeuterated Pyrococcus furiosus rubredoxin: implication of hydronium ions and protonation state equilibria in redox changes. *Angewandte Chemie* **52**, 1022-1025, (2013).

153 Vijayakrishnan, S., Kelly, S. M., Gilbert, R. J., Callow, P., Bhella, D., Forsyth, T., Lindsay, J. G. & Byron, O. Solution structure and characterisation of the human pyruvate dehydrogenase complex core assembly. *Journal of molecular biology* **399**, 71-93, (2010).

154 Rochel, N., Ciesielski, F., Godet, J., Moman, E., Roessle, M., Peluso-Iltis, C., Moulin, M., Haertlein, M., Callow, P., Mely, Y., Svergun, D. I. & Moras, D. Common architecture of nuclear receptor heterodimers on DNA direct repeat elements with different spacings. *Nature structural & molecular biology* **18**, 564-570, (2011).

155 Cuypers, M. G., Trubitsyna, M., Callow, P., Forsyth, V. T. & Richardson, J. M. Solution conformations of early intermediates in Mos1 transposition. *Nucleic acids research* **41**, 2020-2033, (2013).

156 Grage, S. L., Keleshian, A. M., Turdzeladze, T., Battle, A. R., Tay, W. C., May, R. P., Holt, S. A., Contera, S. A., Haertlein, M., Moulin, M., Pal, P., Rohde, P. R., Forsyth, V. T., Watts, A., Huang, K. C., Ulrich, A. S. & Martinac, B. Bilayer-mediated clustering and functional interaction of MscL channels. *Biophysical journal* **100**, 1252-1260, (2011).

157 Hellstrand, E., Grey, M., Ainalem, M. L., Ankner, J., Forsyth, V. T., Fragneto, G., Haertlein, M., Dauvergne, M. T., Nilsson, H., Brundin, P., Linse, S., Nylander, T. & Sparr, E. Adsorption of alpha-Synuclein to Supported Lipid Bilayers: Positioning and Role of Electrostatics. *ACS chemical neuroscience*, (2013).

158 Wadsater, M., Laursen, T., Singha, A., Hatzakis, N. S., Stamou, D., Barker, R., Mortensen, K., Feidenhans'l, R., Moller, B. L. & Cardenas, M. Monitoring shifts in the conformation equilibrium of the membrane protein cytochrome P450 reductase (POR) in nanodiscs. *The Journal of biological chemistry* **287**, 34596-34603, (2012).

159 Wadsäter, M., Maric, S., Simonsen, J. B., Mortensen, K. & Cardenas, M. The effect of using binary mixtures of zwitterionic and chaged lipids on nanodisc formation and stability. *Soft Matter* **9**, 2329-2337, (2013).

160 Justesen, B. H., Laursen, T., Weber, G., Fuglsang, A. T., Moller, B. L. & Pomorski, T. G. Isolation of monodisperse nanodisc-reconstituted membrane proteins using free flow electrophoresis. *Analytical chemistry* **85**, 3497-3500, (2013).

161 Justesen, B. H., Hansen, R. W., Martens, H. J., Theorin, L., Palmgren, M. G., Martinez, K. L., Pomorski, T. G. & Fuglsang, A. T. Active plasma membrane P-type H+-ATPase reconstituted into nanodiscs is a monomer. *The Journal of biological chemistry* **288**, 26419-26429, (2013).

162 Pedersen, M. C., Arleth, L. & Mortensen, K. WillItFit: a framework for fitting of constrained models to small-angle scattering data. *Journal of Applied Crystallography* **46**, 1894-1898, (2013).

163 Wadsater, M., Simonsen, J. B., Lauridsen, T., Tveten, E. G., Naur, P., Bjornholm, T., Wacklin, H., Mortensen, K., Arleth, L., Feidenhans'l, R. & Cardenas, M. Aligning nanodiscs at the air-water interface, a neutron reflectivity study. *Langmuir : the ACS journal of surfaces and colloids* **27**, 15065-15073, (2011).

164 Wadsater, M., Barker, R., Mortensen, K., Feidenhans'l, R. & Cardenas, M. Effect of phospholipid composition and phase on nanodisc films at the solid-liquid interface as studied by neutron reflectivity. *Langmuir : the ACS journal of surfaces and colloids* **29**, 2871-2880, (2013).

165 Denisov, I. G., Shih, A. Y. & Sligar, S. G. Structural differences between soluble and membrane bound cytochrome P450s. *Journal of inorganic biochemistry* **108**, 150-158, (2012).

166 Silva, R. A., Hilliard, G. M., Li, L., Segrest, J. P. & Davidson, W. S. A mass spectrometric determination of the conformation of dimeric apolipoprotein A-I in discoidal high density lipoproteins. *Biochemistry* **44**, 8600-8607, (2005).

167 Davidson, W. S. & Silva, R. A. Apolipoprotein structural organization in high density lipoproteins: belts, bundles, hinges and hairpins. *Current opinion in lipidology* **16**, 295-300, (2005).

168 Morgan, C. R., Hebling, C. M., Rand, K. D., Stafford, D. W., Jorgenson, J. W. & Engen, J. R. Conformational transitions in the membrane scaffold protein of phospholipid bilayer nanodiscs. *Molecular & cellular proteomics : MCP* **10**, M111 010876, (2011).

169 Glatter, O. & Kratky, O. *Small Angle X-ray Scattering*. (Academic Press Inc., 1982).

170 Mylonas, E. & Svergun, D. I. Accuracy of molecular mass determination of proteins in solution by small-angle X-ray scattering. *Journal of Applied Crystallography* **40**, 245-249, (2007).

171 Li, J., Callaway, D. J. & Bu, Z. Ezrin induces long-range interdomain allostery in the scaffolding protein NHERF1. *Journal of molecular biology* **392**, 166-180, (2009).

172 Vanatalu, K., Paalme, T., Vilu, R., Burkhardt, N., Junemann, R., May, R., Ruhl, M., Wadzack, J. & Nierhaus, K. H. Large-scale preparation of fully deuterated cell components. Ribosomes from Escherichia coli with high biological activity. *European journal of biochemistry / FEBS* **216**, 315-321, (1993).

173 Junemann, R., Wadzack, J., Triana-Alonso, F. J., Bittner, J. U., Caillet, J., Meinnel, T., Vanatalu, K. & Nierhaus, K. H. In vivo deuteration of transfer RNAs: overexpression and large-scale purification of deuterated specific tRNAs. *Nucleic acids research* **24**, 907-913, (1996).

174 Paliy, O., Bloor, D., Brockwell, D., Gilbert, P. & Barber, J. Improved methods of cultivation and production of deuteriated proteins from E. coli strains grown on fully deuteriated minimal medium. *Journal of applied microbiology* **94**, 580-586, (2003).

175 Artero, J. B., Hartlein, M., McSweeney, S. & Timmins, P. A comparison of refined X-ray structures of hydrogenated and perdeuterated rat gammaE-crystallin in H2O and D2O. *Acta crystallographica. Section D, Biological crystallography* **61**, 1541-1549, (2005).

176 Pernot, P., Round, A., Theveneau, P., Giraud, T., Nogueira-Fernandes, R., Nurrizzo, D., Spruce, D., Surr, J., McSweeney, S., Felisaz, F., Foedinger, L., Gobbo, A., Huet, J., Villard, C. & Cipriani, F. in *XIV International Conference on Small-Angle Scattering* Vol. 247 (2010).

177 Katz, J. J. & Crespi, H. L. Deuterated organisms: cultivation and uses. *Science* **151**, 1187-1194, (1966).

178 Mann, L. R. & Moses, V. Properties of Escherichia coli grown in deuterated media. *Folia microbiologica* **16**, 267-284, (1971).

179 Eibl, H. Synthesis of glycerophospholipids. *Chemistry and physics of lipids* **26**, 405-429, (1980).

180 Yoon, T. H. & Kim, I. H. Phosphatidylcholine isolation from egg yolk phospholipids by high-performance liquid chromatography. *Journal of chromatography. A* **949**, 209-216, (2002).

181 Schneiter, R. & Daum, G. in *Yeast Protocol Methods in Molecular Biology* 41-45 (2005).

182 Dowhan, W. A retrospective: Use of Escherichia coli as a vehicle to study phospholipid synthesis and function. *Bba-Mol Cell Biol L* **1831**, 471-494, (2013).

183 Folch, J., Lees, M. & Sloane Stanley, G. H. A simple method for the isolation and purification of total lipides from animal tissues. *The Journal of biological chemistry* **226**, 497-509, (1957).

184 Bligh, E. G. & Dyer, W. J. A rapid method of total lipid extraction and purification. *Canadian journal of biochemistry and physiology* **37**, 911-917, (1959).

185 Crider, Q. E., Alaupovic, P., Hillsberry, J., Yen, C. & Bradford, R. H. Separation of lipids by Silica Gel G column chromatography. *J Lipid Res* **5**, 479-481, (1964).

186 Rohwedder, W. K. Mass-Spectrometry of Lipids Labeled with Stable Isotopes. *Progress in lipid research* **24**, 1-18, (1985).

187 Schiller, J., Arnhold, J., Benard, S., Muller, M., Reichl, S. & Arnold, K. Lipid analysis by matrix-assisted laser desorption and ionization mass spectrometry: A methodological approach. *Anal Biochem* **267**, 46-56, (1999).

188 Sun, G., Yang, K., Zhao, Z., Guan, S., Han, X. & Gross, R. W. Matrix-assisted laser desorption/ionization time-of-flight mass spectrometric analysis of cellular glycerophospholipids enabled by multiplexed solvent dependent analyte-matrix interactions. *Analytical chemistry* **80**, 7576-7585, (2008).

189 Mikhail Bogdanov, P. H., Ziqiang Guan, and William Dowhan. Plasticity of lipid-protein interactions in the function and topogenesis of the membrane protein lactose permease from *Escherichia coli*. *Proceedings of the National Academy of Sciences* **107**, 15057-15062, (2010).

190 White, T., Bursten, S., Federighi, D., Lewis, R. A. & Nudelman, E. High-resolution separation and quantification of neutral lipid and phospholipid species in mammalian cells and sera by multi-one-dimensional thin-layer chromatography. *Anal Biochem* **258**, 109-117, (1998).

191 Rouser, G., Siakotos, A. N. & Fleischer, S. Quantitative analysis of phospholipids by thin-layer chromatography and phosphorus analysis of spots. *Lipids* **1**, 85-86, (1966).

192 Petkovic, M., Schiller, J., Muller, M., Benard, S., Reichl, S., Arnold, K. & Arnhold, J. Detection of individual phospholipids in lipid mixtures by matrix-assisted laser desorption/ionization time-of-flight mass spectrometry: phosphatidylcholine prevents the detection of further species. *Anal Biochem* **289**, 202-216, (2001).

193 Fuchs, B., Muller, K., Goritz, F., Blottner, S. & Schiller, J. Characteristic oxidation products of choline plasmalogens are detectable in cattle and roe deer spermatozoa by MALDI-TOF mass spectrometry. *Lipids* **42**, 991-998, (2007).

194 Schiller, J., Suss, R., Arnhold, J., Fuchs, B., Lessig, J., Muller, M., Petkovic, M., Spalteholz, H., Zschornig, O. & Arnold, K. Matrix-assisted laser desorption and ionization time-of-flight (MALDI-TOF) mass spectrometry in lipid and phospholipid research. *Progress in lipid research* **43**, 449-488, (2004).

195 Fuchs, B., Suss, R. & Schiller, J. An update of MALDI-TOF mass spectrometry in lipid research. *Progress in lipid research* **49**, 450-475, (2010).

196 Law, J. H. Biosynthesis of Cyclopropane Rings. *Accounts of Chemical Research* **4**, 199-203, (1971).

197 Dufourc, E. J., Smith, I. C. & Jarrell, H. C. A 2H-NMR analysis of dihydrosterculoyl-containing lipids in model membranes: structural effects of a cyclopropane ring. *Chemistry and physics of lipids* **33**, 153-177, (1983).

198 Magnuson, K., Jackowski, S., Rock, C. O. & Cronan, J. E., Jr. Regulation of fatty acid biosynthesis in Escherichia coli. *Microbiological reviews* **57**, 522-542, (1993).

199 Harlos, K. & Eibl, H. Influence of calcium on phosphatidylglycerol. Two separate lamellar structures. *Biochemistry* **19**, 895-899, (1980).

200 Sixl, F. & Watts, A. Interactions between phospholipid head groups at membrane interfaces: a deuterium and phosphorus nuclear magnetic resonance and spin-label electron spin resonance study. *Biochemistry* **21**, 6446-6452, (1982).

201 Sixl, F. & Watts, A. Headgroup interactions in mixed phospholipid bilayers. *Proceedings of the National Academy of Sciences of the United States of America* **80**, 1613-1615, (1983).

202 Saito, K., Kawaguchi, A., Okuda, S., Seyama, Y. & Yamakawa, T. Incorporation of hydrogen atoms from deuterated water and stereospecifically deuterium-labeled nicotin amide nucleotides into fatty acids with the Escherichia coli fatty acid synthetase system. *Biochimica et biophysica acta* **618**, 202-213, (1980).

203 Gally, H. U., Pluschke, G., Overath, P. & Seelig, J. Structure of Escherichia coli membranes. Glycerol auxotrophs as a tool for the analysis of the phospholipid head-group region by deuterium magentic resonance. *Biochemistry* **20**, 1826-1831, (1981).

204 Kanemasa, Y., Akamatsu, Y. & Nojima, S. Composition and turnover of the phospholipids in Escherichia coli. *Biochimica et biophysica acta* **144**, 382-390, (1967).

205 Seelig, J. & Seelig, A. Deuterium magnetic resonance studies of phospholipid bilayers. *Biochemical and biophysical research communications* **57**, 406-411, (1974).
206 Seelig, A. & Seelig, J. Bilayers of dipalmitoyl-3-sn-phosphatidylcholine. Conformational differences between the fatty acyl chains. *Biochimica et biophysica acta* **406**, 1-5, (1975).
207 Seelig, J. Deuterium magnetic resonance: theory and application to lipid membranes. *Quarterly reviews of biophysics* **10**, 353-418, (1977).
208 Martinez-Morales, F., Schobert, M., Lopez-Lara, I. M. & Geiger, O. Pathways for phosphatidylcholine biosynthesis in bacteria. *Microbiology* **149**, 3461-3471, (2003).
209 Raetz, C. R. Enzymology, genetics, and regulation of membrane phospholipid synthesis in Escherichia coli. *Microbiological reviews* **42**, 614-659, (1978).
210 Kaneko, H., Hosohara, M., Tanaka, M. & Itoh, T. Lipid composition of 30 species of yeast. *Lipids* **11**, 837-844, (1976).
211 DeChavigny, A., Heacock, P. N. & Dowhan, W. Sequence and inactivation of the pss gene of Escherichia coli. Phosphatidylethanolamine may not be essential for cell viability. *The Journal of biological chemistry* **266**, 10710, (1991).
212 Maric, S., Skar-Gislinge, N., Midtgaard, S. R., Thygesen, M. B., Schiller, J., Frielinghaus, H., Moulin, M., Haertlein, M., Forsyth, V. T., Pomorski, T. G. & Arleth, L. Stealth Carriers for Low-Resolution Structure Determination of Membrane Proteins in solution. *Acta Crystallographica Section D* **70**, 317-328 (2014).
213 Eibisch, M., Zellmer, S., Gebhardt, R., Suss, R., Fuchs, B. & Schiller, J. Phosphatidylcholine dimers can be easily misinterpreted as cardiolipins in complex lipid mixtures: a matrix-assisted laser desorption/ionization time-of-flight mass spectrometric study of lipids from hepatocytes. *Rapid communications in mass spectrometry : RCM* **25**, 2619-2626, (2011).
214 Grinkova, Y. V., Denisov, I. G. & Sligar, S. G. Functional reconstitution of monomeric CYP3A4 with multiple cytochrome P450 reductase molecules in Nanodiscs. *Biochemical and biophysical research communications* **398**, 194-198, (2010).
215 QtiKWS program (http://www.qtikws.de).
216 Pedersen, J. S., Posselt, D. & Mortensen, K. Analytical treatment of the resolution function for small-angle scattering. *Journal of Applied Crystallography* **23**, 321-333, (1990).
217 Pedersen, J. S., Hansen, S. & Bauer, R. The aggregation behavior of zinc-free insulin studied by small-angle neutron scattering. *European biophysics journal : EBJ* **22**, 379-389, (1994).
218 Stuhrmann, H. in *Small-angle X-ray Scattering* (eds Otto Glatter & Otto Kratky) 197-213 (Academic Press, 1982).
219 Andersen, H. D., Wang, C. H., Arleth, L., Peters, G. H. & Westh, P. Reconciliation of opposing views on membrane-sugar interactions. *Proceedings of the National Academy of Sciences of the United States of America* **108**, 1874-1878, (2011).
220 The AxPyMOL Molecular Graphics System, Version 1.5.0.4 (2010).
221 Montelione, G. T., Wuthrich, K., Burgess, A. W., Nice, E. C., Wagner, G., Gibson, K. D. & Scheraga, H. A. Solution structure of murine epidermal growth factor determined by NMR spectroscopy and refined by energy minimization with restraints. *Biochemistry* **31**, 236-249, (1992).
222 Ogiso, H., Ishitani, R., Nureki, O., Fukai, S., Yamanaka, M., Kim, J. H., Saito, K., Sakamoto, A., Inoue, M., Shirouzu, M. & Yokoyama, S. Crystal structure of the complex

of human epidermal growth factor and receptor extracellular domains. *Cell* **110**, 775-787, (2002).

223 Ferguson, K. M., Berger, M. B., Mendrola, J. M., Cho, H. S., Leahy, D. J. & Lemmon, M. A. EGF activates its receptor by removing interactions that autoinhibit ectodomain dimerization. *Molecular cell* **11**, 507-517, (2003).

224 Zhang, X., Gureasko, J., Shen, K., Cole, P. A. & Kuriyan, J. An allosteric mechanism for activation of the kinase domain of epidermal growth factor receptor. *Cell* **125**, 1137-1149, (2006).

225 Bocharov, E. V., Mineev, K. S., Volynsky, P. E., Ermolyuk, Y. S., Tkach, E. N., Sobol, A. G., Chupin, V. V., Kirpichnikov, M. P., Efremov, R. G. & Arseniev, A. S. Spatial structure of the dimeric transmembrane domain of the growth factor receptor ErbB2 presumably corresponding to the receptor active state. *The Journal of biological chemistry* **283**, 6950-6956, (2008).

226 Svergun, D. I., Richard, S., Koch, M. H., Sayers, Z., Kuprin, S. & Zaccai, G. Protein hydration in solution: experimental observation by x-ray and neutron scattering. *Proceedings of the National Academy of Sciences of the United States of America* **95**, 2267-2272, (1998).

227 Lunin, V. V., Dobrovetsky, E., Khutoreskaya, G., Zhang, R., Joachimiak, A., Doyle, D. A., Bochkarev, A., Maguire, M. E., Edwards, A. M. & Koth, C. M. Crystal structure of the CorA Mg2+ transporter. *Nature* **440**, 833-837, (2006).

228 Palczewski, K., Kumasaka, T., Hori, T., Behnke, C. A., Motoshima, H., Fox, B. A., Le Trong, I., Teller, D. C., Okada, T., Stenkamp, R. E., Yamamoto, M. & Miyano, M. Crystal structure of rhodopsin: A G protein-coupled receptor. *Science* **289**, 739-745, (2000).

229 Shintre, C. A., Pike, A. C., Li, Q., Kim, J. I., Barr, A. J., Goubin, S., Shrestha, L., Yang, J., Berridge, G., Ross, J., Stansfeld, P. J., Sansom, M. S., Edwards, A. M., Bountra, C., Marsden, B. D., von Delft, F., Bullock, A. N., Gileadi, O., Burgess-Brown, N. A. & Carpenter, E. P. Structures of ABCB10, a human ATP-binding cassette transporter in apo- and nucleotide-bound states. *Proceedings of the National Academy of Sciences of the United States of America* **110**, 9710-9715, (2013).

230 Shinoda, T., Ogawa, H., Cornelius, F. & Toyoshima, C. Crystal structure of the sodium-potassium pump at 2.4 A resolution. *Nature* **459**, 446-450, (2009).

231 Higgins, M. K., Eswaran, J., Edwards, P., Schertler, G. F., Hughes, C. & Koronakis, V. Structure of the ligand-blocked periplasmic entrance of the bacterial multidrug efflux protein TolC. *Journal of molecular biology* **342**, 697-702, (2004).

232 Svergun, D. I. Restoring low resolution structure of biological macromolecules from solution scattering using simulated annealing. *Biophysical journal* **76**, 2879-2886, (1999).

233 Svergun, D. I., Petoukhov, M. V. & Koch, M. H. Determination of domain structure of proteins from X-ray solution scattering. *Biophysical journal* **80**, 2946-2953, (2001).

234 Kucerka, N., Nagle, J. F., Feller, S. E. & Balgavy, P. Models to analyze small-angle neutron scattering from unilamellar lipid vesicles. *Physical review. E, Statistical, nonlinear, and soft matter physics* **69**, 051903, (2004).

235 Makhatadze, G. I., Clore, G. M. & Gronenborn, A. M. Solvent isotope effect and protein stability. *Nature structural biology* **2**, 852-855, (1995).

236 Hagn, F., Etzkorn, M., Raschle, T. & Wagner, G. Optimized phospholipid bilayer nanodiscs facilitate high-resolution structure determination of membrane proteins. *Journal of the American Chemical Society* **135**, 1919-1925, (2013).

237 Majewski, J., Kuhl, T. L., Wong, J. Y. & Smith, G. S. X-ray and neutron surface scattering for studying lipid/polymer assemblies at the air-liquid and solid-liquid interfaces. *Journal of biotechnology* **74**, 207-231, (2000).

238 Akesson, A., Lind, T. K., Barker, R., Hughes, A. & Cardenas, M. Unraveling dendrimer translocation across cell membrane mimics. *Langmuir : the ACS journal of surfaces and colloids* **28**, 13025-13033, (2012).

239 Molloy, S. Reactive resistance. *Nature reviews. Genetics* **11**, 240, (2010).

Publications

Article I

Wadsäter, M. H., Maric, S., Simonsen, J. B., Mortensen, K. and Cardenas Gomez, M. 2013, The effect of using binary mixtures of zwitterionic and charged lipids on nanodisc formation and stability, ***Soft Matter*** *9, (7)* 2329-2337.

Article II

Maric, S., Thygesen, M. B., Schiller, J., Moulin, M., Marek, M., Haertlein, M., Forsyth, V. T., Arleth, L. and Pomorski, T. G. 2014. Biosynthetic preparation of selectively deuterated phosphatidylcholine in genetically modified *Escherichia coli*. ***In preparation for Journal of Lipid Research***.

Article III

Maric, S., Skar-Gislinge, N., Midtgaard, S. R., Thygesen, M. B., Schiller, J., Frielinghaus, H., Moulin, M., Haertlein, M., Forsyth, V. T., Pomorski, T. G., and Arleth, L. 2013. Stealth Carriers for Low-Resolution Structure Determination of Membrane Proteins in Solution, ***Acta Crystallographica Section D70.*** 317-328

Article I

Soft Matter

RSC Publishing

PAPER

View Article Online
View Journal | View Issue

Cite this: *Soft Matter*, 2013, **9**, 2329

The effect of using binary mixtures of zwitterionic and charged lipids on nanodisc formation and stability†

Maria Wadsäter,[a] Selma Maric,[b] Jens B. Simonsen,*[c] Kell Mortensen[d] and Marité Cardenas*[a]

Nanodiscs are self-assembled ~10 nm particles composed of lipid bilayer patches, stabilized by helical amphipathic belt proteins. The size, monodispersity and well-defined structure make the nanodiscs a popular model for the biological cell membrane, especially for structural and functional studies of membrane proteins. The structures and properties of nanodiscs made of zwitterionic lipids are well known. However, the biological cell membrane is negatively charged and thus nanodiscs containing anionic lipids should provide a better mimic of the native environment for membrane proteins. Despite the broad potential of charged nanodiscs, a systematic study of the influence of charged lipids on the nanodisc structure and stability has not yet been accomplished. In this paper, binary systems of zwitterionic DMPC mixed with the anionic lipids DMPG or DMPA or with the cationic synthetic DMTAP are used to prepare negatively and positively charged nanodiscs, respectively. Size exclusion chromatography analysis shows that nanodiscs can be prepared with high yield at all compositions of DMPC and DMPG, while mixtures of DMPC with either DMPA or DMTAP impair nanodisc formation. The presence of DMPG improves the stability of the nanodisc, both thermally and over time upon storage at −20 °C, as compared to pure DMPC nanodiscs. This stabilization is attributed to favourable electrostatic interactions between the anionic head of DMPG and cationic charges of the belt protein and inter-nanodisc repulsion that prevents aggregation of nanodiscs. In contrast, even small fractions of DMPA result in a faster degradation at −20 °C. These results suggest that the mixing of DMPC and DMPG provides nanodiscs that are better suited for studies of the function and structure of membrane proteins not only due to their inherent charge but also due to their improved thermal and storage stability compared to pure DMPC nanodiscs.

Received 29th August 2012
Accepted 17th December 2012

DOI: 10.1039/c2sm27000e

www.rsc.org/softmatter

Introduction

Nanodiscs are small monodispersed disc-like particles that self-assemble from mixtures of phospholipids and amphipathic helical proteins. Sligar and co-workers optimized the primary structure of apolipoprotein A-I in human high density lipoproteins in terms of producing monodispersed and well-defined nanolipoprotein particles.[1] This resulted in a synthetic gene from which Membrane Scaffold Proteins (MSP) were expressed. Upon mixing MSP with lipids and detergents at appropriate stoichiometries, well-defined monodispersed particles self-assemble, typically known as "nanodiscs".[2] The diameter of these lipid bilayer discs is controlled by the length of the MSP, which in turn can be varied by insertions of 22-mer amphipathic α-helices in the approximately 200 residues long original MSP sequence.[1,2] Lately these nanodiscs have attracted significant interest within the research communities due to their peculiar structure of small lipid bilayer patches that can efficiently serve as a native-like model of the cell membrane for membrane proteins.[3,4]

The formation and structure of nanodiscs prepared from different zwitterionic phospholipids have been extensively studied.[1,2,4–15] Size exclusion chromatography (SEC) was used to evaluate the quality of 1,2-dipalmitoyl-*sn-glycero*-3-phosphocholine DPPC nanodisc preparations using different types of MSP and lipid to protein ratios.[1,2] Using atomic force microscopy (AFM), the disc-like structure of DPPC nanodiscs was confirmed and a rough measurement of the height of the lipid bilayer was accomplished.[1] Small angle neutron and X-ray scattering (SANS and SAXS) studies revealed the overall structure and dimensions of nanodiscs made of different

[a]*Nano-Science Center and Institute of Chemistry, Faculty of Science, University of Copenhagen, DK-2100, Copenhagen, Denmark. E-mail: cardenas@nano.ku.dk*

[b]*Structural Biophysics, Niels Bohr Institute, University of Copenhagen, Bülowsvej 17, DK-1870 Frederiksberg C, Denmark*

[c]*Department of Basic Sciences and Environment, Faculty of Life Sciences, University of Copenhagen, Thorvaldsensvej 40, DK-1871 Frederiksberg C, Denmark. E-mail: jbsi@life.ku.dk*

[d]*Nano-Science Center and Niels Bohr Institute, Universitetsparken 5, 2200, Copenhagen, Denmark*

† Electronic supplementary information (ESI) available. See DOI: 10.1039/c2sm27000e

phosphatidylcholines[11,12,16] and an intrinsic, slightly temperature-dependent elliptical shape of the nanodisc was reported.[12] Moreover, in nanodiscs, the 1,2-dilauroyl-*sn-glycero*-3-phosphocholine (DLPC)[12] bilayer was found to be laterally compressed, while 1-palmitoyl-2-oleoyl-*sn-glycero*-3-phosphocholine (POPC)[12] and DPPC[16] bilayers were laterally expanded as compared to that in large liposomes. These observations were attributed to the adaptation of lipids to the thickness of the hydrophobic double belt at the MSP–lipid interface. This hydrophobic matching effect of the lipid tail and the belt protein is also reflected in interfacial structures of high order for gel phase DMPC nanodiscs, while the disorder in terms of interfacial roughness increases for fluid phase DMPC and gel phase DPPC nanodiscs.[17]

As most biological cell membranes carry a net negative charge, the inclusion of negatively charged lipids in the nanodisc is expected to improve its biomimetic properties.[18] Cationic phospholipids do not naturally occur in biological membranes but synthetic insoluble surfactants (often referred to as lipids) are frequently used in, for instance, drug and gene delivery systems as they bind to negatively charged molecules such as DNA.[19] The use of negatively or positively charged nanodiscs can provide an additional degree of freedom when creating alternative systems both for drug-carrier systems[20] and for fundamental studies of the structure and dynamics of membrane proteins. For instance, electrostatic forces of attraction between negatively charged nanodiscs and insoluble cationic surfactants were used to form a completely hydrated well-aligned nanodisc layer below the air–water interface.[21] Moreover, charged nanodiscs may allow for assembly of alternating anionic and cationic matrices that could be used for crystallographic purposes or in studies of interactions of different membrane proteins. Despite the biomimetic relevance of anionic nanodiscs and the potential of charged nanodiscs in alternative experimental systems for membrane protein studies, a systematic study of the influence of charged lipids on nanodisc structure and stability has not yet been accomplished. Hence, in this paper we attempted to prepare stable negatively charged nanodiscs using the membrane scaffolding protein MSP1D1[2] and binary mixtures of zwitterionic 1,2-dimyristoyl-*sn-glycero*-3-phosphocholine (DMPC) and anionic phospholipids 1,2-dimyristoyl-*sn-glycero*-3-phospho-(1′-*rac*-glycerol) (DMPG) or 1,2-dimyristoyl-*sn-glycero*-3-phosphate (sodium salt) (DMPA) (Fig. 1B) at various compositions. The possibility of forming stable monodispersed positively charged nanodiscs from mixtures of DMPC and the cationic 1,2-dimyristoyl-3-trimethylammonium-propane (DMTAP) is also studied. Fig. 1 gives schematics of the nanodisc structure and the chemical structures of the lipids used in this work.

In this study, SEC is used to evaluate the nanodisc yield as a function of composition of the assembly mixtures. In this case, the nanodisc yield relates to the relative yield between the nanodisc elution peak and those for lipid free proteins and other protein–lipid aggregates in the SEC chromatogram. In this way we show that monodispersed nanodiscs can be formed with high yield at all compositions for DMPC and DMPG mixtures, while this was not the case for mixtures of DMPA and DMPC. In the latter case, a high yield of nanodiscs was obtained

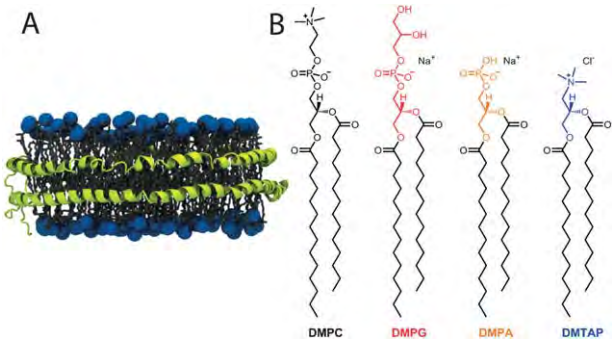

Fig. 1 (A) Schematic representation of the structure of the nanodisc seen from the plane of the lipid bilayer. (B) Chemical structures of the phospholipids used to prepare charged nanodiscs in this work.

only for $X_{DMPA} \leq 0.25$. The inclusion of only 10 mol% cationic DMTAP ($X_{DMTAP} = 0.1$) in the assembly considerably deteriorates the nanodisc yield. A considerably greater stability upon storage at −20 °C is observed for nanodiscs containing 25 mol% DMPG, as compared to pure DMPC nanodiscs. On the contrary, the use of DMPA has a negative impact on the stability over time of the nanodisc, even though the lipid to protein ratio used gave good yields of nanodiscs upon assembly. In addition, DSC showed that the presence of DMPG significantly increased the thermal stability of the nanodisc complex. These results are discussed in terms of the importance of lipid–lipid and lipid–protein interactions for the self-assembly and the stability of the nanodiscs.

Materials and methods

Materials

DMPC, DMPG, DMPA and DMTAP in organic solution were all purchased from Avanti Polar Lipids, Inc. and used as received. Sodium phosphates ($Na_2HPO_4 \cdot 12H_2O$ and $NaH_2PO_4 \cdot H_2O$), tris-(hydroxymethyl) aminomethane (Tris), sodium chloride (NaCl), sodium cholate, chloroform, methanol, molybdate reagent ($(NH_4)_6Mo_7O_{24}$), sulphuric acid, ascorbic acid and primuline were purchased from Sigma Aldrich and used as received. Ultrapure water (Ultra Clear Basic, SG, resistivity 18.2 MΩ cm) was exclusively used in all work.

Nanodisc preparation

The amphipathic scaffold protein was expressed and purified according to Bayburt *et al.*[1] with further modification resulting in MSP1D1.[2] The samples that were analyzed by size exclusion chromatography and phosphorus analysis were prepared in Tris buffer, while the nanodiscs destined for DSC were prepared using a sodium phosphate buffer as the pH of Tris buffer is known to vary with temperature. Nanodisc samples were prepared according to a protocol described elsewhere.[1,2] Briefly, the different lipids were mixed in appropriate quantities to obtain the desired molar ratios and the organic solvent was rapidly removed under a nitrogen stream. The dried mixtures were then exposed to high vacuum for 3 hours to remove

residual traces of the organic solvent. The dried lipid films were then resuspended in a Tris or phosphate buffer (20 mM Tris/sodium phosphate, 100 mM sodium chloride at pH 7.4) including 100 mM sodium cholate and then mixed with the aqueous solution of MSP1D1. After 1 h incubation of the detergent–lipid–MSP1D1 solutions at a temperature close to the gel–liquid crystalline phase transition temperature of the lipids, BioBeads SM-2 Absorbent (Bio-Rad) was added to remove the detergent and initiate the assembly process. The samples were filtered through 0.22 μm centrifugal filters (Millipore) and separated by size exclusion chromatography (0.5 ml min^{-1}) while monitoring the absorbance at 280 nm (Superdex 200 10/300 GL column, ÄKTA purifier system, GE Healthcare). In this way the assembled nanodiscs could not only be distinguished from other lipid–protein aggregates and free MSP1D1 but the chromatograms also provided an indication of the particle size distribution and the nanodisc yield of the preparation. The central fractions of the nanodisc retention peak (corresponding to ~30% of the total volume in the retention peak) were collected, pooled and used for the phosphorus analysis, DSC studies and the test of stability upon storage. Choosing a small fraction of the total volume peak was previously shown to improve the monodispersity of the nanodisc preparation.[5]

Differential Scanning Calorimetry (DSC)

DSC measurements were carried out in a VP-DSC system from MicroCal. The samples were heated at a rate of 1 °C min^{-1} at constant pressure (~1.7 bar). All nanodisc samples had a lipid concentration ranging from 0.8 to 1.7 mM. The Origin software package from MicroCal was used to reduce the calorimetric data. First, a reference scan (buffer in both chambers) was subtracted from the sample data to eliminate the impact of instrument-related differences in the performance of the two chambers, *e.g.* different heat transfer to the chambers. A baseline subtraction is required due to the different heat capacity of the nanodiscs and the solvent. The baseline was defined using a cubic function to connect the baselines on each side of the endothermic peak corresponding to the phase transition. The data were normalized to the lipid concentration and to the maximal intensity of the gel to liquid crystalline phase transition peak of the nanodisc lipids.

Thin Layer Chromatography (TLC) and phosphorus analysis

In order to estimate the overall composition of lipids in the nanodiscs made from mixtures of DMPG and DMPC, the lipids were extracted after nanodisc formation according to the method of Bligh and Dyer.[22] Briefly, the following procedure was repeated thrice: (i) addition of chloroform, methanol and water to the nanodisc sample and (ii) extraction of the lipid containing chloroform phase upon phase separation. DMPC and DMPG were then separated on TLC plates developed in chloroform/acetone/methanol/acetic acid/water (30 : 40 : 10 : 10 : 5, v/v/v/v/v). Approximately 100 nmol lipids were loaded to a TLC plate (silica gel 60 F_{254}, Merck) and were separated upon migration in the mobile phase that is drawn up by capillary forces. The separations were visualized in UV-light after spraying primuline solution (5 mg primuline in 100 ml acetone/water, 80/20, v/v) over the plate. The separated spots were compared to reference DMPG and DMPC spots and scraped off using a razor blade.

The lipid concentration of the extracted nanodisc lipids in each of the spots recovered from the TLC plate was determined by analysis of the phosphoric amount in the sample according to the method of Rouser *et al.*[23] The lipids were heated in 70% perchloric acid at 180 °C for 30 minutes followed by addition of ammonium molybdate and ascorbic acid and further heated to 80 °C for 10 minutes. The absorbance at 780 nm was measured and the total phosphorus concentration was determined using a phosphorus standard curve.

Results

The formation of monodispersed charged nanodiscs

The initial evaluation of the nanodisc preparation in terms of heterogeneity of the assembled sample was assessed *via* SEC. The size exclusion chromatograms were normalized to the maximal nanodisc peak intensity and the relative yield of nanodiscs compared to large aggregates and lipid-free MSP after sample filtration.[2,24] This relative nanodisc yield is in this text referred to as the nanodisc yield.

The nanodisc yield is improved by using mixed lipid–detergent micelles instead of lipid lamellar phases in the nanodisc assembly.[1] The anionic detergent sodium cholate is a bile salt known to disrupt vesicles due to the formation of mixed micelles.[25] The size exclusion chromatograms of DMPC nanodiscs prepared in the presence and absence of sodium cholate did indeed show an increase in nanodisc yield for samples prepared using detergent (Fig. SI 1, ESI†). The overall shape and the position of the nanodisc retention peak were however not affected by use of detergent. Moreover, the gel to liquid crystalline phase transition of the nanodisc lipids, probed by differential scanning calorimetry (Fig. SI 2, ESI†), was similar for the two nanodisc samples, indicating that no or at least only a very minor fraction of sodium cholate may be present in the sample after incubation with biobeads. Thus, given that the co-addition of cholate actually improves the nanodisc yield and given that no influences from detergent in the nanodisc samples are expected in this case, we decided to perform nanodisc assembly with charged lipids in the presence of cholate.

Bayburt *et al.* compared the size exclusion chromatograms of MSP1D1-based nanodiscs made of DPPC for different lipid to protein molar ratios to determine the optimal stoichiometry for obtaining a high yield of nanodiscs.[24] An optimal DPPC to MSP1D1 ratio of 75–100 : 1 was found and the nanodiscs contained on average 81 DPPC per MSP1D1 as measured by scintillation counting while the overall disc-like structure was confirmed by SAXS.[2] We thus have attempted to create nanodiscs for DMPC and its mixture with charged nanodiscs at lipid to belt protein ratios close to this value. Fig. 2A gives the size exclusion chromatograms of pure DMPC nanodiscs prepared at lipid to MSP1D1 molar ratios ($\theta_{lipid/MSP1D1}$) ranging from 60, 80, 90 to 100 : 1. Nanodiscs were eluted in between 12.3 and

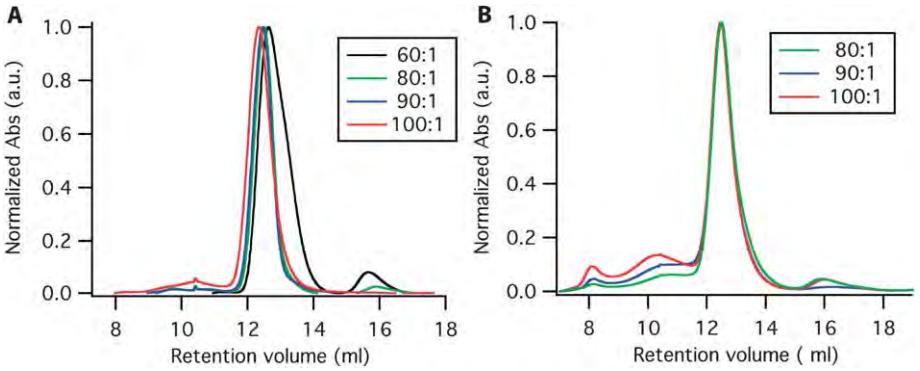

Fig. 2 Size exclusion chromatograms of (A) pure DMPC and (B) $X_{DMPA} = 0.25$ nanodiscs prepared at different DMPC to MSP1D1 ratios indicated in the figure label. Nanodiscs eluted at $V = 12.3$–12.6 ml, while lipid free proteins eluted at $V = 16$ ml and other lipid–protein aggregates eluted at $V = 8$–11 ml.

12.6 ml, while lipid-free MSP1D1 eluted at ~16 ml and other larger lipid–protein-aggregates showed a retention volume of 8–11 ml. The chromatograms suggest an optimal $\theta_{lipid/MSP1D1} =$ 80–90, as the nanodisc peak relative to the peaks corresponding to lipid-free MSP1D1 and other larger lipid–protein-aggregates is maximized at these stoichiometries. Furthermore, the nanodisc peak is narrowest at these stoichiometries, thus indicating less polydispersity in the nanodisc preparation. This optimal $\theta_{lipid/MSP1D1}$ is in excellent agreement with that previously reported for DPPC nanodiscs.[2] Reported values for the cross-sectional area occupied by DMPC and DPPC[26] are relatively similar both in the gel (47.2 Å^2 at 10 °C for DMPC[27] and 47.9 Å^2 at 20 °C for DPPC) and in the liquid crystalline phase (59.6 Å^2 at 30 °C for DMPC[26] and 64 Å^2 at 50 °C for DPPC). Thus the result supports previous SAXS and SANS studies, which measured a similar total area of the lipid bilayer core for nanodiscs prepared from different lipids and suggested that the area of the lipid bilayer disc is mainly controlled by the MSP1D1 belt protein.[12]

The introduction of 25 mol% anionic DMPA in the nanodisc assembly mixture ($X_{DMPA} = 0.25$) did not seem to alter the optimal $\theta_{lipid/MSP1D1}$ for nanodisc formation (Fig. 2B). Indeed, the lipid to protein ratio is expected to deviate by maximally ±9 lipids for the different charged lipids used in this work, based on the assumption that the area observed for the DPPC nanodisc lipid core[2] is fixed and that the cross-sectional area of any of the charged lipids differs by maximally ±5 Å^2 of that for the cross sectional area of DPPC. Therefore, a $\theta_{lipid/MSP1D1} = 90$ is expected to provide enough lipids to produce well filled nanodiscs for DMTAP, DMPG and DMPA and this ratio was hereafter used in all nanodisc preparations.

The size exclusion chromatograms of the nanodiscs prepared from binary mixtures of DMPC and either of the anionic DMPG or DMPA with molar fractions equal to 0, 0.25, 0.5, 0.75 and 1 (= pure system) expressed in terms of the charged lipids (X_{DMPG} and X_{DMPA}, respectively) are shown in Fig. 3. This figure also includes the corresponding data for binary mixtures of DMPC and the cationic DMTAP with a $X_{DMTAP} = 0.1$ molar fraction. Again, the ratio between the amount of nanodiscs relative to both lipid-free MSP1D1 and other larger lipid–protein-aggregates (eluted at 8–11 ml) serves as a simple assessment of the nanodisc self-assembly process.[15] The chromatograms indicate that well-defined nanodiscs could be produced with high yield at all proportions of DMPC and DMPG, while a high yield of nanodiscs was obtained for only $X_{DMPA} = 0.25$. The yield of the nanodiscs composed of mixtures of DMPC and DMPG (Fig. 3A) increased with increasing DMPG fraction, as the peak intensities for large aggregates and lipid-free MSP1D1 decreased in relation to that of nanodiscs. Even though DMPA also carries a negative charge, the retention peak of the lipid–protein assemblies that elute at 12.5 ml splits into two different peaks for $X_{DMPA} \geq 0.5$. For $X_{DMPA} > 0.5$, the retention volume between these peaks increased with increasing DMPA fraction. Moreover, a large fraction of the material was eluted in the void volume of the SEC column for $X_{DMPA} = 0.5$ and 0.75, suggesting the formation of aggregates much larger than nanodiscs (the exclusion limit of the superdex 200 size exclusion column used is ~1.3×10^6 g mol^{-1} for globular proteins, as compared to ~1.7×10^5 g mol^{-1} for DMPC nanodiscs).

The inclusion of DMTAP in the assembly mixture of lipids and MSP1D1 considerably impaired the quality of the nanodisc sample as a significant amount of large aggregates appeared already at $X_{DMTAP} = 0.1$. At higher molar fractions of DMTAP ($X_{DMTAP} = 0.3$) a turbid solution was obtained after the removal of the biobeads, indicating precipitation into micrometer-sized aggregates. No further analysis of the precipitated DMTAP-containing sample was undertaken.

Generally, compared to pure zwitterionic nanodiscs, the SEC retention peak of nanodiscs prepared from anionic–zwitterionic lipid mixtures shifted toward smaller retention volumes (Fig. 3A and B), while the retention peak for nanodiscs prepared from cationic–zwitterionic mixtures shifted toward larger retention volumes. If size-related, these shifts would correspond to the fact that larger nanodiscs are assembled from anionic than cationic lipids. However, this is unlikely given that MSP1D1 is expected to control the nanodisc area as discussed below and that $\theta_{lipid/MSP1D1}$ remained constant regardless of the DMPG/DMPC composition (Table 1). Thus, this shift is more likely related to attractive and repulsive interactions between the agarose–dextran matrix of the superdex 200 column and the charged nanodiscs (the direction of the shift is indeed

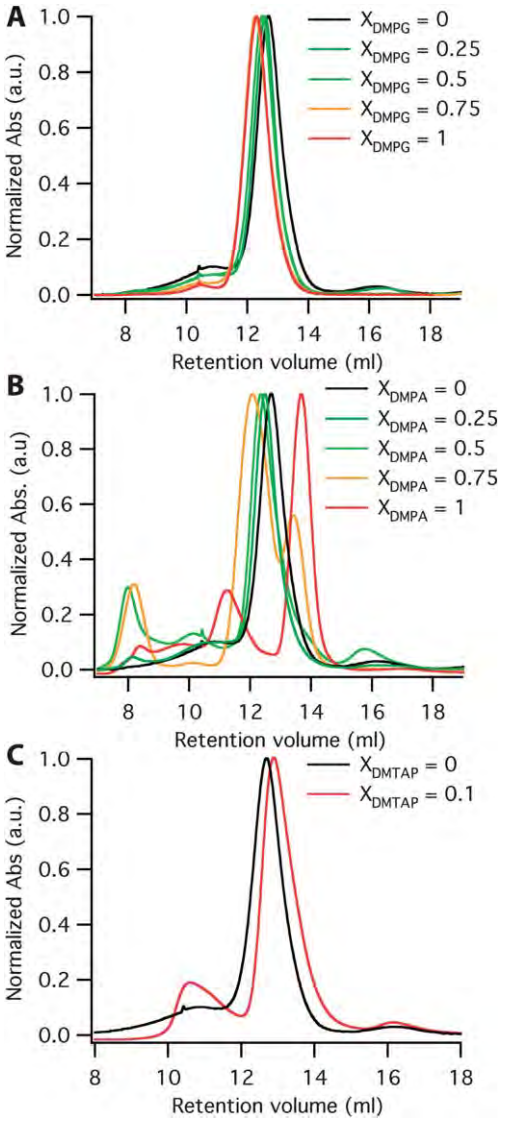

Fig. 3 Size exclusion chromatograms of samples prepared from mixtures of DMPC and the anionic lipids (A) DMPG or (B) DMPA with the molar fractions of 0, 0.25, 0.5, 0.75 and 1, or the cationic synthetic lipid (C) DMTAP with the molar fractions of 0 and 0.1.

Table 1 Measured lipid/protein stoichiometry and lipid composition in the DMPG/DMPC nanodiscs

X_{DMPG} in the assembly mixture	Lipids/MSP1D1	X_{DMPG} in nanodiscs[b]
0	90 ± 5	NA[a]
0.25	88 ± 1	0.26
0.5	91 ± 1	0.50
0.75	92 ± 1	0.78
1.0	91 ± 6	NA[a]

[a] Not applicable. [b] Typically the measured fraction of DMPG in extracted lipids from nanodiscs varies by less than ±5% units among separate nanodisc preparations and analyses.

dependent on the charge of the additional lipid used in the assembly mixture).

Nanodisc stability under storage at −20 °C as a function of composition

The nanodisc is supposed to serve as a tool for studies of membrane proteins. For biophysical characterization at, for instance, large-scale facilities, samples are typically prepared and frozen prior to measurements. Thus, the stability over time of the nanodisc samples upon storage is central for routine studies in the lab. The effect of lipid composition on nanodisc stability after storage in a freezer at −20 °C was examined by running the samples a second time over the SEC column after

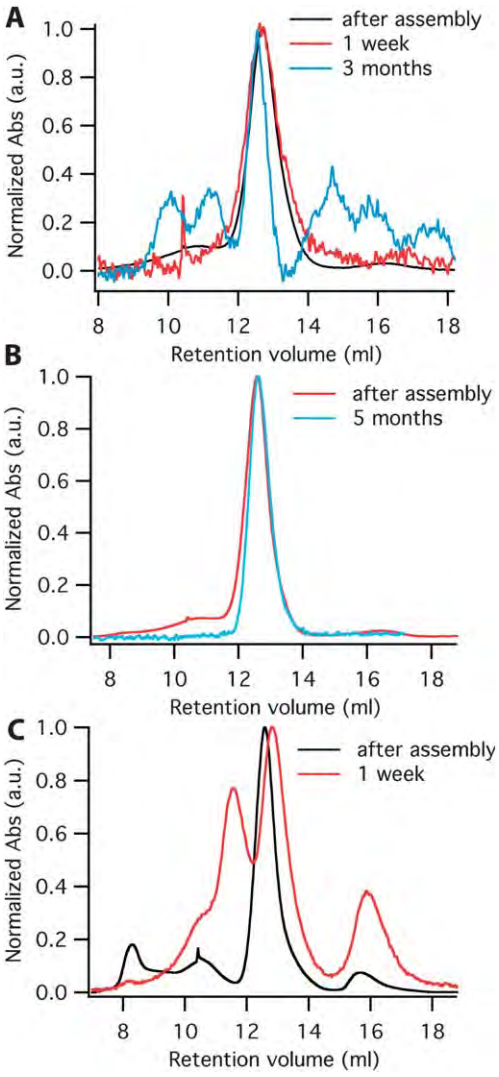

Fig. 4 Size exclusion chromatograms of fresh and stored nanodiscs. The fresh nanodiscs are taken directly after assembly (*i.e.* less than one day). About 30% of the nanodisc peak was collected and stored at −20 °C and re-subjected to SEC: (A) fresh pure DMPC nanodiscs and after storage at −20 °C for 1 week and 3 months, (B) fresh X_{DMPG} = 0.25 nanodiscs and after storage for 5 months at −20 °C, (C) fresh X_{DMPA} = 0.25 nanodiscs and after storage for 1 week. The concentration of the sample loaded 1 week and 3 months after preparation was considerably lower for the DMPC nanodiscs than for the DMPG and DMPA containing nanodiscs and the noise is thus more apparent in these chromatograms.

different periods of storage (Fig. 4). The stability of the sample was evaluated by comparison of the relative peak intensities of the elution of nanodiscs, lipid-free proteins and other protein–lipid aggregates. Storage for 1 week did not induce large changes in the integrity of the DMPC nanodisc sample, while considerable degradation was observed after three months of storage at −20 °C (Fig. 4A). In contrast, the $X_{DMPG} = 0.25$ nanodiscs showed no signs of degradation even after storage for 5 months at −20 °C (Fig. 4B). Interestingly, enhanced stability upon storage was not observed for the anionic DMPA, instead the nanodiscs prepared from a DMPA containing assembly mixture ($X_{DMPA} = 0.25$) were significantly degraded already after storage for 1 week at −20 °C (Fig. 4C). Given their poor storage stability, the nanodiscs prepared from DMPA were not further analysed.

Thermal stability of the nanodiscs as a function of DMPG/DMPC composition

Given the remarkable stability upon storage in the freezer of the DMPG containing nanodiscs, further evaluation of their thermal stability was achieved by differential scanning calorimetry (DSC). Temperature scans covering a range from 5 to 105 °C for the nanodiscs, prepared from assembly mixtures with DMPG molar fractions equal to $X_{DMPG} = 0$, 0.25, 0.5, 0.75 and 1, are shown in Fig. 5. In general, lipids in nanodiscs display a relatively broad gel–liquid phase transition since the small number of lipids in each nanodisc have a less cooperative effect[13,28] as compared to vesicles. Moreover, for DMPC (and other lipid nanodisc systems like DPPC nanodiscs), the gel to liquid crystalline phase transition temperature (T_m) was found to shift by 3–4 °C to higher temperatures in nanodiscs as compared to vesicles.[28] The increase in T_m was attributed to the lateral surface pressure provided by the protein belt on the lipid bilayer[13] but could also be due to the fact that about one-third of the lipids are interfacing the MSP1D1 protein and may experience strong lipid–protein interactions.[28]

Each of the DSC scans displays one or two endothermic peaks. The first peak occurred between 24.8 and 28 °C for all compositions (Fig. 5), and corresponds to the lipid phase transition confirming the bilayer structure of the nanodiscs. The second endothermic peak present at ~90 °C was present for $X_{DMPG} = 0$, 0.25 and 0.5 nanodiscs only and is attributed to the MSP1D1 protein denaturation, as in previous DSC studies of lipid–apolipoprotein A-I particles.[29] The figure shows that the protein denaturation peak shifts gradually to slightly higher temperatures when the fraction of DMPG increases from 0 to 50% (T_d = ~89, 91 and 93 °C for $X_{DMPG} = 0$, 0.25 and 0.5 respectively). At a higher fraction of DMPG (>50%) the peak completely disappears from the detected temperature range.

In general, the gel–liquid crystalline phase transition is similar to previous results for nanodiscs of pure DMPC or DPPC.[13,28] Our results for the $T_m = 28.0$ °C of DMPC nanodiscs are in excellent agreement with those observed by Shaw *et al.*[28] This shows that the small modification performed on the MSP to generate MSP1D1, which included the deletion of the first 11 *N*-terminal amino acids and the replacement of the factor X cleavage site by a TEV protease recognition site and a linker,[2] does not noticeably affect the thermotropic behaviour of the lipid bilayer in the nanodisc.

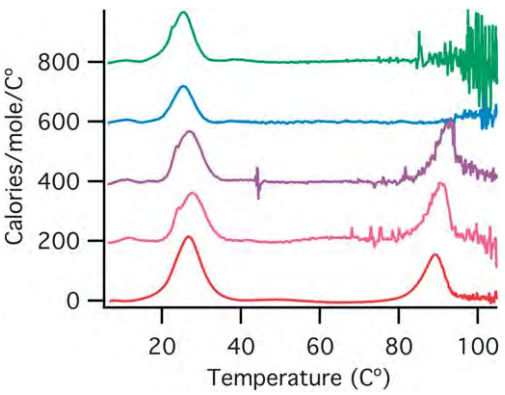

Fig. 5 The enthalpy per mole lipid measured by DSC in thermal scans of $X_{DMPG} =$ 0 (red), 0.25 (pink), 0.5 (purple), 0.75 (blue) and 1 (green) nanodiscs. The curves were normalized to the lipid concentration and the maximum intensity in the lipid phase transition peak.

Composition of DMPG/DMPC nanodiscs

Although the overall structure for multicomponent mixtures may seem to be monodisperse, as for the DMPG/DMPC nanodiscs, discrete polydispersity[5] and compositional variability[30] may occur. In order to determine the overall composition of the DMPG/DMPC nanodisc assemblies, the total lipid and protein concentrations were estimated by analysis of the phosphoric amount of the nanodiscs and the absorbance measured at 280 nm, respectively (Table 1). Interestingly, the number of lipids per MSP1D1 is found to be independent of DMPG/DMPC composition, thus supporting our assumption of fixed nanodisc size and validating our choice of $\theta_{lipid/MSP1D1} = 80$–90 in the mixed lipid nanodisc preparation. Furthermore, the lipid composition of the extracted lipids was analysed by separating the extracted lipids by TLC. These results verify that the composition of the initial mixture of DMPG, DMPC and MSP1D1 is indeed kept in the assembly of nanodiscs, although compositional variance among individual nanodiscs may still occur.

Discussion

It is clear that stable nanodiscs can be made from mixtures of DMPC and DMPG with increasing yield (Fig. 3) and stability (Fig. 4 and 5) upon increasing DMPG content. In contrast, increasing the content of DMPA resulted in lower nanodisc yield and decreased nanodisc stability (Fig. 3 and 4). Finally, nanodiscs prepared from DMPC and the cationic DMTAP could only be prepared at 10% DMTAP (Fig. 3C) at lower relative yields than for pure DMPC and with poor storage stability.

Previous studies of the interaction of human apolipoprotein A-I and other apolipoproteins with a mixture of DMPC and DMPG showed that most apolipoproteins bind more strongly to DMPG than to DMPC.[29,31,32] The strong DMPG–apolipoprotein

A-I interaction was attributed to favourable electrostatic interactions between the anionic phosphate group of the DMPG head and cationic sites in the apolipoprotein.[29] In contrast, the interaction of the apolipoprotein with zwitterionic DMPC was proposed to be mainly of hydrophobic character[33] as the interactions with the negatively charged phosphate group in the zwitterionic PC head were suggested to be both electrostatically and sterically screened due to the positively charged and bulky choline moiety (see schematics in Fig. 1B).[32] As MSP1D1 is a genetically modified version of apolipoprotein A-I (ref. 1) it is expected to possess a similar pattern of charges as its precursor. Thus, strong electrostatic interactions between the negatively charged PG head and cationic residues in MSP1D1 could facilitate the nanodisc formation as supported by the observations of increased yield of nanodiscs with increasing fraction of DMPG in the size exclusion chromatograms (Fig. 3A).

Despite the similarities between DMPG and DMPA in terms of negative charge, a drastic reduction in nanodisc yield occurred when including DMPA in the nanodisc preparation (Fig. 3). Using DSC and ^{31}P-NMR spectroscopy, the interaction of DMPA with apolipophorin III was found to be weaker than for both DMPC and DMPG at pH 7.2, when the DMPA carries a single charge.[32] Hydrogen bonding among the PA head groups[34] was proposed to impair the PA–protein interactions.[32] Moreover, DMPA and DMPC exhibit a non-ideal mixing behaviour for which DMPA–DMPC complexes or dimers are proposed to form.[35] Such lipid complexation may overcome the MSP1D1–lipid interactions necessary for nanodisc assembly. Moreover, other factors beyond lipid–lipid interactions such as the hydration bonding capacity of the PA head groups and the packing parameter for DMPA are expected to influence the MSP1D1–lipid interaction, since nanodiscs could not be formed from pure DMPA (Fig. 3B). In contrast, DMPG and DMPC present a nearly ideal mixing behaviour at all compositions and pH 7 (ref. 36) and thus no strong lipid–lipid interactions are expected to occur for DMPC–DMPG nanodiscs. Finally, the net charge of the anionic lipid is different at the conditions for nanodisc formation and size exclusion separation (pH 7.4, 100 mM NaCl buffer). For DMPA, the majority (85%) of the molecules ($pK_{a2} = 8$ for DMPA in 100 mM NaCl (ref. 37)) are expected to carry a single negative charge, while only 15% carry a double negative charge in comparison with the single charge carried by DMPG at the same pH. Such differences in net charge may have an important effect on the interplay between the DMPC, DMPA/DMPG and MSP1D1 molecules.

In analogy with the argument of favorable electrostatic interactions between the single negative charge of PG and the cationic sites of MSP1D1, repelling interactions between the TAP head group and the cationic charges of MSP1D1 upon adopting the belt structure in the nanodisc may make the nanodisc an unfavorable structure, resulting in low nanodisc yield as observed by SEC (Fig. 3C). Alternatively, strong non-ideal mixing behavior for DMTAP and DMPC[38] due to attracting interactions between the TAP and PC head groups could further interfere with the necessary lipid–protein interactions in the nanodisc structure thus decreasing their stability. Finally, MSP1D1 does indeed carry a net negative charge at pH 7.4, and strong electrostatic interactions between the TAP head groups and another region of the MSP1D1 protein may overcome the lipid–lipid and lipid–protein interactions present in the nanodisc structure, thus impairing the proper folding of MSP1D1 in the best conformation and resulting in low nanodisc yields as observed by SEC (Fig. 3C) due to the induction of other types of lipid–protein aggregates and phase separation, as typically observed for oppositely charged biopolymer–surfactant mixtures.[39,40]

DSC scans (Fig. 5) allowed the probing of not only the lipid phase transition of the nanodisc lipids (first endothermic peak) but also the MSP1D1 protein unfolding and/or structural degradation of the nanodisc (second endothermic peak). An increasing thermal stability of the MSP protein, and thereby the entire nanodisc structure, is observed for increasing content of DMPG as the protein unfolding peak shifts to higher temperatures until completely disappearing from the detected temperature range (up to 105 °C) for $X_{DMPG} > 0.5$. This is in agreement with previous results for complexes of human apolipoprotein A-I and DMPC, in which the apolipoprotein was relatively easily denatured as compared to apolipoprotein A-I in complex with DMPG.[29]

Regarding nanodisc stability, it is clear that both the thermal stability and stability upon storage at −20 °C of the nanodiscs are closely related to the relative yield of nanodiscs obtained from the self-assembly process (Fig. 3, 4 and 5). Attractive electrostatic PG–MSP1D1 interactions or near ideal lipid–lipid interactions for DMPG and DMPC may stabilize the DMPG containing nanodiscs while non-ideal interactions of DMPA with DMPC may dominate over the lipid–protein interactions making the nanodiscs a less stable aggregate in solution. The remarkable thermal (Fig. 5) and storage (Fig. 4) stability measured for nanodiscs containing a small fraction of DMPG may be attributed to the attractive electrostatic interactions between the anionic DMPG and positively charged residues of the protein. A very dynamic nature of the nanodisc prepared from 1,2-dioleoyl-*sn-glycero*-3-phosphocholine (DOPC) was proposed since correlated unfolding events of the MSP were observed *via* hydrogen/deuterium exchange mass spectrometry.[41] The electrostatic interactions within the DMPG containing nanodiscs may "fix" the helical conformation of MSP1D1 and protect it from denaturation upon occasional unfolding events during storage, thawing or thermal heating. Moreover, the high net charge of the DMPG containing nanodiscs is also expected to give more stable aggregates in solution due to longer-range inter-nanodisc repulsion. Indeed, complexes formed by DMPG and apolipoprotein A-I were proposed to be thermodynamically stable over a range of temperatures above the phase transition temperature of the lipid,[29] while complexes formed by DMPC and apolipoprotein A-I were shown to have a complex stability largely controlled by kinetic factors,[42] in agreement with our results on stability upon storage.

Conclusions

The rapidly increasing use of nanodiscs as a carrier system and as a tool in membrane protein studies has resulted in a need for

charged nanodiscs since the scientific community is now facing new challenges regarding the effect of lipid charge on the protein function. We intended to prepare both anionic and cationic monodispersed and stable nanodiscs using either the negatively charged DMPG or DMPA and the positively charged DMTAP. The charge density was altered by pre-mixing charged phospholipids with the zwitterionic DMPC in the initial assembling solution. We found that a high yield of well-defined nanodiscs can be obtained from mixtures of DMPG at all proportions but only for 25 mol% DMPA. Indeed, nanodiscs could only be formed from assembly mixtures containing 10 mol% DMTAP, although the amount of lipid-free MSP1D1 and large lipid–protein aggregates is relatively high already at this low fraction of DMTAP. A larger fraction of DMTAP ($X_{DMTAP} = 0.3$) resulted in precipitation observed as turbidity of the solutions. Based on the size exclusion chromatograms, the optimal lipid to MSP1D1 molar ratio in the assembly mixture is 80–90 : 1. Analysis of the phosphoric amount in the DMPG based nanodisc samples showed that the number of lipids per MSP1D1 in these nanodiscs was independent of the fraction of DMPG and suggested a constant area of the nanodiscs regardless of DMPC/DMPG composition. Moreover, the presence of 25 mol% DMPA destabilizes the nanodisc complex, which was considerably degraded already after one week of storage at −20 °C. In contrast to DMPA, the introduction of 25 mol% DMPG in the DMPC nanodiscs has a remarkable stabilizing effect on the nanodisc structure, which showed no sign of degradation after five months of storage at −20 °C. The stabilizing effect on nanodiscs by DMPG was further demonstrated as an increase in denaturation temperature for increasing fraction of DMPG. Thus, the inclusion of a low fraction of DMPG in nanodiscs should be an advantage in various applications of nanodiscs as it results in a high yield of monodispersed and well-defined nanodiscs, which better mimic the native cell membranes and can be stored at −20 °C for at least five months. These results suggest that mixing DMPC and DMPG provides nanodiscs that are better suited for studies of the function and structure of membrane proteins not only due to their inherent charge but also due to their thermal and storage stability.

Acknowledgements

The authors thank Tomas Laursen for help with illustrations and acknowledge financial support from the “Center for Synthetic Biology” at Copenhagen University funded by the UNIK research initiative of the Danish Ministry of Science, Technology and Innovation. J.B.S. would also like to acknowledge the VKR Foundation and the “IMK Almene” Foundation for funding.

References

1 T. H. Bayburt, Y. V. Grinkova and S. G. Sligar, *Nano Lett.*, 2002, **2**, 853–856.
2 I. G. Denisov, Y. V. Grinkova, A. A. Lazarides and S. G. Sligar, *J. Am. Chem. Soc.*, 2004, **126**, 3477–3487.
3 T. H. Bayburt and S. G. Sligar, *FEBS Lett.*, 2010, **584**, 1721–1727.
4 A. Nath, W. M. Atkin and S. G. Sligar, *Biochemistry*, 2007, **46**, 2059–2069.
5 C. D. Blanchette, B. W. Segelke, N. Fischer, M. H. Corzett, E. A. Kuhn, J. A. Cappuccio, W. H. Benner, M. A. Coleman, B. A. Chromy, G. Bench, P. D. Hoeprich and T. A. Sulchek, *Int. J. Mol. Sci.*, 2009, **10**, 2958–2971.
6 R. A. Silva, G. M. Hilliard, L. Li, J. P. Segrest and W. S. Davidson, *Biochemistry*, 2005, **44**, 8600–8607.
7 S. E. Panagotopulos, E. M. Horace, J. N. Maiorano and W. S. Davidson, *J. Biol. Chem.*, 2001, **276**, 42965–42970.
8 A. Shaw, *FEBS Lett.*, 2004, **556**, 260–264.
9 V. Koppaka, L. Silvestro, J. A. Engler, C. G. Brouillette and P. H. Axelsen, *J. Biol. Chem.*, 1999, **274**, 14541–14544.
10 Y. Li, A. Z. Kijac, S. G. Sligar and C. M. Rienstra, *Biophys. J.*, 2006, **91**, 3819–3828.
11 M. Nakano, M. Fukuda, T. Kudo, M. Miyazaki, Y. Wada, N. Matsuzaki, H. Endo and T. Handa, *J. Am. Chem. Soc.*, 2009, **131**, 8308–8312.
12 N. Skar-Gislinge, J. B. Simonsen, K. Mortensen, R. Feidenhans'l, S. G. Sligar, B. L. Moller, T. Bjornholm and L. Arleth, *J. Am. Chem. Soc.*, 2010, **132**, 13713–13722.
13 I. G. Denisov, M. A. McLean, A. W. Shaw, Y. V. Grinkova and S. G. Sligar, *J. Phys. Chem. B*, 2005, **109**, 15580–15588.
14 C. P. Wan, M. H. Chiu, X. Wu, S. K. Lee, E. J. Prenner and P. M. Weers, *Biochim. Biophys. Acta*, 2011, **1808**, 606–613.
15 B. A. Chromy, E. Arroyo, C. D. Blanchette, G. Bench, H. Benner, J. A. Cappuccio, M. A. Coleman, P. T. Henderson, A. K. Hinz, E. A. Kuhn, J. B. Pesavento, B. W. Segelke, T. A. Sulchek, T. Tarasow, V. L. Walsworth and P. D. Hoeprich, *J. Am. Chem. Soc.*, 2007, **129**, 14348–14354.
16 I. G. Denisov, Y. V. Grinkova, A. A. Lazarides and S. G. Sligar, *J. Am. Chem. Soc.*, 2004, **126**, 3477–3487.
17 M. Wadsäter, R. Barker, K. Mortensen, R. Feidenhans'l and M. Cárdenas, *Langmuir*, 2012.
18 G. M. Cooper, *The Cell, A Molecular Approach*, Sinauer Associates, Sunderland (MA), 2nd edn, 2000.
19 J. O. Rädler, I. Koltover, T. Salditt and C. R. Safinya, *Science*, 1997, **275**, 810–814.
20 S. K. Kim, M. B. Foote and L. Huang, *Biomaterials*, 2012, **33**, 3959–3966.
21 M. Wadsäter, J. B. Simonsen, T. Lauridsen, E. Grytli Tveten, P. Naur, T. Bjørnholm, H. Wacklin, K. Mortensen, L. Arleth, R. Feidenhans'l and M. Cardenas, *Langmuir*, 2011, **27**, 15065–15073.
22 E. G. Bligh and W. J. Dyer, *Can. J. Biochem. Physiol.*, 1959, **37**, 911–917.
23 G. Rouser, A. N. Siakotos and S. Fleisher, *Lipids*, 1966, **1**, 85–86.
24 T. H. Bayburt, Y. V. Grinkova and S. G. Sligar, *Nano Lett.*, 2002, **2**, 853–856.
25 M. Cárdenas, K. Schillen, V. Alfredsson, R.-D. Duang, L. Nyberg and T. Arnebrant, *Chem. Phys. Lipids*, 2008, **151**, 10–17.
26 J. F. Nagel, *Biochim. Biophys. Acta*, 2000, **1469**, 159–195.

27 S. Tristram-Nagle, Y. Liu, J. Legleiter and J. F. Nagle, *Biophys. J.*, 2002, **83**, 3324–3335.
28 A. W. Shaw, M. A. McLean and S. G. Sligar, *FEBS Lett.*, 2004, **556**, 260–264.
29 W. K. Surewicz, R. M. Epand, H. J. Pownall and S. W. Hui, *J. Biol. Chem.*, 1986, **261**, 6191–6197.
30 A. Åkesson, T. Lind, N. Ehrlich, D. Stamou, H. Wacklin and M. CLardenas, *Soft Matter*, 2012, **8**, 5658–5665.
31 R. M. Epand, J. P. Segrest and G. M. Anantharamaiah, *J. Biol. Chem.*, 1990, **34**, 20829–20832.
32 Y. P. Zhang, R. Lewis, R. N. McElhaney and R. O. Ryan, *Biochemistry*, 1993, **32**, 3942–3952.
33 D. J. Reijngoud, S. Lund-Katz, H. Hauser and M. C. Phillips, *Biochemistry*, 1982, **21**, 2977–2983.
34 J. M. Boggs, *Biochim. Biophys. Acta*, 1987, **906**, 353–404.
35 P. Garidel, C. Johann and A. Blume, *Biophys. J.*, 1997, **72**, 2196–2210.
36 P. Garidel, C. Johann, L. Mennicke and A. Blume, *Eur. Biophys. J.*, 1997, **26**, 447–459.
37 D. Marsh, *CRC Handbook of Lipid Bilayers*, CRC Press, Boca Raton, 1990.
38 R. Zantl, L. Baicu, F. Artzner, I. Sprenger, G. Rapp and J. O. Rädler, *J. Phys. Chem. B*, 1999, **103**, 10300–10310.
39 R. Dias, S. Mel'nikov, B. Lindman and M. G. Miguel, *Langmuir*, 2000, **16**, 9577–9583.
40 A. K. Moren and A. Khan, *Langmuir*, 1995, **11**, 3636–3643.
41 C. M. Hebling, C. R. Morgan, K. D. Rand, D. W. Stafford, J. W. Jorgenson and J. R. Engen, *Mol. Cell. Proteomics*, 2011, DOI: 10.1074/mcp.M111.010876.
42 R. M. Epand, *Biochim. Biophys. Acta*, 1982, **712**, 146–151.

Article II

Biosynthetic preparation of selectively deuterated phosphatidylcholine in genetically modified *Escherichia coli*

Selma Maric[1,2], Mikkel B. Thygesen[3], Jürgen Schiller[4], Magdalena Marek[2], Martine Moulin[5,6], Michael Haertlein[5], V. Trevor Forsyth[5,6], Lise Arleth[1] and Thomas Günther Pomorski[2].

[1]Structural Biophysics, Niels Bohr Institute, Faculty of Science, University of Copenhagen, Universitetsparken 5, 2100 Copenhagen, Denmark. [2]Center for Membrane Pumps in Cells and Disease, Dept. Plant and Environmental Sciences, Faculty of Science, University of Copenhagen, Thorvaldsensvej 40, 1871 Frederiksberg C, Denmark. [3]CARB Centre, Department of Chemistry, Faculty of Science, University of Copenhagen.Thorvaldsensvej 40, 1871 Frederiksberg C, Denmark. [4]Institut für Medizinische Physik und Biophysik, Medizinische Fakultät, Universität Leipzig, Härtelstrasse 16-18, 04107 Leipzig, Germany. [5]Life Sciences Group, Institut Laue Langevin, 6 rue Jules Horowitz, CEDEX 9, BP156, 38042 Grenoble, France. [6]EPSAM/ISTM, Keele University, Staffordshire ST5 5BG, United Kingdom.

Corresponding author: Thomas Günther Pomorski

+ 45 3533 3373

tgp@plen.ku.dk

Abstract

Phosphatidylcholine (PC) is a major component of eukaryotic cell membranes and one of the most commonly used phospholipids for reconstitution of membrane proteins into carrier systems such as lipid vesicles, micelles and nanodiscs. Selectively deuterated versions of this lipid have many applications especially in structural studies using techniques such as NMR, neutron reflectivity and small-angle neutron scattering. Here we present a comprehensive study of selective deuteration of phosphatidylcholine through biosynthesis in a genetically modified strain of *Escherichia coli*. By carefully tuning the deuteration level in *E.coli* growth media and varying the deuteration of supplemented carbon sources we show that it is possible to achieve controlled deuteration for three distinct parts of the PC lipid molecule, namely the (a) lipid head group, (b) glycerol backbone and (c) fatty acyl tail. This biosynthetic approach paves the way for the synthesis of specifically deuterated, physiologically relevant phospholipid species that are otherwise not available through standard chemical synthesis.

Supplementary keywords: glycerophospholipids, phosphatidylcholine, selective deuteration, biosynthesis, *E. coli*, neutron scattering, NMR, mass spectrometry

Introduction

Deuterium-labelled phospholipids were originally developed for the analysis of lipid pathways and for the purposes of mass spectrometry as internal standards (1). They have also found use in solid state NMR and neutron diffraction techniques for the study of structural organization and dynamics of biological membranes (2-4). Additionally, deuterated phospholipids are used in membrane-mimicking carriers to study membrane proteins (2, 4). In ^{1}H NMR studies of complex membrane protein systems, full lipid deuteration leads to the complete suppression of their ^{1}H signal (2, 5). This results in lipid 'transparency' and significantly simplifies data analysis enabling both secondary and tertiary structural analysis of embedded membrane proteins (2). In neutron reflectometry, the advantages lie in obtaining different contrasts for different parts of the lipid bilayer (3). Controlling the deuteration levels allows specific parts of the lipid molecules to be highlighted (6). This can then be exploited not only in studies of the effects of the lipid environment on membrane protein systems but allows for the study of different lipid systems and their interactions with various ligands and potential drugs (3, 7). In small-angle neutron scattering (SANS) studies, specific deuteration of lipids allows solvent contrast variation to render membrane protein carrier systems such as lipid vesicles (8) or other membrane-mimicking carriers (4) fully or nearly invisible. This potentially allows for analysing the SANS data with well-established data analysis methods originally developed for proteins in solution (9).

The available labelling approaches for production of biomolecules such as lipids and proteins are chemical synthesis and microbial synthesis/expression or a combination of the two, when different levels of deuteration within the molecules are required (10). For recombinant proteins, microbial expression is the preferred deuteration method – often with *Escherichia coli*, as the expression host (11). This organism can be adapted to grow in minimal media in high levels of D_2O (11), and the use of D_2O can be combined with different deuterated carbon sources such as sodium acetate, glycerol, or glucose. This type of approach is now widely used in neutron protein crystallography (12, 13), SANS (14-16) and neutron reflectivity (17, 18). Deuterated phospholipids, on the other hand, are generally produced by chemical synthesis, which allows for the combination of various fatty acyl residues to obtain the desired mixtures of partially labelled or perdeuterated, saturated phospholipid species as well as selective deuteration of specific groups (10). However, the synthesis of selectively deuterated versions of physiologically relevant unsaturated phosphatidylcholines (PC), which are the major membrane-forming phospholipids in eukaryotes (19), still remains difficult. For example, obtaining PC with non-identical fatty acyl residues at

positions *sn*-1 and -2 of glycerol requires rather complex organic synthesis. In addition, adjustments of the head-group deuteration level at the final stages of lipid synthesis can lead to modifications of the double bonds in unsaturated acyl tails (20). These mono-unsaturated PC species with a fatty acyl length between 16 and 18 carbon atoms are, however, the physiologically most relevant for biophysical and biochemical studies of membranes and membrane proteins due to their ability to form stable bilayers at a broad range of pH, temperature and ionic strength. Thus, they are the lipids of choice for the reconstitution of membrane proteins into various carrier-systems such as lipid vesicles, micelles and nanodiscs.

We recently reported a small-angle neutron scattering study of a so-called "stealth nanodisc system". I.e. a version of the ApoA1-derived nanodisc carrier (21), which is contrast optimized for SANS based structural studies of membrane proteins in solution (4). This SANS contrast optimization is crucial step in our general quest towards developing the nanodisc carrier for low resolution structural studies of membrane proteins in solution or at interfaces (22-25). Here we describe in more detail the novel methods that were developed for this work to produce selectively deuterated, physiologically relevant PCs using *E. coli* strain AL95/pAC-PCSlp-Sp-Gm genetically engineered to produce PC instead of its wild-type lipid phosphatidylethanolamine (PE) (26). These methods allow controlled, site-specific deuteration of three distinct parts of the PC lipid molecule (lipid head group, glycerol backbone, fatty acyl tail) by varying the D_2O concentration of the media as well as deuteration of the supplemented carbon sources. This choice of the host enabled the possibility of reaching very high degrees of deuteration (27) while the very simple phospholipid composition of *E. coli* (28) (as compared to yeast for example (29)), facilitated both biosynthesis and subsequent lipid extraction and purification. This has established a new platform for the preparation of physiologically relevant deuterium-labelled PCs and should be applicable also for the deuteration of other phospholipids and membrane components.

Materials and Methods

Materials

All chemicals and solvents were obtained (in the highest commercially available purity) from Sigma-Aldrich (Denmark) and used as supplied unless stated otherwise. Deuterated glycerol (D8, 99%) and deuterated choline chloride (Trimethyl-D9, 98%) were from Eurisotop (ST-Aubin Cedex, France) and Silantes® rich deuterated medium was purchased from Silantes GmbH (München, Germany). Phospholipid standards were purchased from Avanti Polar Lipids Inc. (Birmingham,

AL, USA) and used as supplied. MALDI matrices used were acidic 2,5-dihydroxybenzoic acid (DHB) as 0.5 M solution in methanol (30) and basic 9-aminoacridine (9-AA) hemihydrate (Acros Organics, Geel, Belgium) applied as 10 mg/ml solution in 60/40 (v/v) isopropanol/acetonitrile (31). Thin-layer chromatography (TLC) silica gel 60 plates were from Merck (Darmstadt, Germany). Ultrapure water (Ultra Clear Basic, SG, resistivity 18.2 MΩ×cm) was exclusively used throughout this study.

Bacterial strain and cultivation conditions

E. coli strain AL95 carrying the plasmid pAC-PCSlp-Sp-Gm which allows for the expression of PC synthase encoded by the *Legionella pneumophila pcsA* gene under control of an arabinose inducible promotor (32) was adapted to minimal deuterated medium after a multi-stage adaptation process according to a modified method by Artero *et al.* (33). Briefly, a fresh overnight culture of AL95 strain carrying the plasmid and grown in Luria-Bertani broth (LB) supplemented with 50 mM $MgCl_2$ was diluted to an initial cell density of 0.95 (A_{600}) into flasks containing: 6.86 g/l $(NH_4)_2SO_4$, 1.56 g/l KH_2PO_4, 6.48 g/l $Na_2HPO_4{\cdot}2H_2O$, 0.49 g/l diammoniumhydrogen-citrate, 0.25 g/l $MgSO_4{\cdot}7H_2O$, 1.0 ml/l of a salt mix (0.5 g/l $CaCl_2{\cdot}2H_2O$, 16.7 g/l $FeCl_3{\cdot}6H_2O$, 0.18 g/l, $ZnSO_4{\cdot}7H_2O$, 0.16 g/l $CuSO_4{\cdot}5H_2O$, 0.15 g/l $MnSO_4{\cdot}4H_2O$, 0.18 g/l $CoCl_2{\cdot}6H_2O$, 20.1 g/l EDTA), with 5 g/l glycerol and 10 mg/l gentamicin in H_2O. To ensure initial growth divalent metal ions in the form of 50 mM $MgSO_4$ solution were added to the flask cultures in addition to 10% Silantes rich medium. After overnight incubation at 37°C this process was repeated daily over a course of three weeks. After adaptation to non-deuterated minimal medium the cells were amplified (1 in 10) in minimal medium based on D_2O also containing 50 mM $MgSO_4$ solution and 10% deuterated Silantes® rich medium. This process was then repeated for one week.

The adapted starting cultures were amplified in minimal medium containing different levels of D_2O as well as different variations of the used deuterated carbon sources; glycerol and choline (Table 1 in Figure 4). The cells were induced with 0.2% arabinose (non-deuterated), and 2 mM choline chloride as previously described (32). After incubation at 37˚C for 24 h cells were harvested by centrifugation (10,000 × g, 20 min, 4°C), and washed with MiliQ water.

Phospholipid extraction and purification

Total lipids were extracted by a modified method of Bligh and Dyer (34). In short, cell pellets were re-suspended in H_2O (5 ml H_2O/g of cell paste) and sonicated (10 × 2 s pulses at about 20%

power using a Branson Sonifier® 450 Sonicator). Methanol (2.2 ml) and chloroform (1 ml) were added per 1-ml cell suspension aliquot. After 30 min at 25°C phase separation was induced by addition of chloroform (1 ml) and H_2O (1 ml) followed by centrifugation (800 × g, 10 min, 4°C). The chloroform phase was collected and the process repeated two more times. The chloroform phase was stored at -20°C and the residual rest of the water phase was subsequently removed. The final chloroform phase was dried using a stream of nitrogen, and lipid extracts were stored at -20°C. For further purification 50 mg of total lipid extracts were applied to a silica gel column (1 × 15 cm, Silica Gel 60, 230/400 mesh, 6 g), and lipids were separated according to phospholipid head-group by eluting with varying ratios of chloroform/methanol [9:1 (200 ml), 4:1 (200 ml), 1:1 (200 ml), 1:4 (200 ml), 100% methanol (300 ml)] mixtures.

Phospholipid analysis

Phospholipids were separated by thin-layer chromatography (TLC) using chloroform/ethanol/water/triethylamine (30/35/7/35, v/v/v/v) and identified through comparison with known standards chromatographed on the same plate after staining with primuline (5 mg primuline in 100 ml acetone/water, 80/20, v/v) (35). For further analysis, lipid spots from primuline stained TLC were scraped off and extracted three times with 100 µl chloroform/methanol/0.9% aqueous NaCl (1/1/1, v/v/v). Total phospholipid content was determined by digesting lipids in deionized water and perchloric acid for 1 h at 180°C followed by addition of ammonium molybdate and ascorbic acid. After further heating to 80°C for 10 min, the sample was cooled and the absorbance was read at 812 nm to quantify total lipid phosphorus as previously described (36).

MALDI-TOF mass spectrometry.

For MS analysis, lipid spots from primuline stained TLC were scraped off and extracted as described above. The obtained lipid fractions (concentrated to a volume of 10 µl) as well as total extracts (10 µl) were independently pre-mixed 1:1 (v/v) with the different matrix compounds (DHB and 9-AA) prior to deposition onto the MALDI target and investigated by positive and negative ion-mode MALDI-TOF MS, respectively. MALDI-TOF mass spectra were acquired on a Bruker Autoflex mass spectrometer (Bruker Daltonics, Bremen, Germany) which utilizes a pulsed nitrogen laser, emitting at 337 nm. The extraction voltage was 20 kV and gated matrix suppression was applied to prevent the saturation of the detector by matrix ions (37). For each mass spectrum, 100 single laser shots were averaged. In order to enhance the resolution, all spectra were acquired in the

reflector mode using delayed extraction conditions. See (38, 39) for a more detailed methodological description of MALDI-TOF MS with the focus on lipid analysis. All data were processed with the software "Flex Analysis" version 2.2 (Bruker Daltonics). Selected lipids were also analyzed subsequent to phosphoplipase A_2 (PLA_2) digestion in order to determine the fatty acyl composition as previously described (38).

Deuteration level determination

The level of deuteration, $X_{DPC,}$ for the lipid species obtained from adapted AL95 preparations with varying levels of D_2O were determined by mass spectrometry through comparison of the lipid species actual mass with the calculated theoretical mass for its fully deuterated analogue and calculated using:

$$X_D = \frac{m_{DPC} - m_{HPC}}{m_{100\%\,DPC} - m_{HPC}} \quad (1)$$

Where m_{DPC} is the average mass obtained for the deuterated species, m_{HPC} is the mass of non-deuterated PC and $m_{100\%\,DPC}$ is the theoretical mass of fully deuterated phospholipid.

NMR spectroscopy.

The localization of the incorporated deuterium on the lipid PC molecules was determined by ^{1}H-NMR spectroscopy through comparison of ca. 5% (v/v) solutions of deuterated phosphatidylcholine with an equivalent solution of non-deuterated phosphatidylcholine also synthesized by *E. coli*. All lipids were dissolved in chloroform-d (99.96%, 0.03 % (v/v) tetramethylsilane (TMS)) and all spectra were recorded on a Bruker Avance 300 MHz instrument.

Results

Growing *E. coli* AL95/pAC-PCSlp-Sp-Gm bacteria in a deuterated medium required a process of adaptation (40). Initial amplification of the strain in minimal medium according to the

method by Artero *et al.* (33) resulted in no significant cell growth neither in non-deuterated nor deuterated conditions (data not shown). This result was expected as the auxotroph strain requires most amino acids and high amounts of divalent metal ions for growth (32, 41). Supplementation with 10% rich medium (Silantes®) was necessary to reach a cell density (OD_{600}) of 2 upon overnight growth (Fig. 1A, black squares). However, the required high amount of magnesium salts proved to be insoluble in rich Silantes® media as well as in minimal media due to their high phosphate content. After a three week long adaptation period of daily culture amplification using Silantes® medium in all preparations, a significant increase in bacterial cell growth was observed resulting in cell densities (OD_{600}) of 9 for the adapted AL95 strain (Fig. 1A, grey circles). After the initial adaptation phase the strain was able to grow on minimal medium without any kind of supplementation.

The adaptation to minimal medium led to substantial changes in the lipid composition of the strain. While the original AL95/pAC-PCSlp-Sp-Gm produced predominantly PC, phosphatidylglycerol (PG) and cardiolipin (CL), with only a negligible contribution of PE, a clear reversion to high amounts of PE was detected in the D_2O adapted AL95 strain (Fig. 1B). It has previously been shown that magnesium is a requirement for PE suppression and that growth of the cells in the absence of high levels of divalent metal ions leads to increased levels of PE (32, 41) Therefore it is most likely that the relapse to a more wild type-like lipid composition in adapted AL95 was not only due to the deuterium isotope effect on the organism but was a result of the lower concentration of divalent metal ions used in the preparations.

Figure 1C shows the proportion of the four individual phospholipid classes in wild-type *E. coli* (WT), AL95/pAC-PCSlp-Sp-Gm before adaptation (AL95) and AL95/pAC-PCSlp-Sp-Gm after adaptation (Adapted AL95). Before adaptation, the lipid composition of the PC producing strain consisted of up to 60% PC together with 40% CL and a small contribution (less than 1.5%) of PG. The well-adapted strain, however, showed more than 50% PE together with almost equal amounts of PC and PG, with 22% and 23%, respectively, and a small contribution (less than 1%) of CL. Even under conditions of the reversion to a more wild type-like lipid composition for the well-adapted strain, the ability to synthesize PC was obvious, leading to a, for *E. coli*, new lipid distribution of the four most abundant phospholipids. This might explain the improved bacterial growth in minimal conditions as compared to AL95/pAC-PCSlp-Sp-Gm bacteria before adaptation and wild-type *E. coli*.

Fatty acyl distribution of deuterated phospholipids from adapted E. coli AL95

After the initial adaptation process, the adapted *E. coli* AL95 was cultured in deuterated medium and the phospholipids were extracted, purified using silica gel column chromatography and characterized by mass spectrometry. For a preparation of adapted AL95 where 100% D_2O was used together with deuterated glycerol as carbon source, this gave a narrow distribution of highly deuterated phospholipid species enabling the determination of their fatty acyl composition (Figure 2). Lipids extracted from the strain harvested in the stationary phase showed predominantly 1-palmitoyl-2-palmitoleoyl (16:0/16:1) PC and its cyclopropane modified analogue (16:0/17:0 cyc) (4) (see fig 3A).

The species containing the cyclopropane residue was the most abundant, as is usually the case with E.coli lipids, and was further analysed (Figure 2). The peak maximum at *m/z* 810 (H^+ adduct) corresponded to the PC species where 63 hydrogen atoms are replaced by deuterium. This assignment could be made because it is known that 9-AA results primarily in H^+ adduct formation while the generation of Na^+ adducts (*m/z* 832) plays only a minor role (31). In contrast to PC which is preferentially detected as positive ion, all other phospholipids of interest were more easily detectable in the negative ion mode. PE 16:0/17:0 cyc and PG 16:0/17:0 cyc were detected at *m/z* 769 and 802, respectively, which indicated the incorporation of either 66 or 68 deuterium atoms and, thus, gave data comparable to PC. Remarkably, there was in all cases a signal with a marked isotope pattern at *m/z* 769 (PC), 728 (PE) and 761 (PG). These signals could not be assigned so far. However, the mass difference in comparison to the most intense signals was always 41 mass units. This made an assignment even more difficult because the head-groups of all discussed phospholipids are different and, thus, the generation of fragment ions during the MS process was very unlikely. Although we were also able to detect some deuterated cardiolipin (CL) species, these particular species are not discussed here due to poor signal-to-noise ratio in accordance with the previous study on CL detection (42) in particular since deuteration leads to an additional decrease of sensitivity.

Deuteration levels of phosphatidylcholine in adapted E. coli AL95

Adapted AL95 was cultivated in an increasing level of D_2O in order to monitor the effects of D_2O on PC molecules with deuterated minimal medium ranging from 50% to 100% D_2O. This was done in the presence of both deuterated and non-deuterated glycerol, while the choline carbon source, used for induction, was kept non-deuterated. The deuteration level for the resulting PC

species was determined through comparison of the actual average mass with that of the theoretical mass of fully deuterated species according to Equation 1. This calculation assumes that no major changes in the fatty acyl composition are present as a result of deuteration, as it was shown by comparing the highly deuterated species produced in 100% D_2O with the analogous lipids produced in H_2O (Fig. 2). As expected, the increased level of D_2O in the growth medium resulted in increased deuteration of PC for preparations with non-deuterated as well as deuterated glycerol (Fig. 3B black and red respectively). It was observed that the PC lipids biosynthesized in both 50% and 75% D_2O displayed a very broad *m/z* distribution when analysed by mass spectrometry. This was most likely a result of random deuterium incorporation in the lipid molecules leading to different species of partially deuterated PC and making the fatty acyl analysis challenging. Assuming 80 possible deuterium atoms for fully deuterated 16:0/17:0cyc PC it can be seen that with non-deuterated glycerol as carbon source the deuteration of the most abundant PC species increased from 21% to 83% (Fig. 3B black) while for the preparations with deuterated glycerol the deuteration of PC naturally increased from 43% to 90% (Fig. 3B red). Full deuteration was not observed for any of the species indicating that the non-deuterated choline chloride used for induction was also incorporated into the lipid molecules and lowered the overall deuteration levels.

NMR analysis of the PC extracted and purified from preparations grown in an increasing level of D_2O showed a gradual decrease of the ^1H resonance (Fig. 3C). This was most obvious for the large signal at 1.2 ppm corresponding to the majority of the hydrogens of the fatty acyl chains which become increasingly deuterated with increasing level of D_2O in the growth medium. The signals at 3.9 ppm and 4.4 ppm belonging to the ethylene hydrogens and the signal at 3.4 ppm corresponding to the methyl groups (all belonging to the choline head-group) were observed in all preparations where the supplemented choline was non-deuterated. The glycerol signals, on the other hand, at 4.0 ppm, 4.2 ppm and 5.2 ppm were not observed in all the preparations where deuterated glycerol was used as a supplement. These data indicated that the carbon source had an effect on the PC head-group deuteration while the increasing fatty acyl residue deuteration depended particularly on the total amount of D_2O. This is consistent with previous studies where fatty acyl residues obtained from *E. coli* cells grown in D_2O showed replacement of almost every hydrogen by deuterium without supplementation of deuterated carbon sources (43).

Head-group deuteration of PC synthesized in adapted AL95

To determine the effect of deuteration for both, the glycerol and the choline moiety of the PC head-group, the adapted AL95 was cultivated in growth medium supplemented with deuterated glycerol and deuterated choline and their non-deuterated analogues according to Fig 4**.**

The positive ion MALDI-TOF mass spectra of PC lipids synthesized in deuterated media at ~100% D_2O while varying the deuteration of both, the glycerol and the choline moiety, is shown in Figure 5. The PC species were compared to commercially available hydrogenated POPC and D_{31}-POPC (Avanti Polar Lipids Inc.) after digestion with phospholipase PLA_2 (that is known to cleave exclusively the fatty acyl chain in *sn*-2 position) to yield LPC 16:0 which helps to obtain a more accurate differentiation of both fatty acyl residues. This method was chosen because our MALDI MS does not possess a dedicated collision cell.. The peaks at *m/z* 526.5 and 549.5 correspond to the respective proton and sodium adducts of 16:0 LPC with fully deuterated fatty acyl residues and a hydrogenated head. LPC was obtained from D_{31}-POPC after digestion with PLA_2 and showed a rather narrow mass distribution due to the lacking possibility of exchange reactions with the solvent. A similar mass distribution was also observed for highly deuterated preparations of PC obtained through *E. coli* biosynthesis. PC extracted from cells cultivated with non-deuterated carbon sources ($H_{gly}H_{cho}$-PC) showed an almost identical profile as that of D31-POPC with major peaks at *m/z* 526.5 and 548.5 corresponding to the proton and sodium adduct of LPC 16:0, respectively. Deuterated PC extracted from cells cultivated with deuterated glycerol ($D_{gly}H_{cho}$-PC) showed an increase of exactly five amu as compared with $H_{gly}H_{cho}$-PC resulting in peaks at *m/z* 531.5 and 553.5. This favourably agrees with the mass of five deuterium atoms of the glycerol moiety in the lipid molecule. In contrast to this, the preparation of PC where deuterated choline was used together with non-deuterated glycerol ($H_{gly}D_{cho}$-PC) resulted in a mass difference of exactly nine amu (*m/z* 535.6 and 557.6) corresponding favourably to the nine available deuterium atoms from the supplemented choline. The $D_{gly}D_{cho}$-PC preparation, where both carbon sources were deuterated showed peaks at *m/z* 540.6 and 562.6, i.e. an increase of 14 amu when compared to both $H_{gly}H_{cho}$-PC and D_{31}-POPC. This mass difference agrees well with the difference between the protonated and deuterated carbon sources added to the media with choline possessing nine and glycerol with five hydrogen atoms.

The extent of deuteration of the remaining cellular lipids from adapted AL95 preparations with varying deuterated carbon source (Table 1 in Figure 4) was also determined by MALDI-TOF MS and the masses of the most abundant phospholipid species are summarized in Table 2. While

deuterium enriched glycerol and choline had an effect on the deuteration of the obtained PC, the remaining lipids were affected solely by glycerol. These data showed that choline was not metabolized into the WT *E. coli* lipids and confirmed the lipid synthesis pathways as suggested by Dowhan (44).

Deuterium localization in PC synthesized in adapted AL95

For PC species obtained from preparations of adapted AL95 cultivated in deuterated media and varying deuterated carbon sources (according to Table 1) the localization of the deuterium atoms within the head-group was investigated by ^{1}H-NMR (Fig. 6.). The preparation of PC in the presence of non-deuterated carbon sources ($H_{gly}H_{cho}$-PC) showed a head-group identical to that of non-deuterated PC. The two signals seen at 4.04 ppm and 4.50 ppm in the $D_{gly}D_{cho}$-PC preparation (Fig. 6, $D_{gly}D_{cho}$-PC) were in agreement with the ethylene hydrogens of the choline head-group (Fig. 4). Although the deuterated species gave a chemical shift slightly downfield-shifted in comparison to the hydrogenated sample, these signals were present in all preparations and this could also be confirmed by ^{13}C-NMR (data not shown). The signal at 3.4 ppm assigned to the methyl groups of the choline moiety was present in both preparations of PC where non-deuterated choline was used ($H_{gly}H_{cho}$-PC and $D_{gly}H_{cho}$-PC). However this signal was completely lacking in preparations where deuterated choline was used ($H_{gly}D_{cho}$-PC and $D_{gly}D_{cho}$-PC) confirming the direct choline incorporation into the PC head-group. Similarly, the ^{1}H signals at 4.0 ppm and 4.2 ppm as well as 5.2 ppm (corresponding to the glycerol backbone of the PC) were absent in preparations where deuterated glycerol was used ($D_{gly}H_{cho}$-PC and $D_{gly}D_{cho}$-PC) but were still present in PC obtained from preparations where the growth medium was supplemented with non-deuterated glycerol. The many small signals seen in NMR for the deuterated analogues (Fig. 3C and our previous study) were associated with the acyl residues and indicated that the remaining hydrogens were randomly distributed throughout the fatty acyl chains.

The combined ^{1}H-NMR and MALDI-TOF data showed that both glycerol and choline were taken up by adapted AL95 and incorporated directly into the PC head-groups without modifications. The data presented clearly indicate that head-group deuteration of PC can be controlled by carbon source supplementation while the degree of deuteration for the fatty acyl chains is dependent on the total amount of D_2O in the media. Therefore, it should also be possible to prepare PC species with selective head-group deuteration while the fatty acyl chains are kept non-deuterated. Examples of the selectively deuterated PC species obtained at ~100% D_2O are illustrated in Figure 7.

Discussion

Adaptation to deuterated conditions is harsh for any organism and in most cases only possible at low levels of deuteration. Microorganisms appear to have considerable difficulty adapting to growth in D_2O as compared to adjusting to a single deuterated carbon source only (40). For bacteria such as *E. coli*, the deuterium adaptation process, when successful, has been shown to lead to many unusual features (40). In this work we have shown that the *E. coli* strain AL95/pAC-PCSlp-Sp-Gm, designed so that phosphatidylcholine (PC) replaces the native phospholipid phosphatidylethanolamine (PE), could be adapted to grow under fully deuterated minimal conditions. This was, however, accompanied by severe metabolic modifications of the strain as a function of the growth medium. The austerity of the adaptation process and the limiting choice of deuterated supplements, led to changes in both auxotrophy and lipid composition of the strain. A clear reversion towards the production of high amounts of PE was observed after the adaptation process as had previously been observed for preparations with insufficient Mg^{2+} concentration in the growth media (32, 41). While the adapted strain continued to produce PC, the adaptation process resulted in a novel lipid composition which was associated by an enhanced biomass production.

The yields of deuterated PC that could be obtained through the biosynthetic approach are in the range of 50 mg/l for flask cultures - clearly sufficient for use in techniques such as NMR, SANS and neutron reflectivity. Based on the amount of cell paste obtained in a pilot fermentation study, it is also possible to scale the production up to over 200 mg/l. While this is 100-fold lower in comparison to partial or perdeuterated synthetic PC, the approach allows access to partially deuterated versions of the physiologically relevant monounsaturated PC lipids. The PC lipids can easily be extracted and purified in high yields using established methods. However, enabling purification procedures by means of preparative high-performance liquid chromatography (HPLC) may be preferable for large-scale preparations.

Mass spectrometry showed no major difference in fatty acyl length or degree of saturation for the biosynthetically deuterated PC species when compared to their hydrogenated analogues with possibilities for regulation of the fatty acyl composition during biosynthesis. The cyclopropanated residues are typical of *E. coli* lipids from cells harvested in the stationary growth phase (45) and have been shown to improve stability while maintaining the overall membrane fluidity (46, 47). The fatty acyl distribution can be regulated during the bacterial growth cycle (45) but harvesting cells in

stationary growth phase is recommended if the highest biomass and therefore the highest yield of phospholipid is of interest for the lowest cost of deuterated medium.

The biologically produced PC lipids can be deuterated to a very high extent and the level of deuteration can be easily controlled by adjusting the total level of D_2O in the growth medium. Direct carbon source incorporation into the PC head groups provides additional control to selectively deuterate this part of the molecule through supplementation of selectively deuterated carbon sources to the growth media. While the *E. coli* strain AL95/pAC-PCSlp-Sp-Gm was originally engineered to test the effects of the eukaryotic model lipids on bacterial membrane proteins, this project showed that it can also be used as a production platform for physiologically relevant deuterium-labelled phosphatidylcholines and that this approach is also applicable for the deuteration of other physiologically relevant phospholipids and membrane components.

Acknowledgements

The authors gratefully acknowledge the access to the Deuteration Laboratory PSB platform with ILL's Life Sciences Group, at the Institut Laue-Langevin in Grenoble. We thank Professor William Dowhan and his group at the University of Texas, US for their kind contribution in providing of the PC producing *E. coli* strain. Finally we thank the European Spallation Source, the UNIK research initiative of the Danish Ministry of Science, Technology and Innovation through the "Center for Synthetic Biology" at University of Copenhagen, by the Danish National, and the Research Foundation through the PUMPKIN Center of Excellence for co-funding of the project. Dr Schiller thanks the German Research Council (SFB 1052/B6) for financial support. Professor Forsyth acknowledges support from the UK Engineering and Physical Sciences Research Council (EPSRC) for the ILL Deuteration Laboratory under grants GR/R99393/01 and EP/C015452/1, from the EU NMI3 programme under FP7, and also through the EU CRISP programme (grant number 283745).

References

1. Rohwedder, W. K. 1985. Mass-Spectrometry of Lipids Labeled with Stable Isotopes. *Progress in Lipid Research* **24**: 1-18.

2. Hagn, F., M. Etzkorn, T. Raschle, and G. Wagner. 2013. Optimized phospholipid bilayer nanodiscs facilitate high-resolution structure determination of membrane proteins. *Journal of the American Chemical Society* **135**: 1919-1925.
3. Akesson, A., T. K. Lind, R. Barker, A. Hughes, and M. Cardenas. 2012. Unraveling dendrimer translocation across cell membrane mimics. *Langmuir : the ACS Journal of Surfaces and Colloids* **28**: 13025-13033.
4. Maric, S., N. Skar-Gislinge, S. R. Midtgaard, M. B. Thygesen, J. Schiller, H. Frielinghaus, M. Moulin, M. Haertlein, V. T. Forsyth, T. G. Pomorski, and L. Arleth. 2014. Stealth Carriers for Low-Resolution Structure Determination of Membrane Proteins in solution. *Acta Crystallographica. Section D* **70**.
5. Varga, K., L. Aslimovska, I. Parrot, M. T. Dauvergne, M. Haertlein, V. T. Forsyth, and A. Watts. 2007. NMR crystallography: the effect of deuteration on high resolution 13C solid state NMR spectra of a 7-TM protein. *Biochimica et Biophysica Acta* **1768**: 3029-3035.
6. Majewski, J., T. L. Kuhl, J. Y. Wong, and G. S. Smith. 2000. X-ray and neutron surface scattering for studying lipid/polymer assemblies at the air-liquid and solid-liquid interfaces. *Journal of Biotechnology* **74**: 207-231.
7. Molloy, S. 2010. Reactive resistance. *Nature Reviews. Genetics* **11**: 240.
8. Hunt, J. F., P. D. McCrea, G. Zaccai, and D. M. Engelman. 1997. Assessment of the aggregation state of integral membrane proteins in reconstituted phospholipid vesicles using small angle neutron scattering. *Journal of Molecular Biology* **273**: 1004-1019.
9. Konarev, P. V., M. V. Petoukhov, V. V. Volkov, and D. I. Svergun. 2006. *Atsas* 2.1, a program package for small-angle scattering data analysis. *Journal of Applied Crystallography* **39**: 277-286.
10. Bragina, N. A., and V. V. Chupin. 1997. Methods of synthesis of deuterium-labelled lipids. *Russian Chemical Reviews* **66**: 975-986.
11. Leiting, B., F. Marsilio, and J. F. O'Connell. 1998. Predictable deuteration of recombinant proteins expressed in Escherichia coli. *Analytical Biochemistry* **265**: 351-355.
12. Howard, E. I., M. P. Blakeley, M. Haertlein, I. Petit-Haertlein, A. Mitschler, S. J. Fisher, A. Cousido-Siah, A. G. Salvay, A. Popov, C. Muller-Dieckmann, T. Petrova, and A. Podjarny. 2011. Neutron structure of type-III antifreeze protein allows the reconstruction of AFP-ice interface. *Journal of Molecular Recognition : JMR* **24**: 724-732.
13. Cuypers, M. G., S. A. Mason, M. P. Blakeley, E. P. Mitchell, M. Haertlein, and V. T. Forsyth. 2013. Near-atomic resolution neutron crystallography on perdeuterated Pyrococcus furiosus rubredoxin: implication of hydronium ions and protonation state equilibria in redox changes. *Angewandte Chemie* **52**: 1022-1025.
14. Vijayakrishnan, S., S. M. Kelly, R. J. Gilbert, P. Callow, D. Bhella, T. Forsyth, J. G. Lindsay, and O. Byron. 2010. Solution structure and characterisation of the human pyruvate dehydrogenase complex core assembly. *Journal of Molecular Biology* **399**: 71-93.
15. Rochel, N., F. Ciesielski, J. Godet, E. Moman, M. Roessle, C. Peluso-Iltis, M. Moulin, M. Haertlein, P. Callow, Y. Mely, D. I. Svergun, and D. Moras. 2011. Common architecture of nuclear receptor heterodimers on DNA direct repeat elements with different spacings. *Nature Structural & Molecular Biology* **18**: 564-570.
16. Cuypers, M. G., M. Trubitsyna, P. Callow, V. T. Forsyth, and J. M. Richardson. 2013. Solution conformations of early intermediates in Mos1 transposition. *Nucleic Acids Research* **41**: 2020-2033.
17. Grage, S. L., A. M. Keleshian, T. Turdzeladze, A. R. Battle, W. C. Tay, R. P. May, S. A. Holt, S. A. Contera, M. Haertlein, M. Moulin, P. Pal, P. R. Rohde, V. T. Forsyth, A. Watts, K. C. Huang, A. S.

Ulrich, and B. Martinac. 2011. Bilayer-mediated clustering and functional interaction of MscL channels. *Biophysical Journal* **100**: 1252-1260.

18. Hellstrand, E., M. Grey, M. L. Ainalem, J. Ankner, V. T. Forsyth, G. Fragneto, M. Haertlein, M. T. Dauvergne, H. Nilsson, P. Brundin, S. Linse, T. Nylander, and E. Sparr. 2013. Adsorption of alpha-Synuclein to Supported Lipid Bilayers: Positioning and Role of Electrostatics. *ACS Chemical Neuroscience*.
19. van Meer, G., D. R. Voelker, and G. W. Feigenson. 2008. Membrane lipids: where they are and how they behave. *Nature Reviews. Molecular Cell Biology* **9**: 112-124.
20. de Kruijff, B., E. J. van Zoelen, and L. L. van Deenen. 1978. Glycophorin facilitates the transbilayer movement of phosphatidylcholine in vesicles. *Biochimica et Biophysica Acta* **509**: 537-542.
21. Bayburt, T. H., Y. V. Grinkova, and S. G. Sligar. 2002. Self-assembly of discoidal phospholipid bilayer nanoparticles with membrane scaffold proteins. *Nano Letters* **2**: 853-856.
22. Skar-Gislinge, N., J. B. Simonsen, K. Mortensen, R. Feidenhans'l, S. G. Sligar, B. Lindberg Moller, T. Bjornholm, and L. Arleth. 2010. Elliptical structure of phospholipid bilayer nanodiscs encapsulated by scaffold proteins: casting the roles of the lipids and the protein. *Journal of the American Chemical Society* **132**: 13713-13722.
23. Wadsater, M., J. B. Simonsen, T. Lauridsen, E. G. Tveten, P. Naur, T. Bjornholm, H. Wacklin, K. Mortensen, L. Arleth, R. Feidenhans'l, and M. Cardenas. 2011. Aligning nanodiscs at the air-water interface, a neutron reflectivity study. *Langmuir : the ACS Journal of Surfaces and Colloids* **27**: 15065-15073.
24. Wadsater, M., T. Laursen, A. Singha, N. S. Hatzakis, D. Stamou, R. Barker, K. Mortensen, R. Feidenhans'l, B. L. Moller, and M. Cardenas. 2012. Monitoring shifts in the conformation equilibrium of the membrane protein cytochrome P450 reductase (POR) in nanodiscs. *The Journal of Biological Chemistry* **287**: 34596-34603.
25. Kynde, S. A. R., N. Skar-Gislinge, M. C. Pedersen, S. R. Midtgaard, J. B. Simonsen, R. Schweins, K. Mortensen, and L. Arleth. 2014. Small-angle scattering gives direct structural information about a membrane protein inside a lipid environment. *Acta Crystallographica. Section D* **70**.
26. Bogdanov, M., P. Heacock, Z. Guan, and W. Dowhan. 2010. Plasticity of lipid-protein interactions in the function and topogenesis of the membrane protein lactose permease from Escherichia coli. *Proceedings of the National Academy of Sciences of the United States of America* **107**: 15057-15062.
27. Paliy, O., D. Bloor, D. Brockwell, P. Gilbert, and J. Barber. 2003. Improved methods of cultivation and production of deuteriated proteins from E. coli strains grown on fully deuteriated minimal medium. *Journal of Applied Microbiology* **94**: 580-586.
28. Raetz, C. R. 1978. Enzymology, genetics, and regulation of membrane phospholipid synthesis in Escherichia coli. *Microbiological Reviews* **42**: 614-659.
29. Kaneko, H., M. Hosohara, M. Tanaka, and T. Itoh. 1976. Lipid composition of 30 species of yeast. *Lipids* **11**: 837-844.
30. Schiller, J., J. Arnhold, S. Benard, M. Muller, S. Reichl, and K. Arnold. 1999. Lipid analysis by matrix-assisted laser desorption and ionization mass spectrometry: A methodological approach. *Analytical Biochemistry* **267**: 46-56.
31. Sun, G., K. Yang, Z. Zhao, S. Guan, X. Han, and R. W. Gross. 2008. Matrix-assisted laser desorption/ionization time-of-flight mass spectrometric analysis of cellular glycerophospholipids enabled by multiplexed solvent dependent analyte-matrix interactions. *Analytical chemistry* **80**: 7576-7585.
32. Mikhail Bogdanov, P. H., Ziqiang Guan, and William Dowhan. 2010. Plasticity of lipid-protein interactions in the function and topogenesis of the membrane protein lactose permease from

Escherichia coli. *Proceedings of the National Academy of Sciences of the United States of America* **107**: 15057-15062.

33. Artero, J. B., M. Hartlein, S. McSweeney, and P. Timmins. 2005. A comparison of refined X-ray structures of hydrogenated and perdeuterated rat gammaE-crystallin in H2O and D2O. *Acta Crystallographica. Section D* **61**: 1541-1549.
34. Bligh, E. G., and W. J. Dyer. 1959. A rapid method of total lipid extraction and purification. *Canadian Journal of Biochemistry and Physiology* **37**: 911-917.
35. White, T., S. Bursten, D. Federighi, R. A. Lewis, and E. Nudelman. 1998. High-resolution separation and quantification of neutral lipid and phospholipid species in mammalian cells and sera by multi-one-dimensional thin-layer chromatography. *Analytical Biochemistry* **258**: 109-117.
36. Rouser, G., A. N. Siakotos, and S. Fleischer. 1966. Quantitative analysis of phospholipids by thin-layer chromatography and phosphorus analysis of spots. *Lipids* **1**: 85-86.
37. Petkovic, M., J. Schiller, M. Muller, S. Benard, S. Reichl, K. Arnold, and J. Arnhold. 2001. Detection of individual phospholipids in lipid mixtures by matrix-assisted laser desorption/ionization time-of-flight mass spectrometry: phosphatidylcholine prevents the detection of further species. *Analytical Biochemistry* **289**: 202-216.
38. Fuchs, B., K. Muller, F. Goritz, S. Blottner, and J. Schiller. 2007. Characteristic oxidation products of choline plasmalogens are detectable in cattle and roe deer spermatozoa by MALDI-TOF mass spectrometry. *Lipids* **42**: 991-998.
39. Schiller, J., R. Suss, J. Arnhold, B. Fuchs, J. Lessig, M. Muller, M. Petkovic, H. Spalteholz, O. Zschornig, and K. Arnold. 2004. Matrix-assisted laser desorption and ionization time-of-flight (MALDI-TOF) mass spectrometry in lipid and phospholipid research. *Progress in Lipid Research* **43**: 449-488.
40. Katz, J. J., and H. L. Crespi. 1966. Deuterated organisms: cultivation and uses. *Science* **151**: 1187-1194.
41. DeChavigny, A., P. N. Heacock, and W. Dowhan. 1991. Sequence and inactivation of the pss gene of Escherichia coli. Phosphatidylethanolamine may not be essential for cell viability. *The Journal of Biological Chemistry* **266**: 10710.
42. Eibisch, M., S. Zellmer, R. Gebhardt, R. Suss, B. Fuchs, and J. Schiller. 2011. Phosphatidylcholine dimers can be easily misinterpreted as cardiolipins in complex lipid mixtures: a matrix-assisted laser desorption/ionization time-of-flight mass spectrometric study of lipids from hepatocytes. *Rapid Communications in Mass Spectrometry : RCM* **25**: 2619-2626.
43. Saito, K., A. Kawaguchi, S. Okuda, Y. Seyama, and T. Yamakawa. 1980. Incorporation of hydrogen atoms from deuterated water and stereospecifically deuterium-labeled nicotin amide nucleotides into fatty acids with the Escherichia coli fatty acid synthetase system. *Biochimica et Biophysica Acta* **618**: 202-213.
44. Dowhan, W. 2013. A retrospective: Use of Escherichia coli as a vehicle to study phospholipid synthesis and function. *BBA-Molecular and Cell Biology of Lipids* **1831**: 471-494.
45. Magnuson, K., S. Jackowski, C. O. Rock, and J. E. Cronan, Jr. 1993. Regulation of fatty acid biosynthesis in Escherichia coli. *Microbiological Reviews* **57**: 522-542.
46. Law, J. H. 1971. Biosynthesis of Cyclopropane Rings. *Accounts of Chemical Research* **4**: 199-203.
47. Dufourc, E. J., I. C. Smith, and H. C. Jarrell. 1983. A 2H-NMR analysis of dihydrosterculoyl-containing lipids in model membranes: structural effects of a cyclopropane ring. *Chemistry and Physics of Lipids* **33**: 153-177.

Figure 1. Adaptation of *E. coli* AL95/pAC-PCSlp-Sp-Gm to growth in D_2O. (**a**) AL95 carrying the plasmid pAC-PCSlp-Sp-Gm growth curves in minimal deuterated medium supplemented with 10% Silantes® supplementation (black squares) and adapted AL95 in minimal medium without any supplementation (grey circles). Results are the means from two independent experiments; the S.D. is less than 5% of the mean for all data shown. (**b**) Total lipid extracts separated by thin-layer chromatography from wild-type *E. coli* (1), AL95 before adaptation to minimal medium (AL95) and after D_2O adaptation (Adapted AL95). Lipids were visualized by primuline staining. (**c**) Phospholipid composition of wild type *E. coli* (WT), AL95 before adaptation (AL95) and after D_2O adaptation (Adapted AL95). Phosphatidylethanolamine, PE, (black), phosphatidylcholine, PC, (white), phosphatidylglycerol, PG, (grey) and cardiolipin, CL, (striped). Results are the means from four independent experiments; the S.D. is less than 3% of the mean for all data shown.

Figure 2. Positive phosphatidylcholine (PC) and negative ion (all other phospholipids) MALDI-TOF mass spectra of phospholipid species extracted from adapted AL95 grown in ~100% D_2O supplemented with deuterated glycerol and non-deuterated choline. Spectra were recorded in the presence of 9-aminacridine as the matrix and only the most abundant species 16:0/17:0 cyc were investigated in more detail and compositional details are given exclusively for this species. Abbreviations: phosphatidylcholine (PC), phosphatidylethanolamine (PE), phosphatidylglycerol (PG), cardiolipin (CL). Although CL species were detectable, they were not investigated in more detail due to the poor signal-to-noise ratio.

Figure 3. Increased levels of D_2O lead to increasingly deuterated phosphatidylcholine PC. (**A**) The two most abundant PC species from adapted AL95 cultivated in non-deuterated medium and harvested in the stationary phase. (**B**) Level of deuteration in the PC molecule as a function of the D_2O level in the growth medium containing non-deuterated glycerol (black) and deuterated glycerol (red). Deuteration levels were calculated from mass spectrometry data through comparison of the average mass obtained with the calculated theoretical mass of fully deuterated species. (**C**) ^{1}H-NMR spectra of increasingly deuterated PC normalized to the intensity of choline ethylene resonance. From top to bottom: PC synthesized in AL95 under non-deuterated conditions (Control), PC produced in adapted AL95 cultivated in 50% D_2O (50% D_2O), PC produced in adapted AL95 cultivated in 75% D_2O (75% D_2O) and PC produced in adapted AL95 cultivated in 100% D_2O (100% D_2O) with deuterated glycerol and non-deuterated choline in the three preparations. *Insert:*

hydrogen positions and the corresponding peaks are indicated with red letters for aliphatic methylene groups from increasingly deuterated medium and for choline methyl and ethylene groups from non-deuterated supplementation. The asterisks indicate signals of minor contaminants present in two of the samples.

Figure 4. Deuterium-enriched carbon source supplementation of the growth medium. (A) Glycerol $C_3D_8O_3$ and (B) choline chloride $C_5H_5D_9ClNO$. *Insert*: Table 1: Deuterium variation in bacterial growth media.

Figure 5. Positive ion MALDI-TOF spectra of the different species of purified PC extracted from adapted AL95 cultivated in deuterated media and varying carbon source deuteration subsequent to digestion with phospholipase PLA_2 shows selective deuteration. From top to bottom: synthetic hydrogenated LPC (obtained by digestion of POPC), synthetic LPC with hydrogenated head-group and deuterated fatty acyl chain (from D_{31}-POPC), PC synthesized in 100% D_2O supplemented with H-glycerol ($C_3H_8O_3$) and H-choline ($C_5H_{14}ClNO$) ($H_{gly}H_{cho}$-PC), PC synthesized in 100% D_2O supplemented with D-glycerol ($C_3D_8O_3$) and H-choline ($C_5H_{14}ClNO$) ($D_{gly}H_{cho}$-PC), PC synthesized in 100% D_2O supplemented with H-glycerol ($C_3H_8O_3$) and D-choline ($C_5H_5D_9ClNO$) ($H_{gly}D_{cho}$-PC), PC synthesized in 100% D_2O supplemented with D-glycerol ($C_3D_8O_3$) and D-choline ($C_5H_5D_9ClNO$) ($D_{gly}D_{cho}$-PC). Spectra were recorded in the presence of DHB as matrix. Peaks are marked with their *m/z* values and assignments are indicated.

Figure 6. Selective head-group deuteration of phosphatidylcholine (PC) can be monitored through ^{1}H-NMR. From top to bottom: PC synthesized in AL95 under non-deuterated conditions (Control), PC synthesized in deuterated media containing hydrogenated glycerol and hydrogenated choline ($H_{gly}H_{cho}$-PC), PC synthesized in deuterated media containing deuterated glycerol and non-deuterated choline ($D_{gly}H_{cho}$-PC), PC synthesized in deuterated media supplemented with non-deuterated glycerol and deuterated choline ($H_{gly}D_{cho}$-PC) and PC synthesized in deuterated media with deuterated glycerol and deuterated choline ($D_{gly}D_{cho}$-PC). Spectrum intensities are normalized to the choline ethylene signals. Signals at 3.55 ppm originate from alkene protons. *Insert* PC head-group with hydrogen positions and their corresponding protons indicated by red letters.

Figure 7. Molecular structures of PC synthesized by *E. coli* in dependence on the extent of deuteration. Examples of main species for (**a**) PC synthesized in deuterated media containing both non-deuterated glycerol and non-deuterated choline ($H_{Gly}H_{Cho}$-PC). (**b**) PC synthesized in deuterated media supplemented with D_8-glycerol and non-deuterated choline ($D_{Gly}H_{Cho}$-PC). (**c**) PC synthesized in deuterated media containing non-deuterated glycerol and D_9-choline ($H_{Gly}D_{Cho}$-PC). (**d**) PC synthesized in adapted AL95 grown in deuterated media supplemented with D_8-glycerol and D_9-choline ($D_{Gly}D_{Cho}$-PC).

Figure 1.

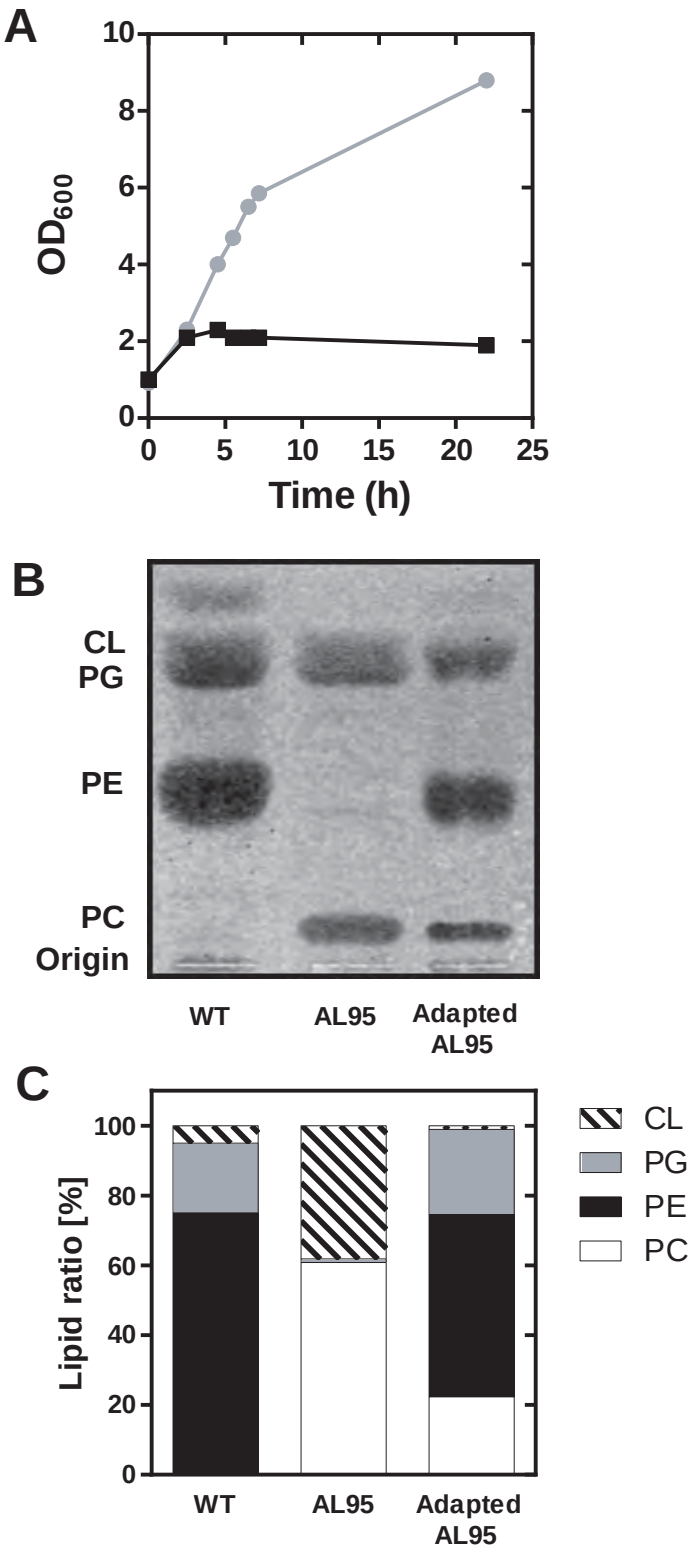
A
10
8
6
4
2
0
OD600
0
5
10
15
20
25
Time (h)
B
CL
PG
PE
PC
Origin
WT
AL95
Adapted AL95
C
100
80
60
40
20
0
Lipid ratio [%]
WT
AL95
Adapted AL95
CL
PG
PE
PC

Figure 2.

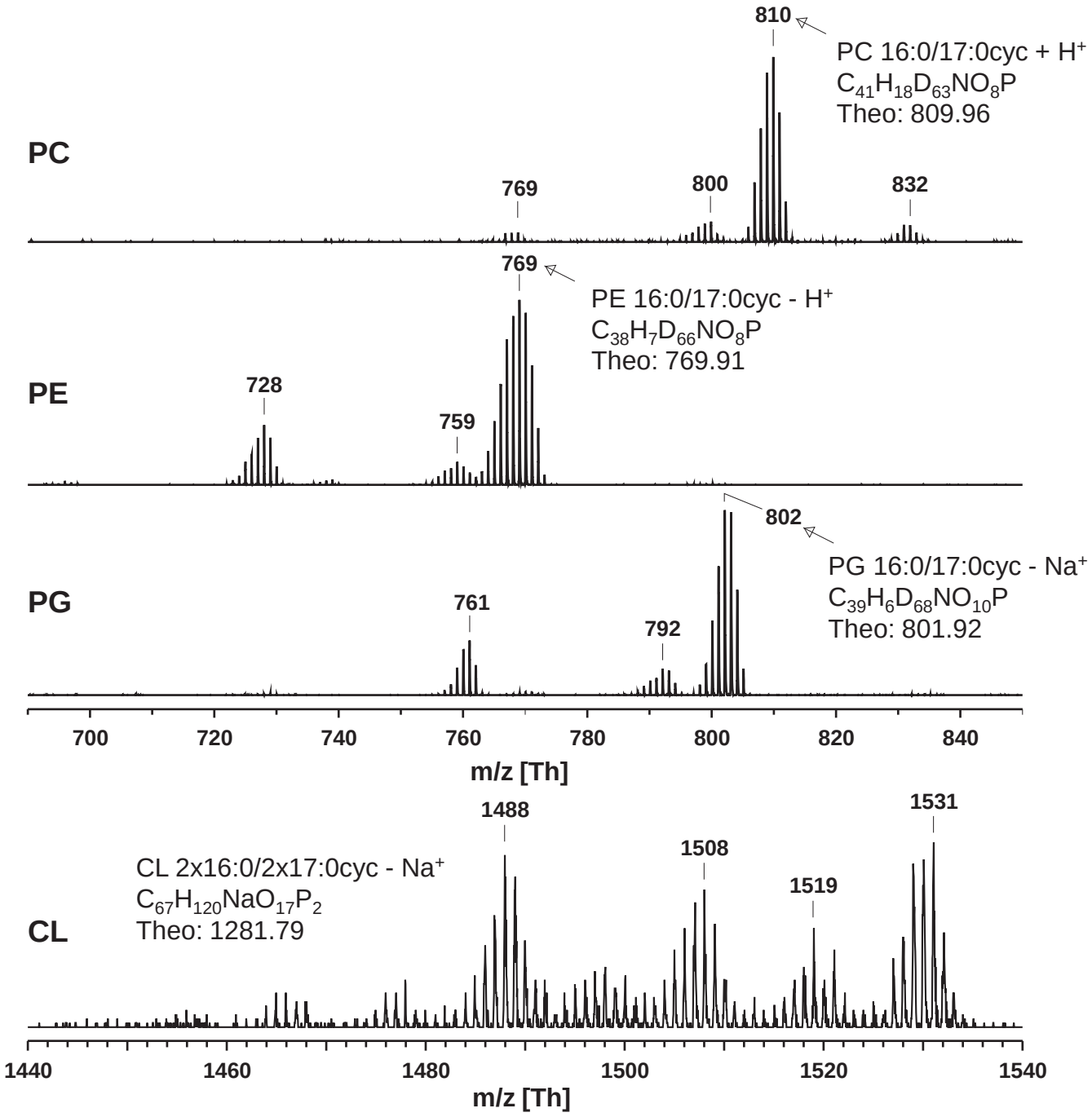
PC
810
PC 16:0/17:0cyc + H+
C41H18D63NO8P
Theo: 809.96
769
800
832
PE
769
PE 16:0/17:0cyc - H+
C38H7D66NO8P
Theo: 769.91
728
759
PG
802
PG 16:0/17:0cyc - Na+
C39H6D68NO10P
Theo: 801.92
761
792
700
720
740
760
780
800
820
840
m/z [Th]
CL
CL 2x16:0/2x17:0cyc - Na+
C67H120NaO17P2
Theo: 1281.79
1488
1508
1519
1531
1440
1460
1480
1500
1520
1540
m/z [Th]

Figure 3.

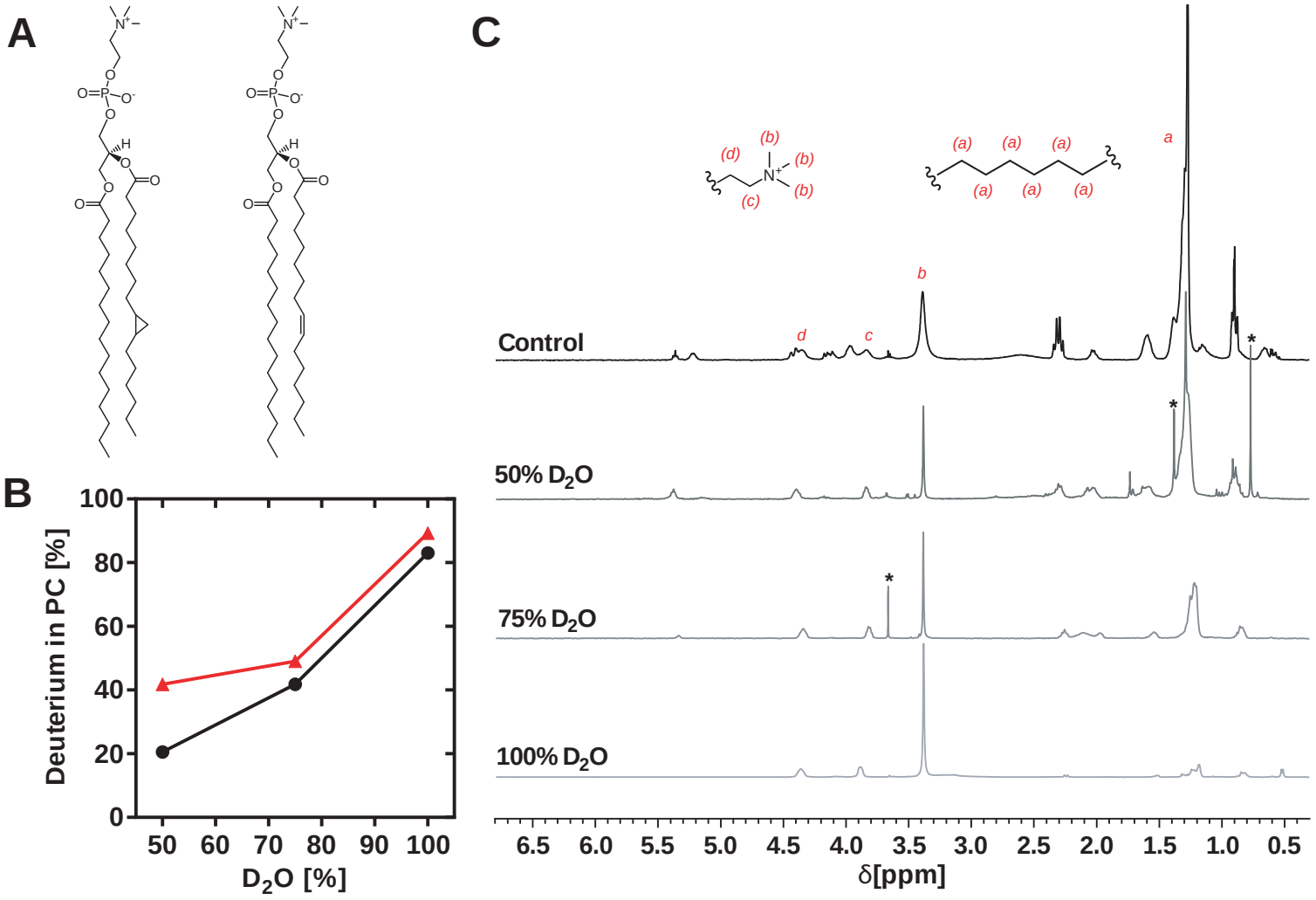

Figure 4.

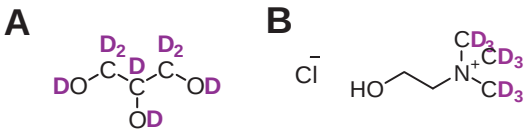

Table 1. Deuterium variation in carbon source supplemented to growth medium

Growth media preparation	Carbon source	
	Glycerol	Choline
$D_{gly}D_{cho}$	$C_3D_8O_3$	$C_5H_5D_9ClNO$
$D_{gly}H_{cho}$	$C_3D_8O_3$	$C_5H_{14}ClNO$
$H_{gly}D_{cho}$	$C_3H_8O_3$	$C_5H_5D_9ClNO$
$H_{gly}H_{cho}$	$C_3H_8O_3$	$C_5H_{14}ClNO$

Figure 5.

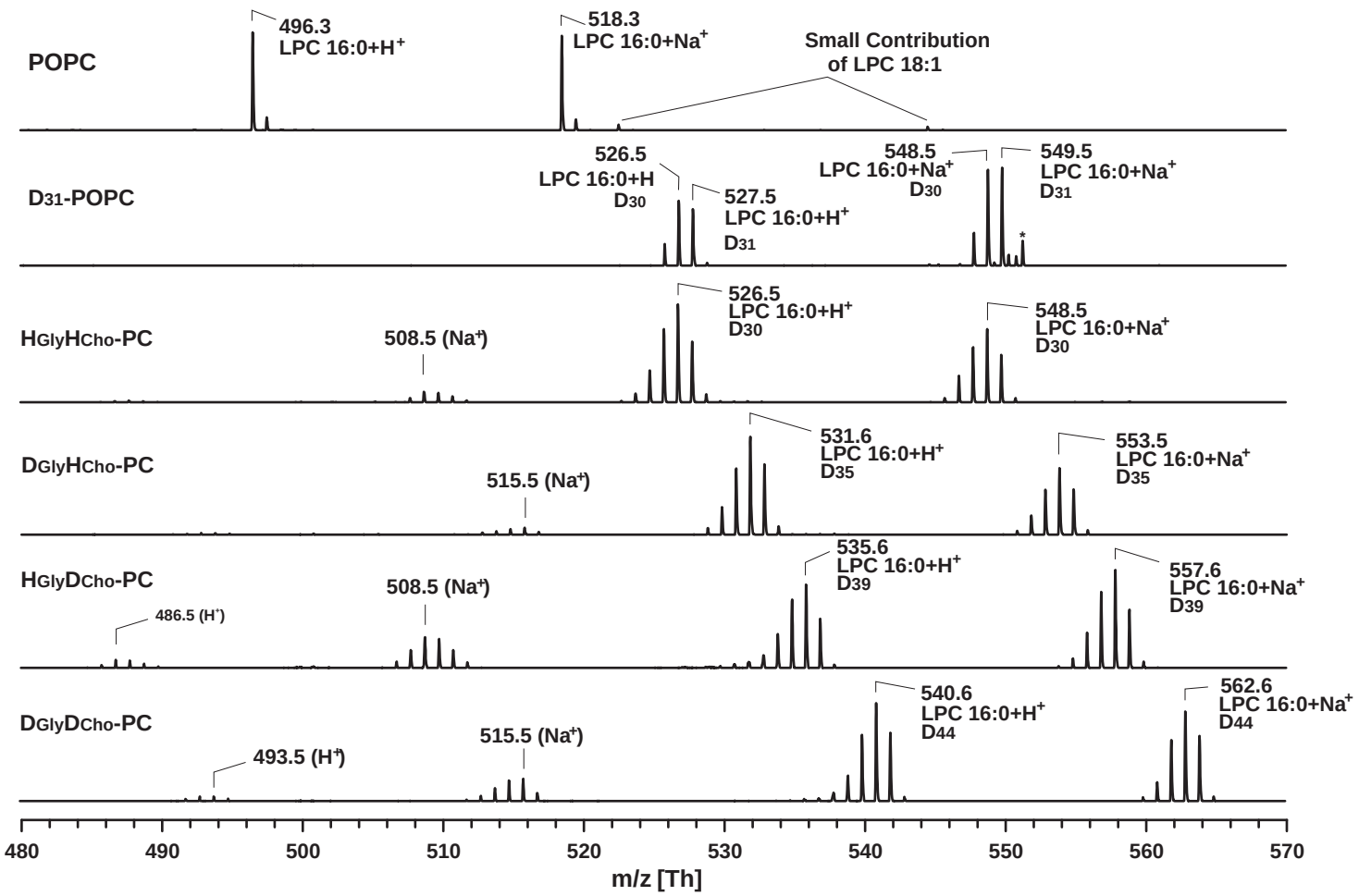
POPC
496.3
LPC 16:0+H+
518.3
LPC 16:0+Na+
Small Contribution
of LPC 18:1
D31-POPC
526.5
LPC 16:0+H
D30
527.5
LPC 16:0+H+
D31
548.5
LPC 16:0+Na+
D30
549.5
LPC 16:0+Na+
D31
*
HGlyHCho-PC
508.5 (Na+)
526.5
LPC 16:0+H+
D30
548.5
LPC 16:0+Na+
D30
DGlyHCho-PC
515.5 (Na+)
531.6
LPC 16:0+H+
D35
553.5
LPC 16:0+Na+
D35
HGlyDCho-PC
486.5 (H+)
508.5 (Na+)
535.6
LPC 16:0+H+
D39
557.6
LPC 16:0+Na+
D39
DGlyDCho-PC
493.5 (H+)
515.5 (Na+)
540.6
LPC 16:0+H+
D44
562.6
LPC 16:0+Na+
D44
480
490
500
510
520
530
540
550
560
570
m/z [Th]

Figure 6.

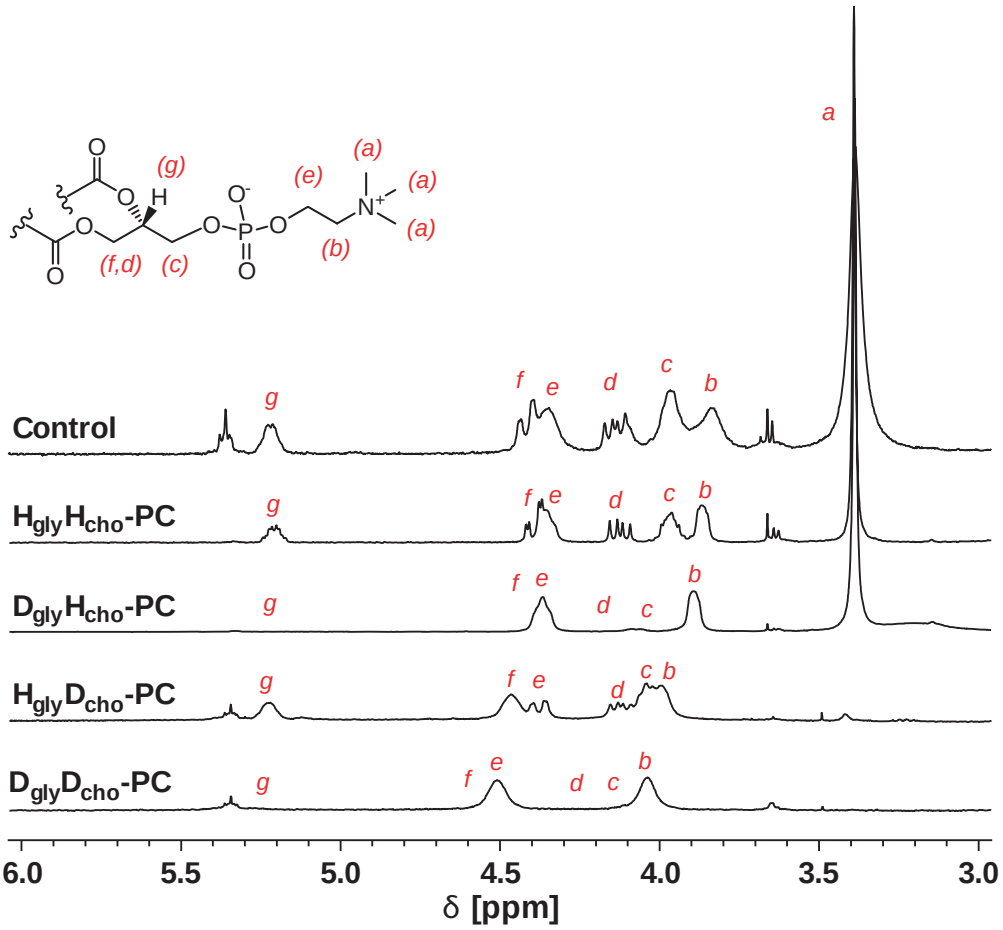
(g)
(e)
(a)
(a)
(a)
(b)
(f,d)
(c)
a
Control
$H_{gly}H_{cho}$-PC
$D_{gly}H_{cho}$-PC
$H_{gly}D_{cho}$-PC
$D_{gly}D_{cho}$-PC
6.0
5.5
5.0
4.5
4.0
3.5
3.0
δ [ppm]

Figure 7.

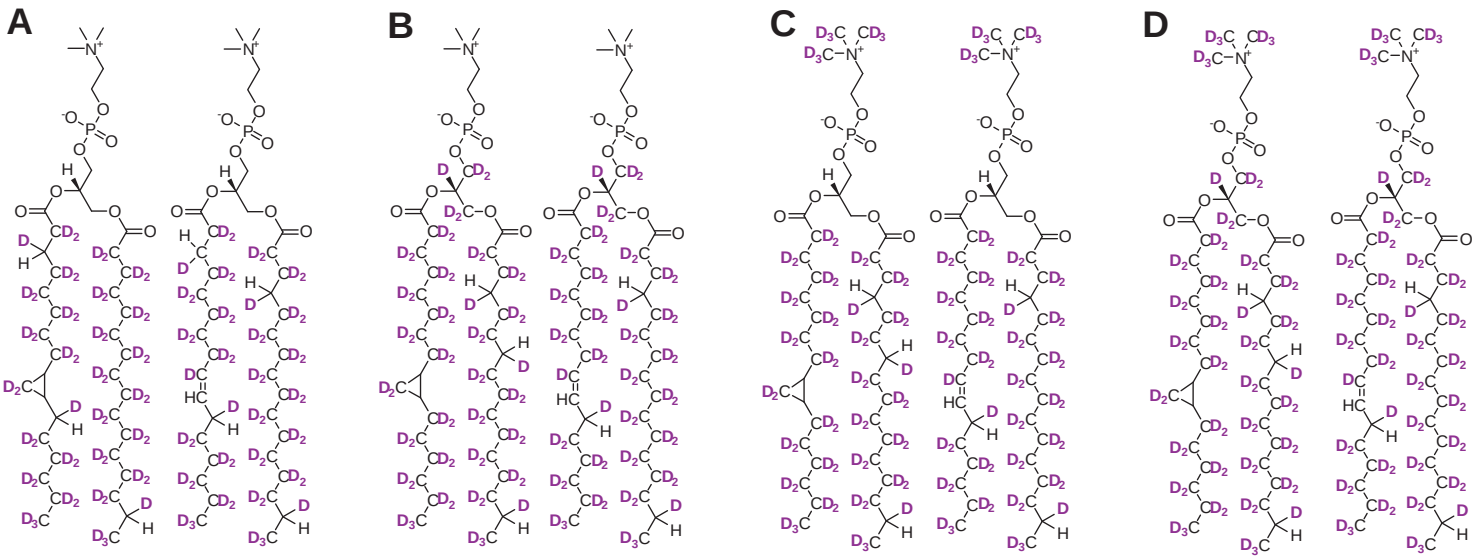

Table 2. *m/z* values (determined by MALDI-TOF MS) of major lipid species from AL95 after deuterium variation in bacterial growth media

Lipid species		Mass			
		$D_{gly}D_{cho}$	$D_{gly}H_{cho}$	$H_{gly}D_{cho}$	$H_{gly}H_{cho}$
PC	16:0/17cyc	818	810	813	804
PE	16:0/17cyc	774	769	763	763
PG	16:0/17cyc	806	802	792	792

Article III

Acta Crystallographica Section D
Biological Crystallography
ISSN 1399-0047

Stealth carriers for low-resolution structure determination of membrane proteins in solution

Selma Maric, Nicholas Skar-Gislinge, Søren Midtgaard, Mikkel B. Thygesen, Jürgen Schiller, Henrich Frielinghaus, Martine Moulin, Michael Haertlein, V. Trevor Forsyth, Thomas Günther Pomorski and Lise Arleth

Acta Cryst. (2014). D**70**, 317–328

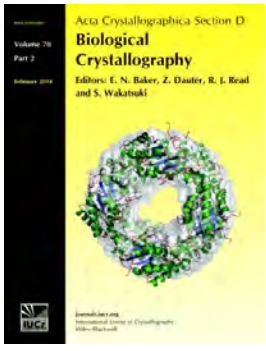

Acta Crystallographica Section D: Biological Crystallography welcomes the submission of papers covering any aspect of structural biology, with a particular emphasis on the structures of biological macromolecules and the methods used to determine them. Reports on new protein structures are particularly encouraged, as are structure–function papers that could include crystallographic binding studies, or structural analysis of mutants or other modified forms of a known protein structure. The key criterion is that such papers should present new insights into biology, chemistry or structure. Papers on crystallographic methods should be oriented towards biological crystallography, and may include new approaches to any aspect of structure determination or analysis. Papers on the crystallization of biological molecules will be accepted providing that these focus on new methods or other features that are of general importance or applicability.

Acta Crystallographica Section D
Biological Crystallography
ISSN 1399-0047

Stealth carriers for low-resolution structure determination of membrane proteins in solution

Selma Maric,[a] Nicholas Skar-Gislinge,[a] Søren Midtgaard,[a] Mikkel B. Thygesen,[b] Jürgen Schiller,[c] Henrich Frielinghaus,[d] Martine Moulin,[e,f] Michael Haertlein,[e] V. Trevor Forsyth,[e,f] Thomas Günther Pomorski[g] and Lise Arleth[a]*

[a]Niels Bohr Institute, University of Copenhagen, Universitetsparken 5, 2100 Copenhagen, Denmark, [b]CARB Centre, Department of Chemistry, University of Copenhagen, Thorvaldsensvej 40, 1871 Frederiksberg C, Denmark, [c]Institut für Medizinische Physik und Biophysik, Medizinische Fakultät, Universität Leipzig, Härtelstrasse 16-18, 04107 Leipzig, Germany, [d]Forschungszentrum Jülich GmbH, Jülich Centre for Neutron Scattering, TUM FRM-2, Lichtenbergstrasse 1, 85747 Garching, Germany, [e]Life Sciences Group, Institut Laue–Langevin, 6 Rue Jules Horowitz, 38042 Grenoble, France, [f]EPSAM/ISTM, Keele University, Staffordshire ST5 5BG, England, and [g]Center for Membrane Pumps in Cells and Disease, Department of Plant and Environmental Sciences, University of Copenhagen, Thorvaldsensvej 40, Frederiksberg C, Denmark

Correspondence e-mail: arleth@nbi.ku.dk

Received 14 June 2013
Accepted 7 October 2013

Structural studies of membrane proteins remain a great experimental challenge. Functional reconstitution into artificial nanoscale bilayer disc carriers that mimic the native bilayer environment allows the handling of membrane proteins in solution. This enables the use of small-angle scattering techniques for fast and reliable structural analysis. The difficulty with this approach is that the carrier discs contribute to the measured scattering intensity in a highly nontrivial fashion, making subsequent data analysis challenging. Here, an elegant solution to circumvent the intrinsic complexity brought about by the presence of the carrier disc is presented. In combination with small-angle neutron scattering (SANS) and the D_2O/H_2O-based solvent contrast-variation method, it is demonstrated that it is possible to prepare specifically deuterated carriers that become invisible to neutrons in 100% D_2O at the length scales relevant to SANS. These 'stealth' carrier discs may be used as a general platform for low-resolution structural studies of membrane proteins using well established data-analysis tools originally developed for soluble proteins.

1. Introduction

Despite significant recent breakthroughs in the field of membrane-protein X-ray crystallography (Rasmussen *et al.*, 2007; Cherezov *et al.*, 2007; Rosenbaum *et al.*, 2007; Rasmussen, Choi *et al.*, 2011; Rasmussen, DeVree *et al.*, 2011), including the award of the 2012 Nobel Prize in Chemistry to Lefkowitz and Kobilka for their contributions toward the understanding of G-protein-coupled receptor systems (Roth & Marshall, 2012), there is still an important lack of structural insight into membrane proteins and their complexes (Bhattacharya, 2009; White, 2009). This is most clearly illustrated by the extremely low number of unique membrane-protein structures available in the Protein Data Bank compared with their 30% prevalence in the human proteome (Fagerberg *et al.*, 2010) and their importance as targets for about 50% of all current drugs (Terstappen & Reggiani, 2001; Xia *et al.*, 2006). Of the 80 000 available protein structures to date, only 400 represent membrane proteins, with around a dozen of these being human membrane-protein structures (Baker, 2010). This creates an obvious need for alternative methods that complement crystallography, nuclear magnetic resonance (NMR) and (cryo) transmission electron microscopy (TEM) approaches for this important class of drug targets.

Over the last decade, small-angle X-ray scattering (SAXS) and small-angle neutron scattering (SANS) have become increasingly important methods in structural studies of water-

soluble protein systems (Jacques & Trewhella, 2010; Petoukhov & Svergun, 2012; Blanchet & Svergun, 2013; Rambo & Tainer, 2013). Recent developments of these techniques at synchrotron radiation and neutron beam sources, in combination with sophisticated sample-preparation procedures and better, more robust and more general data-analysis software tools (Konarev *et al.*, 2006; Jacques *et al.*, 2012), makes small-angle scattering (SAS) an increasingly important tool for the study of biomolecular systems. While SAS only has a structural resolution of the order of 10 Å, which does not provide information at the sorts of length scales accessible to protein crystallography or NMR, it has the significant advantage of allowing rapid protein studies in solution and native-like environments. Furthermore, the solution properties may easily be varied in a way that allows parametric studies such as those relating to temperature, buffer conditions and pH (Round *et al.*, 2008; Toft *et al.*, 2008; Hura *et al.*, 2009). This is powerful for studies of structural flexibility, which is of central importance in protein function, self-assembly and dynamic metabolon formation. Previously, SAS studies have been carried out using membrane proteins stabilized with detergent micelles or liposomes (Chan & Boxer, 2007) or using more advanced systems such as amphipoles (Pocanschi *et al.*, 2006) or nanodiscs (Nath *et al.*, 2007). The requirements for sample volumes and sample concentrations have been brought down to about 10–20 µl at protein concentrations of a few milligrams per millilitre for SAXS and 100–300 µl at a similar protein concentration for SANS (Jacques & Trewhella, 2010). This is compatible with what is typically attainable for many membrane-protein systems (Midgett & Madden, 2007; Tate, 2010). Nevertheless, SAS has to date only provided limited structural knowledge on membrane proteins despite a few breakthroughs (Hunt *et al.*, 1997; Berthaud *et al.*, 2012; Calcutta *et al.*, 2012), mainly because it is difficult to extract the low-resolution structure of the membrane protein alone from SAS data measured on a complex multi-component system.

We have now developed a versatile and robust methodology to circumvent this intrinsic complexity through the use of the well tested and structurally well defined nanodisc system for membrane-protein reconstitution (Bayburt *et al.*, 2002; Nath *et al.*, 2007; Ritchie *et al.*, 2009). In combination with the D_2O/H_2O-based contrast-variation method in neutron scattering (Jacrot, 1976), we demonstrate that it is possible to control the *Escherichia coli*-based biosynthesis of deuterated phosphatidylcholines as well as the expression of membrane-scaffolding proteins to prepare specifically deuterated analogues of the nanodisc which give a minimal contribution to the neutron scattering data when used in 100% D_2O. In this context, a particular challenge has been to control the deuteration levels in the phospholipid head and tail groups, respectively. The stealth discs produced in this way should be generally usable in low-resolution structural studes of many membrane proteins and their complexes in solution. The analysis of SANS data for this platform is greatly simplified and allows the application of existing data analysis tools that are already available for soluble proteins.

2. Materials and methods

2.1. Expression and purification of deuterated membrane-scaffold protein MSP1D1 (D-MSP1S1)

D-MSP1D1 was overexpressed in *E. coli* strain BL21 (DE3) using a pET-28a vector after an initial adaptation process of the strain to minimal deuterated medium as described previously (Artero *et al.*, 2005). High cell-density cultures were grown in 85% deuterated minimal medium containing glycerol as a carbon source (Rochel *et al.*, 2011). The protein was purified according to a modified version of the established method (Ritchie *et al.*, 2009). All sets of protein lipid deuteration were carried out in collaboration with the Deuteration Laboratory PSB platform within the Life Sciences Group at the Institut Laue–Langevin (ILL), Grenoble, France.

2.2. Production and purification of deuterated phosphatidylcholine

E. coli strain AL95 carrying the plasmid pAC-PCSlp-Sp-Gm allowing the biosynthesis of phosphatidylcholine (PC; Bogdanov *et al.*, 2010) was adapted to minimal deuterated medium according to previously established procedures (Artero *et al.*, 2005). Selective deuteration of PC with the relevant scattering-length density was achieved by amplifying the adapted starting culture in ∼100% deuterated minimal medium (Artero *et al.*, 2005) containing 0.2% arabinose (Sigma–Aldrich), 5% deuterated glycerol (1,1,2,3,3-d_5, 99%; Eurisotop) and 2 m*M* deuterated choline chloride (trimethyl-d_9, 98%; Eurisotop). To obtain partial deuteration, hydrogenated glycerol, as well as hydrogenated choline, were used instead. After cultivation at 310 K for 24 h, the cells were harvested by centrifugation and the total cellular lipids were extracted by the method of Bligh & Dyer (1959). Lipid extracts were separated into individual phospholipids using silica-gel chromatography with varying ratios of chloroform and methanol [9:1 (0.2 l), 4:1 (0.2 l), 1:1 (0.2 l), 1:4 (0.2 l) and 100% methanol (0.3 l)].

2.3. Phospholipid analysis

Phospholipid species were separated by thin-layer chromatography (TLC) using chloroform/ethanol/water/triethylamine [30:35:7:35(*v*:*v*:*v*:*v*)] and identified by comparison with known standards chromatographed on the same plate after staining with primuline [5 mg primuline in 100 ml 80:20(*v*:*v*) acetone:water; White *et al.*, 1998]. For further analysis, lipid spots were scraped off and extracted three times with 100 µl chloroform/methanol/0.9% aqueous NaCl [1:1:1(*v*:*v*:*v*)]. The lipid concentration was quantified by determination of the total phosphorus as described previously (Rouser *et al.*, 1966).

2.4. MALDI–TOF mass spectrometry

The extracted lipids were analysed using matrix-assisted laser desorption/ionization time-of-flight (MALDI–TOF) mass spectrometry as described previously (Schiller *et al.*, 2004). The lipid fractions were independently pre-mixed in a

1:1(*v*:*v*) ratio with different matrix compounds [2,5-dihydroxybenzoic acid (DHB) and 9-aminoacridine (9-AA)] prior to deposition onto the MALDI target and were investigated by both positive and negative ion-mode MALDI–TOF MS on a Bruker Autoflex mass spectrometer (Bruker Daltonics; Petkovic *et al.*, 2001). The lipids were also analysed subsequent to PLA_2 digestion in order to determine the fatty-acyl composition, as described previously (Fuchs *et al.*, 2007).

2.5. NMR spectroscopy

The locations of the incorporated deuterium atoms in the lipid molecules were determined by ^{1}H NMR through comparison of 5% solutions of hydrogenated PC, of partially deuterated PC synthesized with hydrogenated glycerol and hydrogenated choline and of deuterated PC synthesized with deuterated glycerol and deuterated choline all achieved in *E. coli*. The lipids were dissolved in chloroform-d [99.96%, 0.03%(*v*:*v*) TMS as internal reference] and measured on a 300 MHz NMR spectrometer (Bruker).

2.6. Stealth carrier disc preparation

Liposomes were prepared by extrusion of the stealth PC lipids in D_2O buffer solution (20 m*M* Tris–HCl, 100 m*M* NaCl pH 7.5) through 100 nm polycarbonate filters (Avanti Polar Lipids Inc). Liposomes at different D_2O:H_2O ratios were achieved through dilution of the D_2O-based liposome stock preparation with an adequate amount of H_2O buffer solution (20 m*M* Tris–HCl, 100 m*M* NaCl pH 7.5). This allowed liposomes to be obtained at 60–100% D_2O for subsequent SANS measurements. The liposome size was confirmed through dynamic light scattering on a BI-200SM System (Brookhaven Instruments). Stealth nanodiscs were reconstituted using the deuterated version of MSP1D1 together with the deuterated stealth PC lipids through the previously described self-assembly-based procedure (Ritchie *et al.*, 2009). All SAXS measurements were performed in H_2O-based buffer. Prior to the SANS measurements, the H_2O-based buffer used in the initial nanodisc preparation was substituted for a 100% D_2O-based buffer solution using centrifugal spin-filters with a cutoff of 50 kDa (Millipore). To achieve the H_2O:D_2O ratios required for the subsequent SANS measurements (60–100% D_2O), the nanodisc stock solution in 100% D_2O was diluted with an adequate amount of H_2O buffer solution.

2.7. SANS contrast variation

All reported contrast-variation SANS data were collected at 25°C using the KWS1 instrument at the Forschungs-Neutronenquelle Heinz Maier-Leibnitz (FRMII) in Munich, while initial pilot data as well as the data from nanodiscs prepared with commercially available POPC (Avanti Polar Lipids Inc.) were obtained using the D11 instrument at the Institut Laue–Langevin (ILL), Grenoble. All reported measurements from FRMII were performed with 4.5 Å neutrons with a wavelength spread $\Delta\lambda/\lambda$ of 10% FWHM. A combination of two to three instrumental settings were used to obtain a sufficiently wide q-range: high q-values (0.035–0.45 Å^{-1}) were covered with a sample-to-detector distance of 1.5 m and a collimation length of 4 m. Intermediate q-values (0.0057–0.077 Å^{-1}) were covered with a sample-to-detector distance of 8 m and a collimation length of 8 m. Low q-values (0.0022–0.03 Å^{-1}) were covered with a sample-to-detector distance of 20 m and a collimation length of 20 m. Owing to the small size of the nanodiscs, these were only measured at high and intermediate q-values, while the liposomes, which have structural features ranging from the ∼40 Å bilayer thickness to the ∼1200 Å liposome diameter, had to be measured at all three settings. Absolute scale calibration was performed using a calibrated Plexiglas sample as an external reference and following the standard procedures at the facility. Radial averaging, background subtraction and absolute scale calibration to convert the data into scattering intensity $I(q)$ in units of cm^{-1} as a function of momentum transfer $q = 4\pi\sin\theta/\lambda$ (where θ is the half scattering angle and λ is the wavelength of the incoming beam) was carried out using the *QtiKWS* software (Pipich, 2007). Small resolution effects were present in the SANS data, mainly owing to the non-negligible wavelength spread of the incoming neutrons. These were taken into account in the subsequent model-based data analysis by smearing of the fit function with the calculated resolution function (Pedersen *et al.*, 1990). All samples were measured in flat rectangular Hellma quartz cells. The samples in 85–100% D_2O were measured in cells with a path length of 2 mm, whereas the samples in 60–80% D_2O were measured in cells with a path length of 1 mm in order to optimize the signal-to-noise ratio and to minimize incoherent background and multiple-scattering effects.

2.8. SAXS structural analysis

The nanodiscs were characterized by SAXS using the Bio-SAXS instrument BM29 at the European Synchrotron Radiation Facility (ESRF), Grenoble. All SAXS data were collected at 20°C at q-values ranging from 0.0040 to 0.45 Å^{-1} with $q = 4\pi\sin\theta/\lambda$ using the fixed instrument setup described for the now disassembled beamline ID14-3 (Pernot *et al.*, 2010), a predecessor of the current beamline. Data processing, including radial averaging, background subtraction and conversion of the data into $I(q)$ (units of cm^{-1}) was performed using the *ATSAS* package (Konarev *et al.*, 2006). Calibration of the scattering intensity into absolute units of cm^{-1} was performed using the forward scattering intensity of bovine serum albumin prepared at a concentration of 3.2 mg ml^{-1} as an external reference. Resolution effects were considered to be negligible owing to the very high monochromaticity of the incoming beam, a very small beam diameter and close to perfect collimation. The data were analysed using an established approach for the nanodisc system (Skar-Gislinge & Arleth, 2011; Skar-Gislinge *et al.*, 2010).

2.9. Determination of forward scattering intensity *I*(0)

For each contrast measurement, the forward scattering was estimated by the indirect Fourier transform method with overlap optimization and background correction (Glatter,

1977; Pedersen *et al.*, 1994) and by taking the resolution effects into account (Pedersen *et al.*, 1990). The absolute scaled data for the liposome and nanodisc samples were normalized by sample concentration and the match points were derived in the standard way (Stuhrmann, 1982) by fitting a second-order polynomial to the forward scattering plotted as a function of volume fraction of D_2O in the buffer solution.

2.10. Model calculation of liposomes

The theoretical scattering signal for D_{64}-POPC liposomes was calculated using the same approach and Fortran77 implementation of the analytical model as previously described in Andersen *et al.* (2011). However, to adapt the calculations to the D_{64}-POPC case, the following total lipid scattering lengths, b, and partial specific molecular volumes, ν, were applied: PC head group, $b = 6.0 \times 10^{-12}$ cm, $\nu = 319$ Å^3; PO tail group, $b = 6.4 \times 10^{-11}$ cm, $\nu = 927$ Å^3. The model calculations assume that the liposomes are measured on a background of 100% D_2O with a scattering length density of 6.38×10^{10} cm^{-2}. An average liposome radius of 500 Å in a Gaussian distribution with $\Delta\sigma/\sigma = 0.25$ was assumed, with a liposome bilayer thickness of 40 Å. This is an idealized model calculation which does not take into account incoherent background effects or other small effects that are typically present in the experimental situation and that contribute to the overall observed scattering.

2.11. Model calculation of protein scattering signal

The theoretical scattering signal for the epidermal growth factor receptor (EGFR) was based on a combination of available crystal structures (PDB entries 1ivo, 1nql, 2jwa, 1egf and 2gs6) which were assembled manually using *PyMOL* (v.1.5.0.4; Schrödinger) based on available structural information for the system (Montelione *et al.*, 1992; Ogiso *et al.*, 2002; Ferguson *et al.*, 2003; Zhang *et al.*, 2006; Bocharov *et al.*, 2008). Assuming one active dimer per nanodisc, the scattering data were then calculated using the program *CRYSON* (Svergun *et al.*, 1998). The theoretical scattering signal for CorA (PDB entry 2bbj; Lunin *et al.*, 2006) was calculated using *CRYSON* assuming one pentameric complex per disc. The data were normalized in relation to the nanodisc data by exploiting the fact that the absolute forward scattering intensity for a dilute system of particles in solution can be calculated as $I(0) = nV^2(\Delta\rho)^2$, where n is the concentration (mol l^{-1}), V is the partial specific molecular volume of the protein, which is 1.35 g cm^3 (Mylonas & Svergun, 2007), and $\Delta\rho$ is the excess scattering-length density of the (hydrogenated) protein in D_2O, which is 3×10^{10} cm^{-2} (Jacrot, 1976).

3. Results

3.1. The stealth nanodisc system: reaching invisibility

The theoretical deuteration levels required for total 'invisibility' of the nanodisc system differ for the various components of this lipid–protein particle. This results from natural differences in the scattering-length density (SLD) between proteins and phospholipids as well as between the head groups and the fatty-acyl residues of the phospholipid bilayer alone (Engelman & Moore, 1975; Jacrot, 1976). The SLD can be calculated by summing over the scattering lengths of the single atoms in a molecule and dividing by the partial specific molecular volume (Glatter & Kratky, 1982).

A buffer based on 100% D_2O is generally favoured in SANS studies in order to minimize the hydrogen incoherent scattering associated with the use of H_2O (Jacrot, 1976). Consequently, for the stealth membrane-protein carriers, zero contrast in 100% D_2O at all of the SANS-relevant length scales is preferable to minimize both the hydrogen incoherent scattering as well as the coherent signal arising from the carrier molecules (Fig. 1).

For the prototype stealth nanodisc we have chosen a PC-based lipid bilayer together with the membrane scaffold protein MSP1D1 (Nath *et al.*, 2007), as several successful reconstitutions of membrane proteins have previously been reported for this nanodisc system. We used PC composed of mixed acyl unsaturated fatty-acyl residues of 16–18 C atoms in length because these are physiologically the most relevant and therefore are most often chosen as model bilayer lipids for the reconstitution of membrane proteins (van Meer *et al.*, 2008).

For a PC-based bilayer in 100% D_2O we calculated that total matching can be achieved when 78% of the head-group atoms and 92% of the acyl-chain H atoms have been

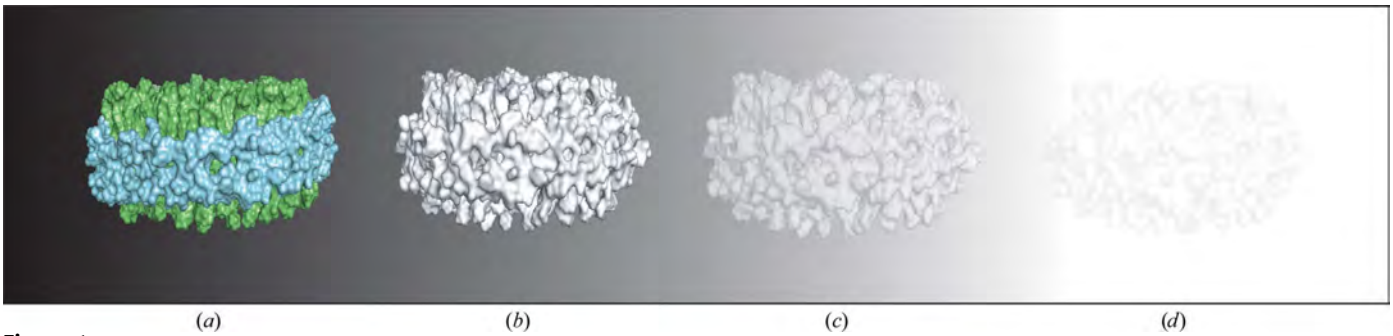

Figure 1
Schematic representation of the stealth nanodisc in buffer solution with a gradually increasing level of D_2O (decreasing greyscale). (*a*) Hydrogenated nanodisc consisting of a phospholipid bilayer (green) and membrane scaffold protein MSP (light blue). (*b*) Stealth nanodisc comprised of deuterated lipid and deuterated MSP at 60% D_2O. (*c*) Stealth nanodisc at 80% D_2O. (*d*) Stealth nanodisc at 100% D_2O.

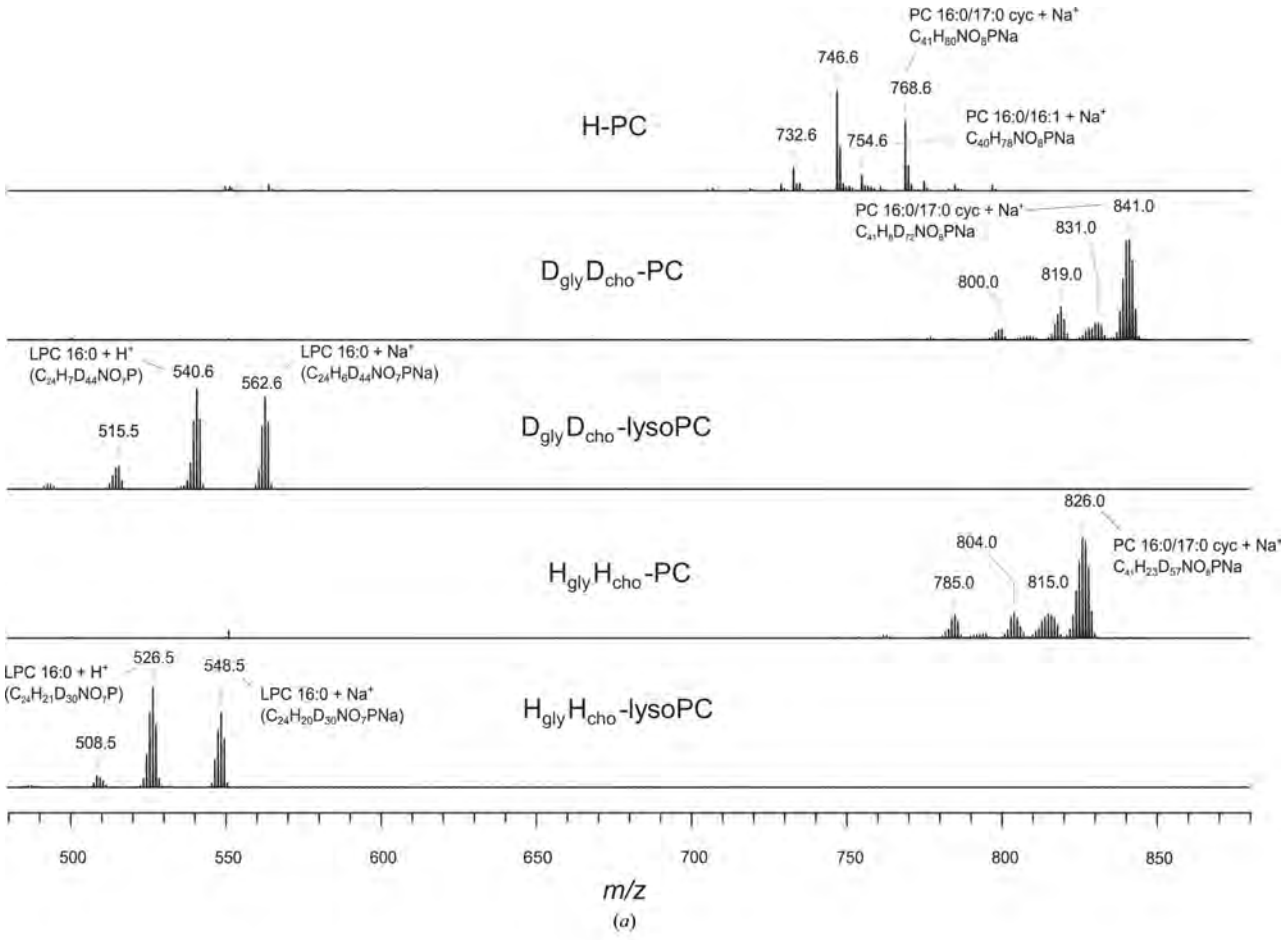

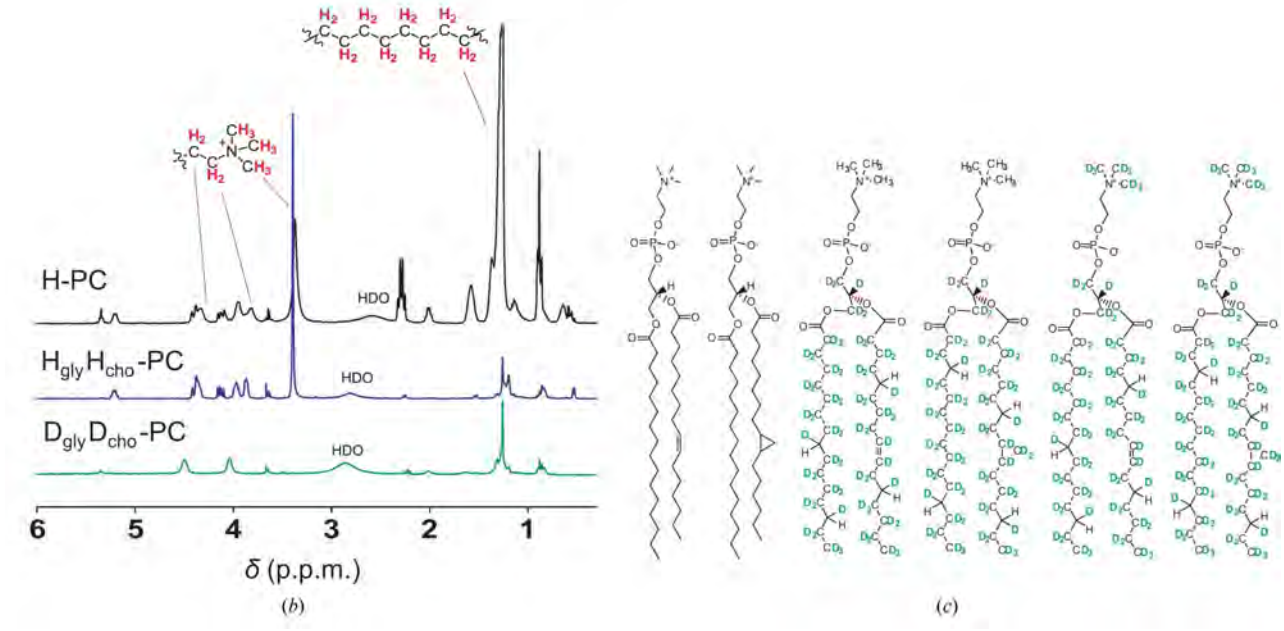

Figure 2
Selective deuteration of phosphatidylcholine in genetically modified *E. coli*. (*a*) Positive-ion MALDI–TOF spectra of purified phosphatidylcholine (PC) obtained from a genetically modified *E. coli* strain grown in hydrogenated medium (trace H-PC), in deuterated medium supplemented with deuterated glycerol and deuterated choline before (trace $D_{gly}D_{cho}$-PC) and after (trace $D_{gly}D_{cho}$-lysoPC) treatment with PLA_2 as well as in deuterated medium supplemented with hydrogenated glycerol and hydrogenated choline before (trace $H_{gly}H_{cho}$-PC) and after (trace $H_{gly}H_{cho}$-lysoPC) treatment with PLA_2. Peaks are marked with their *m*/*z* values and assignments are indicated. (*b*) NMR spectra showing H-PC (black), $H_{gly}H_{cho}$-PC (blue) and $D_{gly}D_{cho}$-PC (green) with HDO representing water traces in the samples. (*c*) Molecular structure of the *E. coli*-produced PC (examples of the main species according to deuteration).

exchanged to deuterium. For the membrane scaffold protein MSP1D1 encircling the bilayer, as for all other proteins, the required level of deuteration is reached when on average 70% of the non-exchangeable H atoms are replaced by D atoms (Engelman & Moore, 1975; Jacrot, 1976; Li *et al.*, 2009). Owing to the exchangeability of the H atoms bound to O, N and S atoms, this leads to an overall level of deuteration of about 75% when the protein is dispersed in 100% D_2O solution.

3.2. Engineering of the stealth-nanodisc components

While several versions of partially deuterated 1-palmitoyl-2-oleoyl-PC and dipalmitoyl-PC (16:0/18:1 and 16:0/16:0, respectively) are commercially available (Bragina & Chupin, 1997), monounsaturated mixed-acyl versions of PC with the specific deuteration levels that would result in stealth properties in 100% D_2O are not. This is because chemical synthesis of these lipids is highly challenging (Bragina & Chupin, 1997). Previous chemical syntheses of deuterated PC have utilized methods that do not allow differentiation between the fatty-acyl residues at positions 1 and 2 of the glycerol (Bragina & Chupin, 1997). Selective deuteration of the head group in unsaturated deuterated phospholipids is accompanied by modifications of the double bonds (de Kruijff *et al.*, 1978). We therefore chose to produce the required PC lipids through biological deuteration in a recently engineered *E. coli* strain (AL95) that produces PC (Bogdanov *et al.*, 2010). *E. coli* may be deuterated to a very high degree (Paliy *et al.*, 2003) and has a very simple lipid composition (Raetz, 1978) compared, for example, with yeast (Kaneko *et al.*, 1976), and was therefore chosen in order to facilitate biosynthesis as well as subsequent extraction and lipid isolation.

Minimal medium was chosen for the production of both deuterated nanodisc components in order to obtain better control of the deuteration levels. For the bacterial lipids we were able to achieve targeted head-group deuteration through the addition of deuterated glycerol, while the deuteration of the acyl chains could be controlled through the total level of D_2O in the growth medium. Also, the addition of commercially available partially deuterated choline chloride retaining a protonated ethylene group (trimethylammonium-d_9) enabled an additional level of control of head-group deuteration. Furthermore, choline supplementation resulted in higher yields of PC, as seen for its hydrogenated analogue (Bogdanov *et al.*, 2010).

The fatty-acyl distribution of *E. coli* phospholipids is dependent on the growth conditions (de Mendoza *et al.*, 1983). For this particular strain, cells harvested in the stationary growth phase resulted in a lipid extract containing 1-palmitoyl-2-palmitoleoyl-*sn*-glycero-3-phosphocholine (16:0/16:1 PC) as shown by positive-ion MALDI–TOF analysis (Fuchs *et al.*, 2010), with *m*/*z* 732.6 and 754.6 corresponding to the proton and sodium adducts, respectively (Fig. 2*a*, trace H-PC). The data also showed the presence of primarily PC with a cyclopropane-modified fatty-acyl residue at *m*/*z* 746.6 and 768.6 (16:0/17:0cyc PC) typical of *E. coli* lipids (Magnuson *et al.*, 1993). These cyclopropanated residues appear to improve stability and are less reactive to oxidative modifications than the corresponding unsaturated fatty-acyl residues, while keeping the overall membrane fluidity unchanged (Law, 1971; Dufourc *et al.*, 1983).

The PC biosynthesized in deuterated medium at ∼100% D_2O in the presence of deuterated glycerol and partially deuterated choline chloride (trimethylammonium-d_9) exhibited a narrow distribution of highly deuterated PC with no major changes in the fatty-acyl distribution (Fig. 2*a*, trace $D_{gly}D_{cho}$-PC). The peaks at *m*/*z* 800.0 and 819.0 were assigned to the H^+ adducts of highly deuterated 16:0/16:1 PC and 16:0/17:0cyc PC, respectively, whereas the two peaks at *m*/*z* 831.0 and 841.0 were assigned to the respective Na^+ adducts of the same two species. While the Na^+ adduct of completely deuterated 16:0/17:0cyc PC (d_{80}) should result in *m*/*z* 849.0, the observed lower value of 841.0 for the most abundant species can be explained by incompletely deuterated 16:0/17:0cyc PC with a remaining average of eight H atoms ($C_{41}H_8D_{72}NO_8PNa$). This interpretation was further confirmed through characterization of the PC fraction after digestion with phospholipase PLA_2, an enzyme that selectively cleaves the fatty-acyl residue in the *sn*-2 position (Fuchs *et al.*, 2007). Prior to digestion, the most abundant peak was at *m*/*z* 841.0 and after digestion it was at *m*/*z* 562.6 (Fig. 2*a*, traces $D_{gly}D_{cho}$-PC and $D_{gly}D_{cho}$-lysoPC). Fully deuterated lysoPC 16:0 would give a mass of 568.6 for the Na^+ adduct; however, the lower value of 562.6 observed for the most abundant species can be assigned to a partially deuterated lysoPC containing six H atoms ($C_{24}H_6D_{44}NO_7PNa$). This indicates a loss of two H atoms after the deletion of the fatty-acyl residue in the *sn*-2 position. The biosynthesis approach gave a narrow distribution of deuteration level for PC, with an observed standard deviation of 1.3 atomic mass units (amu) within the single species. When compared with the 80 possible D atoms in the 16:0/17:0cyc PC this corresponds to a ∼1.6% deviation in the deuteration level for the overall lipid. The biosynthesis of PC in ∼100% D_2O in the presence of protonated carbon sources showed a similar fatty-acyl distribution but with a shift in *m*/*z* from 841.0 to 826.0 (Fig. 2*a*, trace $H_{gly}H_{cho}$-PC). Assuming no change in fatty-acyl distribution, this decrease of 15 amu corresponds well to the difference between the protonated and deuterated carbon sources added to the medium (choline possessing nine and glycerol five H atoms). An exact decrease of 14 amu can be observed when comparing the lyso fractions of both $D_{gly}D_{cho}$-PC and $H_{gly}H_{cho}$-PC subsequent to PLA_2 digestion, with a shift from *m*/*z* 562.6 for a deuterated carbon-source preparation to *m*/*z* 548.5 for a protonated carbon-source preparation (Fig. 2*a*, traces $D_{gly}D_{cho}$-lysoPC and $H_{gly}H_{cho}$-lysoPC), indicating completely hydrogenated head groups in this partially deuterated species.

The localization of the residual H atoms in the two aforementioned deuterated versions of PC was investigated by ^{1}H NMR by comparison to the hydrogenated analogue (Fig. 2*b*). The two signals observed at 4.04 and 4.50 p.p.m. in $D_{gly}D_{cho}$-PC were in agreement with the ethylene H atoms of the choline head group (Fig. 2*b*, trace $D_{gly}D_{cho}$-PC green). Although they were slightly downfield-shifted compared with

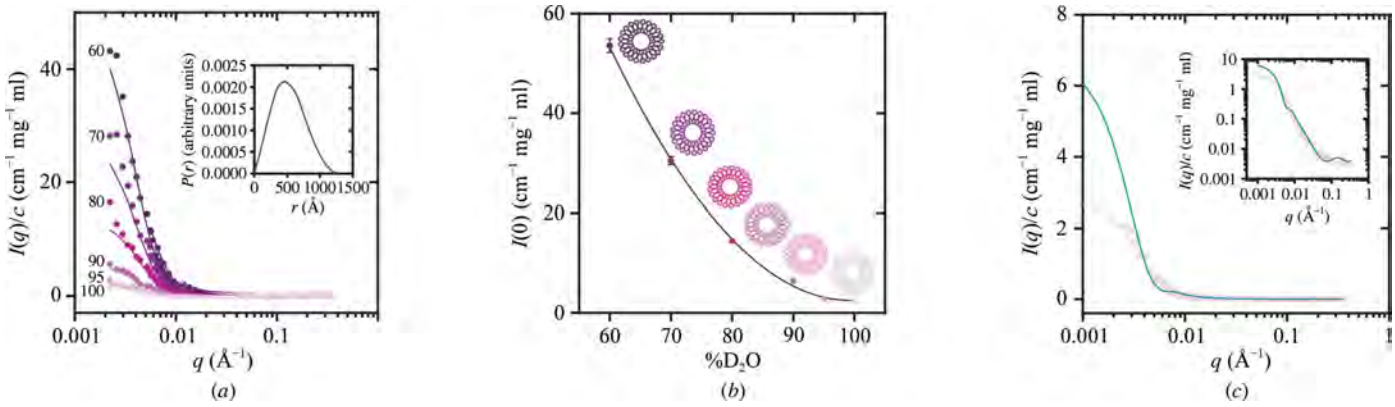

Figure 3
Stealth liposome SANS contrast variation. (*a*) SANS data together with IFT fits showing the decrease in scattering intensity from the stealth liposomes with the indicated increasing levels of D_2O in the buffer. The inset shows the pair distance distribution function for stealth liposomes at 60% D_2O. (*b*) SANS forward scattering as a function of the D_2O content of the buffer. Inset: a schematic representation of stealth liposomes with decreasing contrast in D_2O. (*c*) Stealth liposome SANS data (light purple) and theoretical SANS data calculated for liposomes with commercially available D_{64}-POPC (Avanti Polar Lipids; petrol). The insert shows a comparison of the two versions of deuterated liposomes (light purple and dark cyan) on a logarithmic scale.

the hydrogenated sample, this assignment was confirmed by ^{13}C NMR (65.9 and 60.3 p.p.m., respectively). If these two aforementioned peaks are assumed to correspond to two H atoms each, as is the case for the added choline, this gives a total of approximately four H atoms in the fatty-acyl signal at around 1.2 p.p.m. (Fig. 2*b*, green trace). NMR analysis of $H_{gly}H_{cho}$-PC obtained from *E. coli* grown with hydrogenated carbon sources, as shown in Fig. 2(*b*) (blue), confirmed head-group incorporation of protonated glycerol and choline, while the fatty-acyl residues remained highly deuterated. The glycerol and choline signals between 3.5 and 5.5 p.p.m. were identical to the hydrogenated sample, whereas the acyl signals were similar to the highly deuterated sample. The many small signals observed in NMR for the two deuterated analogues (Fig. 2*b*, blue and green traces) are associated with the acyl residues and indicate that the remaining H atoms were randomly distributed throughout the chains. The combined MALDI–TOF and ^1H NMR data allowed the calculation of the deuteration levels for the most abundant $D_{gly}D_{cho}$-PC species 16:0/17:0cyc PC. For the 18 head-group H atoms present in normal hydrogenated conditions, the remaining four H atoms gave 78% deuteration. For the acyl chains, 58 of the 62 H atoms were exchanged to deuterium, corresponding to 93% deuteration. Fig. 2(*c*) illustrates examples of the most abundant species before and after deuteration.

The stealth version of MSP1D1 with the 'match-out' deuteration level was expressed in *E. coli* BL21 (DE3) cells grown in 85% deuterated minimal medium according to established protocols for protein deuteration (Leiting *et al.*, 1998). The initial yields of the two nanodisc components achieved using this approach were in the region of ~50 mg l^{-1} for deuterated PC and ~25 ml^{-1} for deuterated MSP1D1. These amounts are sufficient for several nanodisc assemblies that can be used in subsequent SAXS and SANS analysis. Based on the amount of cell paste obtained in a pilot fermentation study, this can be scaled up to over 200 mg l^{-1} for PC. A similar scale-up is also expected to be possible for MSP1D1 through fermentation.

3.3. Stealth carrier assembly and SANS contrast variation

Small unilamellar liposomes were prepared from purified $D_{gly}D_{cho}$-PC (Supporting Fig. S1*a*[1]). These stealth liposomes showed an average diameter of 110 nm when probed by dynamic light scattering. The liposome size was also confirmed through SANS, in which model fitting (Kucerka *et al.*, 2004) and the pair distance distribution function, $p(r)$, obtained by indirect Fourier transformation gave a maximum dimension of 120 nm (Fig. 3*a*, insert). Contrast-variation SANS data collected over a broad q-range for the prepared liposomes at increasing D_2O content in the buffer showed a systematic decrease in scattering intensity with increasing level of D_2O (Fig. 3*a*). The minimum in scattering intensity for the liposomes derived from the SANS forward scattering as a function of D_2O content is observed to be close to 100% D_2O (Fig. 3*b*). A comparison of the scattering from the stealth liposomes to the theoretically expected results for the commercially available D_{64}-POPC deuterated lipids in 100% D_2O is provided in Fig. 3(*c*). The plot shows that the forward scattering of the liposomes is minimized in the stealth lipid system. This is expected, as the commercially available D_{64}-POPC lipids are not matched out at 100% D_2O, which is the optimal contrast in order to maximize the signal-to-noise ratio of an inserted membrane protein. However, and more importantly, the oscillation at intermediate to high q that is present in the commercial system owing to the different internal scattering length densities in the lipids is much less visible in the stealth lipids. Since the scattering signal from a typical membrane protein is expected to be present in this region (Fig. 5) this is an important result. Fig. 3(*c*) also shows that while the

[1] Supporting information has been deposited in the IUCr electronic archive (Reference: KW5078).

biosynthetically produced lipids minimize the scattering from the liposomes, the scattering intensity at 100% D_2O is unfortunately not zero. A complete $I(q) = 0$ is impossible to obtain owing to internal deuteration fluctuations within the single lipids. However, the data indicate that an even better match-out could potentially be achieved through further fine-tuning of the growth conditions. This will be pursued in future work.

SAXS analysis of deuterated MSP1D1 on its own showed that the purified amphipathic protein belts formed large disordered aggregates when dissolved in aqueous solution, making subsequent SANS contrast-variation investigations unreliable.

However, by combining the produced $D_{gly}D_{cho}$-PC (Supporting Fig. S1*a*) and deuterated MSP1D1 (Supporting Fig. S1*b*) using standard nanodisc-preparation procedures (Ritchie *et al.*, 2009), successful assembly of nanodiscs was achieved. Size-exclusion chromatography showed an elution profile (Supporting Fig. S1*c*) commonly observed for hydrogenated nanodiscs (Ritchie *et al.*, 2009). A small shoulder observed on the chromatogram indicated that the ratio of phospholipid to membrane-scaffold protein was not at the optimal level for reconstitution. Non-optimal ratios can arise from slight discrepancies in concentration measurements when dealing with deuterated versions of the phospholipids and MSP and would lead to fractions of slightly larger lipid–protein aggregates. Therefore, only the fractions thought to contain nanodiscs of typical size were used for further analysis (Supporting Fig. S1*c*, green). Successful nanodisc assembly was supported by SAXS analysis. The very distinct SAXS curve characteristic of the nanodisc system (Fig. 4*a*, green) gave a $p(r)$ function that indicated a maximum size of approximately 12 nm for the discs. This was consistent with the previously observed size of nanodiscs with attached His tags, which was also the case in this preparation (Skar-Gislinge *et al.*, 2010). Finally, a recently derived mathematical model of the nanodisc (Skar-Gislinge *et al.*, 2010; Skar-Gislinge & Arleth, 2011) was fitted to the experimental data (Fig. 4*a*, black) and confirmed that the SAXS data were fully consistent with the nanodiscs having approximately the same structure as has previously been observed by our group (Skar-Gislinge *et al.*, 2010; Skar-Gislinge & Arleth, 2011).

The SANS contrast-variation study of the stealth nanodisc showed a systematic decrease in scattering intensity with an increasing level of deuterium in the solvent and revealed a clear minimum in the overall scattering intensity at 100% D_2O (Figs. 4*b* and 4*c*). This initial preparation of the stealth carriers resulted in a small residual signal for both the stealth liposomes and the nanodiscs. This could be owing to the aforementioned statistical fluctuations in the deuteration of the lipids and the MSP1D1. The observed intensity decreased to a level only slightly above that of the experimental background and was therefore difficult to measure accurately. In Fig. 4(*d*) we compare the residual nanodisc signal with the SANS signal of a nanodisc assembled with D-MSP1D1 in combination with commercially available chemically synthesized D_{64}-POPC (Avanti Polar Lipids) containing fully deuterated fatty-acyl chains and protonated head groups. While the forward scattering signals from both of the deuterated nanodisc samples are over ∼150-fold lower than that of a protonated nanodisc (Fig. 4*d*, inset), the biosynthesized stealth nanodisc clearly shows an improvement, with a lowered

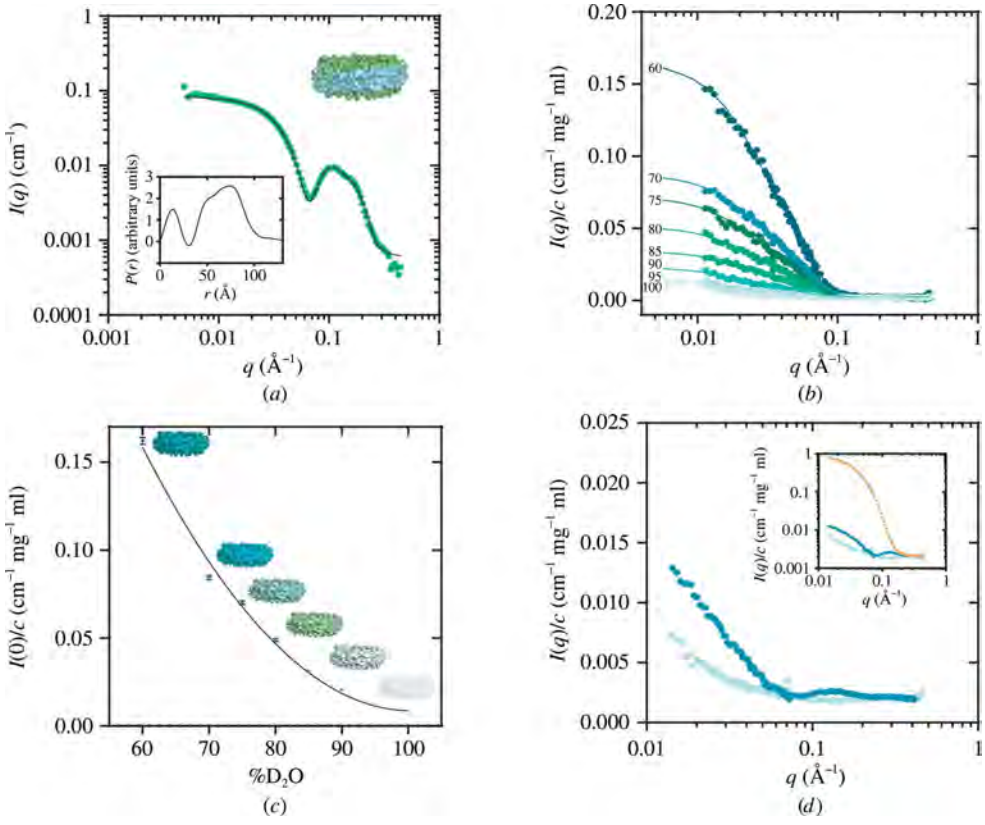

Figure 4
Stealth nanodisc assembly and SANS contrast variation. (*a*) Small-angle X-ray scattering data from nanodiscs in H_2O (green) shown together with the fitted structural model (black). The inset shows the pair distance distribution function for the stealth discs with information about the disc size. (*b*) SANS data together with IFT fits showing the decrease in scattering intensity from the stealth nanodiscs with the indicated increasing buffer content of D_2O in solution. (*c*) SANS forward scattering as a function of the D_2O content of the buffer. (*d*) Stealth nanodisc SANS data (light green) and SANS data measured for nanodiscs assembled with D-MSP1D1 and commercially available D_{64}-POPC (Avanti Polar Lipids; petrol). The inset shows a comparison of the two versions of deuterated discs (light green and blue) with a protonated version of the nanodisc (orange) on a logarithmic scale.

scattering intensity in the entire q-range when compared with the chemically synthesized version of the disc. An even better match-out could potentially be achievable through further optimization of the deuteration levels of both the lipid bilayer and the membrane-scaffold protein.

In order to obtain insight into the potential performance of the developed stealth nanodiscs, a comparison of the residual stealth nanodisc signal was performed with a range of possible protein targets of different sizes (Fig. 5), where the theoretical scattering intensity was generated using the program *CRYSON* (Svergun *et al.*, 1998). For EGFR, for which the complete structure has yet to be resolved, the scattering data were based on a manual assembly of the available structural parts (Zhang *et al.*, 2006; Ferguson *et al.*, 2003; Bocharov *et al.*, 2008; Ogiso *et al.*, 2002; Montelione *et al.*, 1992), while for the other proteins the curves were generated using already available structural information (Palczewski *et al.*, 2000; Shintre *et al.*, 2013; Pedersen *et al.*, 2007; Shinoda *et al.*, 2009; Higgins *et al.*, 2004). For larger protein complexes such as EGFR with one active dimer per nanodisc, a ∼120-fold larger forward scattering intensity could be observed for the protein compared with the stealth nanodisc carrier, while for the CorA pentameric complex (Lunin *et al.*, 2006) the signal is ∼45-fold larger than that of the stealth nanodisc. In such cases the signal from the nanodisc can be ignored to the first order, allowing the use of the stealth nanodisc system in combination with already tested bead-modelling and rigid-body approaches (Svergun, 1999; Svergun *et al.*, 2001) to obtain a good low-resolution determination of the membrane-protein structure. In the case of smaller membrane-protein systems, it will be beneficial to include a primitive model of the weakly scattering stealth nanodisc in order to resolve the membrane-protein signal. In all cases, combining the bead-modelling approach with an approximate model of the weakly scattering stealth nanodisc should make it possible to further improve the structural resolution of the membrane protein towards the standard ∼10 Å resolution that is typically achievable from small-angle scattering data.

4. Discussion

We have shown that the deuteration level of physiologically relevant PC can be separately controlled for head groups and tails *via* a biosynthetic pathway. This includes targeted substitution of hydrogen by deuterium in the different parts of the phospholipid molecule through systematic addition of deuterated nutrients during biosynthesis. We have exploited this to prepare an advanced carrier system for membrane proteins that becomes 'invisible' to neutrons in 100% D_2O-based buffers. This development offers a general approach to determine the low-resolution structure of membrane proteins and their complexes in solution using already established SAXS/SANS data-analysis methods (Petoukhov & Svergun, 2012; Blanchet & Svergun, 2013).

Using this approach, the deuterated stealth carriers can be produced in sufficiently large amounts to facilititate SANS-based structural studies of membrane proteins that are generally only available in small quantities (Midgett & Madden, 2007; Tate, 2010).

The SAXS analysis of the prepared nanodiscs showed that the overall disc structure did not change compared with POPC nanodiscs that have been described previously (Skar-Gislinge *et al.*, 2010; Skar-Gislinge & Arleth, 2011). This confirmed that the cyclopropane substitution of some of the double bonds in the PC unsaturated fatty-acyl chain that occurs in *E. coli* during the stationary growth phase (Magnuson *et al.*, 1993) and which should not affect the bilayer fluidity (Dufourc *et al.*, 1983) also did not affect nanodisc formation. Harvesting cells in this growth phase is therefore recommended as it leads to the highest biomass and consequently the highest yield of phospholipid for the lowest cost of deuterated medium. The fatty-acyl distribution can be regulated during the bacterial growth cycle (Magnuson *et al.*, 1993), creating additional opportunities for the development of these stealth lipids.

The deuteration approach through biosynthesis also allows the production of different types of specifically deuterated physiologically relevant PCs that may be exploitable using other structural techniques such as NMR and neutron reflectometry. In NMR studies of complex protein–lipid systems a complete cancellation of the ^{1}H signal through the use of fully deuterated PC leads to significant simplification in data analysis (Hagn *et al.*, 2013), while physiologically relevant PC may provide better stability of the incorporated membrane protein (van Meer *et al.*, 2008). In neutron reflectometry, on the other hand, the advantages lie in obtaining different contrasts in different parts of the lipid bilayer, which can be controlled through different deuteration levels, thus highlighting specific parts (Majewski *et al.*, 2000). This can then be exploited not only in studies of the effect of the lipid environment on membrane-protein systems but also in studies of

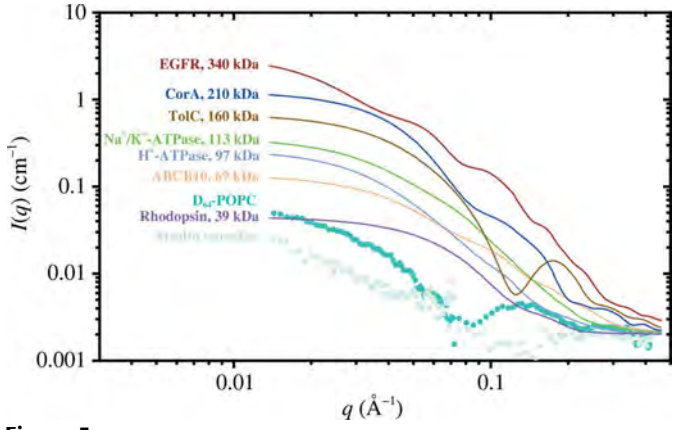

Figure 5
Comparison of the stealth nanodisc SANS signal with those of model proteins. SANS data from stealth nanodiscs in 100% D_2O (green) and D_{64}-POPC nanodiscs (petrol) shown together with the theoretical scattering signals for bovine rhodopsin (purple), ATP-binding cassette transporter (ABCB10; orange), H^+-ATPase (light blue), Na^+/K^+-ATPase (green), trimeric TolC protein from *E. coli* (brown), bacterial magnesium transporter CorA (dark blue) and the epidermal growth factor receptor EGFR (dark red). All scattering curves were generated using *CRYSON* and PDB entries available for each protein (PDB entries 1f88, 4ayw, 3b8c, 2zxe, 1tqq and 2bbj), while the EGFR structure was combined in *PyMOL* (http://www.pymol.org) using PDB entries 1ivo, 1nql, 2jwa, 2gs6 and 1egf.

various ligands and potential drugs and their interactions with the membrane (Akesson *et al.*, 2012). In this context, using the lipids to understand, for example, the interactions of antimicrobial peptides with bacterial membranes could lead to novel insights into the increasing problem of antibiotic resistance in bacteria (Molloy, 2010).

In the case of the reported stealth nanodiscs and liposomes, a residual signal is visible for both carriers when investigated by SANS in 100% D_2O. This signal is negligible by comparison with that of a possible protein signal in 100% D_2O, as shown in the comparison of the nanodisc carrier with a range of model membrane-protein signals. In these examples, the signal caused by the nanodisc can to a good approximation be ignored when reconstructing the low-resolution membrane-protein structure from SANS data. However, for studies of small membrane proteins with a size of ∼50 kDa, for which the membrane-protein signal is also relatively weak in 100% D_2O, the residual nanodisc signal needs either to be incorporated in the data analysis or needs further reduction to achieve the same negligibility.

Stealth liposomes naturally give a larger residual signal than the nanodiscs owing to the much larger size of the particles. However, they can be used as an alternative carrier for larger membrane-protein systems where reconstitution into nanodiscs is not appropriate or where a more cell-like environment is desired, for example in electrolyte or pH-gradient studies.

For accurate and reliable data interpretation in terms of the structural parameters, the scattering data should be obtained from a pure and well defined sample, as with any other systems studied by SAS. As with regular nanodiscs, the reconstitution conditions should be optimized for each membrane protein under study (Ritchie *et al.*, 2009). Based on the initial stealth nanodisc assembly shown in this article, we do not foresee that the reconstitution conditions will differ significantly for these specifically deuterated nanodiscs. The use of D_2O-based buffer in SANS can in unfavourable cases give rise to greater protein instability (Makhatadze *et al.*, 1995), that may compromise the SANS data quality.

Nevertheless, for membrane-protein complexes the nanodisc-based approach of 'mimicked solubility' has already led to an improved understanding of membrane-protein function in a more native-like environment (Ritchie *et al.*, 2009) as well as structure, using for example NMR (Hagn *et al.*, 2013). We therefore anticipate that both the stealth nanodiscs as well as the stealth liposomes will be a great advantage as 'neutron-invisible' carriers to be used as a platform for SANS structural studies of membrane proteins in solution. Combined with the advancement of *ab initio* and rigid-body modelling programs for structural data analysis and the development of powerful next-generation neutron sources, data obtained through this development may lead to further insights into the dynamics, protein–ligand binding and conformational changes of membrane proteins in a solution environment. Collectively, this approach establishes an experimental basis for using the system for low-resolution structural studies of membrane proteins using the same data-analysis tools as are already available for soluble proteins in solution (Konarev *et al.*, 2006; Petoukhov & Svergun, 2012; Blanchet & Svergun, 2013).

The authors gratefully acknowledge the access to the large-scale facility SANS and SAXS beamtime at SANS beamline KWS1 at Forschungs Neutronenquelle Heinz Maier-Leibnitz (FRM II), Munich, SANS beamline D11 at the Institut Laue–Langevin (ILL), Grenoble, the BM29 Bio-SAXS beamline at the European Synchrotron Radiation Facility (ESRF), Grenoble and the Deuteration Laboratory PSB platform operated together with the ILL Life Sciences Group, Grenoble. In particular, the authors would like to thank Dr Adam Round, Dr Petra Pernot and Dr Ralph Schweins for beamline support in Grenoble. The authors also wish to thank Professor William Dowhan and his group at the University of Texas, USA for their kind contribution in providing the PC-producing *E. coli* strain. The authors would like to thank Martin Cramer Pedersen for help with model calculation data and Professor Birger Lindberg Møller for critical reading of the manuscript. Finally, we thank the European Spallation Source and the Danish Government-funded UNIK Synthetic Biology program for co-funding of the project as well as the Danish Research Council-funded DanScatt organization for providing financial support for travel to the large-scale facility SAXS and SANS beamlines. JS thanks the German Research Council for financial support (SFB 1052/B6). VTF acknowledges support from the UK Engineering and Physical Sciences Research Council (EPSRC) for the ILL Deuteration Laboratory under grants GR/R99393/01 and EP/C015452/1, from the EU NMI3 programme under FP7 and also through the EU CRISP programme (grant No. 283745).

References

Akesson, A., Lind, T. K., Barker, R., Hughes, A. & Cardenas, M. (2012). *Langmuir*, **28**, 13025–13033.
Andersen, H. D., Wang, C., Arleth, L., Peters, G. H. & Westh, P. (2011). *Proc. Natl Acad. Sci. USA*, **108**, 1874–1878.
Artero, J.-B., Härtlein, M., McSweeney, S. & Timmins, P. (2005). *Acta Cryst.* D**61**, 1541–1549.
Baker, M. (2010). *Nature (London)*, **465**, 823–826.
Bayburt, T. H., Grinkova, Y. V. & Sligar, S. G. (2002). *Nano Lett.* **2**, 853–856.
Berthaud, A., Manzi, J., Pérez, J. & Mangenot, S. (2012). *J. Am. Chem. Soc.* **134**, 10080–10088.
Bhattacharya, A. (2009). *Nature (London)*, **459**, 24–27.
Blanchet, C. E. & Svergun, D. I. (2013). *Annu. Rev. Phys. Chem.* **64**, 37–54.
Bligh, E. G. & Dyer, W. J. (1959). *Can. J. Biochem. Physiol.* **37**, 911–917.
Bocharov, E. V., Mineev, K. S., Volynsky, P. E., Ermolyuk, Y. S., Tkach, E. N., Sobol, A. G., Chupin, V. V., Kirpichnikov, M. P., Efremov, R. G. & Arseniev, A. S. (2008). *J. Biol. Chem.* **283**, 6950–6956.
Bogdanov, M., Heacock, P., Guan, Z. & Dowhan, W. (2010). *Proc. Natl Acad. Sci. USA*, **107**, 15057–15062.
Bragina, N. A. & Chupin, V. V. (1997). *Russ. Chem. Rev.* **66**, 975–986.
Calcutta, A., Jessen, C. M., Behrens, M. A., Oliveira, C. L., Renart, M. L., González-Ros, J. M., Otzen, D. E., Pedersen, J. S., Malmendal, A. & Nielsen, N. C. (2012). *Biochim. Biophys. Acta*, **1818**, 2290–2301.
Chan, Y.-H. M. & Boxer, S. G. (2007). *Curr. Opin. Chem. Biol.* **11**, 581–587.

Cherezov, V., Rosenbaum, D. M., Hanson, M. A., Rasmussen, S. G., Thian, F. S., Kobilka, T. S., Choi, H. J., Kuhn, P., Weis, W. I., Kobilka, B. K. & Stevens, R. C. (2007). *Science*, **318**, 1258–1265.

Dufourc, E. J., Smith, I. C. & Jarrell, H. C. (1983). *Chem. Phys. Lipids*, **33**, 153–177.

Engelman, D. M. & Moore, P. B. (1975). *Annu. Rev. Biophys. Bioeng.* **4**, 219–241.

Fagerberg, L., Jonasson, K., von Heijne, G., Uhlén, M. & Berglund, L. (2010). *Proteomics*, **10**, 1141–1149.

Ferguson, K. M., Berger, M. B., Mendrola, J. M., Cho, H.-S., Leahy, D. J. & Lemmon, M. A. (2003). *Mol. Cell*, **11**, 507–517.

Fuchs, B., Müller, K., Göritz, F., Blottner, S. & Schiller, J. (2007). *Lipids*, **42**, 991–998.

Fuchs, B., Süss, R. & Schiller, J. (2010). *Prog. Lipid Res.* **49**, 450–475.

Glatter, O. (1977). *J. Appl. Cryst.* **10**, 415–421.

Glatter, O. & Kratky, O. (1982). *Small Angle X-ray Scattering.* New York: Academic Press.

Hagn, F., Etzkorn, M., Raschle, T. & Wagner, G. (2013). *J. Am. Chem. Soc.* **135**, 1919–1925.

Higgins, M. K., Eswaran, J., Edwards, P., Schertler, G. F., Hughes, C. & Koronakis, V. (2004). *J. Mol. Biol.* **342**, 697–702.

Hunt, J. F., McCrea, P. D., Zaccaï, G. & Engelman, D. M. (1997). *J. Mol. Biol.* **273**, 1004–1019.

Hura, G. L., Menon, A. L., Hammel, M., Rambo, R. P., Poole, F. L. II, Tsutakawa, S. E., Jenney, F. E. Jr, Classen, S., Frankel, K. A., Hopkins, R. C., Yang, S., Scott, J. W., Dillard, B. D., Adams, M. W. W. & Tainer, J. A. (2009). *Nature Methods*, **6**, 606–612.

Jacques, D. A., Guss, J. M., Svergun, D. I. & Trewhella, J. (2012). *Acta Cryst.* D**68**, 620–626.

Jacques, D. A. & Trewhella, J. (2010). *Protein Sci.* **19**, 642–657.

Jacrot, B. (1976). *Rep. Prog. Phys.* **39**, 911–953.

Kaneko, H., Hosohara, M., Tanaka, M. & Itoh, T. (1976). *Lipids*, **11**, 837–844.

Konarev, P. V., Petoukhov, M. V., Volkov, V. V. & Svergun, D. I. (2006). *J. Appl. Cryst.* **39**, 277–286.

Kruijff, B. de, van Zoelen, E. J. & van Deenen, L. L. (1978). *Biochim. Biophys. Acta*, **509**, 537–542.

Kucerka, N., Nagle, J. F., Feller, S. E. & Balgavý, P. (2004). *Phys. Rev. E Stat. Nonlin. Soft Matter Phys.* **69**, 051903.

Law, J. H. (1971). *Acc. Chem. Res.* **4**, 199–203.

Leiting, B., Marsilio, F. & O'Connell, J. F. (1998). *Anal. Biochem.* **265**, 351–355.

Li, J., Callaway, D. J. & Bu, Z. (2009). *J. Mol. Biol.* **392**, 166–180.

Lunin, V. V., Dobrovetsky, E., Khutoreskaya, G., Zhang, R., Joachimiak, A., Doyle, D. A., Bochkarev, A., Maguire, M. E., Edwards, A. M. & Koth, C. M. (2006). *Nature (London)*, **440**, 833–837.

Magnuson, K., Jackowski, S., Rock, C. O. & Cronan, J. E. Jr (1993). *Microbiol. Rev.* **57**, 522–542.

Majewski, J., Kuhl, T. L., Wong, J. Y. & Smith, G. S. (2000). *J. Biotechnol.* **74**, 207–231.

Makhatadze, G. I., Clore, G. M. & Gronenborn, A. M. (1995). *Nature Struct. Biol.* **2**, 852–855.

Meer, G. van, Voelker, D. R. & Feigenson, G. W. (2008). *Nature Rev. Mol. Cell Biol.* **9**, 112–124.

Mendoza, D. de, Klages Ulrich, A. & Cronan, J. E. (1983). *J. Biol. Chem.* **258**, 2098–2101.

Midgett, C. R. & Madden, D. R. (2007). *J. Struct. Biol.* **160**, 265–274.

Molloy, S. (2010). *Nature Rev. Genet.* **11**, 240.

Montelione, G. T., Wüthrich, K., Burgess, A. W., Nice, E. C., Wagner, G., Gibson, K. D. & Scheraga, H. A. (1992). *Biochemistry*, **31**, 236–249.

Mylonas, E. & Svergun, D. I. (2007). *J. Appl. Cryst.* **40**, s245–s249.

Nath, A., Atkins, W. M. & Sligar, S. G. (2007). *Biochemistry*, **46**, 2059–2069.

Ogiso, H., Ishitani, R., Nureki, O., Fukai, S., Yamanaka, M., Kim, J.-H., Saito, K., Sakamoto, A., Inoue, M., Shirouzu, M. & Yokoyama, S. (2002). *Cell*, **110**, 775–787.

Palczewski, K., Kumasaka, T., Hori, T., Behnke, C. A., Motoshima, H., Fox, B. A., Le Trong, I., Teller, D. C., Okada, T., Stenkamp, R. E., Yamamoto, M. & Miyano, M. (2000). *Science*, **289**, 739–745.

Paliy, O., Bloor, D., Brockwell, D., Gilbert, P. & Barber, J. (2003). *J. Appl. Microbiol.* **94**, 580–586.

Pedersen, B. P., Buch-Pedersen, M. J., Morth, J. P., Palmgren, M. G. & Nissen, P. (2007). *Nature (London)*, **450**, 1111–1114.

Pedersen, J. S., Hansen, S. & Bauer, R. (1994). *Eur. Biophys. J.* **22**, 379–389.

Pedersen, J. S., Posselt, D. & Mortensen, K. (1990). *J. Appl. Cryst.* **23**, 321–333.

Pernot, P., Round, A., Theveneau, P., Giraud, T., Nogueira-Fernandes, R., Nurrizzo, D., Spruce, D., Surr, J., McSweeney, S., Felisaz, F., Foedinger, L., Gobbo, A., Huet, J., Villard, C. & Cipriani, F. (2010). *J. Phys. Conf. Ser.* **247**, 012009.

Petkovic, M., Schiller, J., Müller, M., Benard, S., Reichl, S., Arnold, K. & Arnhold, J. (2001). *Anal. Biochem.* **289**, 202–216.

Petoukhov, M. V. & Svergun, D. I. (2012). *Int. J. Biochem. Cell Biol.* **45**, 429–437.

Pipich, V. (2007). *QtiKWS*. http://iffwww.iff.kfa-juelich.de/~pipich/dokuwiki/doku.php/qtikws.

Pocanschi, C. L., Dahmane, T., Gohon, Y., Rappaport, F., Apell, H. J., Kleinschmidt, J. H. & Popot, J. L. (2006). *Biochemistry*, **45**, 13954–13961.

Raetz, C. R. (1978). *Microbiol. Rev.* **42**, 614–659.

Rambo, R. P. & Tainer, J. A. (2013). *Annu. Rev. Biophys.* **42**, 415–441.

Rasmussen, S. G. F., Choi, H.-J. *et al.* (2011). *Nature (London)*, **469**, 175–180.

Rasmussen, S. G. F., Choi, H.-J., Rosenbaum, D. M., Kobilka, T. S., Thian, F. S., Edwards, P. C., Burghammer, M., Ratnala, V. R., Sanishvili, R., Fischetti, R. F., Schertler, G. F., Weis, W. I. & Kobilka, B. K. (2007). *Nature (London)*, **450**, 383–387.

Rasmussen, S. G. F., DeVree, B. T. *et al.* (2011). *Nature (London)*, **477**, 549–555.

Ritchie, T. K., Grinkova, Y. V., Bayburt, T. H., Denisov, I. G., Zolnerciks, J. K., Atkins, W. M. & Sligar, S. G. (2009). *Methods Enzymol.* **464**, 211–231.

Rochel, N., Ciesielski, F., Godet, J., Moman, E., Roessle, M., Peluso-Iltis, C., Moulin, M., Haertlein, M., Callow, P., Mély, Y., Svergun, D. I. & Moras, D. (2011). *Nature Struct. Mol. Biol.* **18**, 564–570.

Rosenbaum, D. M., Cherezov, V., Hanson, M. A., Rasmussen, S. G. F., Thian, F. S., Kobilka, T. S., Choi, H.-J., Yao, X.-J., Weis, W. I., Stevens, R. C. & Kobilka, B. K. (2007). *Science*, **318**, 1266–1273.

Roth, B. L. & Marshall, F. H. (2012). *Nature (London)*, **492**, 57.

Round, A. R., Franke, D., Moritz, S., Huchler, R., Fritsche, M., Malthan, D., Klaering, R., Svergun, D. I. & Roessle, M. (2008). *J. Appl. Cryst.* **41**, 913–917.

Rouser, G., Siakotos, A. N. & Fleischer, S. (1966). *Lipids*, **1**, 85–86.

Schiller, J., Süss, R., Arnhold, J., Fuchs, B., Lessig, J., Müller, M., Petković, M., Spalteholz, H., Zschörnig, O. & Arnold, K. (2004). *Prog. Lipid Res.* **43**, 449–488.

Shinoda, T., Ogawa, H., Cornelius, F. & Toyoshima, C. (2009). *Nature (London)*, **459**, 446–450.

Shintre, C. A. *et al.* (2013). *Proc. Natl Acad. Sci. USA*, **110**, 9710–9715.

Skar-Gislinge, N. & Arleth, L. (2011). *Phys. Chem. Chem. Phys.* **13**, 3161–3170.

Skar-Gislinge, N., Simonsen, J. B., Mortensen, K., Feidenhans'l, R., Sligar, S. G., Lindberg Møller, B., Bjørnholm, T. & Arleth, L. (2010). *J. Am. Chem. Soc.* **132**, 13713–13722.

Stuhrmann, H. (1982). *Small-angle X-ray Scattering*, edited by O. Glatter & O. Kratky, pp. 197–213. New York: Academic Press.

Svergun, D. I. (1999). *Biophys. J.* **76**, 2879–2886.

Svergun, D. I., Petoukhov, M. V. & Koch, M. H. J. (2001). *Biophys. J.* **80**, 2946–2953.

Svergun, D. I., Richard, S., Koch, M. H. J., Sayers, Z., Kuprin, S. & Zaccai, G. (1998). *Proc. Natl Acad. Sci. USA*, **95**, 2267–2272.

Tate, C. G. (2010). *Methods Mol. Biol.* **601**, 187–203.

Terstappen, G. C. & Reggiani, A. (2001). *Trends Pharmacol. Sci.* **22**, 23–26.
Toft, K. N., Vestergaard, B., Nielsen, S. S., Snakenborg, D., Jeppesen, M. G., Jacobsen, J. K., Arleth, L. & Kutter, J. P. (2008). *Anal. Chem.* **80**, 3648–3654.
White, S. H. (2009). *Nature (London)*, **459**, 344–346.
White, T., Bursten, S., Federighi, D., Lewis, R. A. & Nudelman, E. (1998). *Anal. Biochem.* **258**, 109–117.
Xia, Y., Lu, L. J. & Gerstein, M. (2006). *J. Mol. Biol.* **357**, 339–349.
Zhang, X., Gureasko, J., Shen, K., Cole, P. A. & Kuriyan, J. (2006). *Cell*, **125**, 1137–1149.